

Washington University in St. Louis

Washington University Open Scholarship

Arts & Sciences Electronic Theses and
Dissertations

Arts & Sciences

Spring 5-15-2023

Dynamics of Epithelial Differentiation Following Intestinal Villus Injury

Takahiro Erick Ohara

Follow this and additional works at: https://openscholarship.wustl.edu/art_sci_etds

Recommended Citation

Ohara, Takahiro Erick, "Dynamics of Epithelial Differentiation Following Intestinal Villus Injury" (2023). *Arts & Sciences Electronic Theses and Dissertations*. 2900.
https://openscholarship.wustl.edu/art_sci_etds/2900

This Dissertation is brought to you for free and open access by the Arts & Sciences at Washington University Open Scholarship. It has been accepted for inclusion in Arts & Sciences Electronic Theses and Dissertations by an authorized administrator of Washington University Open Scholarship. For more information, please contact digital@wumail.wustl.edu.

WASHINGTON UNIVERSITY IN ST. LOUIS

Division of Biology and Biomedical Sciences
Immunology

Dissertation Examination Committee:

Thaddeus Stappenbeck, Chair

Marco Colonna, Co-Chair

Maxim Artyomov

Samantha Morris

David Ornitz

Steven Van Dyken

Dynamics of Epithelial Differentiation Following Intestinal Villus Injury

by

Takahiro Erick Ohara

A dissertation presented to
Washington University in St. Louis
in partial fulfillment of the
requirements for the degree
of Doctor of Philosophy

May 2023
St. Louis, Missouri

© 2023, Takahiro Erick Ohara

Table of Contents

List of Figures	iv
List of Tables	viii
Acknowledgements	ix
Abstract	xii
Chapter 1: Introduction	1
1.1 Introduction	2
1.2 Figures	16
1.3 References	18
Chapter 2: Modeling Intestinal Villus Injury-Repair Using Poly(I:C)	27
2.1 Introduction	28
2.2 Materials and Methods	31
2.3 Results	35
2.4 Discussion	37
2.5 Figures	40
2.6 References	45
Chapter 3: Identification of an Atrophy-Induced Villus Epithelial Cell Type	50
3.1 Introduction	51
3.2 Materials and Methods	55
3.3 Results	62
3.4 Discussion	69
3.5 Figures	73
3.6 Tables	95

3.7	References.....	96
Chapter 4: YAP Signaling Mediates Intestinal Barrier Re-establishment.....		104
4.1	Introduction.....	105
4.2	Materials and Methods.....	110
4.3	Results.....	116
4.4	Discussion.....	123
4.5	Figures.....	127
4.6	Tables.....	152
4.7	References.....	154
Chapter 5: Characterizing Atrophy-Induced Stromal Changes		160
5.1	Introduction.....	161
5.2	Materials and Methods.....	166
5.3	Results.....	172
5.4	Discussion.....	178
5.5	Figures.....	182
5.6	Tables.....	199
5.7	References.....	200
Chapter 6: Summary and Future Directions		205
6.1	Summary.....	206
6.2	Future Directions	210
6.3	Closing Remarks.....	218
6.4	Figures.....	219
6.5	References.....	222

List of Figures

Chapter 1

- Figure 1.1.** Tissue architecture of epithelial barriers..... 16
- Figure 1.2.** Structure and turnover of the intestinal epithelium..... 17

Chapter 2

- Figure 2.1.** Schematic of epithelial cell death induced by double-stranded RNA.....40
- Figure 2.2.** Poly(I:C) induces robust villus injury in the proximal small intestine.....41
- Figure 2.3.** Poly(I:C) preferentially kills differentiated epithelial cells over stem/progenitor cells and does not discriminate between absorptive and secretory lineage cells.....42
- Figure 2.4.** Robust villus repair and regeneration following poly(I:C)-induced injury.....43
- Figure 2.5.** Intestinal stem cells are spared from poly(I:C)-induced injury.....44

Chapter 3

- Figure 3.1.** Transient suppression of enterocyte markers following villus injury..... 73
- Figure 3.2.** Characterization of villus atrophy-induced epithelial changes.....75
- Figure 3.3.** Villus injury induces a disease-associated epithelial cell type.....77
- Figure 3.4.** aVECs acquire a fetal-like transcriptional program.....78
- Figure 3.5.** scRNA-seq workflow for IECs from the homeostatic and atrophic intestine.....79
- Figure 3.6.** Analysis of scRNA-seq data.....81
- Figure 3.7.** Fetal markers are enriched in atrophy-associated IECs that transcriptionally resemble homeostatic villus-top enterocytes the most..... 83

Figure 3.8. aVECs are transcriptionally distinct from normal enterocytes and are comprised of cells within the enterocyte and goblet cell lineage.....	84
Figure 3.9. Identification of Crohn’s disease-associated enterocyte and goblet cell populations by scRNA-seq.....	85
Figure 3.10. aVEC-like cells are present in Crohn’s disease samples.....	87
Figure 3.11. aVECs express lineage-specific and differentiation markers.....	88
Figure 3.12. Lineage dynamics during villus injury-repair.....	89
Figure 3.13. aVECs are terminally differentiated.....	90
Figure 3.14. aVECs arise from transit-amplifying cells.....	92
Figure 3.15. aVECs are short-lived and transiently cover damaged villi.....	94

Chapter 4

Figure 4.1. YAP-dependent mechanisms of ISC recovery after injury.....	127
Figure 4.2. Defining a core transcriptional signature for intestinal barrier restoration.....	128
Figure 4.3. YAP is activated in aVECs.....	129
Figure 4.4. YAP promotes adaptive epithelial differentiation.....	130
Figure 4.5. WAE cells retain remnants of colonocyte and goblet cell identity.....	131
Figure 4.6. YAP is activated in WAE cells.....	132
Figure 4.7. <i>Yap^{AIEC}</i> and <i>Yap^{fl/fl}</i> mice exhibit a similar level of poly(I:C)-induced damage.....	134
Figure 4.8. Proper barrier re-establishment and aVEC morphology depend on YAP.....	135
Figure 4.9. scRNA-seq overview of the damaged intestine from <i>Yap^{AIEC}</i> and <i>Yap^{fl/fl}</i> mice.....	136
Figure 4.10. scRNA-seq analysis of the damaged intestine from <i>Yap^{AIEC}</i> and <i>Yap^{fl/fl}</i> mice.....	137
Figure 4.11. Cell-type specific responses to YAP deficiency during villus atrophy.....	139

Figure 4.12. <i>In situ</i> hybridization validation and pathway analysis of scRNA-seq data.....	140
Figure 4.13. YAP is functionally required for proper adaptive differentiation.....	142
Figure 4.14. Analysis of Wnt signaling and cell proliferation in the absence of YAP.....	143
Figure 4.15. Defining the extent to which YAP controls the fetal and aVEC program.....	144
Figure 4.16. Loss of YAP results in impaired villus regeneration.....	145
Figure 4.17. Inability to delete YAP in differentiated cells using <i>Krt20^{CreER}/Yap^{fl/fl}</i> mice.....	147
Figure 4.18. Impaired villus regeneration in <i>Yap^{ΔIEC}</i> mice is accompanied by a persistent maladapted aVEC state and abnormal epithelial differentiation.....	148
Figure 4.19. Eventual recovery of villus structures in <i>Yap^{ΔIEC}</i> mice one-week post-injury and possible compensation by stromal EREG.....	150

Chapter 5

Figure 5.1. aVECs are induced at the tip region of partially blunted villi.....	182
Figure 5.2. aVECs are present on atrophic villi in germ-free mice.....	183
Figure 5.3. Remodeling of the stromal microenvironment following villus injury.....	184
Figure 5.4. The PGE2-PTGER4 axis is not required for YAP nuclear localization and aVEC formation.....	186
Figure 5.5. The PGE2-PTGER4 axis is dispensable for villus regeneration.....	188
Figure 5.6. Defining the villus atrophy-induced intestinal secretome.....	190
Figure 5.7. Induction of a fetal-like, YAP-activated program in intestinal spheroids regardless of differentiation status or PGE2 treatment.....	191
Figure 5.8. Differentiated spheroids, but not ALI cells, feature nuclear YAP expression.....	192
Figure 5.9. YAP is essential for adaptive differentiation <i>in vitro</i>	193
Figure 5.10. EREG supplementation partially rescues YAP deficiency.....	195

Figure 5.11. Maladaptive differentiation in *APC^{Min/+}* tumors..... 196

Figure 5.12. YAP deficient mice are highly susceptible to double-poly(I:C) challenge..... 198

Chapter 6

Figure 6.1. Overall summary of findings..... 219

Figure 6.2. Mechanisms of tissue repair..... 220

Figure 6.3. Role of adaptive differentiation in pathogen defense and disease..... 221

List of Tables

Chapter 3

Table 3.1. Primers used for qRT-PCR, related to Figure 3.13.....95

Chapter 4

Table 4.1. Genes commonly induced in aVECs and WAE cells, related to Figure 4.2..... 152

Table 4.2. Genes expressed by aVECs and/or YAP-dependent, related to Figure 4.15..... 153

Chapter 5

Table 5.1. Primers used for qRT-PCR, related to Figure 5.3..... 199

Acknowledgements

I probably would not be writing this dissertation if it had not been for a talk given by Dr. Debora Farber in 2013 when I was an undergraduate student at UCLA. Her research on retinitis pigmentosa—an untreatable disease that runs in my family—helped me realize the importance of basic science research in advancing medical therapies. After dedicating myself to a research career over the past several years, I have been blessed with incredible mentors, starting with Dr. Xian-Jie Yang at UCLA, Dr. Maria Morasso at the NIH, Dr. Thaddeus Stappenbeck (now at Cleveland Clinic), and Dr. Marco Colonna at Washington University in St. Louis. Thank you all for your support and guidance in my journey toward becoming a physician-scientist.

I especially want to thank my two mentors in graduate school, Thad and Marco. Thad, I have learned so much from you. Thank you for teaching me how to write grants, pushing me to always see the big picture, and helping me write a coherent, impactful research story. Even when things got tough, you always found a way to cheer me up. Marco, I cannot thank you enough for taking me under your wings. Without your generosity, my final few years of graduate school would not have been nearly as successful. To both Thad and Marco, thank you for creating a lab environment where I felt valued and where I was free to explore as a scientist.

To the past and present members of the Stappenbeck lab, it has been an honor working with all of you. In particular, I would like to thank Yi Wang and Kelli VanDussen for being incredibly talented and inspiring scientists. Qiuhe Lu for being the smartest and funniest person I know. Satoru Fujii for letting me practice my Japanese language skills. Brian Muegge for advice on bioinformatics. RC Lai for helping me with the colonic biopsy injury system. Steven Ekman for your friendship. And Nikki Malvin for being a terrific lab manager. To all the present

members of the Colonna lab, thank you for welcoming me to your lab and being so accommodating to my needs. I hope we will all cross paths again in the future.

I have also been fortunate to have a wonderful group of scientists as part of my thesis committee. To Max Artyomov, Sam Morris, Dave Ornitz, and Steve Van Dyken: it has been a great pleasure getting to know you all. Thank you for guiding me throughout my PhD training and helping me develop into a better scientist. Your feedback has been greatly appreciated.

I would like to acknowledge some of the cores/facilities at Washington University as well as funding sources that were instrumental in completing this work: the Digestive Disease Research Core Center for paraffin embedding, sectioning, and H&E staining; the Genome Technology Access Center for providing microarray and single-cell RNA sequencing data; the Siteman Flow Cytometry Core (especially Michael Savio) for FACS sorting; the Molecular Microbiology Imaging Facility (especially Wandy Beatty) for transmission electron microscopy images; and training grants from the NIH (5T32 AI007172 and F30 DK120076).

During graduate school, I discovered a passion for teaching. After serving as a teaching assistant for the first-year medical histology course, I decided to continue my involvement in the course for three additional years. It was an incredible, rewarding experience. I would like to thank Dr. Paul Bridgman for giving me this opportunity. I would also like to thank the students for attending my lectures, utilizing my services, and showering me with kind messages. Being voted Teaching Assistant of the Year for two years in a row meant a great deal to me.

The Medical Scientist Training Program has been fundamental in making sure I survive this long and at times difficult journey. Thank you for accepting me into your program and for providing funding support. I am eternally grateful for the opportunity. Many thanks to the extraordinary staff members who run the program: Brian Sullivan, Christy Durbin, Linda

Perniciaro, and Liz Bayer. You have all been so helpful and kind to me. To Dr. Wayne Yokoyama, thank you for being an amazing role model and program director.

While I was not planning on joining the Immunology Program when I first came to Washington University, I am so glad that I did. The immunology community here is incredibly special. I would like to thank all the professors in the department for creating such a collaborative and imaginative place to do science. By far the best part about joining the program was all the friendships and memories I made over the years. There are too many to name, but I want to give a few special shout-outs: Ray Ohara, Takeshi Egawa, and Chyi Hsieh for all the fun times playing tennis; my PhD cohort for introducing me to Dungeons & Dragons; and the Lymphomaniacs team for a fun season of softball. I am lucky to have met so many great people.

Last, but by no means least, I want to thank my close friends and family members. They are my biggest cheerleaders. They remind me that there is a world outside of lab and academia. They are the reason that I was able to come this far. To my sister and my parents, thank you for everything you have done for me. I know I can be stubborn and reserved at times, but I am truly blessed to have you in my life. Your patience, love, and understanding have made this all possible. To my nephew Kai, I cannot wait to see you grow up and make an impact in this world.

Takahiro Erick Ohara

Washington University in St. Louis

May 2023

ABSTRACT OF THE DISSERTATION

Dynamics of Epithelial Differentiation Following Intestinal Villus Injury

by

Takahiro Erick Ohara

Doctor of Philosophy in Biology and Biomedical Sciences

Immunology

Washington University in St. Louis, 2023

Professor Thaddeus S. Stappenbeck, Chair

Professor Marco Colonna, Co-Chair

Millions of finger-like structures called villi line the small intestine, providing an enormous surface area for rapid and efficient nutrient absorption. Collapse of the villus architecture, known as villus atrophy, is often observed in response to pathogen invasion, inflammation, medications, and ischemia due to loss of intestinal epithelial cells, resulting in symptoms of diarrhea and malabsorption. Though removal of the inciting agent generally allows for near complete tissue recovery, some individuals take longer to restore their villi, a condition known as persistent villus atrophy, for reasons that are unknown. How intestinal villi cope with tissue damage and re-establish their structure remains poorly understood, yet their capacity to do so is vital for survival. Here, I developed a robust and highly reproducible injury-repair model that specifically targets the villus compartment of the small intestine. This system, which entails a single intraperitoneal injection of the double-stranded RNA analog poly(I:C) in mice, mimics key aspects of acute viral gastroenteritis and displays a consistent repair and regeneration pattern following injury. Using this model, I identified a transient, damage-induced epithelial cell type covering the surface of atrophic villi. Intriguingly, these atrophy-induced villus epithelial cells

(aVECs) possessed a fetal-like transcriptional profile, yet were terminally differentiated and lineage-committed. The primary function of aVECs was to quickly re-establish the intestinal barrier after villus damage. I further determined yes-associated protein (YAP), one of the major transcriptional mediators of the Hippo signaling pathway, as a crucial regulator of aVEC function. In the absence of YAP, aVECs were unable to properly restore the intestinal barrier post-injury. As a result, villus regeneration was markedly hampered in YAP-deficient mice. Finally, I found evidence of aVEC-like cells in human disease states with villus injury, such as Crohn's and celiac disease. Given that aVECs were derived from progenitor cells in the crypt, I defined a key repair mechanism involving the activation of a fetal-like program during injury-induced differentiation, a process I term "adaptive differentiation". Thus, I propose adaptive differentiation as an important healing mechanism in high turnover tissues such as the intestine.

Chapter 1

Introduction

1.1 Introduction

Architecture of Epithelial Barriers

In 1896, the American architect Louis Sullivan coined the phrase, “form follows function,” a design principle that the shape of a building should reflect its intended purpose. This idea not only impacted modern architecture but also product design and software engineering. We see examples of this everywhere in nature, where Sullivan got his inspiration. While he specifically referenced eagles, clouds, and rivers in his essay, “The Tall Office Building Artistically Considered,” the tissues in our body and the organelles in our cells also exemplify this philosophy (Friedman and Nunnari, 2014; Junt et al., 2008; Russell et al., 2000).

Epithelial barriers, such as the skin, lung, and intestine, line our body surfaces and interface with the external environment. They each possess a unique tissue architecture that supports their distinct functions (**Figure 1.1**). The skin, whose primary role is to withstand mechanical stress, is multi-layered with an epidermis, dermis, and hypodermis (Vig et al., 2017). The lung is the site of gas exchange and accomplishes this through highly vascularized sacculles (Whitsett et al., 2019). The intestine maximizes its absorptive capacity through folding of the mucosa and through finger-like structures called villi (Walton et al., 2016). Thus, the three-dimensional structure of each organ is uniquely suited to efficiently carry out its functions.

Notably, the surface epithelium is integral to the structure and function of these tissues. At the forefront are the specialized differentiated epithelial cells. In the skin, the epidermis is a stratified squamous epithelium composed of keratinocytes that function in resisting mechanical pressure, preventing water loss, and excluding toxins (Simpson et al., 2011). In the lung, a simple squamous epithelium predominantly covered by type I pneumocytes mediates the exchange of oxygen and carbon dioxide (Knudsen and Ochs, 2018). In the intestine, a highly

polarized simple columnar epithelium consisting largely of enterocytes and goblet cells enables the absorption of nutrients and secretion of mucus on the luminal side (Allaire et al., 2018). Given their vital functions, epithelial cells are crucial for maintaining tissue homeostasis. Damage to the epithelium results in collapse of the tissue architecture and potentially organ failure. Furthermore, epithelial damage is a hallmark of many diseases in barrier tissues.

Therefore, it is no surprise that the restoration of the epithelial barrier has become an important therapeutic goal. In fact, nearly all barrier tissues have the capacity to regenerate due to the presence of tissue stem cells, which can self-renew and replenish lost differentiated cells (Fuchs and Blau, 2020). Even before tissue stem cells were identified, Howard Green at the Massachusetts Institute of Technology developed the first stem cell-based therapy using cultured keratinocytes (Fuchs, 2018). Since then, cultured epithelial autografts have been utilized to treat burn patients for several decades (Atiyeh and Costagliola, 2007). In the gut, successful mucosal healing is regarded as an endpoint for disease activity and remission in patients with inflammatory bowel disease (IBD) (Dave and Loftus, 2012). With the advent of intestinal organoid culture systems, organoid-based therapy is currently underway for the treatment of IBD and short bowel syndrome (Nakamura and Sato, 2018; Sato et al., 2009; Sugimoto et al., 2021). Besides transplanting cultured cells, methods to directly reprogram cells toward the epithelial lineage *in vivo* has also shown efficacy in a preclinical mouse model (Kurita et al., 2018).

The epithelial layer does not function alone—it is supported by a network of extracellular matrix proteins, stromal cells, immune cells, vessels, and nerves. During development, epithelial-mesenchymal interactions govern the morphogenesis of epithelial tissues and ectodermal appendages (Arias, 2001). During homeostasis, multiple cell types contribute to the stem cell niche and regulate stem cell activity (Li and Xie, 2005). The hair follicle stem cell niche is one of

the best studied, and the cell types that make up the niche continues to grow. Aside from the dermal papilla, recent studies have identified regulatory T cells, lymphatic capillaries, and sympathetic nerves as components of the stem cell microenvironment (Ali et al., 2017; Gur-Cohen et al., 2019; Shwartz et al., 2020). In comparison, the stem cell niche in the airway and intestine is less characterized and remains to be further elucidated. Specific PDGFR α ⁺ stromal cell populations have been identified in both tissues to support stem cell function (Shoshkes-Carmel et al., 2018; Zepp et al., 2017). T-helper cells also modulate intestinal stem cell renewal and differentiation (Biton et al., 2018). The progeny of stem cells, including transit-amplifying cells and terminally differentiated cells, can feedback to the stem cell compartment (Hsu et al., 2014; Sato et al., 2011). Having multiple niche constituents likely enables precise control over stem cell activity and prevents stem cell failure should any of these malfunction.

In this dissertation, I will examine how barrier tissues restore their architecture after injury with an emphasis on the epithelial layer. Specifically, I will focus on the small intestine, an organ that is lined by millions of crypt-villus units. Villi are finger-like structures that project into the lumen of the gut. They provide an enormous surface area that maximizes nutrient digestion and absorption. Crypts are small invaginations that house stem and progenitor cells. While there is an extensive body of work understanding how the crypt compartment respond to and recover from injury, very little is known regarding how intestinal villi cope with damage. Despite the importance of these structures for our development and well-being, the cellular and molecular processes involved in rebuilding damaged villi remain poorly understood. By understanding villus repair in the context of the three-dimensional structure of the tissue, I hope to provide a framework for which we can identify where this process might fail in disease.

The Intestinal Epithelium

The intestinal epithelium is tasked with the challenge of balancing its absorptive function with its role in host defense. An important feature of the intestinal epithelium is that it constantly renews every 4-5 days (Umar, 2010). Fueling this high turnover rate are the intestinal stem cells (ISCs) and transit-amplifying (TA) cells that reside in the crypt. Specifically, ISCs divide approximately every 24 hours at the base of the crypt and give rise to TA cells (Pennings et al., 2018). TA cells then undergo additional bouts of cell division before exiting the crypt and committing to the various intestinal epithelial cell (IEC) lineages of the intestine, including absorptive enterocytes, mucus-secreting goblet cells, hormone-producing enteroendocrine cells, chemosensory tuft cells, and anti-microbial peptide-producing Paneth cells (Beumer and Clevers, 2021). With the exception of Paneth cells, these differentiated cells migrate along the surface of villi. The colon, which lacks villi, instead feature deeper crypts that house both proliferative and differentiated cells along the length of the crypt. Once epithelial cells reach the tip of the villus in the small intestine or the luminal surface in the colon, they undergo cell death and extrusion through a process termed anoikis (Patankar and Becker, 2020). We illustrate this in **Figure 1.2**.

The organization of the epithelium is tailored to meet the specific demands of the different regions of the intestinal tract. In the duodenum, villi are long, and the epithelium mainly consists of enterocytes that specialize in the absorption of dietary nutrients (Thompson et al., 2018). Along with the jejunum, which is the region after the duodenum, it is the principal site for the absorption of carbohydrates, lipids, and amino acids (Goodman, 2010). In the distal small intestine, also known as the ileum, villi are shorter, and goblet cells are more prevalent to provide lubrication for the passage of stool towards the colon. The ileum is also the main site for the absorption of vitamin B12, bile salts, and any remaining nutrients not absorbed by the

proximal intestine (Tappenden, 2014b). Paneth cells, which secrete anti-microbial peptides such as defensins and lysozyme, are present throughout the small intestine at the base of the crypt interspersed between ISCs (Clevers and Bevins, 2013). In contrast, the colon lacks Paneth cells and contains a high density of goblet cells (Peterson and Artis, 2014). All IECs originate from ISCs, which are distinguished by the expression of LGR5 at the crypt base (Barker et al., 2007).

Several important signaling pathways have been elucidated to govern the intestinal epithelium's high self-renewal capacity, heterogeneity, and gradient of differentiation along the crypt-villus axis. Wnt-R-spondin signaling, in particular, is crucial for maintaining the stem and progenitor cells of the crypt. Essential Wnt ligands are produced by subepithelial stromal cells and constitute the ISC niche (Degirmenci et al., 2018; Shoshkes-Carmel et al., 2018). These ligands confer a basal competency unto ISCs, enabling R-spondin-driven ISC self-renewal (Yan et al., 2017). Loss or inhibition of Wnt signaling causes rapid cessation of proliferation and disruption of tissue integrity (Shoshkes-Carmel et al., 2018; van Es et al., 2012). Furthermore, hyperactivated Wnt signaling leads to adenoma formation and tumorigenesis (Romagnolo et al., 1999; Su et al., 1992). Counteracting the effects of Wnts is Hedgehog and Bmp signaling, which contribute to the differentiation of IECs (Vanuytsel et al., 2013). Hedgehog ligands secreted from the epithelium induce underlying stromal cells to produce Bmps, which feedback to the epithelium to maintain differentiation (Madison et al., 2005). Loss of Hedgehog or Bmp signaling in the gut results in epithelial hyperplasia and ectopic crypt formation (Batts et al., 2006; Madison et al., 2005). Bmp signaling has also been demonstrated to regulate hormone expression of enteroendocrine cells (Beumer et al., 2018). Notch signaling, which is essential for maintaining ISCs, dictates cell fate decisions through lateral inhibition (Sancho et al., 2015; VanDussen et al., 2012). Activation of Notch signaling in progenitors drives the absorptive cell

fate whereas Notch inhibition induces the secretory cell fate (Noah and Shroyer, 2013). Blocking the Notch cascade with a γ -secretase inhibitor converts proliferative crypt cells into post-mitotic goblet cells (van Es et al., 2005). Last, but not least, EGF is a crucial component of the intestinal organoid culture system, and the EGF receptor is highly expressed by ISCs (Sato et al., 2009). EGF signaling is considered to promote stem cell proliferation *in vivo* (Beumer and Clevers, 2016). The current paradigm is that all of these pathways converge to establish a differentiation gradient along the crypt-villus axis, with pro-proliferative signals mediated by Wnts and EGFs being the highest at the crypt and pro-differentiation signals mediated by Bmps and Hedgehog being the lowest at the crypt. What maintains and regulates these signaling gradients are still unclear, but additional regulatory factors including Wnt and Bmp inhibitors likely play a role.

Until recently, there has been a long-standing debate as to what cell(s) provide essential Wnt ligands for ISC maintenance. Multiple different Wnt ligands are produced by various cell types in the gut (Gregorieff et al., 2005). Given that Paneth cells are located adjacent to ISCs and express WNT3A along with other niche factors, they were proposed to serve as a major constituent of the stem cell niche (Sato et al., 2011). In fact, Paneth cell-derived WNT3A is essential for the growth of intestinal organoids (Farin et al., 2012). However, WNT3A and Paneth cells are largely dispensable for the maintenance of ISCs *in vivo* (Durand et al., 2012; Farin et al., 2012). Myofibroblasts express Wnt ligands and were initially candidates for the stem cell niche (Miyoshi, 2017; Valenta et al., 2016). However, Wnt secretion from epithelial cells and myofibroblasts appears to be non-essential for ISC identity and function (San Roman et al., 2014). The breakthrough came when subepithelial fibroblasts known as telocytes, marked by the expression of PDGFRA, FOXL1, and GLI1, were discovered to secrete essential Wnt ligands, making them the long sought-after ISC niche cells (Degirmenci et al., 2018; Shoshkes-Carmel et

al., 2018). While questions remain as to which specific Wnt ligands are crucial for ISC maintenance, these studies illustrate an important role for fibroblast populations located right beneath the epithelial layer in regulating stem cell renewal and intestinal homeostasis.

Adaptive Cellular Responses in the Gut

While much is known about the homeostatic turnover of the intestinal lining since the landmark studies of Cheng and Leblond (Cheng and Leblond, 1974), details of how the epithelium responds to stress, injury, and environmental changes are currently an area of intense research. Recent studies have uncovered a remarkable capacity for the intestinal epithelium to adapt to various local and systemic perturbations, thus enabling host survival and fitness.

Intestinal adaptation after extensive intestinal resection in short bowel syndrome offers a classic example. Following loss of a large portion of the small bowel due to disease, ischemia, trauma, or some other reason, the remnant bowel undergoes a significant structural and functional compensatory response in order to maximize nutrient absorption (Tappenden, 2014a). This generally involves enhanced crypt proliferation and increased villus length (Rubin and Levin, 2016). The mechanisms responsible for this response are likely multiple. Notably, glucagon-like peptide-2 (GLP-2), which is secreted by enteroendocrine L cells, increase in levels following resection, and exogenous treatment of GLP-2 alone enhances crypt and villus height (Ljungmann et al., 2001; Tsai et al., 1997). An analog of GLP-2, teduglutide, is approved for clinical use in adults with short bowel syndrome (Seidner et al., 2013). Since GLP-2 also acts on the enteric nervous system (ENS), these studies suggest a potential enteroendocrine-ENS-epithelium axis in driving resection-associated intestinal adaptation (Bjerknes and Cheng, 2001).

The type of food that we eat and the amount of calorie that we consume have wide-ranging effects on our health. It is well-established that calorie restriction promotes changes in metabolic processes that enhance tissue health and animal lifespan (Hwangbo et al., 2020). On the contrary, obesity promotes tissue dysfunction and is a major risk factor for diseases such as cardiovascular disease, fatty liver disease, type 2 diabetes, and cancer (Goossens, 2017). Importantly, recent studies have revealed that nutrient-sensing and metabolic pathways can control the self-renewal capacity and cell fate choices of ISCs (Alonso and Yilmaz, 2018). During calorie restriction, mTOR1 signaling is reduced in Paneth cells, leading to the production of cyclic ADP ribose, which augments the function of neighboring ISCs (Yilmaz et al., 2012). Additionally, Paneth cells and ISCs form a metabolic partnership wherein Paneth cells, which rely on glycolysis, produce lactate to maintain the function of ISCs, which display high mitochondrial activity (Rodriguez-Colman et al., 2017). In the case of obesity, mice fed with a high-fat diet display increased numbers and function of LGR5⁺ ISCs due to robust induction of PPAR-delta signaling in these cells (Beyaz et al., 2016). Together, these findings provide a mechanistic link between diet and tissue fitness through the regulation of adult stem cells.

The intestinal epithelium must carefully balance its primary function in nutrient absorption and its role in pathogen defense. Emerging evidence reveals a dynamic interplay between IECs and immune cells to mediate these processes. During infection by parasitic helminths such as *Nippostrongylus brasiliensis* and *Heligmosomoides polygyrus*, tuft cells secrete IL-25 to activate group 2 innate lymphoid cells (ILC2s), which then signal to the crypt compartment via IL-13 to promote the differentiation of more tuft cells and goblet cells (von Moltke et al., 2016). In this way, a tuft cell-ILC2 circuit is established to limit parasitic infection in the gut. Tuft cells appear to directly sense helminth-derived metabolites, specifically

succinate, to trigger this circuit (Nadjsombati et al., 2018; Schneider et al., 2018). Recently, it was also shown that $\gamma\delta$ T cells signal to the intestinal epithelium in response to changes in nutrient availability. Specifically, switching from a high protein diet to a high carbohydrate diet in mice triggers a carbohydrate transcriptional program in IECs in a $\gamma\delta$ T cell- and IL-22-dependent manner (Sullivan et al., 2021). Interestingly, tuft cells were implicated in inducing this carbohydrate transcriptional program as well, albeit the mechanism is still unclear (Sullivan et al., 2021). It will be interesting to see how these results fit with other studies that suggest that enterocytes dynamically shift their metabolic program along the villus axis (Moor et al., 2018).

The intestine also harbors a large community of microorganisms that are key to many aspects of health. A large majority of these microbes are bacteria, but viruses, fungi, and protozoa also reside in the gut and contribute to host fitness in unique ways (Valdes et al., 2018). How the intestine adapts to fluctuations in the microbiome during development and our adult life is a key area of research. The intestinal epithelium is now recognized as a central player in responding to microbial signals and shaping the host immune system (Soderholm and Pedicord, 2019). Through expression of various pattern recognition receptors, including toll-like receptors (TLRs), NOD-like receptors (NLRs), and RIG-I-like receptors (RLRs), IECs can directly sense the presence of microbes and relay that information to underlying immune cells (Fukata and Arditi, 2013). This microbiota-IEC crosstalk is essential for defending against pathogens, producing antimicrobial peptides, inducing regulatory T cell differentiation, generating IgA producing plasma cells, and mounting a robust immune response (Okumura and Takeda, 2017).

Lastly, the intestine is vulnerable to a wide variety of insults that can breach the epithelial barrier. These may include certain medications, infectious agents, and inflammatory stimuli. The ability to withstand damage signals and repair the injury are adaptations that ensure the survival

of the animal (Jessen et al., 2015). In examining various injury contexts in the gut, one major theme that has emerged over the years is the importance of cell plasticity (Blanpain and Fuchs, 2014). Many studies have uncovered a high degree of cell plasticity among IECs, particularly in their ability to dedifferentiate and re-acquire stem cell features, thus ensuring a constant pool of ISCs at all times (Beumer and Clevers, 2016). Mechanistically, it is thought that the broadly permissive chromatin landscape of IECs endows them with fate flexibility (Kim et al., 2014). Thus, even when ISCs are destroyed by injury, the intestinal epithelium can quickly adapt to ISC loss by having other cells take over their function (Tian et al., 2011). Interestingly, various stromal cell populations, including group 3 innate lymphoid cells (ILC3s) and PDGFRA⁺ fibroblasts, and cell-extrinsic signals, including gp130 ligands, have been shown to mediate this adaptive response (Greicius et al., 2018; Murata et al., 2020; Romera-Hernandez et al., 2020; Taniguchi et al., 2015). Additionally, IECs display unique responses to superficial injuries to the intestinal barrier through a process traditionally referred to as restitution (Lacy, 1988). When an ulcer or wound forms in the intestinal mucosa, a proliferation-independent mechanism of repair occurs whereby wound-associated epithelial (WAE) cells arise from the crypts adjacent to the injury and cover the surface of the wound to re-establish the barrier (Seno et al., 2009). In particular, prostaglandin E2 (PGE2) production from mesenchymal cells in the wound bed appears to direct WAE cell formation (Miyoshi et al., 2017). Therefore, depending on the context, location, and severity of injury, IECs can acquire unique capabilities owing to signals from the mesenchyme in order to repair wounds and restore tissue architecture. All of the adaptive cellular responses described here provide IECs with the capacity to cope with various perturbations that can occur in the gut, thus ensuring tissue homeostasis and host survival .

Dysregulation of Adaptive Cellular Responses in Disease

The understanding of how IECs adapt to a variety of conditions and how host and microbial factors contribute to these responses have important implications for regenerative medicine and personalized therapy for a number of intestinal and extra-intestinal diseases. Impairment in these adaptive responses is largely thought to underly disease pathology.

Inflammatory bowel disease (IBD) is a group of disorders characterized by chronic inflammation of the digestive tract. There are two main types of IBD. The first one, known as ulcerative colitis, is restricted to the colon and affects mainly the mucosal and submucosal layers of the intestine with crypt loss and ulceration (Gajendran et al., 2019). The second type, known as Crohn's disease, can involve any part of the gastrointestinal tract, though is most prevalent in the terminal ileum. Unlike ulcerative colitis, Crohn's disease can affect all the layers of the gut, featuring transmural inflammation, granulomas, and fistulas (Gajendran et al., 2018). The etiology and pathogenesis of IBD is unknown, but is largely thought to involve a complex interplay between the microbiota, host genetics, and environmental factors (Zhang et al., 2017). Impaired function of the epithelial layer can cause a cascade of events, with enhanced intestinal permeability, perturbed immune homeostasis, and further damage to the epithelium (Coskun, 2014). Whether epithelial dysfunction is a cause or an effect of IBD is not known, but several IBD-associated genes are unique to the function of IECs (McCole, 2014). Importantly, mucosal healing—that is, restoration of the epithelial architecture—is considered to be a successful endpoint in achieving long-term remission in IBD patients (Dave and Loftus, 2012; Schnitzler et al., 2009). Understanding how epithelial cells respond to injury in normal conditions and identifying how this process can go awry in disease will be important moving forward. Recently, we have shown that consumption of a western diet and smoking can exacerbate IBD-like

pathology in mice by triggering defects in Paneth cells (Liu et al., 2021; Liu et al., 2018). In addition, we found that a specific strain of fungus, *Debaryomyces hansenii*, is abundant in inflamed mucosal tissues of Crohn's disease samples, and the presence of *D. hansenii* impairs wound healing in mice through upregulation of type I interferon and CCL5 (Jain et al., 2021). These findings identify new players in IBD pathogenesis and reveal novel therapeutic targets.

Irritable bowel syndrome (IBS) is a common gastrointestinal disorder that is characterized by abdominal pain and diarrhea and/or constipation (Vahedi et al., 2010). The etiology of IBS is poorly understood. It is considered to be a form of intestinal dysmotility, and stress is a well-known trigger of IBS and IBD flares (Lind, 1991; Sun et al., 2019). Stress itself can cause alterations in gastrointestinal motility, antimicrobial immunity, and microbial composition (Rengarajan et al., 2020). Interestingly, this study found that abnormal opening of goblet cell-associated passages (GAPs) was the root cause of stress-induced bacterial translocation in the gut (Rengarajan et al., 2020). IBS can also be triggered after an episode of acute gastroenteritis known as post-infectious irritable bowel syndrome (PI-IBS). The mechanisms underlying the development of PI-IBS is also poorly understood, but several studies implicate a defect in epithelial integrity and an increase in enterochromaffin cell numbers as possible underlying factors (Thabane and Marshall, 2009). While anti-TNF-alpha-based therapies have been proven effective in certain IBD patients (Peyrin-Biroulet, 2010), there are currently no therapies for IBS outside of lifestyle modifications and symptomatic relief.

Celiac disease is another common immune-driven disorder with a complex pathophysiology characterized by damage to the small intestinal villi. In contrast to IBD and IBS, the trigger of celiac disease and the genetic underpinnings are well-defined. Celiac disease is caused by ingestion of wheat gluten, which induces an inflammatory response in the small

intestine (Alaedini and Green, 2005). Overt inflammation results in villus atrophy, crypt hyperplasia, and infiltration of intra-epithelial lymphocytes (Green and Jabri, 2003). Keeping patients on a gluten-free diet is the most effective treatment option (Tye-Din et al., 2018). Despite this, celiac disease remains a global disease that is increasing in prevalence, affecting people of all ages. The immunological basis for celiac disease remains poorly understood, and many questions remain regarding why some people with or without genetic predisposition develop (or not develop) the disease. Furthermore, over one-third of patients (recent numbers suggest this may be higher) experience a refractory form of celiac disease that is resistant to treatment (i.e., a strict gluten-free diet) (Lebwohl et al., 2014; Rubio-Tapia and Murray, 2010). These patients present with persistent villus atrophy for reasons that are unclear (Fernandez-Banares et al., 2021). Surprisingly, little known in regard to how villi normally heal after injury. Understanding this process will be crucial given that there is a significant association between mucosal recovery and reduced mortality in celiac disease patients (Rubio-Tapia et al., 2010).

Finally, colorectal cancer is one of the most commonly diagnosed cancers in both men and women and is the second most common cause of cancer death in the United States (Siegel et al., 2020). Mutations in tumor suppressor genes drive cancer progression, with specific genes involved in the adenoma-carcinoma sequence (Armaghany et al., 2012). Most notably, the adenomatous polyposis coli (APC) gene is the most commonly mutated gene in colorectal cancer (Armaghany et al., 2012). An inherited condition known as familial adenomatous polyposis (FAP), caused by mutations in APC, is characterized by formation of numerous adenomatous polyps in the distal intestine (Jasperson et al., 1993). How mutations in the APC gene confer IECs with a selective growth advantage in the gut is not well understood. Interestingly, pathways that are upregulated during injury-induced repair and regeneration, such as the Hippo-YAP

pathway, appears to be absolutely required for the initiation of APC-associated tumors (Gregorieff et al., 2015). This is consistent with the notion that “cancer is a wound that never heals,” which suggests that adaptive mechanisms of tissue repair can be hijacked by cancer cells to gain selective advantages over non-cancerous cells (Byun and Gardner, 2013).

1.2 Figures

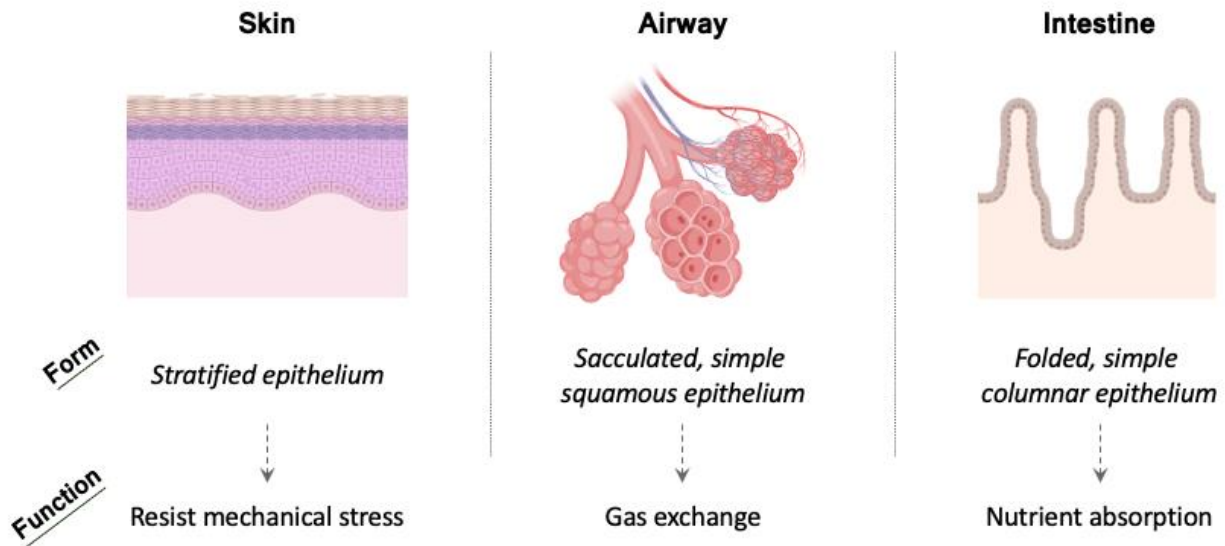


Figure 1.1. Tissue architecture of epithelial barriers

Epithelial barriers such as the skin, airway, and intestine possess a unique tissue architecture that enables their functions. The skin's main function is to resist mechanical tension and it achieves this by having a multilayered structure with an epidermis, dermis, and hypodermis. The airway's main function is to exchange oxygen and carbon dioxide. It achieves this by forming aggregates of saccules that, combined, greatly increases the surface area for gas exchange. The epithelial surface in the airway is also very flat and located adjacent to the extensive capillary network in the lung. The gut's main function is to absorb dietary nutrients. It maximizes this function by extensively folding the epithelial surface through formation of structures called villi. Structures called microvilli found on the apical surface of the epithelium also augments the absorptive area.

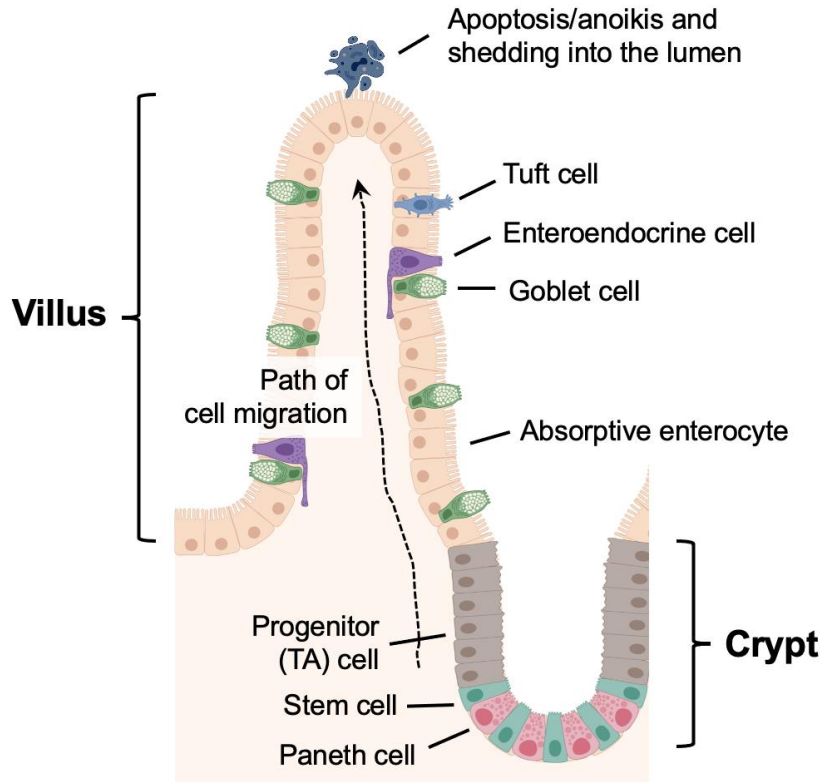


Figure 1.2. Structure and turnover of the intestinal epithelium

The intestinal epithelium renews every 3-5 days. This high turnover rate is driven by the actively cycling stem and progenitor cells in the crypt. At the base of the crypt are stem cells interspersed between Paneth cells. As stem cells move up the crypt compartment, they become transit-amplifying (TA) progenitor cells that undergo additional rounds of cell division. At this stage, TA cells make the decision to commit to one of the various intestinal lineages of the gut, including absorptive enterocytes, goblet cells, enteroendocrine cells, and tuft cells. Once they exit the crypt, TA cells mature into one of these lineages and line the surface of the villus. Intestinal epithelial cells migrate along the villus axis, eventually reaching the tip of the villus where they undergo anoikis, a type of programmed cell death, and shed off into the lumen.

1.3 References

Alaedini, A., and Green, P.H. (2005). Narrative review: celiac disease: understanding a complex autoimmune disorder. *Ann Intern Med* 142, 289-298.

Ali, N., Zirak, B., Rodriguez, R.S., Pauli, M.L., Truong, H.A., Lai, K., Ahn, R., Corbin, K., Lowe, M.M., Scharschmidt, T.C., *et al.* (2017). Regulatory T Cells in Skin Facilitate Epithelial Stem Cell Differentiation. *Cell* 169, 1119-1129 e1111.

Allaire, J.M., Crowley, S.M., Law, H.T., Chang, S.Y., Ko, H.J., and Vallance, B.A. (2018). The Intestinal Epithelium: Central Coordinator of Mucosal Immunity. *Trends Immunol* 39, 677-696.

Alonso, S., and Yilmaz, O.H. (2018). Nutritional Regulation of Intestinal Stem Cells. *Annu Rev Nutr* 38, 273-301.

Arias, A.M. (2001). Epithelial mesenchymal interactions in cancer and development. *Cell* 105, 425-431.

Armaghany, T., Wilson, J.D., Chu, Q., and Mills, G. (2012). Genetic alterations in colorectal cancer. *Gastrointest Cancer Res* 5, 19-27.

Atiyeh, B.S., and Costagliola, M. (2007). Cultured epithelial autograft (CEA) in burn treatment: three decades later. *Burns* 33, 405-413.

Barker, N., van Es, J.H., Kuipers, J., Kujala, P., van den Born, M., Cozijnsen, M., Haegbarth, A., Korving, J., Begthel, H., Peters, P.J., *et al.* (2007). Identification of stem cells in small intestine and colon by marker gene *Lgr5*. *Nature* 449, 1003-1007.

Batts, L.E., Polk, D.B., Dubois, R.N., and Kulesa, H. (2006). Bmp signaling is required for intestinal growth and morphogenesis. *Dev Dyn* 235, 1563-1570.

Beumer, J., Artegiani, B., Post, Y., Reimann, F., Gribble, F., Nguyen, T.N., Zeng, H., Van den Born, M., Van Es, J.H., and Clevers, H. (2018). Enteroendocrine cells switch hormone expression along the crypt-to-villus BMP signalling gradient. *Nat Cell Biol* 20, 909-916.

Beumer, J., and Clevers, H. (2016). Regulation and plasticity of intestinal stem cells during homeostasis and regeneration. *Development* 143, 3639-3649.

Beumer, J., and Clevers, H. (2021). Cell fate specification and differentiation in the adult mammalian intestine. *Nat Rev Mol Cell Biol* 22, 39-53.

Beyaz, S., Mana, M.D., Roper, J., Kedrin, D., Saadatpour, A., Hong, S.J., Bauer-Rowe, K.E., Xifaras, M.E., Akkad, A., Arias, E., *et al.* (2016). High-fat diet enhances stemness and tumorigenicity of intestinal progenitors. *Nature* 531, 53-58.

Biton, M., Haber, A.L., Rogel, N., Burgin, G., Beyaz, S., Schnell, A., Ashenberg, O., Su, C.W., Smillie, C., Shekhar, K., *et al.* (2018). T Helper Cell Cytokines Modulate Intestinal Stem Cell Renewal and Differentiation. *Cell* *175*, 1307-1320 e1322.

Bjerknes, M., and Cheng, H. (2001). Modulation of specific intestinal epithelial progenitors by enteric neurons. *Proc Natl Acad Sci U S A* *98*, 12497-12502.

Blanpain, C., and Fuchs, E. (2014). Stem cell plasticity. Plasticity of epithelial stem cells in tissue regeneration. *Science* *344*, 1242281.

Byun, J.S., and Gardner, K. (2013). Wounds that will not heal: pervasive cellular reprogramming in cancer. *Am J Pathol* *182*, 1055-1064.

Cheng, H., and Leblond, C.P. (1974). Origin, differentiation and renewal of the four main epithelial cell types in the mouse small intestine. V. Unitarian Theory of the origin of the four epithelial cell types. *Am J Anat* *141*, 537-561.

Clevers, H.C., and Bevins, C.L. (2013). Paneth cells: maestros of the small intestinal crypts. *Annu Rev Physiol* *75*, 289-311.

Coskun, M. (2014). Intestinal epithelium in inflammatory bowel disease. *Front Med (Lausanne)* *1*, 24.

Dave, M., and Loftus, E.V., Jr. (2012). Mucosal healing in inflammatory bowel disease—a true paradigm of success? *Gastroenterol Hepatol (N Y)* *8*, 29-38.

Degirmenci, B., Valenta, T., Dimitrieva, S., Hausmann, G., and Basler, K. (2018). GLI1-expressing mesenchymal cells form the essential Wnt-secreting niche for colon stem cells. *Nature* *558*, 449-453.

Durand, A., Donahue, B., Peignon, G., Letourneur, F., Cagnard, N., Slomianny, C., Perret, C., Shroyer, N.F., and Romagnolo, B. (2012). Functional intestinal stem cells after Paneth cell ablation induced by the loss of transcription factor Math1 (Atoh1). *Proc Natl Acad Sci U S A* *109*, 8965-8970.

Farin, H.F., Van Es, J.H., and Clevers, H. (2012). Redundant sources of Wnt regulate intestinal stem cells and promote formation of Paneth cells. *Gastroenterology* *143*, 1518-1529 e1517.

Fernandez-Banares, F., Beltran, B., Salas, A., Comino, I., Ballester-Clau, R., Ferrer, C., Molina-Infante, J., Rosinach, M., Modolell, I., Rodriguez-Moranta, F., *et al.* (2021). Persistent Villous Atrophy in De Novo Adult Patients With Celiac Disease and Strict Control of Gluten-Free Diet Adherence: A Multicenter Prospective Study (CADER Study). *Am J Gastroenterol* *116*, 1036-1043.

Friedman, J.R., and Nunnari, J. (2014). Mitochondrial form and function. *Nature* *505*, 335-343.

- Fuchs, E. (2018). Skin Stem Cells in Silence, Action, and Cancer. *Stem Cell Reports* *10*, 1432-1438.
- Fuchs, E., and Blau, H.M. (2020). Tissue Stem Cells: Architects of Their Niches. *Cell Stem Cell* *27*, 532-556.
- Fukata, M., and Arditi, M. (2013). The role of pattern recognition receptors in intestinal inflammation. *Mucosal Immunol* *6*, 451-463.
- Gajendran, M., Loganathan, P., Catinella, A.P., and Hashash, J.G. (2018). A comprehensive review and update on Crohn's disease. *Dis Mon* *64*, 20-57.
- Gajendran, M., Loganathan, P., Jimenez, G., Catinella, A.P., Ng, N., Umapathy, C., Ziade, N., and Hashash, J.G. (2019). A comprehensive review and update on ulcerative colitis(). *Dis Mon* *65*, 100851.
- Goodman, B.E. (2010). Insights into digestion and absorption of major nutrients in humans. *Adv Physiol Educ* *34*, 44-53.
- Goossens, G.H. (2017). The Metabolic Phenotype in Obesity: Fat Mass, Body Fat Distribution, and Adipose Tissue Function. *Obes Facts* *10*, 207-215.
- Green, P.H., and Jabri, B. (2003). Coeliac disease. *Lancet* *362*, 383-391.
- Gregorieff, A., Liu, Y., Inanlou, M.R., Khomchuk, Y., and Wrana, J.L. (2015). Yap-dependent reprogramming of Lgr5(+) stem cells drives intestinal regeneration and cancer. *Nature* *526*, 715-718.
- Gregorieff, A., Pinto, D., Begthel, H., Destree, O., Kielman, M., and Clevers, H. (2005). Expression pattern of Wnt signaling components in the adult intestine. *Gastroenterology* *129*, 626-638.
- Greicius, G., Kabiri, Z., Sigmundsson, K., Liang, C., Bunte, R., Singh, M.K., and Virshup, D.M. (2018). PDGFRalpha(+) pericryptal stromal cells are the critical source of Wnts and RSPO3 for murine intestinal stem cells in vivo. *Proc Natl Acad Sci U S A* *115*, E3173-E3181.
- Gur-Cohen, S., Yang, H., Baksh, S.C., Miao, Y., Levorse, J., Kataru, R.P., Liu, X., de la Cruz-Racelis, J., Mehrara, B.J., and Fuchs, E. (2019). Stem cell-driven lymphatic remodeling coordinates tissue regeneration. *Science* *366*, 1218-1225.
- Hsu, Y.C., Li, L., and Fuchs, E. (2014). Transit-amplifying cells orchestrate stem cell activity and tissue regeneration. *Cell* *157*, 935-949.
- Hwangbo, D.S., Lee, H.Y., Abozaid, L.S., and Min, K.J. (2020). Mechanisms of Lifespan Regulation by Calorie Restriction and Intermittent Fasting in Model Organisms. *Nutrients* *12*.

- Jain, U., Ver Heul, A.M., Xiong, S., Gregory, M.H., Demers, E.G., Kern, J.T., Lai, C.W., Muegge, B.D., Barisas, D.A.G., Leal-Ekman, J.S., *et al.* (2021). Debaromyces is enriched in Crohn's disease intestinal tissue and impairs healing in mice. *Science* 371, 1154-1159.
- Jasperson, K.W., Patel, S.G., and Ahnen, D.J. (1993). APC-Associated Polyposis Conditions. In *GeneReviews*((R)), M.P. Adam, H.H. Ardinger, R.A. Pagon, S.E. Wallace, L.J.H. Bean, G. Mirzaa, and A. Amemiya, eds. (Seattle (WA)).
- Jessen, K.R., Mirsky, R., and Arthur-Farraj, P. (2015). The Role of Cell Plasticity in Tissue Repair: Adaptive Cellular Reprogramming. *Dev Cell* 34, 613-620.
- Junt, T., Scandella, E., and Ludewig, B. (2008). Form follows function: lymphoid tissue microarchitecture in antimicrobial immune defence. *Nat Rev Immunol* 8, 764-775.
- Kim, T.H., Li, F., Ferreira-Neira, I., Ho, L.L., Luyten, A., Nalapareddy, K., Long, H., Verzi, M., and Shivdasani, R.A. (2014). Broadly permissive intestinal chromatin underlies lateral inhibition and cell plasticity. *Nature* 506, 511-515.
- Knudsen, L., and Ochs, M. (2018). The micromechanics of lung alveoli: structure and function of surfactant and tissue components. *Histochem Cell Biol* 150, 661-676.
- Kurita, M., Araoka, T., Hishida, T., O'Keefe, D.D., Takahashi, Y., Sakamoto, A., Sakurai, M., Suzuki, K., Wu, J., Yamamoto, M., *et al.* (2018). In vivo reprogramming of wound-resident cells generates skin epithelial tissue. *Nature* 561, 243-247.
- Lacy, E.R. (1988). Epithelial restitution in the gastrointestinal tract. *J Clin Gastroenterol* 10 *Suppl 1*, S72-77.
- Lebwohl, B., Murray, J.A., Rubio-Tapia, A., Green, P.H., and Ludvigsson, J.F. (2014). Predictors of persistent villous atrophy in coeliac disease: a population-based study. *Aliment Pharmacol Ther* 39, 488-495.
- Li, L., and Xie, T. (2005). Stem cell niche: structure and function. *Annu Rev Cell Dev Biol* 21, 605-631.
- Lind, C.D. (1991). Motility disorders in the irritable bowel syndrome. *Gastroenterol Clin North Am* 20, 279-295.
- Liu, T.C., Kern, J.T., Jain, U., Sonnek, N.M., Xiong, S., Simpson, K.F., VanDussen, K.L., Winkler, E.S., Haritunians, T., Malique, A., *et al.* (2021). Western diet induces Paneth cell defects through microbiome alterations and farnesoid X receptor and type I interferon activation. *Cell Host Microbe*.
- Liu, T.C., Kern, J.T., VanDussen, K.L., Xiong, S., Kaiko, G.E., Wilen, C.B., Rajala, M.W., Caruso, R., Holtzman, M.J., Gao, F., *et al.* (2018). Interaction between smoking and ATG16L1T300A triggers Paneth cell defects in Crohn's disease. *J Clin Invest* 128, 5110-5122.

- Ljungmann, K., Hartmann, B., Kissmeyer-Nielsen, P., Flyvbjerg, A., Holst, J.J., and Laurberg, S. (2001). Time-dependent intestinal adaptation and GLP-2 alterations after small bowel resection in rats. *Am J Physiol Gastrointest Liver Physiol* *281*, G779-785.
- Madison, B.B., Braunstein, K., Kuizon, E., Portman, K., Qiao, X.T., and Gumucio, D.L. (2005). Epithelial hedgehog signals pattern the intestinal crypt-villus axis. *Development* *132*, 279-289.
- McCole, D.F. (2014). IBD candidate genes and intestinal barrier regulation. *Inflamm Bowel Dis* *20*, 1829-1849.
- Miyoshi, H. (2017). Wnt-expressing cells in the intestines: guides for tissue remodeling. *J Biochem* *161*, 19-25.
- Miyoshi, H., VanDussen, K.L., Malvin, N.P., Ryu, S.H., Wang, Y., Sonnek, N.M., Lai, C.W., and Stappenbeck, T.S. (2017). Prostaglandin E2 promotes intestinal repair through an adaptive cellular response of the epithelium. *EMBO J* *36*, 5-24.
- Moor, A.E., Harnik, Y., Ben-Moshe, S., Massasa, E.E., Rozenberg, M., Eilam, R., Bahar Halpern, K., and Itzkovitz, S. (2018). Spatial Reconstruction of Single Enterocytes Uncovers Broad Zonation along the Intestinal Villus Axis. *Cell* *175*, 1156-1167 e1115.
- Murata, K., Jadhav, U., Madha, S., van Es, J., Dean, J., Cavazza, A., Wucherpfennig, K., Michor, F., Clevers, H., and Shivdasani, R.A. (2020). Ascl2-Dependent Cell Dedifferentiation Drives Regeneration of Ablated Intestinal Stem Cells. *Cell Stem Cell* *26*, 377-390 e376.
- Nadsombati, M.S., McGinty, J.W., Lyons-Cohen, M.R., Jaffe, J.B., DiPeso, L., Schneider, C., Miller, C.N., Pollack, J.L., Nagana Gowda, G.A., Fontana, M.F., *et al.* (2018). Detection of Succinate by Intestinal Tuft Cells Triggers a Type 2 Innate Immune Circuit. *Immunity* *49*, 33-41 e37.
- Nakamura, T., and Sato, T. (2018). Advancing Intestinal Organoid Technology Toward Regenerative Medicine. *Cell Mol Gastroenterol Hepatol* *5*, 51-60.
- Noah, T.K., and Shroyer, N.F. (2013). Notch in the intestine: regulation of homeostasis and pathogenesis. *Annu Rev Physiol* *75*, 263-288.
- Okumura, R., and Takeda, K. (2017). Roles of intestinal epithelial cells in the maintenance of gut homeostasis. *Exp Mol Med* *49*, e338.
- Patankar, J.V., and Becker, C. (2020). Cell death in the gut epithelium and implications for chronic inflammation. *Nat Rev Gastroenterol Hepatol* *17*, 543-556.
- Pennings, S., Liu, K.J., and Qian, H. (2018). The Stem Cell Niche: Interactions between Stem Cells and Their Environment. *Stem Cells Int* *2018*, 4879379.
- Peterson, L.W., and Artis, D. (2014). Intestinal epithelial cells: regulators of barrier function and immune homeostasis. *Nat Rev Immunol* *14*, 141-153.

- Peyrin-Biroulet, L. (2010). Anti-TNF therapy in inflammatory bowel diseases: a huge review. *Minerva Gastroenterol Dietol* 56, 233-243.
- Rengarajan, S., Knoop, K.A., Rengarajan, A., Chai, J.N., Grajales-Reyes, J.G., Samineni, V.K., Russler-Germain, E.V., Ranganathan, P., Fasano, A., Sayuk, G.S., *et al.* (2020). A Potential Role for Stress-Induced Microbial Alterations in IgA-Associated Irritable Bowel Syndrome with Diarrhea. *Cell Rep Med* 1.
- Rodriguez-Colman, M.J., Schewe, M., Meerlo, M., Stigter, E., Gerrits, J., Pras-Raves, M., Sacchetti, A., Hornsveld, M., Oost, K.C., Snippert, H.J., *et al.* (2017). Interplay between metabolic identities in the intestinal crypt supports stem cell function. *Nature* 543, 424-427.
- Romagnolo, B., Berrebi, D., Saadi-Keddoucci, S., Porteu, A., Pichard, A.L., Peuchmaur, M., Vandewalle, A., Kahn, A., and Perret, C. (1999). Intestinal dysplasia and adenoma in transgenic mice after overexpression of an activated beta-catenin. *Cancer Res* 59, 3875-3879.
- Romera-Hernandez, M., Aparicio-Domingo, P., Papazian, N., Karrich, J.J., Cornelissen, F., Hoogenboezem, R.M., Samsom, J.N., and Cupedo, T. (2020). Yap1-Driven Intestinal Repair Is Controlled by Group 3 Innate Lymphoid Cells. *Cell Rep* 30, 37-45 e33.
- Rubin, D.C., and Levin, M.S. (2016). Mechanisms of intestinal adaptation. *Best Pract Res Clin Gastroenterol* 30, 237-248.
- Rubio-Tapia, A., and Murray, J.A. (2010). Classification and management of refractory coeliac disease. *Gut* 59, 547-557.
- Rubio-Tapia, A., Rahim, M.W., See, J.A., Lahr, B.D., Wu, T.T., and Murray, J.A. (2010). Mucosal recovery and mortality in adults with celiac disease after treatment with a gluten-free diet. *Am J Gastroenterol* 105, 1412-1420.
- Russell, B., Motlagh, D., and Ashley, W.W. (2000). Form follows function: how muscle shape is regulated by work. *J Appl Physiol* (1985) 88, 1127-1132.
- San Roman, A.K., Jayewickreme, C.D., Murtaugh, L.C., and Shivdasani, R.A. (2014). Wnt secretion from epithelial cells and subepithelial myofibroblasts is not required in the mouse intestinal stem cell niche in vivo. *Stem Cell Reports* 2, 127-134.
- Sancho, R., Cremona, C.A., and Behrens, A. (2015). Stem cell and progenitor fate in the mammalian intestine: Notch and lateral inhibition in homeostasis and disease. *EMBO Rep* 16, 571-581.
- Sato, T., van Es, J.H., Snippert, H.J., Stange, D.E., Vries, R.G., van den Born, M., Barker, N., Shroyer, N.F., van de Wetering, M., and Clevers, H. (2011). Paneth cells constitute the niche for Lgr5 stem cells in intestinal crypts. *Nature* 469, 415-418.

- Sato, T., Vries, R.G., Snippert, H.J., van de Wetering, M., Barker, N., Stange, D.E., van Es, J.H., Abo, A., Kujala, P., Peters, P.J., *et al.* (2009). Single Lgr5 stem cells build crypt-villus structures in vitro without a mesenchymal niche. *Nature* *459*, 262-265.
- Schneider, C., O'Leary, C.E., von Moltke, J., Liang, H.E., Ang, Q.Y., Turnbaugh, P.J., Radhakrishnan, S., Pellizzon, M., Ma, A., and Locksley, R.M. (2018). A Metabolite-Triggered Tuft Cell-ILC2 Circuit Drives Small Intestinal Remodeling. *Cell* *174*, 271-284 e214.
- Schnitzler, F., Fidder, H., Ferrante, M., Noman, M., Arijs, I., Van Assche, G., Hoffman, I., Van Steen, K., Vermeire, S., and Rutgeerts, P. (2009). Mucosal healing predicts long-term outcome of maintenance therapy with infliximab in Crohn's disease. *Inflamm Bowel Dis* *15*, 1295-1301.
- Seidner, D.L., Schwartz, L.K., Winkler, M.F., Jeejeebhoy, K., Boullata, J.I., and Tappenden, K.A. (2013). Increased intestinal absorption in the era of teduglutide and its impact on management strategies in patients with short bowel syndrome-associated intestinal failure. *JPEN J Parenter Enteral Nutr* *37*, 201-211.
- Seno, H., Miyoshi, H., Brown, S.L., Geske, M.J., Colonna, M., and Stappenbeck, T.S. (2009). Efficient colonic mucosal wound repair requires Trem2 signaling. *Proc Natl Acad Sci U S A* *106*, 256-261.
- Shoshkes-Carmel, M., Wang, Y.J., Wangenstein, K.J., Toth, B., Kondo, A., Massasa, E.E., Itzkovitz, S., and Kaestner, K.H. (2018). Subepithelial telocytes are an important source of Wnts that supports intestinal crypts. *Nature* *557*, 242-246.
- Shwartz, Y., Gonzalez-Celeiro, M., Chen, C.L., Pasolli, H.A., Sheu, S.H., Fan, S.M., Shamsi, F., Assaad, S., Lin, E.T., Zhang, B., *et al.* (2020). Cell Types Promoting Goosebumps Form a Niche to Regulate Hair Follicle Stem Cells. *Cell* *182*, 578-593 e519.
- Siegel, R.L., Miller, K.D., Goding Sauer, A., Fedewa, S.A., Butterly, L.F., Anderson, J.C., Cercek, A., Smith, R.A., and Jemal, A. (2020). Colorectal cancer statistics, 2020. *CA Cancer J Clin* *70*, 145-164.
- Simpson, C.L., Patel, D.M., and Green, K.J. (2011). Deconstructing the skin: cytoarchitectural determinants of epidermal morphogenesis. *Nat Rev Mol Cell Biol* *12*, 565-580.
- Soderholm, A.T., and Pedicord, V.A. (2019). Intestinal epithelial cells: at the interface of the microbiota and mucosal immunity. *Immunology* *158*, 267-280.
- Su, L.K., Kinzler, K.W., Vogelstein, B., Preisinger, A.C., Moser, A.R., Luongo, C., Gould, K.A., and Dove, W.F. (1992). Multiple intestinal neoplasia caused by a mutation in the murine homolog of the APC gene. *Science* *256*, 668-670.
- Sugimoto, S., Kobayashi, E., Fujii, M., Ohta, Y., Arai, K., Matano, M., Ishikawa, K., Miyamoto, K., Toshimitsu, K., Takahashi, S., *et al.* (2021). An organoid-based organ-repurposing approach to treat short bowel syndrome. *Nature* *592*, 99-104.

- Sullivan, Z.A., Khoury-Hanold, W., Lim, J., Smillie, C., Biton, M., Reis, B.S., Zwick, R.K., Pope, S.D., Israni-Winger, K., Parsa, R., *et al.* (2021). gammadelta T cells regulate the intestinal response to nutrient sensing. *Science* 371.
- Sun, Y., Li, L., Xie, R., Wang, B., Jiang, K., and Cao, H. (2019). Stress Triggers Flare of Inflammatory Bowel Disease in Children and Adults. *Front Pediatr* 7, 432.
- Taniguchi, K., Wu, L.W., Grivnenkov, S.I., de Jong, P.R., Lian, I., Yu, F.X., Wang, K., Ho, S.B., Boland, B.S., Chang, J.T., *et al.* (2015). A gp130-Src-YAP module links inflammation to epithelial regeneration. *Nature* 519, 57-62.
- Tappenden, K.A. (2014a). Intestinal adaptation following resection. *JPEN J Parenter Enteral Nutr* 38, 23S-31S.
- Tappenden, K.A. (2014b). Pathophysiology of short bowel syndrome: considerations of resected and residual anatomy. *JPEN J Parenter Enteral Nutr* 38, 14S-22S.
- Thabane, M., and Marshall, J.K. (2009). Post-infectious irritable bowel syndrome. *World J Gastroenterol* 15, 3591-3596.
- Thompson, C.A., DeLaForest, A., and Battle, M.A. (2018). Patterning the gastrointestinal epithelium to confer regional-specific functions. *Dev Biol* 435, 97-108.
- Tian, H., Biehs, B., Warming, S., Leong, K.G., Rangell, L., Klein, O.D., and de Sauvage, F.J. (2011). A reserve stem cell population in small intestine renders Lgr5-positive cells dispensable. *Nature* 478, 255-259.
- Tsai, C.H., Hill, M., Asa, S.L., Brubaker, P.L., and Drucker, D.J. (1997). Intestinal growth-promoting properties of glucagon-like peptide-2 in mice. *Am J Physiol* 273, E77-84.
- Tye-Din, J.A., Galipeau, H.J., and Agardh, D. (2018). Celiac Disease: A Review of Current Concepts in Pathogenesis, Prevention, and Novel Therapies. *Front Pediatr* 6, 350.
- Umar, S. (2010). Intestinal stem cells. *Curr Gastroenterol Rep* 12, 340-348.
- Vahedi, H., Ansari, R., Mir-Nasseri, M., and Jafari, E. (2010). Irritable bowel syndrome: a review article. *Middle East J Dig Dis* 2, 66-77.
- Valdes, A.M., Walter, J., Segal, E., and Spector, T.D. (2018). Role of the gut microbiota in nutrition and health. *BMJ* 361, k2179.
- Valenta, T., Degirmenci, B., Moor, A.E., Herr, P., Zimmerli, D., Moor, M.B., Hausmann, G., Cantu, C., Aguet, M., and Basler, K. (2016). Wnt Ligands Secreted by Subepithelial Mesenchymal Cells Are Essential for the Survival of Intestinal Stem Cells and Gut Homeostasis. *Cell Rep* 15, 911-918.

- van Es, J.H., Haegebarth, A., Kujala, P., Itzkovitz, S., Koo, B.K., Boj, S.F., Korving, J., van den Born, M., van Oudenaarden, A., Robine, S., *et al.* (2012). A critical role for the Wnt effector Tcf4 in adult intestinal homeostatic self-renewal. *Mol Cell Biol* 32, 1918-1927.
- van Es, J.H., van Gijn, M.E., Riccio, O., van den Born, M., Vooijs, M., Begthel, H., Cozijnsen, M., Robine, S., Winton, D.J., Radtke, F., *et al.* (2005). Notch/gamma-secretase inhibition turns proliferative cells in intestinal crypts and adenomas into goblet cells. *Nature* 435, 959-963.
- VanDussen, K.L., Carulli, A.J., Keeley, T.M., Patel, S.R., Puthoff, B.J., Magness, S.T., Tran, I.T., Maillard, I., Siebel, C., Kolterud, A., *et al.* (2012). Notch signaling modulates proliferation and differentiation of intestinal crypt base columnar stem cells. *Development* 139, 488-497.
- Vanuytsel, T., Senger, S., Fasano, A., and Shea-Donohue, T. (2013). Major signaling pathways in intestinal stem cells. *Biochim Biophys Acta* 1830, 2410-2426.
- Vig, K., Chaudhari, A., Tripathi, S., Dixit, S., Sahu, R., Pillai, S., Dennis, V.A., and Singh, S.R. (2017). Advances in Skin Regeneration Using Tissue Engineering. *Int J Mol Sci* 18.
- von Moltke, J., Ji, M., Liang, H.E., and Locksley, R.M. (2016). Tuft-cell-derived IL-25 regulates an intestinal ILC2-epithelial response circuit. *Nature* 529, 221-225.
- Walton, K.D., Freddo, A.M., Wang, S., and Gumucio, D.L. (2016). Generation of intestinal surface: an absorbing tale. *Development* 143, 2261-2272.
- Whitsett, J.A., Kalin, T.V., Xu, Y., and Kalinichenko, V.V. (2019). Building and Regenerating the Lung Cell by Cell. *Physiol Rev* 99, 513-554.
- Yan, K.S., Janda, C.Y., Chang, J., Zheng, G.X.Y., Larkin, K.A., Luca, V.C., Chia, L.A., Mah, A.T., Han, A., Terry, J.M., *et al.* (2017). Non-equivalence of Wnt and R-spondin ligands during Lgr5(+) intestinal stem-cell self-renewal. *Nature* 545, 238-242.
- Yilmaz, O.H., Katajisto, P., Lamming, D.W., Gultekin, Y., Bauer-Rowe, K.E., Sengupta, S., Birsoy, K., Dursun, A., Yilmaz, V.O., Selig, M., *et al.* (2012). mTORC1 in the Paneth cell niche couples intestinal stem-cell function to calorie intake. *Nature* 486, 490-495.
- Zepp, J.A., Zacharias, W.J., Frank, D.B., Cavanaugh, C.A., Zhou, S., Morley, M.P., and Morrisey, E.E. (2017). Distinct Mesenchymal Lineages and Niches Promote Epithelial Self-Renewal and Myofibrogenesis in the Lung. *Cell* 170, 1134-1148 e1110.
- Zhang, M., Sun, K., Wu, Y., Yang, Y., Tso, P., and Wu, Z. (2017). Interactions between Intestinal Microbiota and Host Immune Response in Inflammatory Bowel Disease. *Front Immunol* 8, 942.

Chapter 2

Modeling Intestinal Villus Injury-Repair Using Poly(I:C)

2.1 Introduction

The intestinal epithelium forms a crucial barrier to a broad spectrum of potentially harmful and immunogenic substances within the gut lumen. Small breaches to the barrier can be swiftly repaired due to the constant turnover the epithelium. However, in more severe injuries that disrupt the mucosal architecture, additional mechanisms of repair may be demanded.

Understanding these repair processes in animal models has provided valuable insights as to what could potentially go awry in disease with impaired healing or predisposition for tumor formation.

Various injury models have been developed for both the small intestine and colon. In the small intestine, damage induced by ischemia-reperfusion, intestinal resection, and irradiation have been extensively utilized over the years, as these have direct clinical relevance (Gonzalez et al., 2015; Kim et al., 2017; Sangild et al., 2014). Among these, irradiation-induced injury is perhaps the most widely used due to its simplicity and reproducibility. A diphtheria toxin-mediated LGR5⁺ ISC ablation model has also garnered attention to study stem cell regeneration (Metcalf et al., 2014). Infection by the enteric helminth *H. polygyrus* and other related pathogens have been used to induce type 2 immunity as well as to disrupt the crypt niche (Nusse et al., 2018; Urban et al., 1991; von Moltke et al., 2016). In the distal intestine, many models have centered on recapitulating aspects of inflammatory bowel disease, one of the most complex and prevalent human enteropathies today (Kiesler et al., 2015). Among these, dextran sodium sulfate (DSS)-induced colitis is by far the most widely adopted model for the same reasons as the irradiation injury system—it's simple, short, and reproducible (Chassaing et al., 2014). However, it is important to note that no single model faithfully captures the complexity of the human disease. Other models such as infection by *Citrobacter rodentium* and *Clostridium difficile* have

been utilized to study the immune response to enteric pathogens (Best et al., 2012; Crepin et al., 2016). Ultimately, which model to choose heavily depends on the research question.

One of the major issues in the field has been a paucity of animal models to study how intestinal villi recover after damage in the small intestine. While various crypt injury models exist, as described above, there is surprisingly very few systems to capture the injury-repair process of the villus compartment despite the importance of these structures for animal development and health. Furthermore, villus damage (also known as villus atrophy) is commonly observed in a wide variety of human enteropathies with multiple possible etiologies (Jansson-Knodell et al., 2018). In children, villus atrophy is associated with increased morbidity, mortality, growth failure, and cognitive dysfunction (Keusch et al., 2014). While ischemia-reperfusion injury can effectively trigger villus collapse, this model requires surgical intervention, and the intestine can easily become necrotic and irreparable (Guan et al., 2009). Non-steroidal anti-inflammatory drugs (NSAIDs) frequently damage the small intestinal lining, but they largely induce mucosal ulcers and crypt loss with variable effects (Beck et al., 2000). Villus atrophy is perhaps most notable for being a hallmark feature of celiac disease, which is a gluten-induced enteropathy (Caio et al., 2019). While removing gluten from the diet generally allows for tissue recovery in these patients, over one-third of individuals take longer to restore their villi, a condition known as persistent villus atrophy, for reasons that are unknown (Lebwohl et al., 2014; Rubio-Tapia and Murray, 2010). Animal models for celiac disease have greatly improved in recent years but require complex genetics that make mechanistic studies challenging (Abadie et al., 2020; Ju et al., 2015). Simpler models using a villus-specific pathogen such as rotavirus or a pro-inflammatory cytokine such as TNF trigger some level of damage but not

enough to cause villi to breakdown (Parker et al., 2019; Zou et al., 2018). Therefore, there is a great need for an acute villus atrophy model that is both simple and reproducible.

Exposed to a high concentration of commensal bacteria at steady state as well as facing constant threats from potentially pathogenic organisms, IECs must be able to recognize a diverse array of microbes through pattern recognition receptors (Fukata and Arditi, 2013). One family of pattern recognition receptors, the toll-like receptors (TLRs), signals through IECs and are critical for maintaining intestinal homeostasis (Burgueno and Abreu, 2020). Dysregulated TLR signaling can result in chronic intestinal inflammation and is associated with the development of cancer (Abreu, 2010). Moreover, a single injection of the TLR4 agonist lipopolysaccharide or the TLR3 agonist poly(I:C) induces rapid villus IEC apoptosis in the small intestine (Williams et al., 2013; Zhou et al., 2007). Among these TLR agonists, poly(I:C), which is a double-stranded RNA analog, triggers robust cell death, villus atrophy, and diarrhea in mice, mimicking key aspects of acute viral gastroenteritis (McAllister et al., 2013). Poly(I:C) acts directly on IECs and engages in TLR3-TRIF-caspase 8-dependent apoptosis (**Figure 2.1**; Gunther et al., 2015; McAllister et al., 2013). Given these findings, we hypothesized that poly(I:C)-induced damage can be used as a potential model to examine how intestinal villi repair and regenerate after severe injury.

2.2 Materials and Methods

Animals

C57BL/6J, *Tlr3*^{-/-}, *Lgr5-EGFP-IRES-CreERT2*, and *Rosa-LSL-tdTomato* mice were obtained from the Jackson Laboratory. Experiments that called for only wild-type mice used 8-week-old C57BL/6J male mice. All other experiments involving specific genetic strains used 7- to 10-week-old male and female mice. Mice were housed under specific-pathogen-free conditions and maintained on a 12 h light/dark cycle. All animal studies were conducted in compliance with protocols approved by the Washington University Institutional Animal Care and Use Committee.

Animal procedures

For intraperitoneal injections, the following reagents were prepared and administered at the indicated dose. 1 mg/mL poly(I:C) HMW (InvivoGen) was made according to the manufacturer's instructions and 20 mg/kg was injected. Dibenzazepine (DBZ, STEMCELL Technologies) was finely suspended in 0.5% hydroxypropyl-methylcellulose (Methocel E4M, Linda Samuelson lab) and 0.1% Tween 80 in water using a mortar/pestle to make 10 μmol/mL. Five days prior to poly(I:C) injection, two doses of 100 μmol/kg DBZ were given 6 h apart. Tamoxifen (Sigma) was dissolved in corn oil to make 20 mg/mL and 75 mg/kg was delivered.

Histology and immunostaining

The proximal small intestine was examined for histological studies. Intestinal tissues were pinned out and fixed in 10% neutral buffered formalin overnight at 4°C. Fixed samples were washed in 70% ethanol three times and embedded in 2% agar (Sigma). This was followed by paraffin embedding, sectioning, and hematoxylin/eosin/Alcian blue/PAS staining. Unstained

paraffin sections were de-paraffinized in xylene and rehydrated in isopropanol three times each. Antigen retrieval was performed in Trilogy solution (Sigma) for 20 min under boiling water. For immunohistochemistry (IHC), sections were additionally treated with 3% H₂O₂ in methanol to quench endogenous peroxidase activity. Slides were incubated in blocking solution (1% BSA/PBS containing 0.1% Triton X-100) for 1 h at room temperature before overnight treatment with primary antibodies diluted in blocking solution at 4°C. The following day, slides were treated with secondary antibodies diluted in blocking solution for 1 h at room temperature. For immunofluorescence (IF), sections were counterstained with Hoechst 33258 (Invitrogen) for 15 min and mounted in Fluoromount medium (Sigma). For IHC, sections were treated with VECTASTAIN Elite ABC-HRP Kit (Vector Laboratories), developed with DAB Peroxidase Substrate Kit (Vector Laboratories), counterstained with CAT hematoxylin (Biocare), and mounted in Cytoseal XYL (Thermo Scientific). Washes were performed in PBS. The following primary antibodies were used in this chapter: rabbit anti-cCasp3 (Cell Signaling 9664) and rabbit anti-RFP (Rockland 600-401-379). The following Thermo Fisher highly cross-absorbed IgG secondary antibodies were used: goat anti-rabbit Biotin and donkey anti-rabbit Alexa Fluor 594.

Primary epithelial culture

The establishment, maintenance, and differentiation of mouse IECs as spheroids were previously described (Miyoshi and Stappenbeck, 2013; Miyoshi et al., 2017). In brief, intestinal crypts were harvested by collagenase type I (Gibco) digestion, and stem cell spheroids were grown in 50% L-WRN conditioned medium in Matrigel (Corning 354234) and passaged every 3 days via trypsinization. To induce epithelial differentiation, dissociated stem cells were grown in differentiation medium containing 10 μM EP₄ receptor antagonist (R&D Systems) and

supplemented with 50 ng/mL EGF (PeproTech) for 24 h. Poly(I:C) HMW (InvivoGen) was added on the day of passage and cell viability was determined 18 h after treatment with CellTiter-Glo 3D Cell Viability Assay reagents (Promega) using the Cytation 5 instrument.

RNAscope in situ hybridization

Intestinal tissues were fixed in 4% PFA overnight at 4°C and then incubated in 20% sucrose/PBS overnight at 4°C. Fixed samples were cryo-embedded in O.C.T. compound (Fisher Scientific) and sectioned at 7 µm on a cryotome. *In situ* hybridization was carried out on frozen sections using a RNAscope 2.5 HD Assay-RED Kit (ACDBio) according to the manufacturer's instructions. The following ACDBio mouse probe was used in this chapter: *Olfm4* (311831).

Imaging and quantification

Images were acquired with an Olympus BX51 microscope (bright-field) or a Zeiss Axio Imager M2 Plus wide field fluorescent microscope. The lengths of well-oriented villi and crypts were measured using the cellSens software (Olympus). For histology-based quantifications, each data point represents an average value across 30-100 villi/crypts in the proximal small intestine per animal (see figure legend for exact number). Images were processed with Adobe Photoshop CC.

Statistics and reproducibility

Statistical analyses were performed in GraphPad Prism 8 or 9. *P*-values are indicated in the plots or figure legends with $p < 0.05$ denoted as significant. Data are expressed as mean \pm standard deviation (SD). An unpaired two-tailed Student's *t*-test was used when comparing two groups; a one-way ANOVA was used when comparing three or more groups; and a two-way ANOVA was

used when comparing groups with two experimental variables. Data from independent experiments were pooled when possible. Otherwise, data are representative of at least two independent experiments. Animals that had near 0% weight loss one day after poly(I:C) injection (<10% of all mice) were excluded from the study as these mice did not exhibit intestinal damage. Further statistical details and quantification methods can be found in the figure legends.

2.3 Results

Poly(I:C) injection rapidly triggers IEC death and villus atrophy in the proximal small intestine

In line with previous studies, a single intraperitoneal injection of poly(I:C) in mice rapidly triggered caspase-3 cleavage and apoptosis of villus epithelial cells (VECs) in the proximal small intestine with minimal damage to crypts (**Figure 2.2A,B**). At steady state, IECs undergo a type of programmed cell death known as anoikis as they reach the very tip of the villi (Patankar and Becker, 2020). Within 3 hours post-injection (HPI), there was elevated levels of dying IECs represented by cleaved caspase-3 staining, not just at tip of the villi but also along the sides. By 6 HPI, the villi began to collapse as dead IECs were shed into the lumen and epithelial apoptosis continued to reach to the lower villus. By 12 HPI, nearly all of the VECs appeared to be lost. Throughout this time, there was minimal cell death in the crypt (**Figure 2.2A,B**). Thus, poly(I:C) induces rapid and severe damage to the villus compartment of the small intestine.

Poly(I:C) acts directly on differentiated IECs without bias toward a specific lineage

The mechanism of cell death in this model is proposed to be independent of bone marrow-derived cells and rather a direct effect of poly(I:C) on IECs through TLR3-TRIF-caspase-8 activation (Gunther et al., 2015; McAllister et al., 2013). While the evidence for this is convincing, it has not been definitively proven using epithelial-specific TLR3 or TRIF knockout animals. Using our primary intestinal spheroid culture system, we tested the direct effect of poly(I:C) on IECs in two culture conditions: (1) L-WRN media that promotes stemness and (2) PTGER4-inhibited serum-free media that promotes differentiation (Miyoshi and Stappenbeck, 2013; Miyoshi et al., 2017). Similar to what we see *in vivo*, poly(I:C) preferentially killed differentiated spheroids over stem cell spheroids in a dose-dependent manner (**Figure 2.3A**).

This effect was completely dependent on TLR3 expression (**Figure 2.3A**). As enterocytes constitute the largest proportion of IECs (Moor et al., 2018), we next examined whether poly(I:C)-induced villus injury relied on the abundance of this cell population by administering the Notch γ -secretase inhibitor dibenzazepine (DBZ) prior to injury (**Figure 2.3B**). Mice treated with DBZ exhibited marked secretory cell hyperplasia, as previously reported (Kim et al., 2014; VanDussen et al., 2012), yet experienced a similar degree of villus atrophy following poly(I:C) injection (**Figure 2.3C**), revealing a nondiscriminatory effect of poly(I:C) on VECs.

Intestinal villi repair and regenerate robustly following poly(I:C)-induced injury

Remarkably, villus injury was short-lived in this model. Pronounced villus atrophy was observed by 24 HPI. After this time, crypt depth increased and villi rapidly regenerated in a reproducible fashion, reaching ~50% of their original length by 48 HPI and ~75% by 72 HPI (**Figure 2.4A,B**). The robust regenerative response was likely due to the intact stem cell compartment. To test this, we examined the stem cell response to poly(I:C)-induced injury. By *in situ* hybridization, we first detected no change in the expression of *Olfm4* in the crypt (**Figure 2.5A**), suggesting that ISCs are spared from damage. Moreover, lineage tracing LGR5⁺ ISCs using *Lgr5^{CreER}; R26R^{tdTomato}* mice by tamoxifen induction prior to poly(I:C) injection revealed a robust stem cell-mediated regenerative response (**Figure 2.5B**). Taken together, the consistent timing and location of damage induced by poly(I:C) provided a unique opportunity to study the repair and regeneration of intestinal villi without impacting the stem cell compartment.

2.4 Discussion

Villus atrophy caused by small bowel injury is observed in a variety of enteropathies (Jansson-Knodell et al., 2018). Removal of the causative agent is imperative for disease management, yet a significant number of patients present with chronic symptoms and persistent villus atrophy despite treatment efforts (Congdon et al., 1981; Pink and Creamer, 1967). Therapies designed around enhancing endogenous mechanisms of villus recovery may provide clinical benefit for such patients, yet our understanding of this process is limited. One major challenge has been a lack of simple and robust mouse models that injure intestinal villi. The weaknesses of current models are that they require surgical intervention, minimally induce villus blunting, show progressive and irreversible villus loss, or involve complex genetics that prohibit wider usage (Abadie et al., 2020; Gonzalez et al., 2015; Jung et al., 2019; Zou et al., 2018).

Here, we adopted a poly(I:C)-mediated injury model in mice, in which repair and regeneration of villi reproducibly occurs. The advantage of this model is its simplicity, requiring only a single injection of a commonly utilized laboratory reagent. Additionally, adult mice tolerate systemic poly(I:C) injection incredibly well, though mice that lack an adaptive immune system do not (Kim et al., 2007). This allows investigators to study the process of villus injury-repair in a wide array of genetic strains, enabling detailed mechanistic studies. Furthermore, the consistent location and timing of damage induced by poly(I:C) helps reduce variability.

As a synthetic analog of double-stranded RNA, poly(I:C) is often used to mimic a viral infection. As such, poly(I:C)-induced villus atrophy can be reproduced with intraperitoneal injection of purified genomic double-stranded RNA obtained from rotavirus (Zhou et al., 2007). Therefore, this injury system likely models aspects of acute viral gastroenteritis. Reports of viral-mediated villus damage in humans have been observed in HIV, norovirus, rotavirus, and

astrovirus infections (Batman et al., 2007; Bishop et al., 1973; Sebire et al., 2004; Woodward et al., 2017). It remains unclear whether a similar pronounced level of villus atrophy is also observed in humans with viral gastroenteritis due to the short course of illness and lack of histological documentation in these settings. In addition, the relevance of this model may extend beyond viral infections. RNA released from necrotic or injured cells in the absence of a viral pathogen can activate TLR3-dependent signaling and augment inflammatory responses in mucosal tissues (Cavassani et al., 2008; Kariko et al., 2004; Murray et al., 2008).

Why the proximal small intestine is vulnerable to poly(I:C)-induced damage remains an open question. One possible explanation is that the expression of TLR3 is highest in that region. However, *Tlr3* mRNA appears to be highly expressed in IECs throughout the entire length of the intestine (Gunther et al., 2015). Interestingly, *Tlr3* expression goes up with age and is distributed asymmetrically towards the basolateral side of IECs (Pott et al., 2012; Stanifer et al., 2020). Another possible explanation is that the proximal small intestine is uniquely susceptible to chemical exposure after systemic injection. Consistent with this, intraperitoneal injection of both TNF and lipopolysaccharide preferentially damages the proximal small intestine (Lau et al., 2011; Parker et al., 2019; Piguet et al., 1998; Williams et al., 2013). Retro-orbital sinus injection of poly(I:C) also induces villus atrophy specifically in the proximal region (McAllister et al., 2013). Interestingly, when TNF is delivered chronically (by delivery of a TNF-expressing plasmid) or in *Tnf^{ΔARE}* mice, in which *Tnf* mRNA is stabilized, gut pathology is localized to the ileum, similar to what occurs in Crohn's disease (Kontoyiannis et al., 1999; Parker et al., 2019).

Finally, why differentiated IECs are more susceptible to poly(I:C)-induced cell death compared to stem and progenitor cells is still unclear. Since the intestinal epithelium is a high-turnover system, and VECs are replaced every 3-5 days, rapid induction of cell death and

shedding may be a way to immediately clear out the virus without relying on the immune system. On top of this, stem cells may possess intrinsic anti-viral properties. Indeed, various stem cell populations have been shown to intrinsically express high levels of interferon-stimulated genes (ISGs), making them resistant to viral infection (Wu et al., 2018). Expression of these ISGs decreases upon differentiation, at which point the cells become interferon-responsive (Wu et al., 2018). This suggests that stem cells possess intrinsic mechanisms of viral resistance. In the context of the poly(I:C) injury model, the difference in susceptibility of crypt and villus IECs to poly(I:C) may be in part due to the differential regulation of NF- κ B signaling in these cells. Mice lacking *Ikk β* (IKK- β) but not *Ikk α* (IKK- α) had increased crypt apoptosis following poly(I:C) injection (McAllister et al., 2013). Thus, activation of canonical NF- κ B signaling in the crypt appears to protect stem and progenitor cells from undergoing poly(I:C)-induced cell death.

2.5 Figures

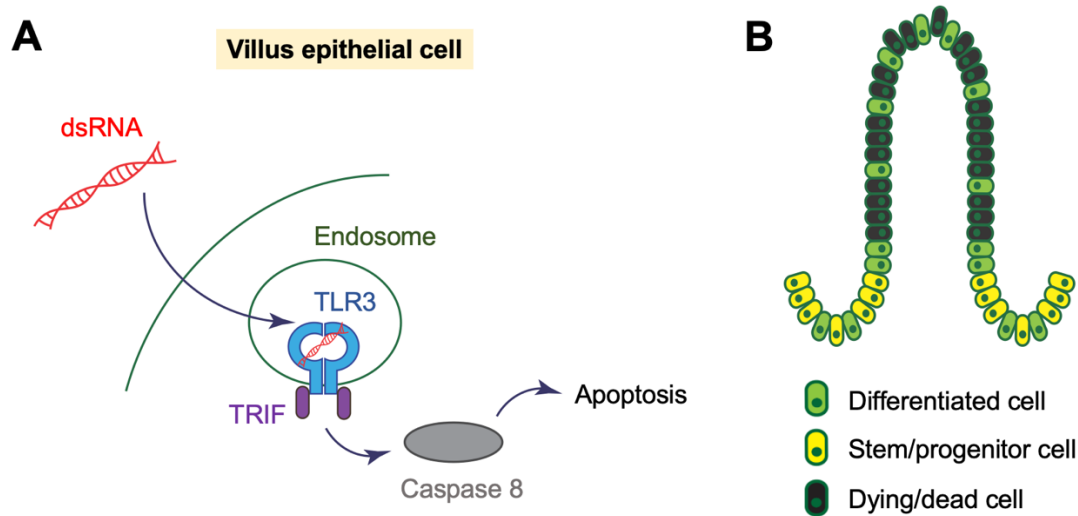


Figure 2.1. Schematic of epithelial cell death induced by double-stranded RNA

(A) In the intestine, double-stranded RNA such as poly(I:C) or a viral genome enters epithelial cells and is sensed by TLR3, a pattern recognition receptor. TLR3 and its adaptor protein TRIF activates caspase-8, leading to induction of the apoptotic pathway. (B) Cell death induced by dsRNA is prominent in villus epithelial cells, while crypt epithelial cells are largely spared.

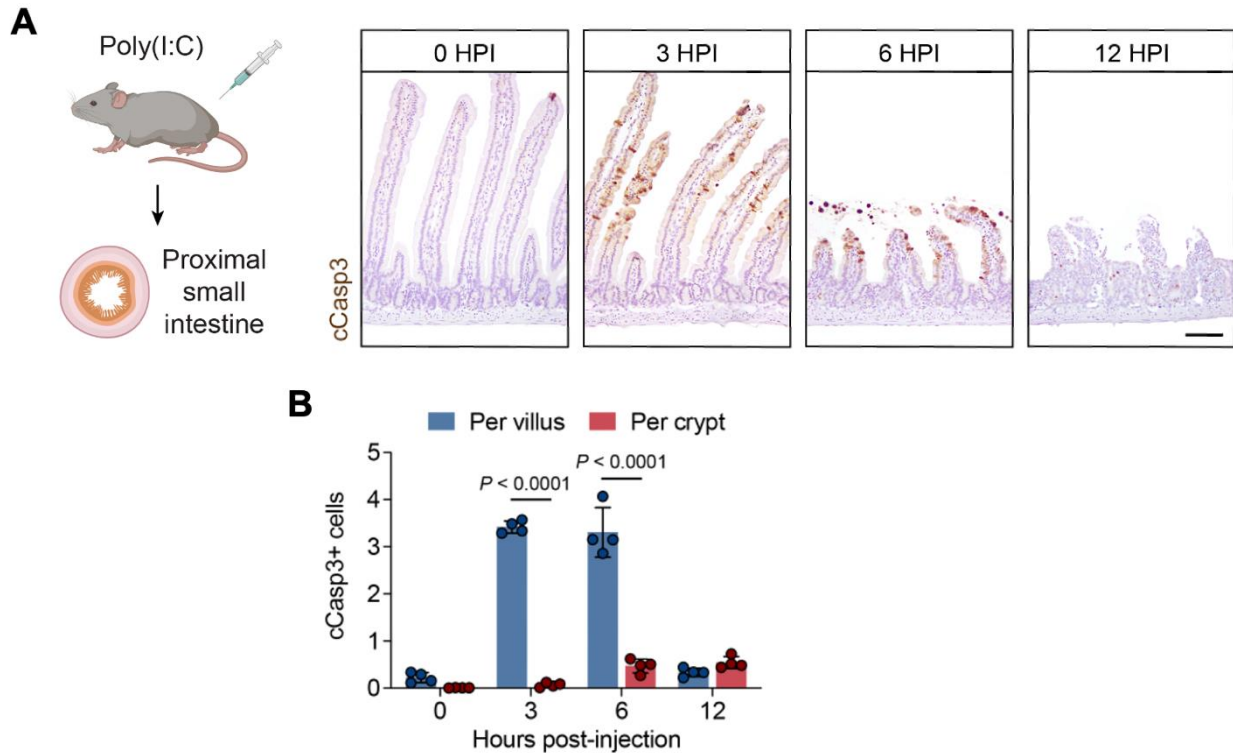


Figure 2.2. Poly(I:C) induces robust villus injury in the proximal small intestine

(A) Poly(I:C) was injected intraperitoneally and the proximal small intestine was analyzed.

Immunohistochemistry (IHC) for cleaved-caspase 3 (cCASP3) (brown) at the indicated hours

post-injection (HPI). Bar: 100 μ m. Images are representative of at least 3 animals. (B) Average

number of cCASP3⁺ cells across 50 villi/crypts was plotted as mean \pm SD. n = 4 mice/group.

Significance was determined by two-way ANOVA and Sidak's multiple comparisons test.

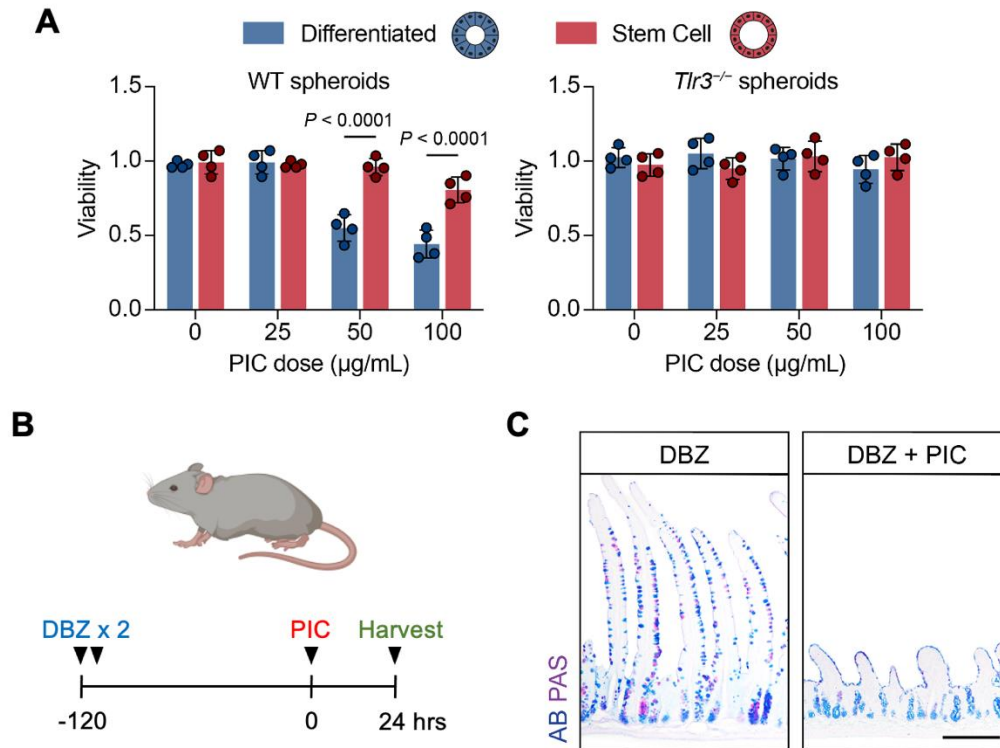


Figure 2.3. Poly(I:C) preferentially kills differentiated epithelial cells over stem/progenitor cells and does not discriminate between absorptive and secretory lineage cells

(A) Poly(I:C) treatment of wild-type or *Tlr3*^{-/-} intestinal epithelial spheroids at different doses. Stem cell spheroids were grown in L-WRN conditioned media and differentiated spheroids were grown in serum-free media. Poly(I:C) was added to the media on the day of passage and treated for 18 h. Cell viability was determined by CellTiter-Glo assay. n = 4 experiments. Values were normalized to media only control and plotted as mean ± SD. Significance was determined by two-way ANOVA and Sidak’s multiple comparisons test. (B) Schematic for dibenzazepine (DBZ) experiment. DBZ was injected twice 5 days prior to poly(I:C) injection. (C) Alcian blue and PAS staining of the intestine before and after poly(I:C)-induced injury. After DBZ injection, there is robust induction of secretory cells. Following poly(I:C) injection, there is still prominent villus atrophy in these mice. Bar: 200 µm. Images are representative of at least 3 animals.

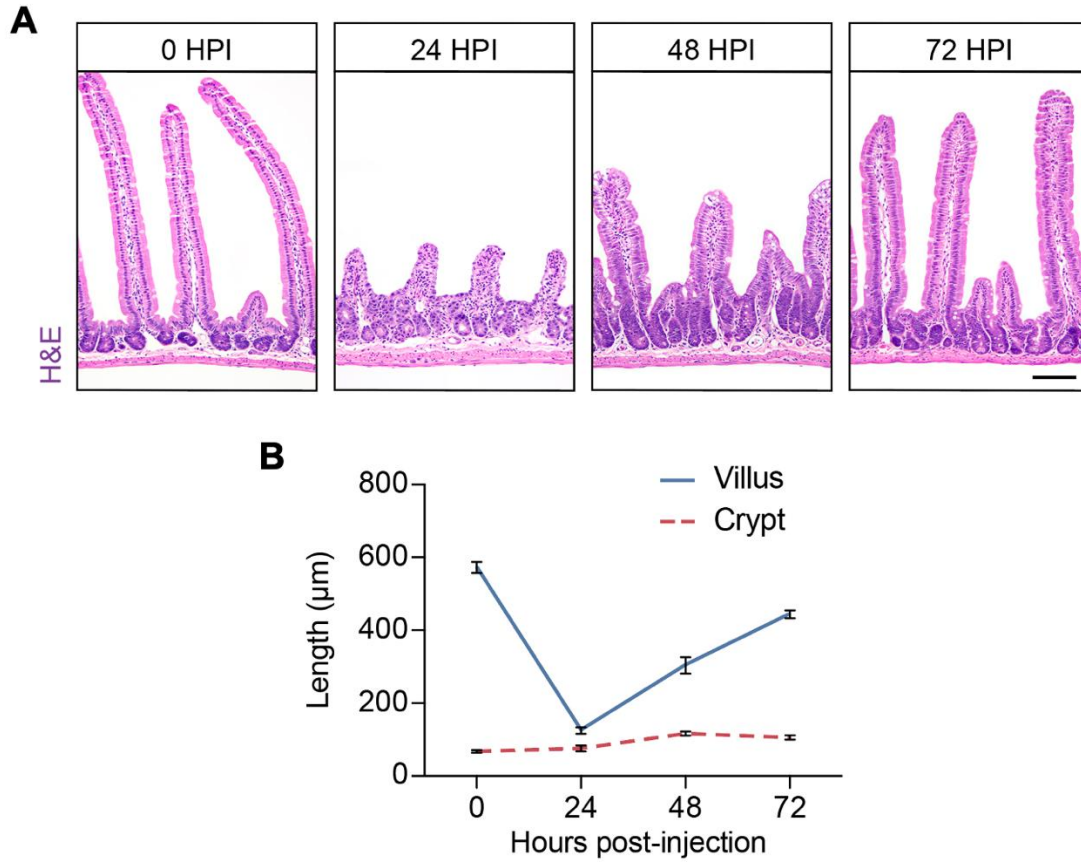


Figure 2.4. Robust villus repair and regeneration following poly(I:C)-induced injury

(A) H&E images of the proximal small intestine at the indicated time points. Bar: 100 µm.

Images are representative of at least 3 animals. (B) Average villus/crypt length across 50 villi/crypts at the indicated time points was plotted as mean ± SD. n = 4 mice/group.

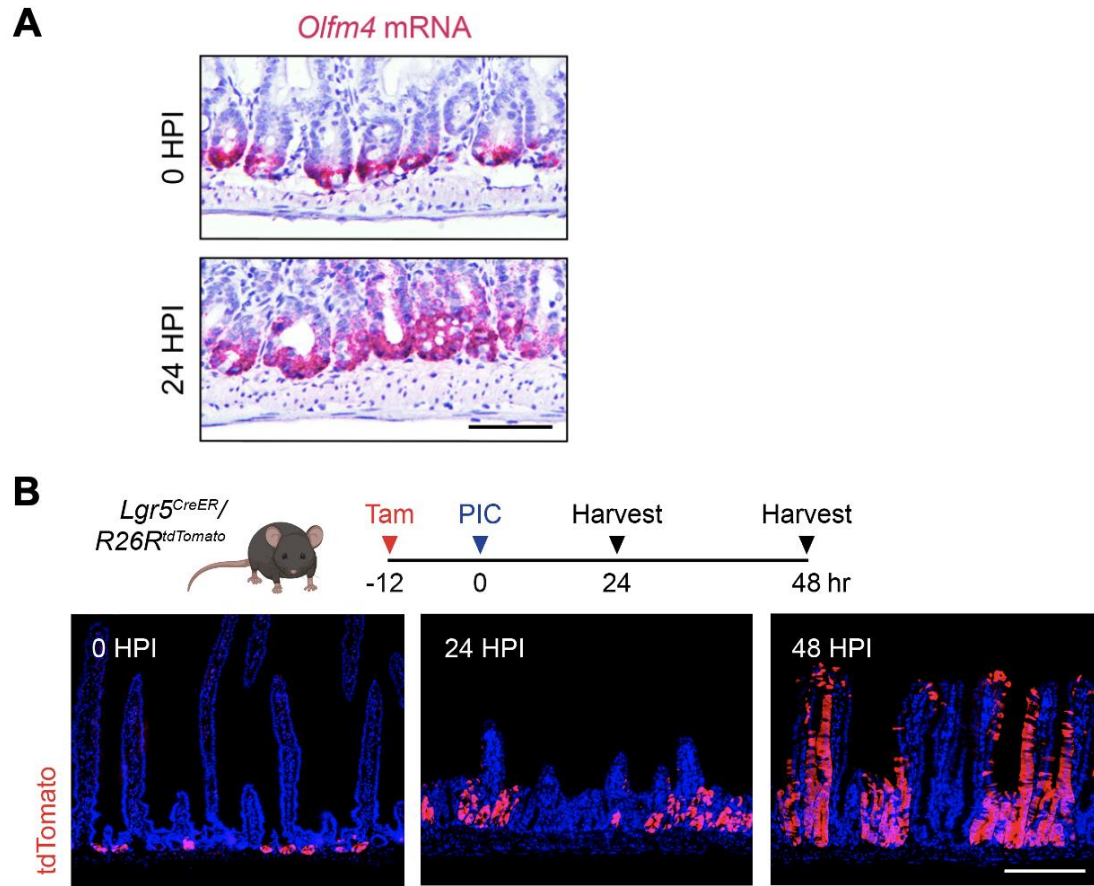


Figure 2.5. Intestinal stem cells are spared from poly(I:C)-induced injury

(A) RNAscope *in situ* hybridization for *Olfm4* in the homeostatic (0 HPI) and atrophic (24 HPI) intestine. Each red dot represents a single mRNA molecule. Bar: 100 μ m. (B) Lineage tracing of LGR5⁺ intestinal stem cells (ISCs). LGR5⁺ ISCs were labeled with tamoxifen 12 h prior to poly(I:C) injection (represented by tdTomato expression in red) in *Lgr5*^{CreER}/*R26R*^{tdTomato} mice and subsequently fate-mapped. Bar: 200 μ m. Images are representative of at least 3 animals.

2.6 References

- Abadie, V., Kim, S.M., Lejeune, T., Palanski, B.A., Ernest, J.D., Tastet, O., Voisine, J., Discepolo, V., Marietta, E.V., Hawash, M.B.F., *et al.* (2020). IL-15, gluten and HLA-DQ8 drive tissue destruction in coeliac disease. *Nature* *578*, 600-604.
- Abreu, M.T. (2010). Toll-like receptor signalling in the intestinal epithelium: how bacterial recognition shapes intestinal function. *Nat Rev Immunol* *10*, 131-144.
- Batman, P.A., Kotler, D.P., Kapembwa, M.S., Booth, D., Potten, C.S., Orenstein, J.M., Scally, A.J., and Griffin, G.E. (2007). HIV enteropathy: crypt stem and transit cell hyperproliferation induces villous atrophy in HIV/Microsporidia-infected jejunal mucosa. *AIDS* *21*, 433-439.
- Beck, P.L., Xavier, R., Lu, N., Nanda, N.N., Dinauer, M., Podolsky, D.K., and Seed, B. (2000). Mechanisms of NSAID-induced gastrointestinal injury defined using mutant mice. *Gastroenterology* *119*, 699-705.
- Best, E.L., Freeman, J., and Wilcox, M.H. (2012). Models for the study of *Clostridium difficile* infection. *Gut Microbes* *3*, 145-167.
- Bishop, R.F., Davidson, G.P., Holmes, I.H., and Ruck, B.J. (1973). Virus particles in epithelial cells of duodenal mucosa from children with acute non-bacterial gastroenteritis. *Lancet* *2*, 1281-1283.
- Burgueno, J.F., and Abreu, M.T. (2020). Epithelial Toll-like receptors and their role in gut homeostasis and disease. *Nat Rev Gastroenterol Hepatol* *17*, 263-278.
- Caio, G., Volta, U., Sapone, A., Leffler, D.A., De Giorgio, R., Catassi, C., and Fasano, A. (2019). Celiac disease: a comprehensive current review. *BMC Med* *17*, 142.
- Cavassani, K.A., Ishii, M., Wen, H., Schaller, M.A., Lincoln, P.M., Lukacs, N.W., Hogaboam, C.M., and Kunkel, S.L. (2008). TLR3 is an endogenous sensor of tissue necrosis during acute inflammatory events. *J Exp Med* *205*, 2609-2621.
- Chassaing, B., Aitken, J.D., Malleshappa, M., and Vijay-Kumar, M. (2014). Dextran sulfate sodium (DSS)-induced colitis in mice. *Curr Protoc Immunol* *104*, 15 25 11-15 25 14.
- Congdon, P., Mason, M.K., Smith, S., Crollick, A., Steel, A., and Littlewood, J. (1981). Small-bowel mucosa in asymptomatic children with celiac disease. Mucosal changes with gluten-free diets. *Am J Dis Child* *135*, 118-121.
- Crepin, V.F., Collins, J.W., Habibzay, M., and Frankel, G. (2016). *Citrobacter rodentium* mouse model of bacterial infection. *Nat Protoc* *11*, 1851-1876.
- Fukata, M., and Arditi, M. (2013). The role of pattern recognition receptors in intestinal inflammation. *Mucosal Immunol* *6*, 451-463.

- Gonzalez, L.M., Moeser, A.J., and Blikslager, A.T. (2015). Animal models of ischemia-reperfusion-induced intestinal injury: progress and promise for translational research. *Am J Physiol Gastrointest Liver Physiol* *308*, G63-75.
- Guan, Y., Worrell, R.T., Pritts, T.A., and Montrose, M.H. (2009). Intestinal ischemia-reperfusion injury: reversible and irreversible damage imaged in vivo. *Am J Physiol Gastrointest Liver Physiol* *297*, G187-196.
- Gunther, C., Buchen, B., He, G.W., Hornef, M., Torow, N., Neumann, H., Wittkopf, N., Martini, E., Basic, M., Bleich, A., *et al.* (2015). Caspase-8 controls the gut response to microbial challenges by Tnf-alpha-dependent and independent pathways. *Gut* *64*, 601-610.
- Jansson-Knodell, C.L., Hujoel, I.A., Rubio-Tapia, A., and Murray, J.A. (2018). Not All That Flattens Villi Is Celiac Disease: A Review of Enteropathies. *Mayo Clin Proc* *93*, 509-517.
- Ju, J.M., Marietta, E.V., and Murray, J.A. (2015). Generating Transgenic Mouse Models for Studying Celiac Disease. *Methods Mol Biol* *1326*, 23-33.
- Jung, H., Leal-Ekman, J.S., Lu, Q., and Stappenbeck, T.S. (2019). Atg14 protects the intestinal epithelium from TNF-triggered villus atrophy. *Autophagy* *15*, 1990-2001.
- Kariko, K., Ni, H., Capodici, J., Lamphier, M., and Weissman, D. (2004). mRNA is an endogenous ligand for Toll-like receptor 3. *J Biol Chem* *279*, 12542-12550.
- Keusch, G.T., Denno, D.M., Black, R.E., Duggan, C., Guerrant, R.L., Lavery, J.V., Nataro, J.P., Rosenberg, I.H., Ryan, E.T., Tarr, P.I., *et al.* (2014). Environmental enteric dysfunction: pathogenesis, diagnosis, and clinical consequences. *Clin Infect Dis* *59 Suppl 4*, S207-212.
- Kiesler, P., Fuss, I.J., and Strober, W. (2015). Experimental Models of Inflammatory Bowel Diseases. *Cell Mol Gastroenterol Hepatol* *1*, 154-170.
- Kim, C.K., Yang, V.W., and Bialkowska, A.B. (2017). The Role of Intestinal Stem Cells in Epithelial Regeneration Following Radiation-Induced Gut Injury. *Curr Stem Cell Rep* *3*, 320-332.
- Kim, K.D., Zhao, J., Auh, S., Yang, X., Du, P., Tang, H., and Fu, Y.X. (2007). Adaptive immune cells temper initial innate responses. *Nat Med* *13*, 1248-1252.
- Kim, T.H., Li, F., Ferreira-Neira, I., Ho, L.L., Luyten, A., Nalapareddy, K., Long, H., Verzi, M., and Shivdasani, R.A. (2014). Broadly permissive intestinal chromatin underlies lateral inhibition and cell plasticity. *Nature* *506*, 511-515.
- Kontoyiannis, D., Pasparakis, M., Pizarro, T.T., Cominelli, F., and Kollias, G. (1999). Impaired on/off regulation of TNF biosynthesis in mice lacking TNF AU-rich elements: implications for joint and gut-associated immunopathologies. *Immunity* *10*, 387-398.

Lau, K.S., Juchheim, A.M., Cavaliere, K.R., Philips, S.R., Lauffenburger, D.A., and Haigis, K.M. (2011). In vivo systems analysis identifies spatial and temporal aspects of the modulation of TNF-alpha-induced apoptosis and proliferation by MAPKs. *Sci Signal* 4, ra16.

Lebwohl, B., Murray, J.A., Rubio-Tapia, A., Green, P.H., and Ludvigsson, J.F. (2014). Predictors of persistent villous atrophy in coeliac disease: a population-based study. *Aliment Pharmacol Ther* 39, 488-495.

McAllister, C.S., Lakhdari, O., Pineton de Chambrun, G., Gareau, M.G., Broquet, A., Lee, G.H., Shenouda, S., Eckmann, L., and Kagnoff, M.F. (2013). TLR3, TRIF, and caspase 8 determine double-stranded RNA-induced epithelial cell death and survival in vivo. *J Immunol* 190, 418-427.

Metcalf, C., Kljavin, N.M., Ybarra, R., and de Sauvage, F.J. (2014). Lgr5+ stem cells are indispensable for radiation-induced intestinal regeneration. *Cell Stem Cell* 14, 149-159.

Miyoshi, H., and Stappenbeck, T.S. (2013). In vitro expansion and genetic modification of gastrointestinal stem cells in spheroid culture. *Nat Protoc* 8, 2471-2482.

Miyoshi, H., VanDussen, K.L., Malvin, N.P., Ryu, S.H., Wang, Y., Sonnek, N.M., Lai, C.W., and Stappenbeck, T.S. (2017). Prostaglandin E2 promotes intestinal repair through an adaptive cellular response of the epithelium. *EMBO J* 36, 5-24.

Moor, A.E., Harnik, Y., Ben-Moshe, S., Massasa, E.E., Rozenberg, M., Eilam, R., Bahar Halpern, K., and Itzkovitz, S. (2018). Spatial Reconstruction of Single Enterocytes Uncovers Broad Zonation along the Intestinal Villus Axis. *Cell* 175, 1156-1167 e1115.

Murray, L.A., Knight, D.A., McAlonan, L., Argentieri, R., Joshi, A., Shaheen, F., Cunningham, M., Alexopolou, L., Flavell, R.A., Sarisky, R.T., *et al.* (2008). Deleterious role of TLR3 during hyperoxia-induced acute lung injury. *Am J Respir Crit Care Med* 178, 1227-1237.

Nusse, Y.M., Savage, A.K., Marangoni, P., Rosendahl-Huber, A.K.M., Landman, T.A., de Sauvage, F.J., Locksley, R.M., and Klein, O.D. (2018). Parasitic helminths induce fetal-like reversion in the intestinal stem cell niche. *Nature* 559, 109-113.

Parker, A., Vaux, L., Patterson, A.M., Modasia, A., Muraro, D., Fletcher, A.G., Byrne, H.M., Maini, P.K., Watson, A.J.M., and Pin, C. (2019). Elevated apoptosis impairs epithelial cell turnover and shortens villi in TNF-driven intestinal inflammation. *Cell Death Dis* 10, 108.

Patankar, J.V., and Becker, C. (2020). Cell death in the gut epithelium and implications for chronic inflammation. *Nat Rev Gastroenterol Hepatol* 17, 543-556.

Piguet, P.F., Vesin, C., Guo, J., Donati, Y., and Barazzone, C. (1998). TNF-induced enterocyte apoptosis in mice is mediated by the TNF receptor 1 and does not require p53. *Eur J Immunol* 28, 3499-3505.

- Pink, I.J., and Creamer, B. (1967). Response to a gluten-free diet of patients with the coeliac syndrome. *Lancet* *1*, 300-304.
- Pott, J., Stockinger, S., Torow, N., Smoczek, A., Lindner, C., McInerney, G., Backhed, F., Baumann, U., Pabst, O., Bleich, A., *et al.* (2012). Age-dependent TLR3 expression of the intestinal epithelium contributes to rotavirus susceptibility. *PLoS Pathog* *8*, e1002670.
- Rubio-Tapia, A., and Murray, J.A. (2010). Classification and management of refractory coeliac disease. *Gut* *59*, 547-557.
- Sangild, P.T., Ney, D.M., Sigalet, D.L., Vegge, A., and Burrin, D. (2014). Animal models of gastrointestinal and liver diseases. Animal models of infant short bowel syndrome: translational relevance and challenges. *Am J Physiol Gastrointest Liver Physiol* *307*, G1147-1168.
- Sebire, N.J., Malone, M., Shah, N., Anderson, G., Gaspar, H.B., and Cubitt, W.D. (2004). Pathology of astrovirus associated diarrhoea in a paediatric bone marrow transplant recipient. *J Clin Pathol* *57*, 1001-1003.
- Stanifer, M.L., Mukenhirm, M., Muenchau, S., Pervolaraki, K., Kanaya, T., Albrecht, D., Odendall, C., Hielscher, T., Haucke, V., Kagan, J.C., *et al.* (2020). Asymmetric distribution of TLR3 leads to a polarized immune response in human intestinal epithelial cells. *Nat Microbiol* *5*, 181-191.
- Urban, J.F., Jr., Katona, I.M., Paul, W.E., and Finkelman, F.D. (1991). Interleukin 4 is important in protective immunity to a gastrointestinal nematode infection in mice. *Proc Natl Acad Sci U S A* *88*, 5513-5517.
- VanDussen, K.L., Carulli, A.J., Keeley, T.M., Patel, S.R., Puthoff, B.J., Magness, S.T., Tran, I.T., Maillard, I., Siebel, C., Kolterud, A., *et al.* (2012). Notch signaling modulates proliferation and differentiation of intestinal crypt base columnar stem cells. *Development* *139*, 488-497.
- von Moltke, J., Ji, M., Liang, H.E., and Locksley, R.M. (2016). Tuft-cell-derived IL-25 regulates an intestinal ILC2-epithelial response circuit. *Nature* *529*, 221-225.
- Williams, J.M., Duckworth, C.A., Watson, A.J., Frey, M.R., Miguel, J.C., Burkitt, M.D., Sutton, R., Hughes, K.R., Hall, L.J., Caamano, J.H., *et al.* (2013). A mouse model of pathological small intestinal epithelial cell apoptosis and shedding induced by systemic administration of lipopolysaccharide. *Dis Model Mech* *6*, 1388-1399.
- Woodward, J., Gkrania-Klotsas, E., and Kumararatne, D. (2017). Chronic norovirus infection and common variable immunodeficiency. *Clin Exp Immunol* *188*, 363-370.
- Wu, X., Dao Thi, V.L., Huang, Y., Billerbeck, E., Saha, D., Hoffmann, H.H., Wang, Y., Silva, L.A.V., Sarbanes, S., Sun, T., *et al.* (2018). Intrinsic Immunity Shapes Viral Resistance of Stem Cells. *Cell* *172*, 423-438 e425.

Zhou, R., Wei, H., Sun, R., and Tian, Z. (2007). Recognition of double-stranded RNA by TLR3 induces severe small intestinal injury in mice. *J Immunol* 178, 4548-4556.

Zou, W.Y., Blutt, S.E., Zeng, X.L., Chen, M.S., Lo, Y.H., Castillo-Azofeifa, D., Klein, O.D., Shroyer, N.F., Donowitz, M., and Estes, M.K. (2018). Epithelial WNT Ligands Are Essential Drivers of Intestinal Stem Cell Activation. *Cell Rep* 22, 1003-1015.

Chapter 3

Identification of an Atrophy-Induced Villus Epithelial Cell Type

3.1 Introduction

The mouse intestinal epithelium offers an excellent system to explore the dynamic regulation of cell turnover and differentiation during injury-induced repair. In the small intestine, distinct zones of proliferation and differentiation are organized into crypt-villus units. Highly active ISC and TA cells are located in the crypt (Barker et al., 2007). The differentiated epithelial lineages, with the exception of Paneth cells, line villi and are replaced every 3-5 days (Gehart and Clevers, 2019). Among the differentiated lineages, enterocytes and goblet cells make up the majority of VECs (Allaire et al., 2018). These cells are columnar in shape and are highly polarized, which enables most of its function to be directed toward the gut lumen. Enterocytes possess microvilli on their apical surface, which further increases the surface area available for nutrient uptake (Crawley et al., 2014). As part of the brush border, microvilli are surrounded by a glycocalyx matrix that is enriched in hydrolytic enzymes and carrier proteins involved in both the terminal steps of nutrient digestion and the initial steps of nutrient absorption (Egberts et al., 1984). Loss of microvilli, as seen in microvillus inclusion disease (MVID) and congenital microvillus atrophy (CMVA), causes life-threatening watery diarrhea and malabsorption in infants (Pecache et al., 2004; Vogel et al., 2016). Goblet cells contain mucin granules apically and are responsible for the production and maintenance of the mucus barrier (Specian and Oliver, 1991). Loss of goblet cells or dysregulation of mucin synthesis leads to exacerbation or spontaneous development of colitis (Nowarski et al., 2015; Van der Sluis et al., 2006). Therefore, the proper polarity and maturation of differentiated IECs is crucial for intestinal homeostasis. Together, IECs are tasked with the challenge of balancing its primary role in nutrient absorption while concurrently serving as a barrier to the harsh external environment.

Breakdown of the intestinal barrier is observed in a variety of pathologies, often triggered by damage to villus epithelial cells (VECs). Several enteric viruses, such as rotavirus, astrovirus, and certain coronavirus strains, have tropism for mature VECs (Ingle et al., 2021; Pensaert et al., 1970; Ramig, 2004). Rotavirus infection in children can result in total villus atrophy (Bishop et al., 1973). Transmissible gastroenteritis virus, a type of coronavirus, causes severe villus atrophy in suckling pigs, with close to 100% mortality rate (Xia et al., 2018). Hypoxic injury and endoplasmic reticulum (ER) stress can lead to the immediate death of villus enterocytes and goblet cells (Hinnebusch et al., 2002; Kaser et al., 2008). In fact, aberrant mucin assembly in goblet cells triggers ER stress, leading to diminished goblet cell numbers and spontaneous colitis (Heazlewood et al., 2008). Furthermore, excessive mucosal inflammation can result in widespread enterocyte destruction (Di Sabatino et al., 2003; Moss et al., 1996). Two classic examples of inflammatory enteropathies are celiac disease and Crohn's disease. In celiac disease, the key genetic underpinnings (human leukocyte antigen (HLA)-DQ2 and HLA-DQ8) and the environmental trigger (gluten) are well-known (Caio et al., 2019). Crohn's disease is much more complex and is generally thought to involve a combination of host genetics, environmental factors, and microbial dysbiosis for disease manifestation (Gajendran et al., 2018). Ischemia-reperfusion injury, which is encountered in surgical and trauma patients, can also profoundly damage the villus compartment (Mallick et al., 2004). This is likely due to the countercurrent shunting of oxygen in the villus—that is, oxygen levels decrease from the crypt to the tip of the villus, making the villus highly sensitive to oxygen changes (Shepherd and Kiel, 1992; Zheng et al., 2015). Finally, various medications have been reported to induce villus atrophy. These include the immunosuppressive drugs azathioprine, mycophenolate mofetil, methotrexate, and NSAIDs (Bosca et al., 2008; Ducloux et al., 1998; Kwo and Tremaine, 1995; Ziegler et al.,

2003). Whatever the etiology, severe loss of differentiated IECs provoked by these assaults can be detrimental, leading to collapse of the villus structure and an impaired absorptive capacity.

Toward understanding key features of small bowel enteropathies, such as Crohn's and celiac disease, multiple studies have identified disease-associated IECs with marked suppression of mature epithelial features. Patients with Crohn's disease have decreased microvilli length and reduced expression of microvilli genes, even in uninfamed regions of the gut (VanDussen et al., 2018). Similar changes in microvilli length were also observed in celiac disease biopsies (Shiner and Birbeck, 1961). Significant reduction of brush border enzymes, including several types of disaccharidases, dipeptidases, and alkaline phosphatase, was seen in both Crohn's and celiac disease patients (Arvanitakis, 1979; Mercer et al., 1990; Prasad et al., 2008). Transcriptomic analyses of Crohn's and celiac disease mucosal samples identified a prominent reduction of enterocyte-related metabolic programs (Dotsenko et al., 2021; Haberman et al., 2014; Loberman-Nachum et al., 2019). While loss of normal enterocytes as a result of injury may partially explain these findings, histological analyses reveal the presence of immature-type IECs lining the damaged or inflamed intestine (Arvanitakis, 1979; Loberman-Nachum et al., 2019). Whether these disease-associated cells are beneficial or pathological remains to be determined. Moreover, whether these epithelial alterations are a result of epithelial dedifferentiation, incomplete epithelial maturation, or an adaptive response to injury is not clear. There are currently no systems to induce or model these cells, making it difficult to study their features and functions.

Recent advances in spatial and single-cell transcriptomics have made it easier to define new cell types and states in normal tissues. In humans, a unique *BEST4/OTOP2*⁺ absorptive cell type has been identified (Parikh et al., 2019; Smillie et al., 2019). These cells are thought to maintain luminal pH through expression of ion channels (Ito et al., 2013; Tu et al., 2018).

Paneth-like cells in the colon have also been described in humans using single-cell technologies (Wang et al., 2020). Furthermore, epithelial lineages that were once thought to be a homogeneous population of cells turns out to have multiple subtypes. Tuft cells, which are the chemosensory cells of the gut, can be divided into an immune-related type and a neuronal type (Haber et al., 2017). Two subtypes of goblet cells, designated as canonical and non-canonical goblet cells, have also been recently identified (Nystrom et al., 2021). Non-canonical goblet cells express genes associated with enterocytes, while canonical goblet cells possess unique functions depending on their location within the crypt or luminal surface (Nystrom et al., 2021). In addition, enterocytes shift their gene expression program as they migrate and traverse across the villus axis (Moor et al., 2018). Together, these studies reveal that there are distinct functional zones within different compartments of the intestine (e.g. villus bottom vs. villus top, crypt vs. surface), and that these local functions are carried out by specialized subtypes of IECs.

Application of single-cell technologies to disease states have also yielded incredible insights to disease pathogenesis. Single-cell profiling of ulcerative colitis and Crohn's disease samples have enabled careful dissection of cell-type-specific responses to inflammation (Elmentaite et al., 2020; Parikh et al., 2019; Smillie et al., 2019). In mice, a unique "revival" stem cell population has been identified following irradiation-induced injury (Ayyaz et al., 2019). These cells expand in response to damage in a YAP-dependent manner and regenerates the epithelium (Ayyaz et al., 2019). We therefore set out to utilize these powerful techniques to define the dynamics of epithelial differentiation in the poly(I:C) intestinal villus injury model.

3.2 Materials and Methods

Animals

C57BL/6J, *Krt20-T2A-CreERT2*, *Lgr5-EGFP-IRES-CreERT2*, *Bmi1-CreER*, and *Rosa-LSL-tdTomato* mice were obtained from the Jackson Laboratory. Experiments that called for only wild-type mice used 8-week-old C57BL/6J male mice. Pregnant C57BL/6J female mice were used to obtain embryos. All other experiments involving specific genetic strains used 7- to 10-week-old male and female mice. Mice were housed under specific-pathogen-free conditions and maintained on a 12 h light/dark cycle. All animal studies were conducted in compliance with protocols approved by the Washington University Institutional Animal Care and Use Committee.

Animal procedures

For intraperitoneal injections, the following reagents were prepared and administered at the indicated dose. 1 mg/mL poly(I:C) HMW (InvivoGen) was prepared in saline and 20 mg/kg was injected. 20 mg/mL tamoxifen (Sigma) was prepared in corn oil and 75 mg/kg was delivered.

Histology and immunostaining

The proximal small intestine was examined for histological studies. To prepare sections for paraffin embedding, intestinal tissues were pinned out and fixed in 10% neutral buffered formalin overnight at 4°C. Fixed samples were washed in 70% ethanol three times and embedded in 2% agar (Sigma). This was followed by paraffin embedding and sectioning. Unstained paraffin sections were de-paraffinized in xylene and rehydrated in isopropanol three times each. Antigen retrieval was performed in Trilogy solution (Sigma) for 20 min under boiling water. Slides were incubated in blocking solution (1% BSA/PBS containing 0.1% Triton X-100) for 1 h

at room temperature before overnight treatment with primary antibodies diluted in blocking solution at 4°C. The following day, slides were treated with secondary antibodies diluted in blocking solution for 1 h at room temperature. For immunofluorescence (IF), sections were counterstained with Hoechst 33258 (Invitrogen) for 15 min and mounted in Fluoromount medium (Sigma). Washes were performed in PBS. The following primary antibodies were used in this chapter: goat anti-Ace2 (R&D Systems AF933), rabbit anti-EpCAM (Abcam ab71916), rabbit anti-Fabp1 (Novus Biologicals NBP1-87695), goat anti-Pdgfra (R&D Systems AF1062), goat anti-IL-33 (R&D Systems AF3626), rabbit anti-Cldn4 (Thermo Fisher 36-4800), rabbit anti-Muc2 (Santa Cruz sc-15334), guinea pig anti-Krt20 (Progen GP-K20), rabbit anti-Aldolase B (Abcam ab75751), goat anti-Mmp7 (R&D Systems AF2967), rabbit anti-Chromogranin A (Abcam ab15160), rabbit anti-Dcamk11 (Abcam ab37994), rabbit anti-RFP (Rockland 600-401-379), rat anti-BrdU (recognizes CldU, Abcam ab6326), and mouse anti-BrdU (recognizes IdU, BD Biosciences 347580). The following Thermo Fisher highly cross-absorbed IgG secondary antibodies were used in this chapter: donkey anti-mouse Alexa Fluor 594, donkey anti-rabbit Alexa Fluor 488/594, donkey anti-rat Alexa Fluor 488, donkey anti-goat Alexa Fluor 488/594, and donkey anti-guinea pig Alexa Fluor 488. For transmission electron microscopy (TEM), intestinal tissues were fixed in 2% PFA/2.5% glutaraldehyde in 100mM cacodylate buffer and subsequently processed and imaged as previously described (Miyoshi et al., 2017).

RNAscope in situ hybridization

Intestinal tissues were fixed in 4% PFA overnight at 4°C and then incubated in 20% sucrose/PBS overnight at 4°C. Fixed samples were cryo-embedded in O.C.T. compound and sectioned at 7 µm on a cryotome. *In situ* hybridization was carried out on frozen sections using a RNAscope 2.5

HD Assay-RED Kit (ACDBio) according to the manufacturer's instructions. The following ACDBio mouse probes were used in this chapter: *Ace2* (417081), *Msln* (443241), *Clu* (427891), and *Alpi* (436781). For co-staining with fluorescent antibodies, sections were treated with the appropriate antibodies using the IF protocol above following *in situ* hybridization staining.

Imaging and quantification

Bright-field images were acquired with an Olympus BX51 microscope. Fluorescent images were acquired with a Zeiss Axiovert 200M inverted microscope and a Zeiss Axio Imager M2 Plus wide field fluorescent microscope. Live spheroid images were acquired with a Zeiss Cell Observer inverted microscope with color camera. Epithelial cell height was measured with the cellSens software (Olympus). For histology-based quantifications, each data point represents an average value across 30-50 well-oriented villi/crypts in the proximal small intestine per animal (exact number is in the figure legends). Images were processed with Adobe Photoshop CC.

Laser-capture microdissection (LCM)-microarray

Intestinal tissues were fixed in methacarn (60% methanol, 30% chloroform, 10% glacial acetic acid) for 4 h at room temperature and processed for paraffin embedding. Paraffin blocks were sectioned at 7 μ m on a microtome. Sections were de-paraffinized in xylene, rehydrated in a series of ethanol washes (70/95/100%), and briefly stained with methyl green (Vector Laboratories). Laser capture microdissection (LCM) was performed using CapSure Micro LCM Caps (Applied Biosystems) on the Arcuturus PixCell Iie system with an Olympus IX51 microscope base. RNA extraction and cDNA synthesis/amplification were carried out using the Arcturus PicoPure RNA Isolation Kit (Applied Biosystems) and Complete Whole Transcriptome Amplification Kit

(WTA2, Sigma) according to the manufacturer's instructions. Amplified cDNA products were purified with the QIAquick PCR Purification Kit (Qiagen), and quality was assessed with the Agilent 2100 Bioanalyzer. Agilent mouse 8x60K v2 microarray chips (Agilent-074809) were used for hybridization. Data normalization, principal component analysis (PCA), and differential gene expression analysis were performed on the Partek software and visualized with Graphpad Prism 8/9. Gene ontology (GO) analysis was carried out with ToppGene Suite and Enrichr (Chen et al., 2013; Kuleshov et al., 2016). Gene set enrichment analysis (GSEA) of the Crohn's disease (Haberman et al., 2014), celiac disease (Dotsenko et al., 2021; Loberman-Nachum et al., 2019), and fetal spheroid (Mustata et al., 2013) signatures (the entire gene list or the top 300 genes in respective studies) were processed using the GSEA v3/4 software (Subramanian et al., 2005). Normalized enrichment scores (NES) and false discovery rates (FDR q -value) are displayed.

Fluorescence-activated cell sorting (FACS)

A standardized protocol for the isolation, dissociation, and sorting of IECs was previously described (Magness et al., 2013). The first 5 cm of the proximal small intestine was used for cell isolation. For downstream qRT-PCR analysis, poly(I:C)-damaged tissues from at least 2 mice were pooled together. Briefly, intestinal tissues were incubated in 30mM EDTA, first on ice for 20 min with 1.5mM DTT and second at 37°C for 10 min without DTT, and then shaken to lift the epithelium. After removal of the muscle layer, single cell dissociation was performed using an enzymatic cocktail containing 1mg/mL Collagenase/Dispase (Roche) and 0.2mg/mL DNase I (Roche) at 37°C for 10 min with intermittent shaking. The cell suspension was additionally subjected to vigorous pipetting and filtered through 70 μ m and 40 μ m strainers. Cells were washed in 10% FBS/PBS and resuspended in FACS buffer containing 2% BSA, 2mM EDTA,

and 25mM HEPES in PBS. 10 μ M Y-27632 (R&D Systems) was added to every solution throughout the experiment. SYTOX-Red (Invitrogen) was used to assess cell viability. Flow cytometry and cell sorting were carried out on the Beckman Coulter MoFlo instrument.

Quantitative real-time PCR (qRT-PCR)

50,000 KRT20-tdT⁺ and KRT20-tdT⁻ cells from *Krt20^{CreER}/R26^{RtdTomato}* mice were sorted directly into Buffer RLT Plus containing β -mercaptoethanol. Total RNA was isolated using the RNeasy Plus Micro Kit (Qiagen). cDNA was synthesized using iScript Reverse Transcription Supermix reagents (Bio-Rad). qPCR was performed using iTaq Universal SYBR Green Supermix reagents (Bio-Rad) on a StepOne Real-Time PCR System (Applied Biosystems). Expression levels were normalized to *B2m*. Primers used in this chapter are listed in **Table 3.1**.

Single-cell spheroid growth assay

Generation of 50% L-WRN conditioned media for intestinal spheroid culture was previously described (Miyoshi and Stappenbeck, 2013). 10,000 KRT20-tdT⁺ and KRT20-tdT⁻ cells from *Krt20^{CreER}/R26^{RtdTomato}* mice were sorted into 50% L-WRN media, spun down, and resuspended in 40 μ L Matrigel (Corning 354234). Cells were cultured in 50% L-WRN media containing 10 μ M ROCK inhibitor for 6 days (media was changed once on day 3). Spheroid efficiency was calculated as the number of spheroids on day 6 over the number of seeded cells (10,000).

Single-cell RNA-sequencing (scRNA-seq) and analysis

FACS purified IECs were resuspended in 10% FBS in DMEM/F12 for single-cell capture and sequencing. Single-cell libraries were constructed using Chromium Single Cell 3' v3 reagents

(10x Genomics) and sequenced on a NovaSeq6000 S4 system (Illumina) with ~50,000 reads per cell. Demultiplexing, alignment, and unique molecular identifier counting were performed with Cell Ranger v4.0. For downstream analysis, filtered gene-barcode matrices generated by Cell Ranger were read into the Seurat package (v3.2.2) on RStudio (v1.3.1056) (Butler et al., 2018). Single-cell transcriptomes from pediatric Crohn's disease patients and healthy controls were obtained from the Gut Cell Survey (Elmentaite et al., 2020) and analyzed in Seurat. Plots generated were adjusted with ggplot2 and Adobe Illustrator CC. In Seurat, low-quality cells with high (>9,000) and low (<500) unique gene counts and high mitochondrial counts (>20%) were first filtered out. The resulting data was log-normalized, and paired samples were integrated. PCA scores were computed on scaled data based on 2,000 of the most highly variable features. The first 15 PCs were used for graph-based clustering (resolution = 0.2-0.3), which was visualized with UMAP-based dimensional reduction (Becht et al., 2018). FindMarkers was used to identify cell types. Immune cells (<1% of total cells) were removed from analysis. Gene expression levels were plotted with FeaturePlot, VlnPlot, and Dotplot functions. Enrichment of the fetal spheroid and aVEC signatures were determined with the AddModuleScore function.

Statistics and reproducibility

Statistical analyses were performed in GraphPad Prism 8 or 9. *P*-values are indicated in the plots or figure legends with $p < 0.05$ denoted as significant. Data are expressed as mean \pm standard deviation (SD). An unpaired two-tailed Student's *t*-test was used when comparing two groups; a one-way ANOVA was used when comparing three or more groups; and a two-way ANOVA was used when comparing groups with two experimental variables. Data from independent experiments were pooled when possible. Otherwise, data are representative of at least two

independent experiments. Animals that had near 0% weight loss one day after poly(I:C) injection (<10% of all mice) were excluded from the study as these mice did not exhibit intestinal damage. Further statistical details and quantification methods can be found in the figure legends.

Data and Code Availability

All sequencing data have been deposited in Gene Expression Omnibus (GEO) under the accession codes GSE168439 (for LCM-microarray) and GSE169718 (for scRNA-seq).

3.3 Results

Villus atrophy is accompanied by a transient loss of mature enterocyte features

To assess the dynamics of epithelial differentiation in the poly(I:C) model throughout the injury-repair process, we first examined the expression pattern of ACE2, a brush border protein and a marker of mature enterocytes, the dominant cell type on villi (Camargo et al., 2009; Zang et al., 2020). During the injury phase (6 HPI), ACE2⁺ enterocytes were shed into the lumen and lost. We defined the atrophy phase (24 HPI) as the nadir of villus height, during which rudimentary villi were covered with epithelial cells that lacked ACE2 protein and mRNA expression (**Figure 3.1A-C**). These cells were prominent on atrophic villi in the proximal small intestine, where injury was most severe (**Figure 3.1D**). Expression of a second enterocyte marker FABP1, involved in lipid metabolism (Gajda and Storch, 2015), was similarly downregulated during the atrophy phase (**Figure 3.1E**). Atrophy-associated epithelial cells were significantly shorter than normal enterocytes (**Figure 3.1F**), indicating an altered differentiation state. These epithelial changes were transient as ACE2⁺ and FABP1⁺ columnar-shaped enterocytes quickly reappeared on villi during the regenerative phase (>48 HPI; **Figure 3.1A-C and 3.1E**).

A reduction of mature enterocyte features occurs in a variety of infectious and inflammatory small bowel enteropathies (Holmes and Lobley, 1989). To determine the scope of the overall transcriptional program present during poly(I:C)-induced villus atrophy, we performed microarray analysis of laser-capture microdissected (LCM) epithelial cells from homeostatic and atrophic villi (**Figure 3.2A,B**). Atrophy-induced VECs (hereafter aVECs) possessed a distinct bulk transcriptional state compared to homeostatic VECs (**Figure 3.2C**). Among the top differentially expressed genes, brush border-related genes were especially downregulated, while repair-associated genes were highly upregulated in aVECs (**Figure 3.2D**).

As such, pathways related to wound healing, such as extracellular matrix (ECM) re-organization and cell migration, were induced in aVECs, whereas pathways linked to intestinal absorption and enterocyte metabolism were suppressed (**Figure 3.2E**). Consistent with these changes, transmission electron microscopy showed that while homeostatic VECs were tall with well-formed microvilli, aVECs were small, had poorly developed microvilli, and contained extensive lipid droplets (**Figure 3.2F**), suggesting a reduced absorptive capacity (Iqbal and Hussain, 2009).

Villus injury triggers a disease-associated epithelial cell type

To test the hypothesis that an aVEC-like state is present in human diseases with injured villi, we compared the transcriptional signature of aVECs in mice to bulk RNA-sequencing datasets of Crohn's and celiac disease biopsies. We found that two established epithelial biomarkers of Crohn's disease, *Duox2* and *Lcn2* (Csillag et al., 2007), were among the most highly upregulated genes in aVECs (**Figure 3.2D**). Gene set enrichment analysis (GSEA) showed significant correlation of a Crohn's disease signature and the aVEC dataset (**Figure 3.3A**; Haberman et al., 2014). We also found significant correlation of two celiac disease signatures with the aVEC dataset, and this correlation was dependent on active disease status with gluten-induced villus atrophy (**Figure 3.3B-D**; Dotsenko et al., 2021; Loberman-Nachum et al., 2019). Therefore, the aVEC signature induced upon poly(I:C)-mediated villus injury can be identified in the transcriptomes of mucosal specimens from multiple human enteropathies.

aVECs possess a fetal-like transcriptional program

During epithelial regeneration, ISCs have been shown to express a fetal-like signature (Gregorieff et al., 2015; Nusse et al., 2018; Wang et al., 2019; Yui et al., 2018). Surprisingly, we

found components of a fetal program in the transcriptome of aVECs (**Figure 3.4A**). GSEA demonstrated significant correlation of this program with the overall bulk transcriptome of aVECs (**Figure 3.4B**; Mustata et al., 2013). We validated that two of the fetal markers, *Msln* and *Clu*, were indeed expressed in the fetal intestinal epithelium and reflective of the fetal signature (**Figure 3.4C,D**). *In situ* hybridization confirmed that *Msln* and *Clu* mRNAs were strongly detectable in aVECs but not expressed in the uninjured epithelium (**Figure 3.4E,F**). Outside of the epithelial layer, *Msln* was also expressed in mesothelial cells (Rinkevich et al., 2012), and *Clu* was also expressed in endothelial cells as previously reported (Andersen et al., 2007).

We further tested the hypothesis that aVECs possess a fetal-like transcriptional program by single-cell RNA sequencing (scRNA-seq) of IECs isolated during homeostasis and poly(I:C)-induced villus atrophy (**Figure 3.5A,B**). Uniform manifold approximation and projection (UMAP) of the integrated dataset identified all major intestinal cell lineages, including three enterocyte clusters reflective of their position on the villus axis (**Figure 3.6A,B**; Moor et al., 2018). Enterocytes were particularly enriched in the homeostasis sample, while crypt-based and secretory cells were enriched in the atrophy sample (**Figure 3.6C**). We validated that in both conditions, epithelial cell procurement by EDTA treatment was complete (**Figure 3.6D**).

Interestingly, we detected highest expression of fetal markers and enrichment of a fetal signature in the villus-top enterocyte cluster (cluster 7) (**Figure 3.7A,B**). In fact, there appeared to be two distinct populations in cluster 7 with the majority of cells possessing the fetal signature in the atrophy sample (**Figure 3.7C**), consistent with the LCM-microarray data. We validated that IL-33 was expressed in aVECs but not in homeostatic VECs (**Figure 3.7D**). However, we also identified several villus-tip markers, including CLDN4 (Tamagawa et al., 2003), that were

expressed by aVECs and homeostatic VECs near the top of villi (**Figure 3.7E**). These results suggest that transcriptionally aVECs most closely resemble enterocytes in the villus-top zone.

Given these findings, we further re-clustered cluster 7 and identified two major sub-clusters as expected. One cluster belonged to homeostatic villus-top enterocytes (cluster 7a) and the other cluster represented aVECs (cluster 7b and 7c). Through this analysis, aVECs were identified as altered versions of *Alpi*⁺ enterocytes and *Muc2*⁺ goblet cells, both enriched for fetal markers such as *Ly6a*, *Msln*, and *Clu* (**Figure 3.8A**). aVECs did not express many of the enterocyte zonation markers present in homeostatic VECs, including purine catabolism genes characteristic of villus-top enterocytes, and were instead enriched for ECM, cell adhesion, and fetal genes (**Figure 3.8B**). Together, these results show that aVECs fall within the enterocyte and goblet cell lineages and resemble most closely to normal enterocytes in the villus-top zone.

aVEC-like cells are present in Crohn's disease samples

As aVECs can be defined in mice at single-cell resolution, we next applied these signatures to a recent scRNA-seq atlas for Crohn's disease (Elmentaite et al., 2020). Analysis of the epithelial cell composition in newly diagnosed Crohn's disease patients and healthy controls yielded 10 clusters, including distinct subsets of enterocytes similar to the original study (**Figure 3.9A,B**). Overall, there was a reduction in the relative abundance of absorptive cells and an increase in crypt-based and secretory cells in Crohn's disease mucosal samples (**Figure 3.9C**). Notably, we observed an expansion of a unique *LCN2*⁺ enterocyte-like population (cluster 9) in Crohn's disease samples that also expressed high levels of *DUOX2* (**Figure 3.9D,E**).

Along with a subset of Crohn's disease-associated *DUOX2*⁺ goblet cells, *LCN2*⁺ enterocytes were enriched for a cell population that shared several markers with aVECs,

including *ITGB6*, *LAMC2*, *PLAUR*, and *ANXA1* (**Figure 3.10A**). In addition, these *DUOX2*⁺ cells were enriched for both aVEC and mouse fetal signatures (**Figure 3.10B,C**), suggesting that an aVEC-like cell type may be present in Crohn's disease and possibly in other enteropathies.

aVECs express lineage-specific markers and are terminally differentiated

Multiple mechanisms have been proposed for how the intestinal epithelium repairs after injury, such as the reversion of differentiated cells to a stem-like state (Beumer and Clevers, 2016). Due to the prominent fetal signature in aVECs, we next tested the stem and lineage properties of these cells. Though aVECs lack expression of many genes associated with the highly specialized functions of mature enterocytes (i.e., *ACE2/FABP1*), these cells nevertheless maintain either an enterocyte or goblet cell identity consistent with our single-cell data: *Alpi* transcripts and *MUC2* were expressed in discrete cells on atrophic villi (**Figure 3.11A**). Furthermore, aVECs expressed the pan-differentiation marker *Krt20* (**Figure 3.11B**). This marker showed complete co-localization with *Msln* and *Clu* mRNAs in aVECs (**Figure 3.11C**).

To assess the extent to which cell differentiation processes were affected during villus repair, we performed immunostaining to evaluate the presence and allocation of all the major intestinal cell lineages (**Figure 3.12**). Unsurprisingly, *ALDOB*⁺ enterocytes were absent on atrophic villi but reappeared on regenerating villi. *MUC2*⁺ goblet cells, while present, had a diminutive theca during villus atrophy, and later during regeneration, co-expressed the Paneth cell marker *MMP7*, featuring an intermediate cell phenotype. *CHGA*⁺ endocrine cells and *DCLK1*⁺ tuft cells were found at similar frequencies on atrophic and regenerating villi. By one-week post-injury, all epithelial lineages largely restored back to homeostatic conditions. Thus, besides a transient increase in intermediate cells during villus regeneration, a cell type commonly

induced in the setting of parasitic infection (Kamal et al., 2002), the distribution of differentiated epithelial cell lineages remained largely intact following injury. Interestingly, the differentiation profile of IECs during villus atrophy (i.e., expression of KRT20/MUC2/*Alpi* and absence of enterocyte protein markers) closely reflect that of the fetal intestine (Guiu et al., 2019).

Clu is expressed in aVECs as we described, but is also a defining marker of the recently identified revSC population, which drives epithelial regeneration after loss of LGR5⁺ ISC to intestinal damage (Ayyaz et al., 2019). Given the close link between the fetal program and regenerative stem cells, we wondered whether aVECs were endowed with stem cell capacity or truly represented a differentiated cell population. To test if aVECs contained stem cell potential, we transiently labeled KRT20-expressing VECs at homeostasis and during atrophy by tamoxifen induction of tdTomato (*Krt20^{CreER}/R26R^{tdTomato}* mice; **Figure 3.13A**). Flow cytometry analysis demonstrated that an average 73% of IECs were tdTomato (tdT)⁺ at homeostasis and 18% during atrophy (**Figure 3.13B**). We validated that KRT20-tdT⁺ aVECs were enriched for the fetal markers *Msln* and *Clu* with reduced expression of *Ace2* compared to KRT20-tdT⁺ homeostatic VECs (**Figure 3.13C**). To functionally test for stemness, we cultured sorted tdT⁺ and tdT⁻ cells in Matrigel/L-WRN conditioned media (Miyoshi and Stappenbeck, 2013). KRT20-tdT⁺ aVECs and homeostatic VECs (as a control) failed to form any spheroids, suggesting a lack of stem cell capacity (**Figure 3.13D,E**). In contrast, KRT20-tdT⁻ cells showed robust spheroid-forming efficiency regardless of injury status as expected of intestinal crypt cells (**Figure 3.13D,E**).

Progenitor cells transiently differentiate into aVECs following injury

In response to ISC damage, rare CLU⁺ cells in the crypt are thought to expand and give rise to revSCs (Ayyaz et al., 2019). To determine the source of aVECs, we first examined

epithelial turnover dynamics by injecting the thymine analogs CldU and IdU prior to injury and during villus atrophy, respectively. These data support the hypothesis that dividing progenitors migrate over damaged villi to become aVECs, which are then replaced by newly emerged IECs during villus regeneration (**Figure 3.14A**). Consistent with this picture, lineage tracing showed that the recent progeny of LGR5⁺ ISC were the dominant source of aVECs relative to BMI1⁺ cells and LGR5⁺ ISCs (**Figure 3.14B,C**). While we cannot exclude the possible contribution of a rare CLU⁺ cell population, our findings favor a model in which TA progenitor cells differentiate into aVECs after injury and acquire a fetal-like profile. Since this program of repair does not involve a cell type conversion, we termed this process “adaptive differentiation”.

The short-lived nature of the aVEC population was further corroborated by the fact that KRT20-labeled cells were absent three weeks post-injury in *Krt20^{CreER}/R26^{RtdTomato}* mice (**Figure 3.15A**). Tracking the fate of *Msln*⁺ cells by *in situ* hybridization showed that aVECs sloughed off at the villus tip during the regenerative phase (**Figure 3.15B**). Taken together, we demonstrate that TA cells adaptively differentiate into aVECs and transiently cover injured villi.

3.4 Discussion

Using a poly(I:C)-mediated injury model in the small intestine, we defined an aVEC population that covers severely damaged villi. Morphologically, aVECs lacked many features typical of mature enterocytes. aVECs were primitive in their appearance with a short cuboidal morphology and diminished brush border. They contained many large fat droplets, which could be a result of lacking the proper machinery to metabolize lipids (Cruz-Garcia and Schlegel, 2014). Importantly, they were reminiscent of surface epithelial cells associated with intestinal injury and disease (Kent and Moon, 1973; Kerzner et al., 1977; Schuffler and Chaffee, 1979). By cross-comparing our aVEC transcriptional dataset with that of Crohn's and celiac disease, we determined that aVEC-like cells were present in human enteropathies. Thus, poly(I:C)-induced villus injury transiently triggers a disease-associated epithelial cell type, offering a unique opportunity to further characterize these cells and examine their role in intestinal biology.

In spite of bearing little resemblance to mature IECs, aVECs were differentiated by all accounts. First, aVECs possessed an *Alpi*⁺ enterocyte or *Muc2*⁺ goblet cell identity based on their transcriptomes. Interestingly, villus IECs in the fetal epithelium have features of epithelial differentiation, yet retain the capacity to serve as precursors to adult intestinal stem cells (Guiu et al., 2019). In contrast, in the injured adult intestine, aVECs did not possess stem cell capacity *in vitro* or *in vivo*. Using a thymidine incorporation assay, aVECs were clearly post-mitotic. When cultured in stem cell media, aVECs did not grow into spheroids. And when lineage-traced, aVECs never re-entered the crypt and acquired a stem-like state to regenerate the epithelium.

Therefore, it was a surprise to find that aVECs possessed a fetal-like profile, which was largely thought to be a defining feature of regenerative stem cells (Nusse et al., 2018; Wang et al., 2019). While studies so far associate this damage-induced state with stemness and

regeneration (Beumer and Clevers, 2021; Nusse et al., 2018; Sprangers et al., 2021), our data suggest that it can also be observed under certain contexts of epithelial differentiation. It is therefore likely that proximity to niche factors in the crypt is crucial for determining stem cell function in the adult intestine (Fuchs et al., 2004; Gehart and Clevers, 2019). Once a cell exits the crypt niche and enters the villus compartment, the surrounding microenvironment likely forces it to undergo cell differentiation. Given that the boundaries between the crypt and villus are mostly intact in the poly(I:C) injury model, we speculate that all the major signaling pathways involved in establishing epithelial proliferation and differentiation during homeostasis, such as the WNT, BMP, and Notch pathways, are still in place even during villus atrophy.

Interestingly, many genes that were upregulated in aVECs were also induced in Crohn's and celiac disease biopsies. This suggested that the lack of mature enterocyte features was not the only commonality between aVECs and disease-associated epithelial cells. The upregulated genes included fetal markers as well as many genes related to pathways involved in wound healing. We will examine the functional role of this reparative program in the next chapter.

By combining spatial transcriptomics with single-cell technology, we were able to obtain a high-resolution view of the various cell states in the atrophic intestine. Previously, LCM and scRNA-seq was combined to understand the heterogeneity of enterocytes along the villus axis (Moor et al., 2018). Similarly, we used LCM data to guide our single-cell analysis and validated our results with single-molecule *in situ* hybridization and immunostaining. LCM is particularly useful for understanding IEC biology as these cells are easy to micro-dissect under the microscope. The ability to characterize these cells in a fixed tissue also minimizes artifacts often associated with tissue dissociation and reduce sampling bias that could result from only collecting surviving cells (Haber et al., 2017; Machado et al., 2021). This is especially a problem

with the differentiated intestinal populations, which are programmed to die once they are lifted from the basement membrane (Grossmann et al., 2001). Despite this, scRNA-seq provides a level of resolution that LCM simply cannot achieve—the ability to transcriptionally profile single cells. Additionally, scRNA-seq enables the ability to see how cells relate to one another with dimensionality reduction (Sun et al., 2019). Thus, using this technology, we were able to determine the heterogeneity of the aVEC population and assess their relation to homeostatic IECs. To our surprise, aVECs clustered very closely to villus-top enterocytes, which are enterocytes found near the tip of the villi. Whether this is due to the spatial positioning of aVECs (as these cells are technically covering the top of atrophic villi) or some other biological phenomenon remains to be known. Villus-top enterocytes are characterized by the expression of AP-1 transcription factors, EGFR, and purine catabolism gene (Moor et al., 2018). It has been suggested that a specific stromal population in the villus tip region, defined by the expression of LGR5, is required for controlling the villus-tip program (Bahar Halpern et al., 2020). Additionally, enterocytes may possess a unique transcriptional profile in the villus tip zone because that is where normal cellular shedding occurs (Patankar and Becker, 2020). Activation of AP-1 transcription factors and EGFR signaling in these cells may help promote changes in cell adhesion, cell-cell junction, and actin cytoskeleton to maintain barrier integrity within that zone (Galvagni et al., 2013; Li et al., 2003; Malliri et al., 1998; Tran et al., 2012).

Another surprise from the scRNA-seq analysis was the fact that aVECs possessed either an enterocyte or goblet cell identity. In fact, atrophic villi were also lined with enteroendocrine and tuft cells at expected frequencies. However, we only saw induction of a fetal program in the enterocyte and goblet cell lineages. This suggests that the allocation of the various intestinal lineages occurs normally even after villus injury but only the enterocyte and goblet cell

populations can acquire a reparative phenotype. Why enteroendocrine and tuft cell lineages fail to acquire fetal characteristics during atrophy is an open question. One reason is that they do not possess the transcriptional machinery to induce such a program. Another possibility is that these cells are so rare and specialized that they are not active participants of repair. Interestingly, both enteroendocrine and tuft cells are thought to interact with nerve cells, suggesting that they are wired differently from enterocytes or goblet cells (Banerjee et al., 2018; Kaelberer et al., 2018).

Importantly, none of the current models of cell reprogramming adequately explains how aVECs form, as these cells originate from immature progenitors. While a fetal-like reprogramming of IECs has been demonstrated before in various crypt injury models, these settings appear to involve a cell type conversion—that is, loss of stem cell and differentiation features and gain of fetal characteristics (Gregorieff et al., 2015; Nusse et al., 2018; Yui et al., 2018). In contrast, aVECs are better described as progenitor-derived cells that exit the cell cycle, undergo lineage commitment, and acquire a fetal-like program but fail to fully mature into normal enterocytes or goblet cells. Thus, the reparative program was likely prioritized over the normal differentiation program during their exit from the crypt. These cells are likely not identical to fetal IECs as not all fetal markers were expressed by aVECs, including TROP2 and CNX43 (Fernandez Vallone et al., 2016). Given that we do not see evidence of reprogramming during aVEC formation, we propose “adaptive differentiation” to explain the process by which stem and progenitor cells differentiate and adapt to the wounded environment to promote tissue repair. We believe this paradigm may be conserved in other organs with high cell turnover rates.

3.5 Figures

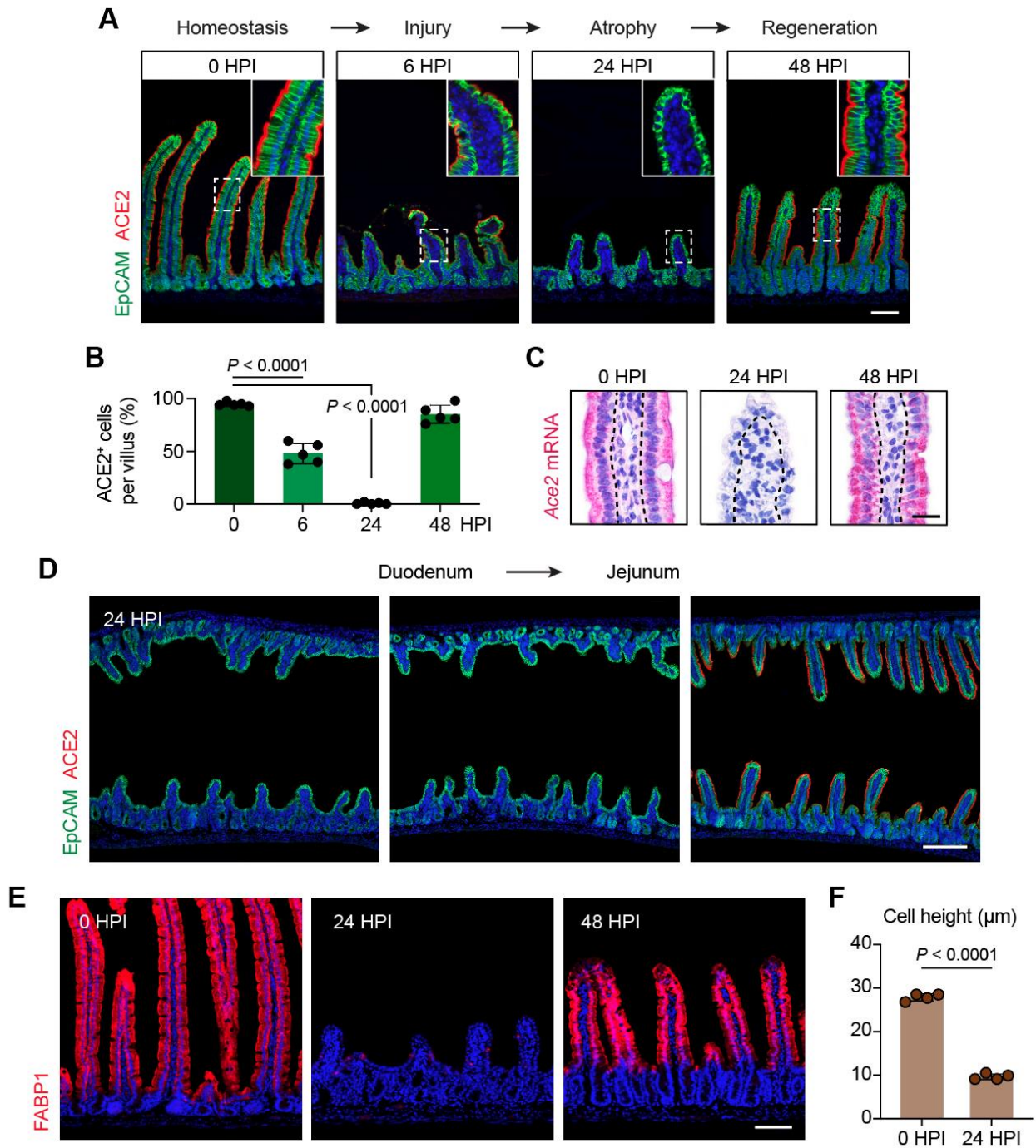


Figure 3.1. Transient suppression of enterocyte markers following villus injury

(A) Immunofluorescence (IF) for EpCAM (green) and ACE2 (red) at the indicated time points/injury-repair stage. Bar: 100 μm (B) Average number of ACE2⁺ cells across 30 villi was plotted as mean \pm SD. n = 5 mice/group. Significance was determined by one-way ANOVA and Tukey's multiple comparison test. (C) RNAscope *in situ* hybridization for *Ace2* in a representative villus at the indicated time points. Each red dot represents a single mRNA molecule. Bar: 25 μm . (D) IF for EpCAM (green) and ACE2 (red) in the small intestine from the duodenum to the proximal jejunum at 24 HPI. Bar: 200 μm . (E) IF for FABP1 (red) at the indicated time points. Bar: 100 μm . (F) Average epithelial cell height across 50 villi based on H&E images was plotted as mean \pm SD. n = 4 mice/group. Significance was determined by unpaired *t*-test. IF and RNAscope images are representative of at least 3 animals.

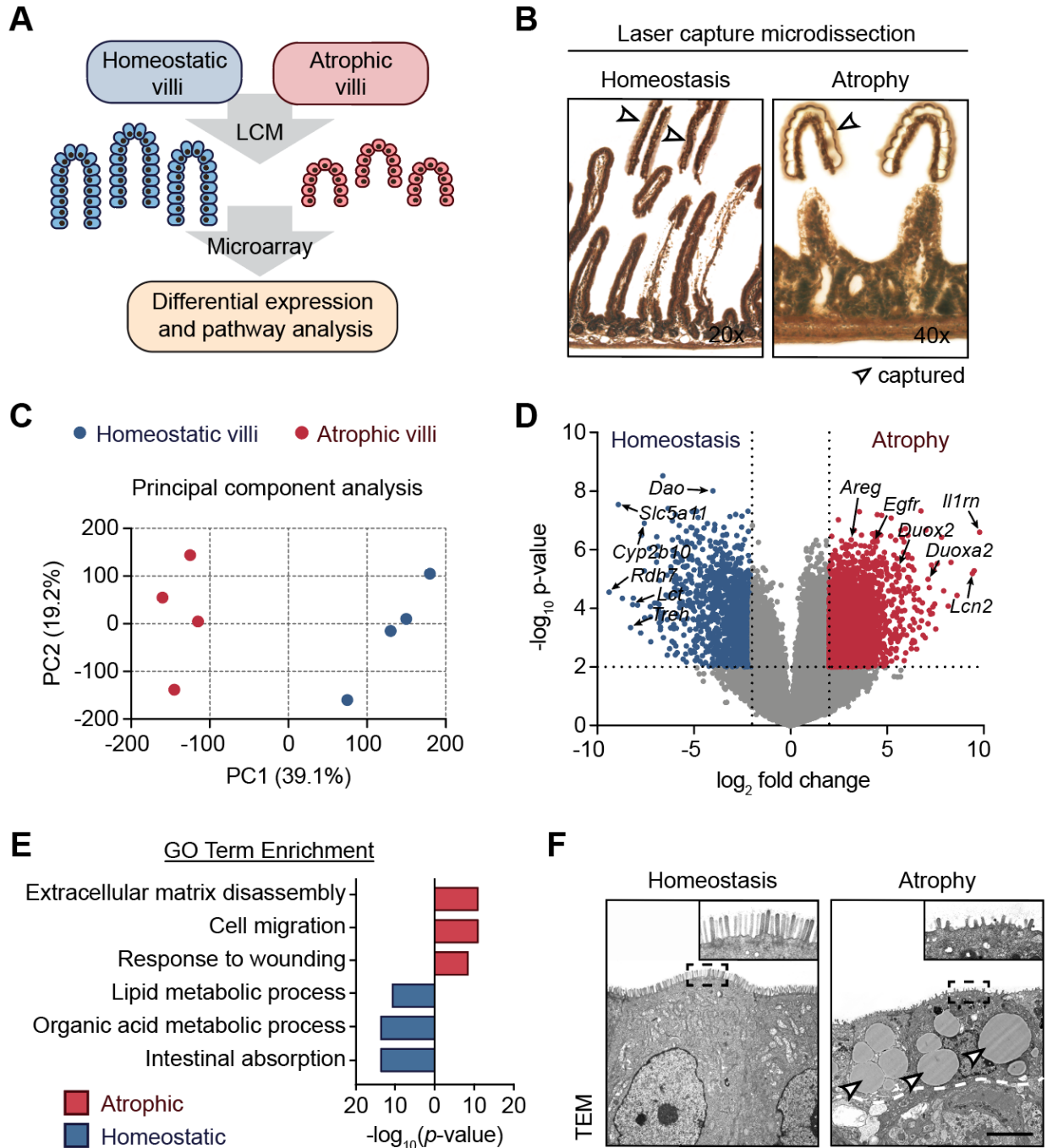


Figure 3.2. Characterization of villus atrophy-induced epithelial changes

(A) Schematic of laser-capture microdissection (LCM)-microarray experiment. Villus epithelial cells (VECs) from 4 mice/group were collected. (B) Example of an LCM experiment showing isolation of villus epithelial cells (VECs) from the homeostatic and atrophic intestine. Arrowheads indicate captured cells. (C) Principal component analysis of bulk transcriptomes from homeostatic VECs and atrophy-induced VECs (aVECs). (D) Volcano plot showing differentially expressed genes between homeostatic VECs and aVECs. Significant genes ($p < 0.01$ and fold-change > 2) were color-coded red or blue. (E) Gene ontology (GO) analysis of the top 500 upregulated and downregulates genes in atrophy-induced VECs (aVECs) compared with homeostatic VECs. (F) Ultrastructure of homeostatic VECs and aVECs. Dashed line represents the epithelial-stromal border. Note that aVECs possess shorter microvilli (inset) and contain many lipid droplets (arrowheads). Bar: 5 μm . Images are representative of at least 3 animals.

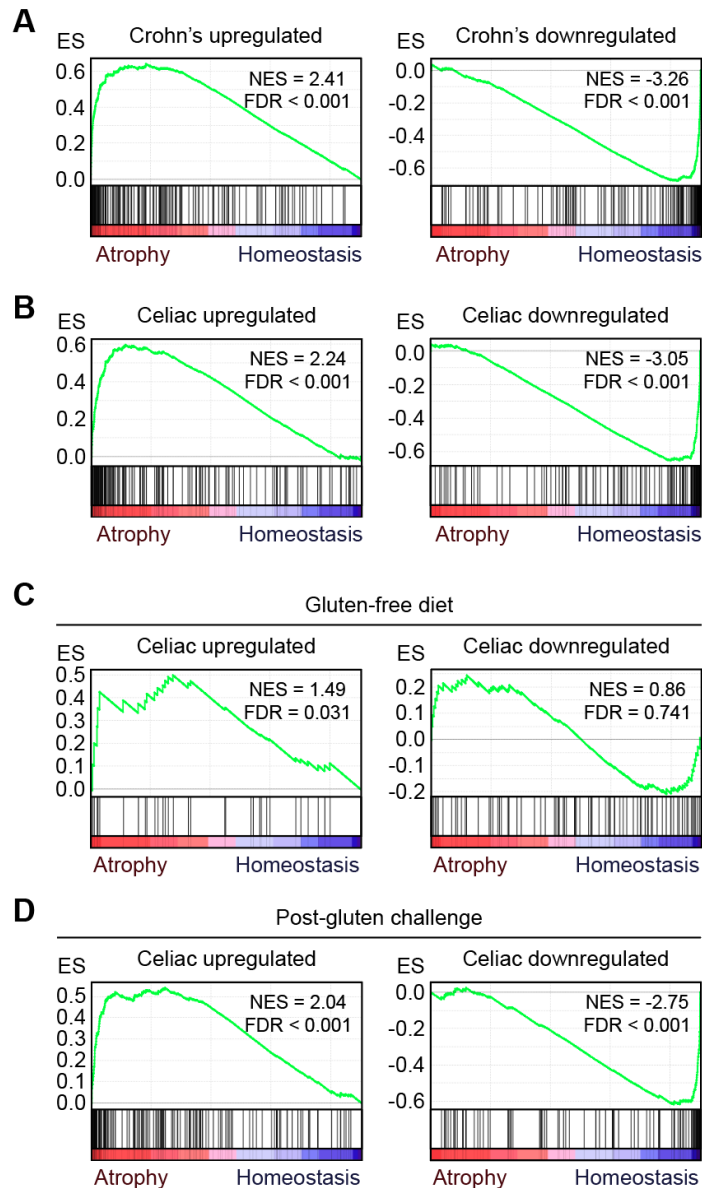


Figure 3.3. Villus injury induces a disease-associated epithelial cell type

(A and B) Gene set enrichment analysis (GSEA) of genes upregulated or downregulated in Crohn's disease (A) and celiac disease (B) in aVECs (Atrophy) compared with homeostatic VECs (Homeostasis). (C and D) GSEA of genes upregulated or downregulated in celiac disease patients on a gluten-free diet (C) or post-gluten challenge (D) in aVECs compared with homeostatic VECs. NES = normalized enrichment score (NES), FDR = false discovery rate.

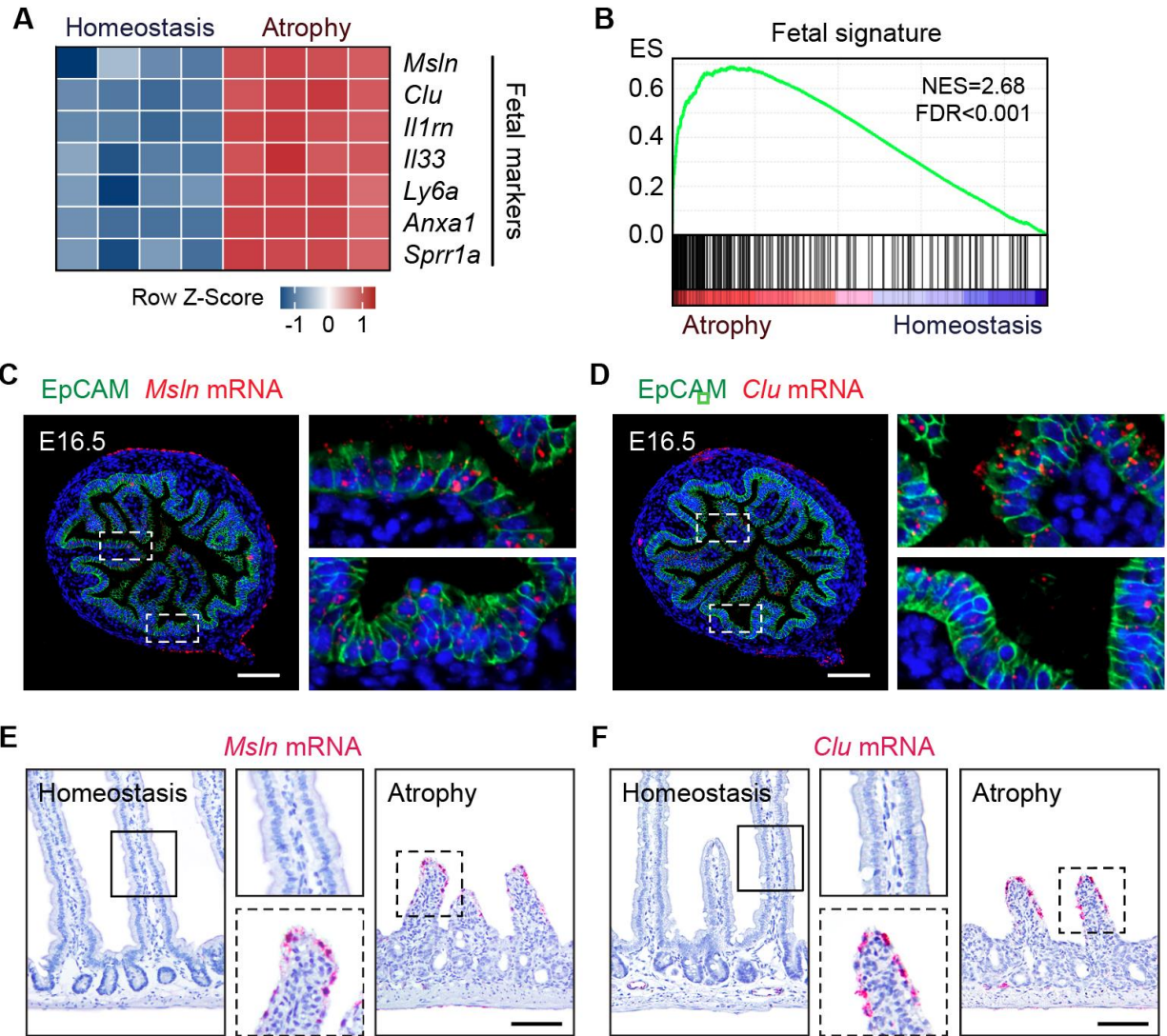


Figure 3.4. aVECs acquire a fetal-like transcriptional program

(A) Heatmap of select fetal markers from the aVEC LCM-microarray dataset. Values were row normalized. n=4 mice/group. (B) GSEA of a fetal spheroid signature in aVECs compared with homeostatic VECs. (C and D) IF/RNAscope *in situ* hybridization for EpCAM (green) and *Msln* or *Clu* (red) in E16.5 intestines. Each red dot represents a single mRNA molecule. (E and F) RNAscope for *Msln* and *Clu* in the homeostatic and atrophic intestine. All bars: 100 μ m.

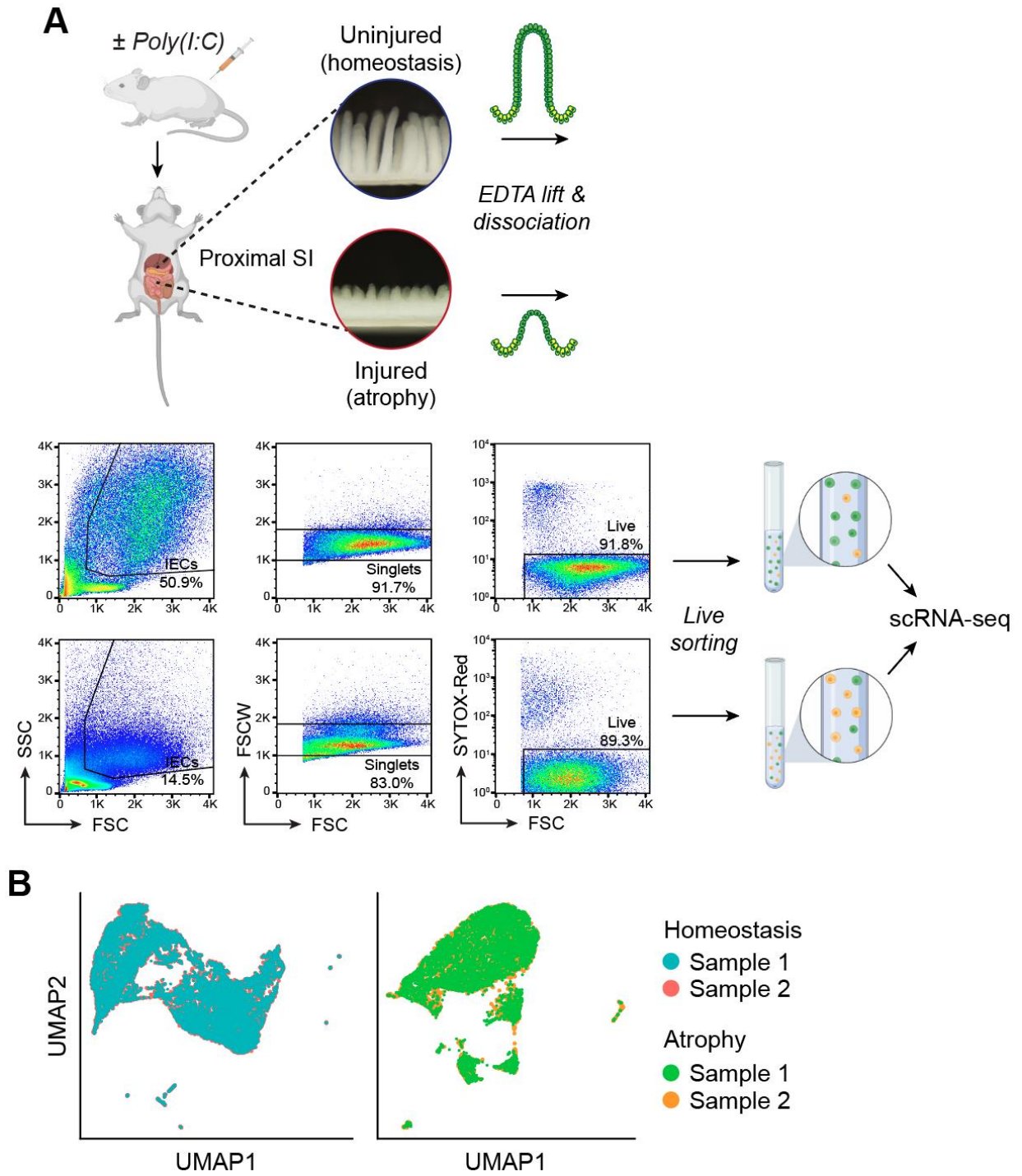


Figure 3.5. scRNA-seq workflow for IECs from the homeostatic and atrophic intestine

(A) Schematic of single-cell RNA sequencing (scRNA-seq) protocol. Intestinal epithelial cells (IECs) from the homeostatic and atrophic intestine were isolated by EDTA treatment, enzymatically dissociated, and sorted based on the gating strategy shown. Sorted IECs were submitted for scRNA-seq using the 10x Genomics system. (B) Uniform manifold approximation and projection (UMAP) visualization of scRNA-seq libraries from two independent homeostasis samples and two independent villus atrophy samples reveals minimal batch-to-batch variation.

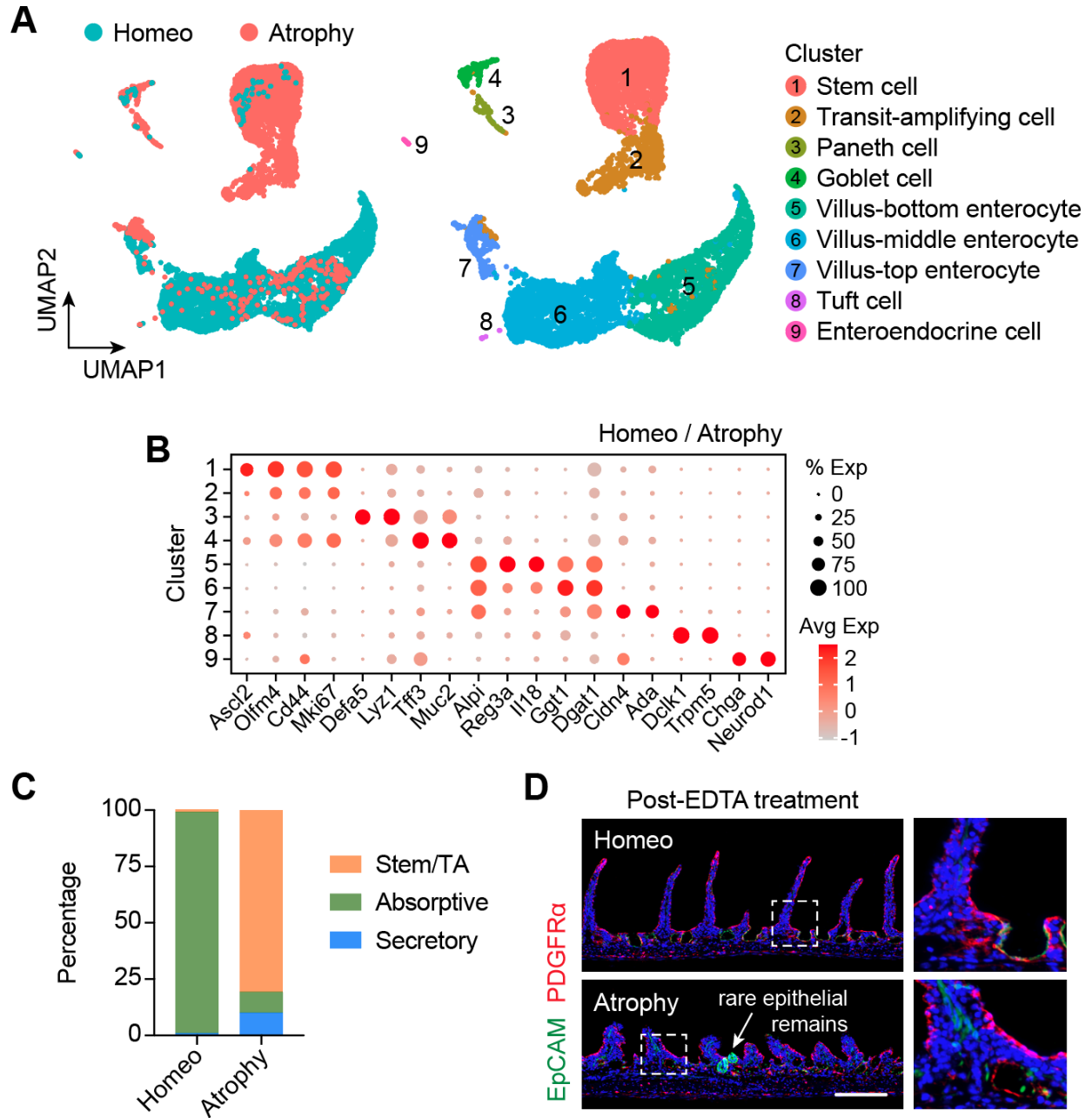


Figure 3.6. Analysis of scRNA-seq data

(A) UMAP visualization of IECs from the homeostatic (4,892 cells) and atrophic (3,650 cells) intestine colored by sample (left) and cell type (right). Clusters were annotated based on expression of known and top marker genes. (B) Dot plot of cell type-specific and enterocyte zonation markers in the homeostasis vs atrophy IEC scRNA-seq dataset. (C) Proportion of stem/progenitor cells, absorptive enterocytes, and secretory cells (i.e., Paneth, goblet, enteroendocrine, and tuft cells) in the homeostatic and atrophic intestine based on scRNA-seq clusters. (D) IF for EpCAM (green) and PDGFR α (red) in the homeostatic and atrophic intestine post-EDTA treatment shows efficient isolation of villus and crypt epithelial cells. Bar: 200 μ m.

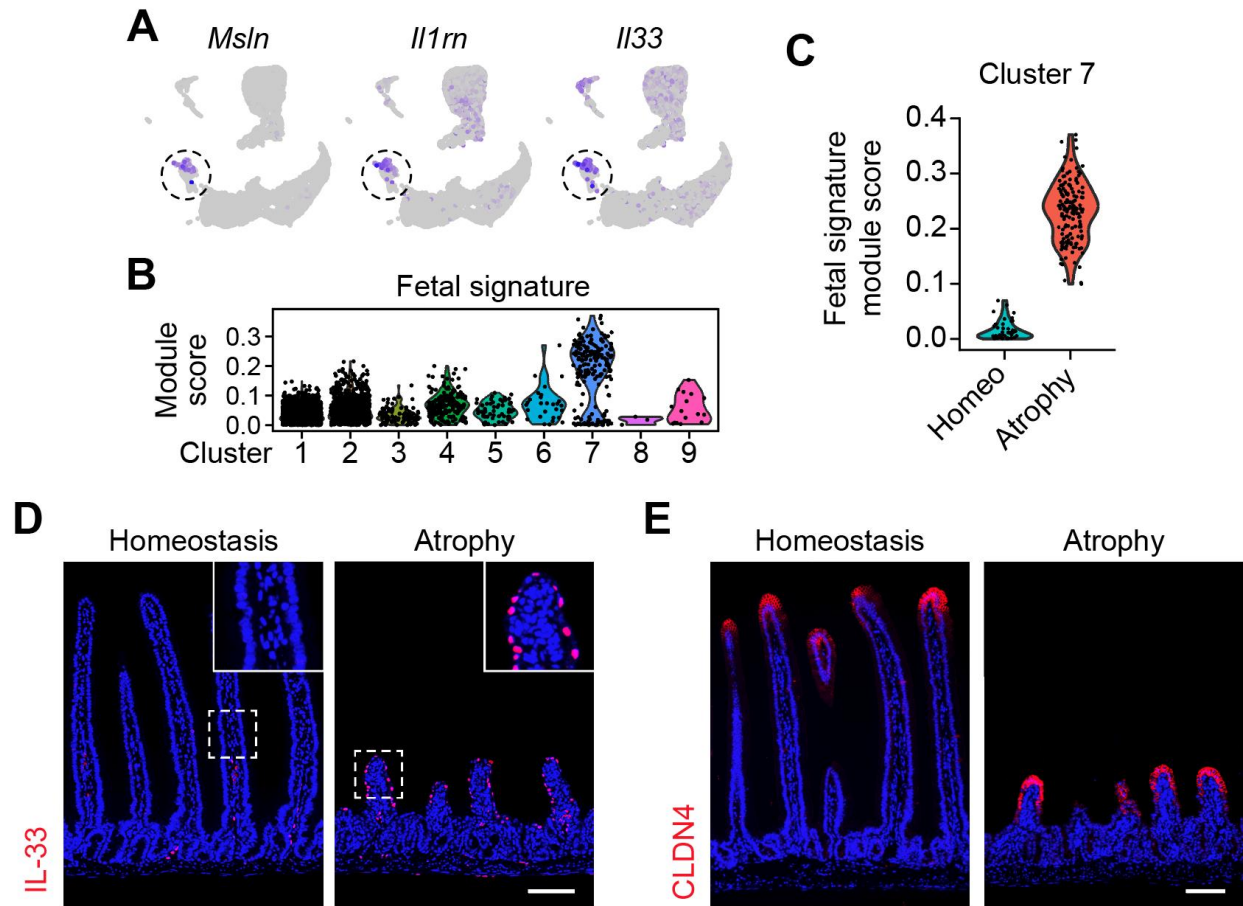


Figure 3.7. Fetal markers are enriched in atrophy-associated IECs that transcriptionally resemble homeostatic villus-top enterocytes the most

(A) Expression of select fetal markers was overlaid on the UMAP plot. Highest expressors were concentrated in a subset of villus-top enterocytes (cluster 7, dashed circle). (B and C) Enrichment analysis of a fetal spheroid signature for each cell separated by cluster (B) and by sample in cluster 7 (C). Each black dot represents one cell. The higher the module score, the better the enrichment. (D) IF for IL-33 (red) in the homeostatic and atrophic intestine. Bar: 100 μ m. (E) IF for CLDN4 (red), a villus-tip marker, in the homeostatic and atrophic intestine. Bar: 100 μ m.

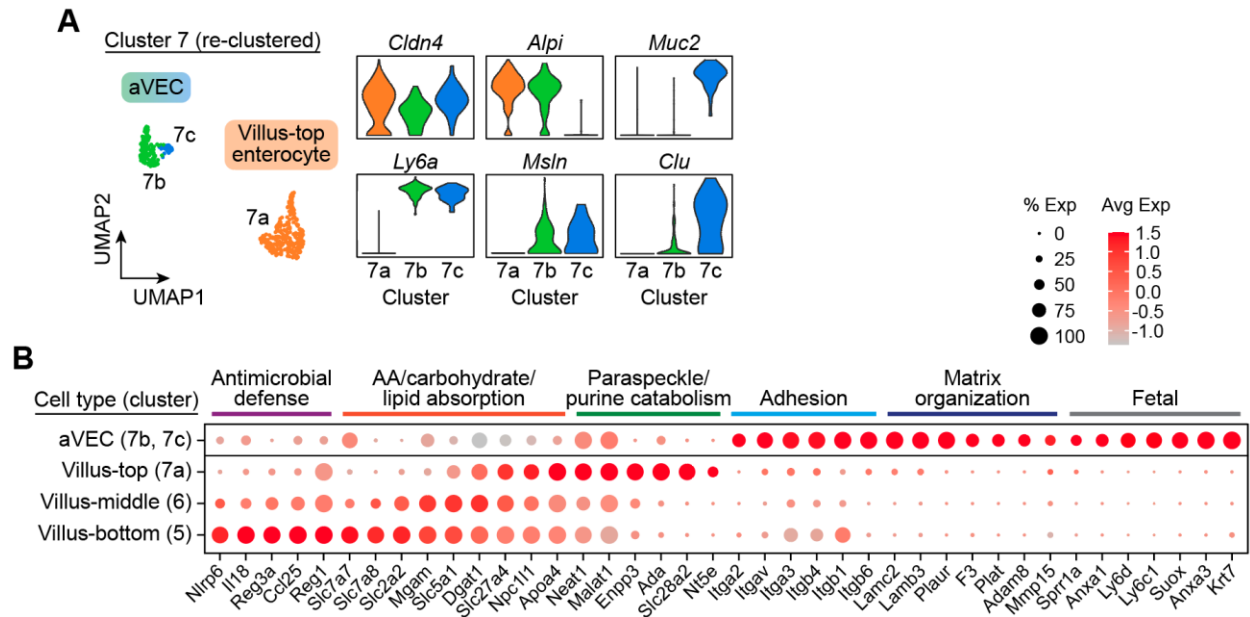


Figure 3.8. aVECs are transcriptionally distinct from normal enterocytes and are comprised of cells within the enterocyte and goblet cell lineage

(A) UMAP visualization of villus-top enterocyte (cluster 7) sub-clusters colored by cell type (left). Expression of villus-tip (*Cldn4*), cell lineage (*Alpi*, *Muc2*), and fetal (*Ly6a*, *Msln*, *Clu*) markers in each sub-cluster (right). Note that aVECs are a heterogeneous population of cells, with some cells possessing an enterocyte identity and other cells a goblet cell identity. (B) Dot plot of enterocyte zonation markers from the villus-bottom to villus-top. Cell-adhesion, extracellular matrix (ECM), and fetal genes expressed by aVECs (atrophy-top cells) are also shown.

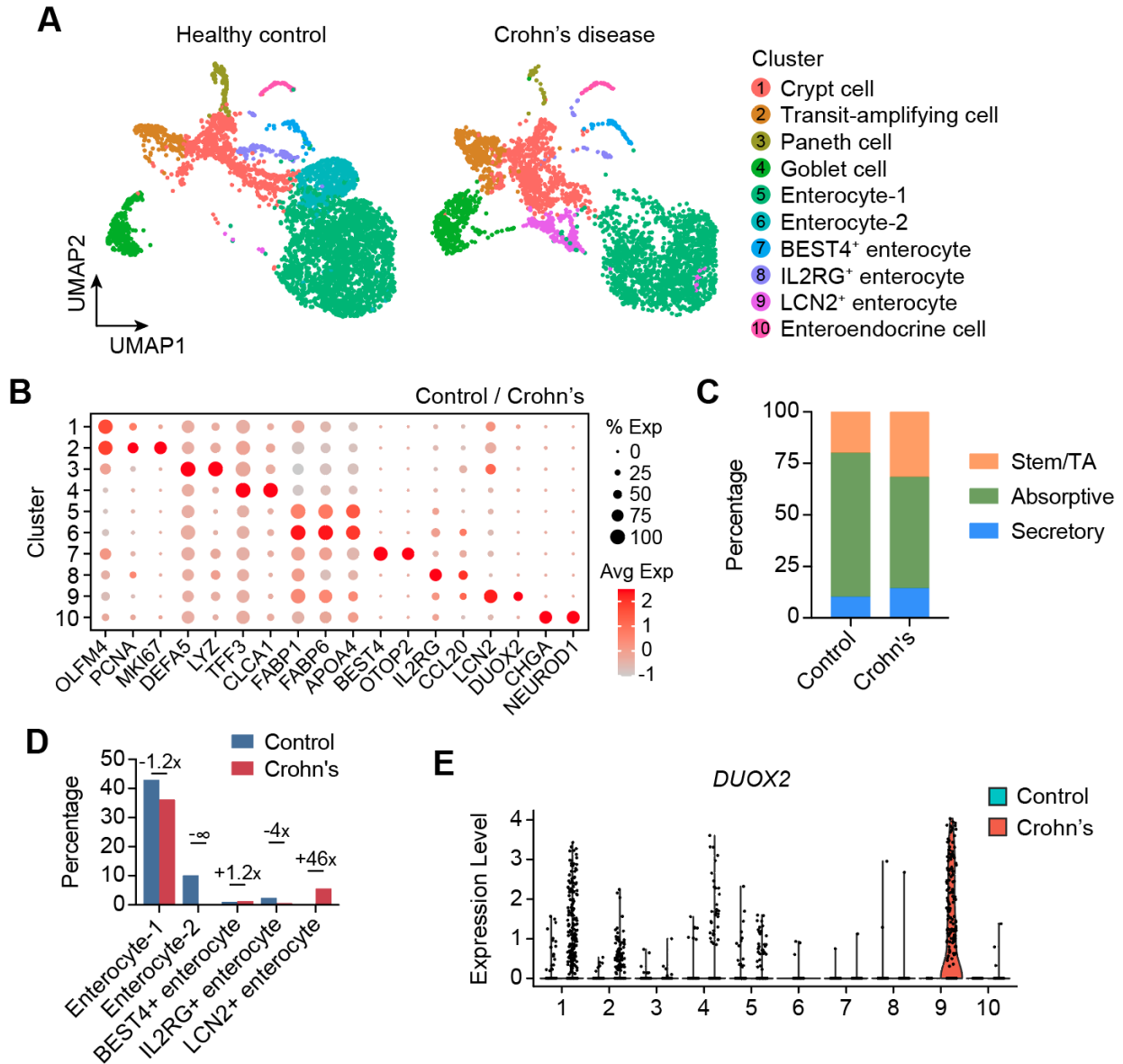


Figure 3.9. Identification of Crohn's disease-associated enterocyte and goblet cell populations by scRNA-seq

(A) UMAP visualization of IECs from healthy control (4,630 cells) and pediatric Crohn's disease (3,545 cells) patients obtained from the Gut Cell Survey. Clusters were annotated based on expression of known and top marker genes. (B) Dot plot of cell type-specific and cluster-defining markers in the healthy control vs pediatric Crohn's disease IEC scRNA-seq dataset. (C) Proportion of stem/progenitor cells, absorptive enterocytes, and secretory cells (i.e., Paneth, goblet, and enteroendocrine cells) in healthy controls and pediatric Crohn's disease patients based on scRNA-seq clusters. (D) Proportion of enterocyte subsets and the relative fold difference between healthy controls and pediatric Crohn's disease patients. Note that *LCN2*⁺ enterocytes (cluster 9) uniquely arise in Crohn's disease. (E) Expression of *DUOX2* in each cluster separated by disease status. Each black dot represents one cell. *DUOX2* is predominantly expressed in Crohn's-associated *LCN2*⁺ enterocytes and in a subset of goblet cells (cluster 4).

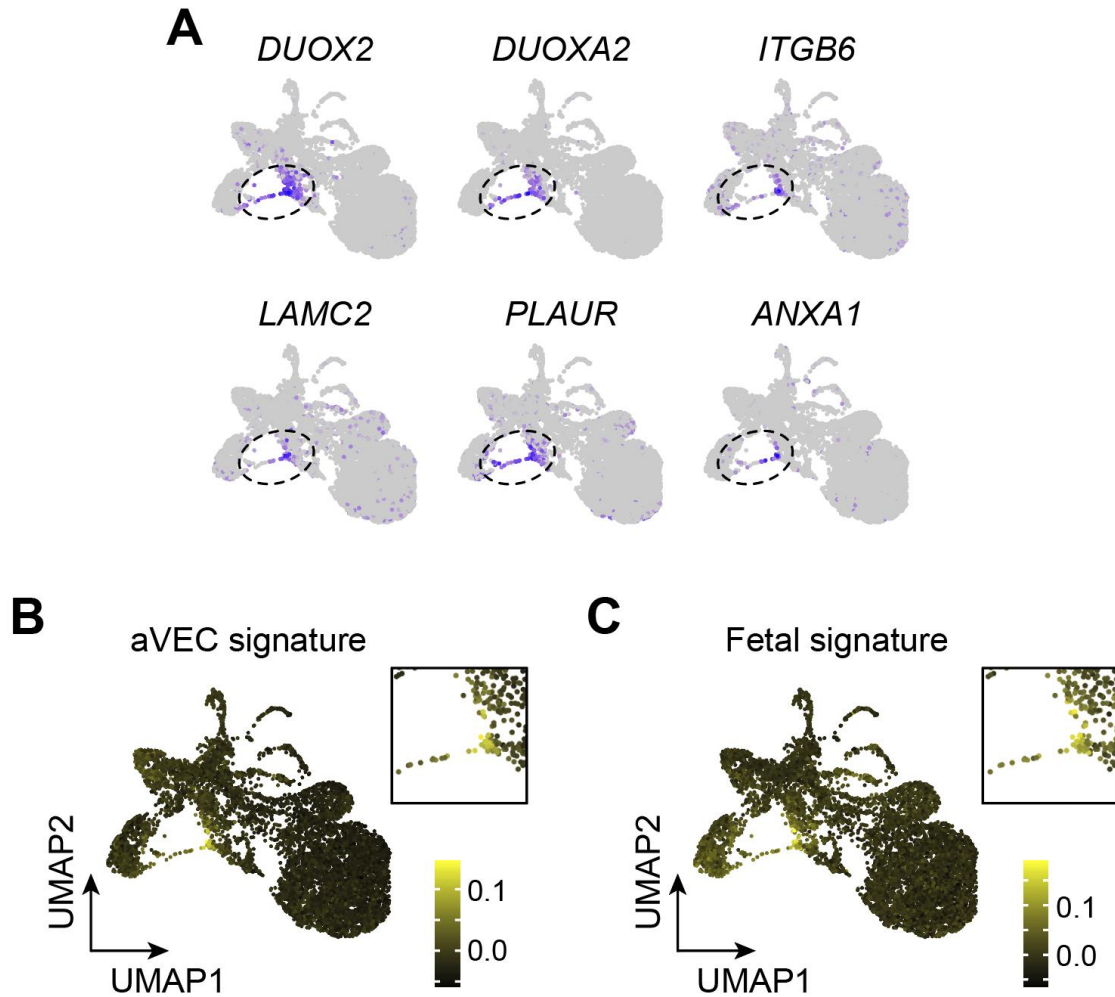


Figure 3.10. aVEC-like cells are present in Crohn's disease samples

(A) Expression of select aVEC markers was overlaid on the UMAP plot. Highest expressors were concentrated in the Crohn's-associated *DUOX2-DUOXA2*⁺ enterocytes and goblet cells. (B and C) Expression of the aVEC (B) and mouse fetal spheroid (C) signature was overlaid on the UMAP plot. Highest expressors (yellow-colored cells) were concentrated in *DUOX2*⁺ cells.

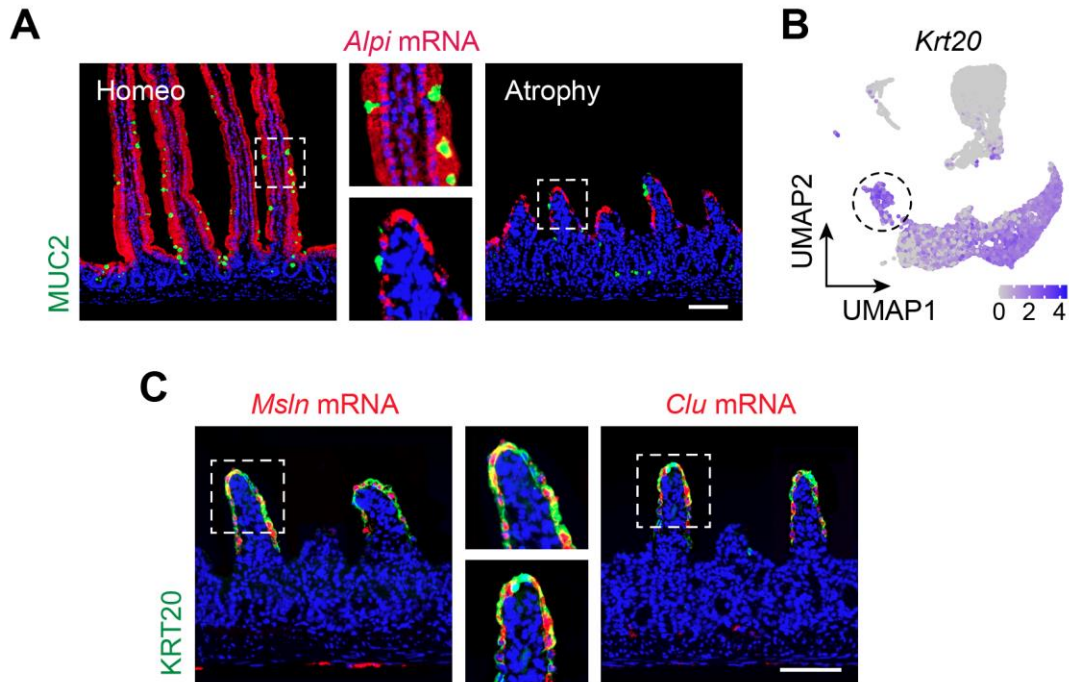


Figure 3.11. aVECs express lineage-specific and differentiation markers

(A) IF/RNAscope for MUC2 (green) and *Alpi* (red) in the homeostatic and atrophic intestine. (B) Expression of *Krt20*, a differentiation marker, was overlaid on the UMAP plot. Villus-top enterocytes (dashed circle) express *Krt20*. (C) IF/RNAscope for KRT20 (green) and *Msln* or *Clu* (red) in the atrophic intestine. Note that *Msln/Clu*⁺ aVECs express KRT20. Bars: 100 μ m.

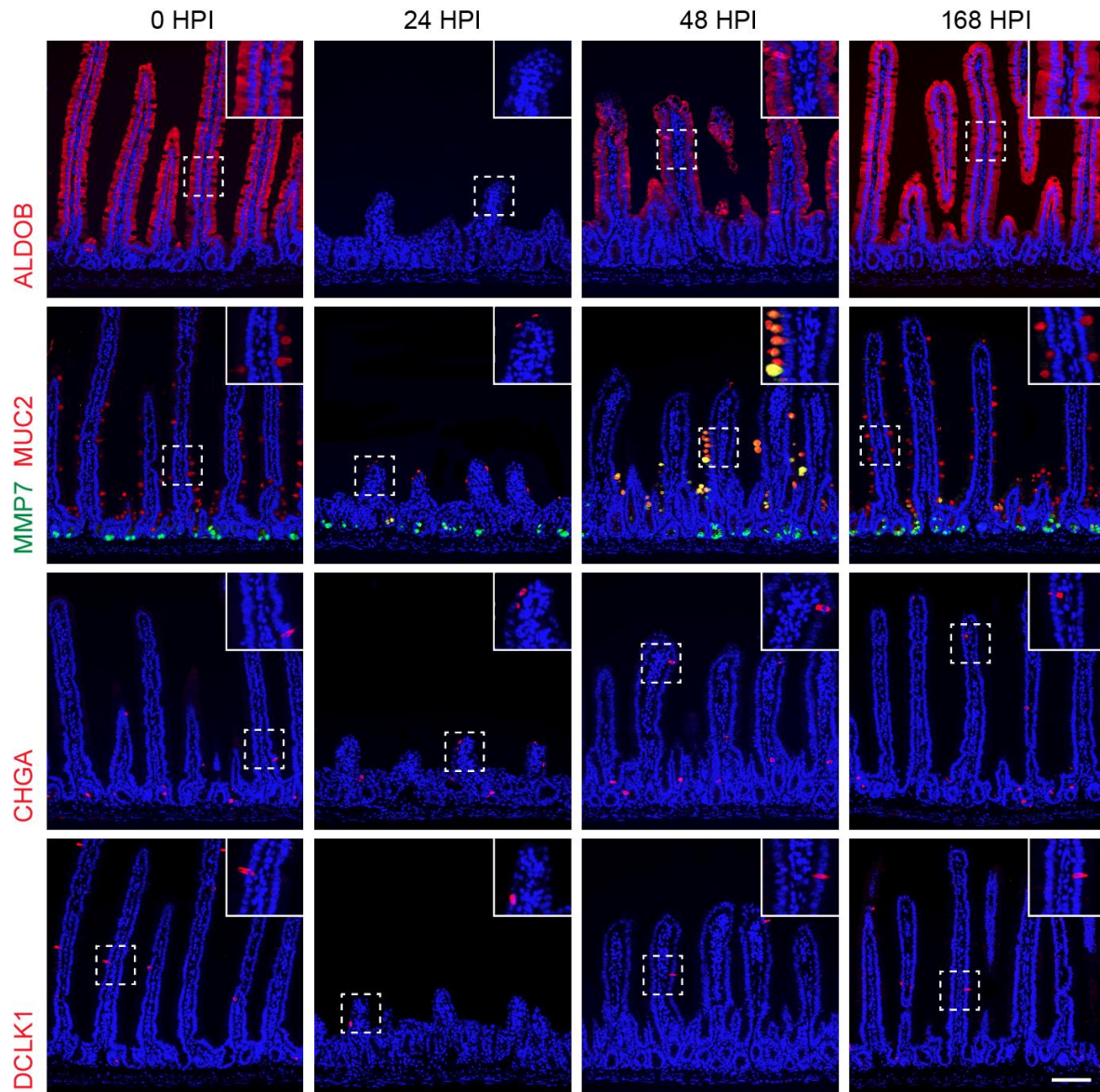


Figure 3.12. Lineage dynamics during villus injury-repair

IF for cell-lineage markers at the indicated time points. Expression of ALDOB (enterocyte), MUC2 (goblet cell), MMP7 (Paneth cell), CHGA (enteroendocrine cell), and DCLK1 (tuft cell) was examined. Note the loss of ALDOB expression during villus atrophy (consistent with loss of ACE2 and FABP1 at this time point) and appearance of MUC2⁺MMP7⁺ intermediate cells during villus regeneration. Images are representative of at least 3 animals. Bar: 100 μ m.

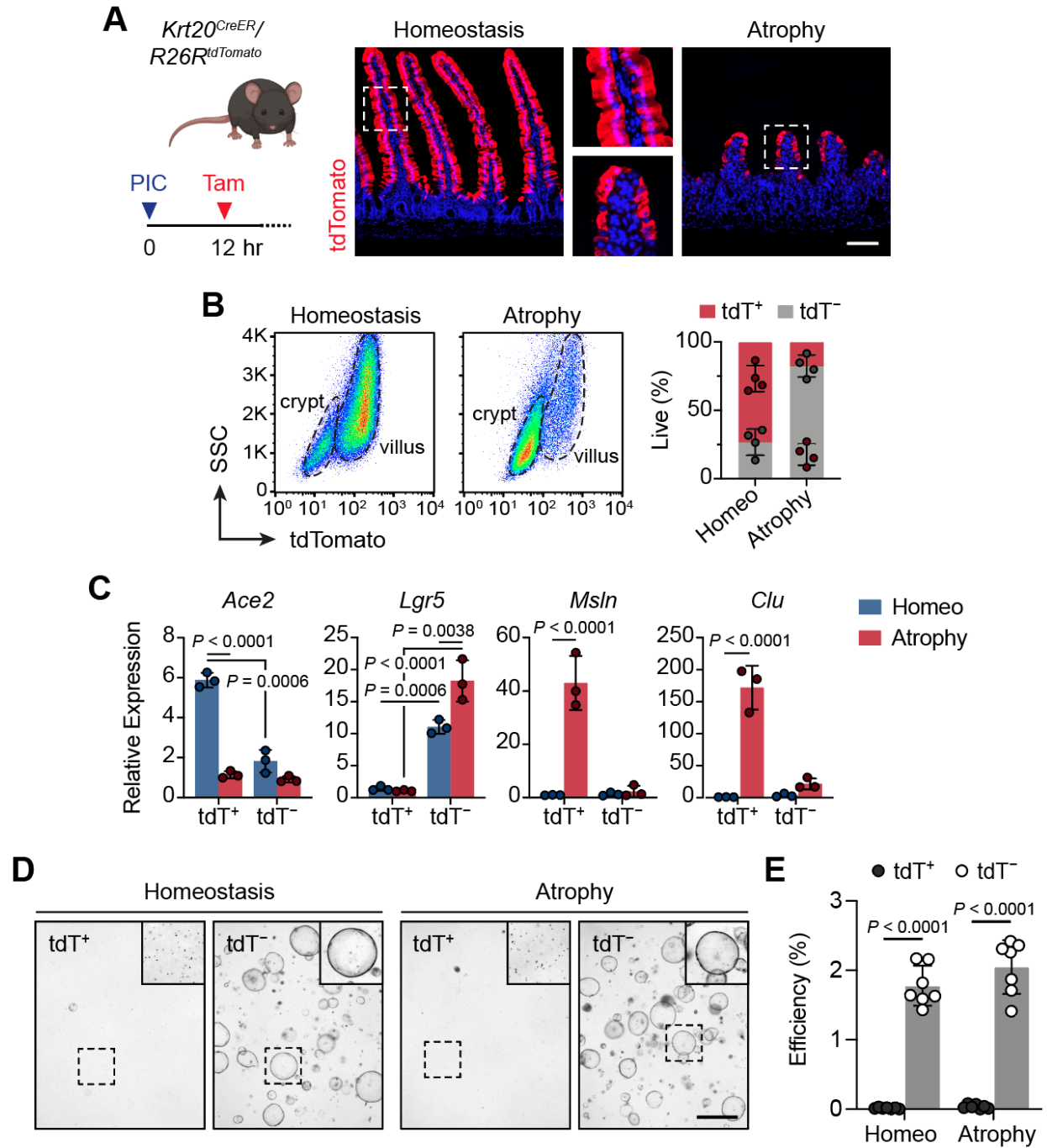


Figure 3.13. aVECs are terminally differentiated

(A) Validation of tamoxifen-mediated fluorescent labeling of KRT20⁺ cells in *Krt20^{CreER}/R26^{tdTomato}* mice during homeostasis and atrophy. Labeled cells express tdTomato (tdT). Bar: 100 μ m. (B) Flow cytometry analysis of KRT20-tdT⁺ and KRT20-tdT⁻ cells during homeostasis and atrophy. Representative plots (left) and relative percentage of each population (right) displayed as mean \pm SD. n = 4 mice/group. (C) qPCR analysis of *Ace2*, *Lgr5*, and fetal markers (*Msln*, *Clu*) in sorted KRT20-tdT⁺ and KRT20-tdT⁻ cells during homeostasis and atrophy. Values were normalized to the lowest expressing sample and plotted as mean \pm SD. n = 3 samples/group (atrophy cells were pooled from multiple mice). Significance was determined by two-way ANOVA and Sidak's multiple comparisons test. (D and E) Sorted KRT20-tdT⁺ and KRT20-tdT⁻ cells were cultured in Matrigel with 50% L-WRN conditioned media. Bright-field images of spheroids were taken on day 6 after plating (D). Insets were enhanced for contrast. Bar: 1000 μ m. Spheroid formation efficiency = number of spheroids formed on day 6 over number of seeded cells on day 0 (E). Values were plotted as mean \pm SD. n = 7 mice/group.

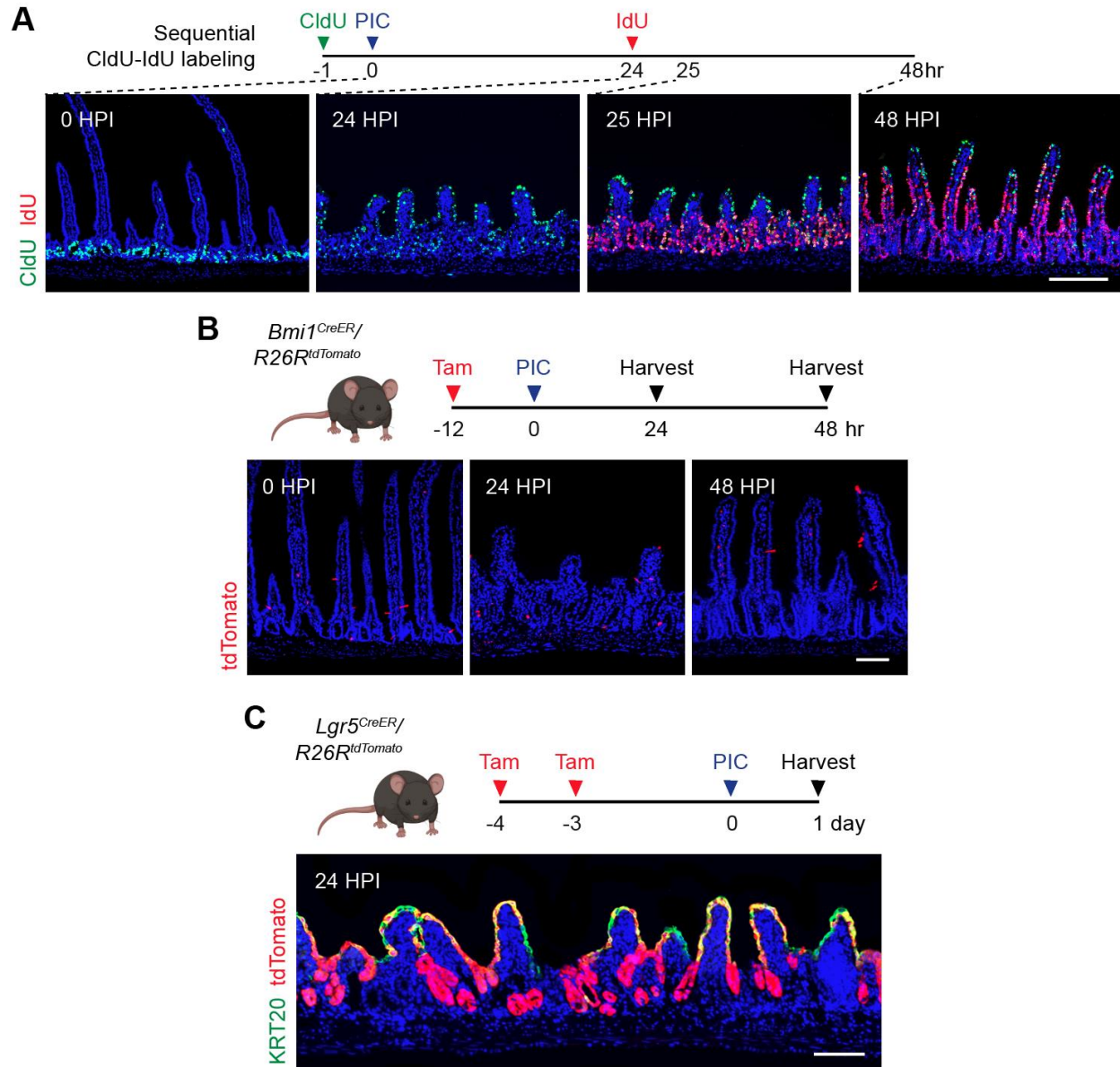


Figure 3.14. aVECs arise from transit-amplifying cells

(A) Assessment of epithelial turnover dynamics. CldU was injected 1 h prior to poly(I:C) injection, and IdU was injected at 24 HPI. IF for CldU (green) and IdU (red) at the indicated time points. Bar: 200 μ m. (B and C) Lineage tracing of BMI1⁺ cells and LGR5-progeny cells during villus injury-repair. BMI1⁺ cells were labeled with tamoxifen 12 h prior to poly(I:C) injection in *Bmi1^{CreER}/R26R^{tdTomato}* mice (B). LGR5-progenies were labeled following tamoxifen-mediated tracing of LGR5⁺ ISCs 3-4 days prior to poly(I:C) injection in *Lgr5^{CreER}/R26R^{tdTomato}* mice (C). The contribution of each cell population to aVECs at 24 HPI and villus regeneration at 48 HPI (for BMI1⁺ cells) are shown. LGR5-progenies are the major source of aVECs (note colocalization with KRT20). Images are representative of at least 4 animals. Bars: 100 μ m.

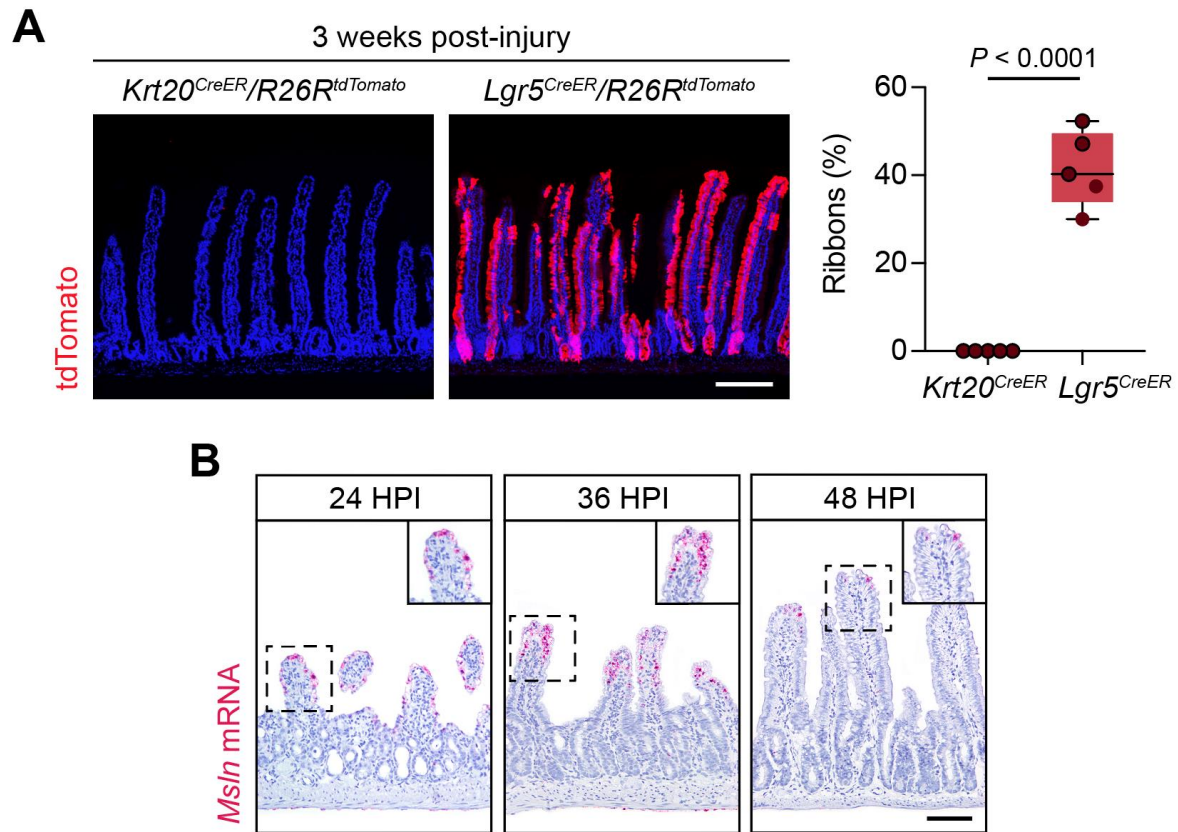


Figure 3.15. aVECs are short-lived and transiently cover damaged villi

(A) Transiently labeled tdT⁺ cells from *Krt20^{CreER}/R26R^{tdTomato}* and *Lgr5^{CreER}/R26R^{tdTomato}* mice were examined 3 weeks post-injury. Bar: 200 μ m. Percentage of ribbons across 50 crypt-villus units was quantified and plotted as a box-whisker plot. n = 5 mice/group. Significance was determined by unpaired *t*-test. (B) RNAscope for *Msln* at the indicated time points. Bar: 100 μ m.

3.6 Tables

Table 3.1. Primers used for qRT-PCR, related to Figure 3.13

<u>Primer Name</u>	<u>Species</u>	<u>Primer Sequence (5' to 3')</u>	<u>Primer Length</u>	<u>Tm (°C)</u>	<u>GC (%)</u>	<u>Product Size</u>	<u>Target</u>	<u>RefSeq</u>
Ace2-F	Mouse	CACTGAAGCTGGGCAGAAGT	20	60.25	55.00	146	Exon 13	NM_001130513
Ace2-R	Mouse	TCAGCCAGTCAAACAACGGT	20	60.11	50.00	146	Exon 14	NM_001130513
B2m-F	Mouse	TTCTGGTGCTTGCTCACTGA	21	59.24	47.62	104	Exon 1	NM_009735
B2m-R	Mouse	CAGTATGTTCCGGCTTCCCATTCC	22	59.39	50.00	104	Exon 2	NM_009735
Clu-F	Mouse	GCTGCTGATCTGGGACAATG	20	58.98	55.00	89	Exon 2	NM_013492
Clu-R	Mouse	ACCTACTCCCTTGAGTGGACA	21	59.85	52.38	89	Exon 3	NM_013492
Lgr5-F	Mouse	CCTACTCGAAGACTTACCCAGT	22	58.65	50.00	165	Exon 12	NM_010195
Lgr5-R	Mouse	GCATTGGGGTGAATGATAGCA	21	58.69	47.62	165	Exon 14	NM_010195
Msln-F	Mouse	GGTCCTGTGGAAGTCCCATCT	21	61.18	57.14	97	Exon 1	NM_018857
Msln-R	Mouse	CTTGCTTTGTAGTCTGGGTCTGC	24	61.33	50.00	97	Exon 2	NM_018857

3.7 References

- Allaire, J.M., Crowley, S.M., Law, H.T., Chang, S.Y., Ko, H.J., and Vallance, B.A. (2018). The Intestinal Epithelium: Central Coordinator of Mucosal Immunity. *Trends Immunol* 39, 677-696.
- Andersen, C.L., Schepeler, T., Thorsen, K., Birkenkamp-Demtroder, K., Mansilla, F., Aaltonen, L.A., Laurberg, S., and Orntoft, T.F. (2007). Clusterin expression in normal mucosa and colorectal cancer. *Mol Cell Proteomics* 6, 1039-1048.
- Arvanitakis, C. (1979). Abnormalities of jejunal mucosal enzymes in ulcerative colitis and Crohn's disease. *Digestion* 19, 259-266.
- Ayyaz, A., Kumar, S., Sangiorgi, B., Ghoshal, B., Gosio, J., Ouladan, S., Fink, M., Barutcu, S., Trcka, D., Shen, J., *et al.* (2019). Single-cell transcriptomes of the regenerating intestine reveal a revival stem cell. *Nature* 569, 121-125.
- Bahar Halpern, K., Massalha, H., Zwick, R.K., Moor, A.E., Castillo-Azofeifa, D., Rozenberg, M., Farack, L., Egozi, A., Miller, D.R., Averbukh, I., *et al.* (2020). Lgr5⁺ telocytes are a signaling source at the intestinal villus tip. *Nat Commun* 11, 1936.
- Banerjee, A., McKinley, E.T., von Moltke, J., Coffey, R.J., and Lau, K.S. (2018). Interpreting heterogeneity in intestinal tuft cell structure and function. *J Clin Invest* 128, 1711-1719.
- Barker, N., van Es, J.H., Kuipers, J., Kujala, P., van den Born, M., Cozijnsen, M., Haegebarth, A., Korving, J., Begthel, H., Peters, P.J., *et al.* (2007). Identification of stem cells in small intestine and colon by marker gene Lgr5. *Nature* 449, 1003-1007.
- Becht, E., McInnes, L., Healy, J., Dutertre, C.A., Kwok, I.W.H., Ng, L.G., Ginhoux, F., and Newell, E.W. (2018). Dimensionality reduction for visualizing single-cell data using UMAP. *Nat Biotechnol*.
- Beumer, J., and Clevers, H. (2016). Regulation and plasticity of intestinal stem cells during homeostasis and regeneration. *Development* 143, 3639-3649.
- Beumer, J., and Clevers, H. (2021). Cell fate specification and differentiation in the adult mammalian intestine. *Nat Rev Mol Cell Biol* 22, 39-53.
- Bishop, R.F., Davidson, G.P., Holmes, I.H., and Ruck, B.J. (1973). Virus particles in epithelial cells of duodenal mucosa from children with acute non-bacterial gastroenteritis. *Lancet* 2, 1281-1283.
- Bosca, M.M., Anon, R., Mayordomo, E., Villagrasa, R., Balza, N., Amoros, C., Corts, J.R., and Benages, A. (2008). Methotrexate induced sprue-like syndrome. *World J Gastroenterol* 14, 7009-7011.

- Butler, A., Hoffman, P., Smibert, P., Papalexi, E., and Satija, R. (2018). Integrating single-cell transcriptomic data across different conditions, technologies, and species. *Nat Biotechnol* *36*, 411-420.
- Caio, G., Volta, U., Sapone, A., Leffler, D.A., De Giorgio, R., Catassi, C., and Fasano, A. (2019). Celiac disease: a comprehensive current review. *BMC Med* *17*, 142.
- Camargo, S.M., Singer, D., Makrides, V., Huggel, K., Pos, K.M., Wagner, C.A., Kuba, K., Danilczyk, U., Skovby, F., Kleta, R., *et al.* (2009). Tissue-specific amino acid transporter partners ACE2 and collectrin differentially interact with hartnup mutations. *Gastroenterology* *136*, 872-882.
- Chen, E.Y., Tan, C.M., Kou, Y., Duan, Q., Wang, Z., Meirelles, G.V., Clark, N.R., and Ma'ayan, A. (2013). Enrichr: interactive and collaborative HTML5 gene list enrichment analysis tool. *BMC Bioinformatics* *14*, 128.
- Crawley, S.W., Mooseker, M.S., and Tyska, M.J. (2014). Shaping the intestinal brush border. *J Cell Biol* *207*, 441-451.
- Cruz-Garcia, L., and Schlegel, A. (2014). Lxr-driven enterocyte lipid droplet formation delays transport of ingested lipids. *J Lipid Res* *55*, 1944-1958.
- Csillag, C., Nielsen, O.H., Vainer, B., Olsen, J., Dieckgraefe, B.K., Hendel, J., Vind, I., Dupuy, C., Nielsen, F.C., and Borup, R. (2007). Expression of the genes dual oxidase 2, lipocalin 2 and regenerating islet-derived 1 alpha in Crohn's disease. *Scand J Gastroenterol* *42*, 454-463.
- Di Sabatino, A., Ciccocioppo, R., Luinetti, O., Ricevuti, L., Morera, R., Cifone, M.G., Solcia, E., and Corazza, G.R. (2003). Increased enterocyte apoptosis in inflamed areas of Crohn's disease. *Dis Colon Rectum* *46*, 1498-1507.
- Dotsenko, V., Oittinen, M., Taavela, J., Popp, A., Peraaho, M., Staff, S., Sarin, J., Leon, F., Isola, J., Maki, M., *et al.* (2021). Genome-Wide Transcriptomic Analysis of Intestinal Mucosa in Celiac Disease Patients on a Gluten-Free Diet and Postgluten Challenge. *Cell Mol Gastroenterol Hepatol* *11*, 13-32.
- Ducloux, D., Ottignon, Y., Semhoun-Ducloux, S., Labbe, S., Saint-Hillier, Y., Miguet, J.P., Carayon, P., and Chalopin, J.M. (1998). Mycophenolate mofetil-induced villous atrophy. *Transplantation* *66*, 1115-1116.
- Egberts, H.J., Koninkx, J.F., van Dijk, J.E., and Mouwen, J.M. (1984). Biological and pathobiological aspects of the glycocalyx of the small intestinal epithelium. A review. *Vet Q* *6*, 186-199.
- Elmentaite, R., Ross, A.D.B., Roberts, K., James, K.R., Ortmann, D., Gomes, T., Nayak, K., Tuck, L., Pritchard, S., Bayraktar, O.A., *et al.* (2020). Single-Cell Sequencing of Developing Human Gut Reveals Transcriptional Links to Childhood Crohn's Disease. *Dev Cell* *55*, 771-783 e775.

Fernandez Vallone, V., Leprovots, M., Strollo, S., Vasile, G., Lefort, A., Libert, F., Vassart, G., and Garcia, M.I. (2016). Trop2 marks transient gastric fetal epithelium and adult regenerating cells after epithelial damage. *Development* *143*, 1452-1463.

Fuchs, E., Tumber, T., and Guasch, G. (2004). Socializing with the neighbors: stem cells and their niche. *Cell* *116*, 769-778.

Gajda, A.M., and Storch, J. (2015). Enterocyte fatty acid-binding proteins (FABPs): different functions of liver and intestinal FABPs in the intestine. *Prostaglandins Leukot Essent Fatty Acids* *93*, 9-16.

Gajendran, M., Loganathan, P., Catinella, A.P., and Hashash, J.G. (2018). A comprehensive review and update on Crohn's disease. *Dis Mon* *64*, 20-57.

Galvagni, F., Orlandini, M., and Oliviero, S. (2013). Role of the AP-1 transcription factor FOSL1 in endothelial cells adhesion and migration. *Cell Adh Migr* *7*, 408-411.

Gehart, H., and Clevers, H. (2019). Tales from the crypt: new insights into intestinal stem cells. *Nat Rev Gastroenterol Hepatol* *16*, 19-34.

Gregorieff, A., Liu, Y., Inanlou, M.R., Khomchuk, Y., and Wrana, J.L. (2015). Yap-dependent reprogramming of Lgr5(+) stem cells drives intestinal regeneration and cancer. *Nature* *526*, 715-718.

Grossmann, J., Walther, K., Artinger, M., Kiessling, S., and Scholmerich, J. (2001). Apoptotic signaling during initiation of detachment-induced apoptosis ("anoikis") of primary human intestinal epithelial cells. *Cell Growth Differ* *12*, 147-155.

Guiu, J., Hannezo, E., Yui, S., Demharter, S., Ulyanchenko, S., Maimets, M., Jorgensen, A., Perlman, S., Lundvall, L., Mamsen, L.S., *et al.* (2019). Tracing the origin of adult intestinal stem cells. *Nature* *570*, 107-111.

Haber, A.L., Biton, M., Rogel, N., Herbst, R.H., Shekhar, K., Smillie, C., Burgin, G., Delorey, T.M., Howitt, M.R., Katz, Y., *et al.* (2017). A single-cell survey of the small intestinal epithelium. *Nature* *551*, 333-339.

Haberman, Y., Tickle, T.L., Dexheimer, P.J., Kim, M.O., Tang, D., Karns, R., Baldassano, R.N., Noe, J.D., Rosh, J., Markowitz, J., *et al.* (2014). Pediatric Crohn disease patients exhibit specific ileal transcriptome and microbiome signature. *J Clin Invest* *124*, 3617-3633.

Heazlewood, C.K., Cook, M.C., Eri, R., Price, G.R., Tauro, S.B., Taupin, D., Thornton, D.J., Png, C.W., Crockford, T.L., Cornall, R.J., *et al.* (2008). Aberrant mucin assembly in mice causes endoplasmic reticulum stress and spontaneous inflammation resembling ulcerative colitis. *PLoS Med* *5*, e54.

- Hinnebusch, B.F., Ma, Q., Henderson, J.W., Siddique, A., Archer, S.Y., and Hodin, R.A. (2002). Enterocyte response to ischemia is dependent on differentiation state. *J Gastrointest Surg* 6, 403-409.
- Holmes, R., and Lobley, R.W. (1989). Intestinal brush border revisited. *Gut* 30, 1667-1678.
- Ingle, H., Hassan, E., Gawron, J., Mihi, B., Li, Y., Kennedy, E.A., Kalugotla, G., Makimaa, H., Lee, S., Desai, P., *et al.* (2021). Murine astrovirus tropism for goblet cells and enterocytes facilitates an IFN-lambda response in vivo and in enteroid cultures. *Mucosal Immunol* 14, 751-761.
- Iqbal, J., and Hussain, M.M. (2009). Intestinal lipid absorption. *Am J Physiol Endocrinol Metab* 296, E1183-1194.
- Ito, G., Okamoto, R., Murano, T., Shimizu, H., Fujii, S., Nakata, T., Mizutani, T., Yui, S., Akiyama-Morio, J., Nemoto, Y., *et al.* (2013). Lineage-specific expression of bestrophin-2 and bestrophin-4 in human intestinal epithelial cells. *PLoS One* 8, e79693.
- Kaelberer, M.M., Buchanan, K.L., Klein, M.E., Barth, B.B., Montoya, M.M., Shen, X., and Bohorquez, D.V. (2018). A gut-brain neural circuit for nutrient sensory transduction. *Science* 361.
- Kamal, M., Dehlawi, M.S., Brunet, L.R., and Wakelin, D. (2002). Paneth and intermediate cell hyperplasia induced in mice by helminth infections. *Parasitology* 125, 275-281.
- Kaser, A., Lee, A.H., Franke, A., Glickman, J.N., Zeissig, S., Tilg, H., Nieuwenhuis, E.E., Higgins, D.E., Schreiber, S., Glimcher, L.H., *et al.* (2008). XBP1 links ER stress to intestinal inflammation and confers genetic risk for human inflammatory bowel disease. *Cell* 134, 743-756.
- Kent, T.H., and Moon, H.W. (1973). The Comparative Pathogenesis of Some Enteric Diseases. Based on Cases Presented at the 22nd Annual Seminar of the American College of Veterinary Pathologists. *Veterinary Pathology* 10, 414-469.
- Kerzner, B., Kelly, M.H., Gall, D.G., Butler, D.G., and Hamilton, J.R. (1977). Transmissible gastroenteritis: sodium transport and the intestinal epithelium during the course of viral enteritis. *Gastroenterology* 72, 457-461.
- Kuleshov, M.V., Jones, M.R., Rouillard, A.D., Fernandez, N.F., Duan, Q., Wang, Z., Koplev, S., Jenkins, S.L., Jagodnik, K.M., Lachmann, A., *et al.* (2016). Enrichr: a comprehensive gene set enrichment analysis web server 2016 update. *Nucleic Acids Res* 44, W90-97.
- Kwo, P.Y., and Tremaine, W.J. (1995). Nonsteroidal anti-inflammatory drug-induced enteropathy: case discussion and review of the literature. *Mayo Clin Proc* 70, 55-61.

Li, G., Gustafson-Brown, C., Hanks, S.K., Nason, K., Arbeit, J.M., Pogliano, K., Wisdom, R.M., and Johnson, R.S. (2003). c-Jun is essential for organization of the epidermal leading edge. *Dev Cell* 4, 865-877.

Loberman-Nachum, N., Sosnovski, K., Di Segni, A., Efroni, G., Braun, T., BenShoshan, M., Anafi, L., Avivi, C., Barshack, I., Shouval, D.S., *et al.* (2019). Defining the Celiac Disease Transcriptome using Clinical Pathology Specimens Reveals Biologic Pathways and Supports Diagnosis. *Sci Rep* 9, 16163.

Machado, L., Geara, P., Camps, J., Dos Santos, M., Teixeira-Clerc, F., Van Herck, J., Varet, H., Legendre, R., Pawlowsky, J.M., Sampaolesi, M., *et al.* (2021). Tissue damage induces a conserved stress response that initiates quiescent muscle stem cell activation. *Cell Stem Cell* 28, 1125-1135 e1127.

Magness, S.T., Puthoff, B.J., Crissey, M.A., Dunn, J., Henning, S.J., Houchen, C., Kaddis, J.S., Kuo, C.J., Li, L., Lynch, J., *et al.* (2013). A multicenter study to standardize reporting and analyses of fluorescence-activated cell-sorted murine intestinal epithelial cells. *Am J Physiol Gastrointest Liver Physiol* 305, G542-551.

Mallick, I.H., Yang, W., Winslet, M.C., and Seifalian, A.M. (2004). Ischemia-reperfusion injury of the intestine and protective strategies against injury. *Dig Dis Sci* 49, 1359-1377.

Malliri, A., Symons, M., Hennigan, R.F., Hurlstone, A.F., Lamb, R.F., Wheeler, T., and Ozanne, B.W. (1998). The transcription factor AP-1 is required for EGF-induced activation of rho-like GTPases, cytoskeletal rearrangements, motility, and in vitro invasion of A431 cells. *J Cell Biol* 143, 1087-1099.

Mercer, J., Eagles, M.E., and Talbot, I.C. (1990). Brush border enzymes in coeliac disease: histochemical evaluation. *J Clin Pathol* 43, 307-312.

Miyoshi, H., and Stappenbeck, T.S. (2013). In vitro expansion and genetic modification of gastrointestinal stem cells in spheroid culture. *Nat Protoc* 8, 2471-2482.

Miyoshi, H., VanDussen, K.L., Malvin, N.P., Ryu, S.H., Wang, Y., Sonnek, N.M., Lai, C.W., and Stappenbeck, T.S. (2017). Prostaglandin E2 promotes intestinal repair through an adaptive cellular response of the epithelium. *EMBO J* 36, 5-24.

Moor, A.E., Harnik, Y., Ben-Moshe, S., Massasa, E.E., Rozenberg, M., Eilam, R., Bahar Halpern, K., and Itzkovitz, S. (2018). Spatial Reconstruction of Single Enterocytes Uncovers Broad Zonation along the Intestinal Villus Axis. *Cell* 175, 1156-1167 e1115.

Moss, S.F., Attia, L., Scholes, J.V., Walters, J.R., and Holt, P.R. (1996). Increased small intestinal apoptosis in coeliac disease. *Gut* 39, 811-817.

Mustata, R.C., Vasile, G., Fernandez-Vallone, V., Strollo, S., Lefort, A., Libert, F., Monteyne, D., Perez-Morga, D., Vassart, G., and Garcia, M.I. (2013). Identification of Lgr5-independent spheroid-generating progenitors of the mouse fetal intestinal epithelium. *Cell Rep* 5, 421-432.

- Nowarski, R., Jackson, R., Gagliani, N., de Zoete, M.R., Palm, N.W., Bailis, W., Low, J.S., Harman, C.C., Graham, M., Elinav, E., *et al.* (2015). Epithelial IL-18 Equilibrium Controls Barrier Function in Colitis. *Cell* 163, 1444-1456.
- Nusse, Y.M., Savage, A.K., Marangoni, P., Rosendahl-Huber, A.K.M., Landman, T.A., de Sauvage, F.J., Locksley, R.M., and Klein, O.D. (2018). Parasitic helminths induce fetal-like reversion in the intestinal stem cell niche. *Nature* 559, 109-113.
- Nystrom, E.E.L., Martinez-Abad, B., Arike, L., Birchenough, G.M.H., Nonnecke, E.B., Castillo, P.A., Svensson, F., Bevins, C.L., Hansson, G.C., and Johansson, M.E.V. (2021). An intercrypt subpopulation of goblet cells is essential for colonic mucus barrier function. *Science* 372.
- Parikh, K., Antanaviciute, A., Fawcner-Corbett, D., Jagielowicz, M., Aulicino, A., Lagerholm, C., Davis, S., Kinchen, J., Chen, H.H., Alham, N.K., *et al.* (2019). Colonic epithelial cell diversity in health and inflammatory bowel disease. *Nature* 567, 49-55.
- Patankar, J.V., and Becker, C. (2020). Cell death in the gut epithelium and implications for chronic inflammation. *Nat Rev Gastroenterol Hepatol* 17, 543-556.
- Pecache, N., Patole, S., Hagan, R., Hill, D., Charles, A., and Papadimitriou, J.M. (2004). Neonatal congenital microvillus atrophy. *Postgrad Med J* 80, 80-83.
- Pensaert, M., Haelterman, E.O., and Burnstein, T. (1970). Transmissible gastroenteritis of swine: virus-intestinal cell interactions. I. Immunofluorescence, histopathology and virus production in the small intestine through the course of infection. *Arch Gesamte Virusforsch* 31, 321-334.
- Prasad, K.K., Thapa, B.R., Nain, C.K., Sharma, A.K., and Singh, K. (2008). Brush border enzyme activities in relation to histological lesion in pediatric celiac disease. *J Gastroenterol Hepatol* 23, e348-352.
- Ramig, R.F. (2004). Pathogenesis of intestinal and systemic rotavirus infection. *J Virol* 78, 10213-10220.
- Rinkevich, Y., Mori, T., Sahoo, D., Xu, P.X., Bermingham, J.R., Jr., and Weissman, I.L. (2012). Identification and prospective isolation of a mesothelial precursor lineage giving rise to smooth muscle cells and fibroblasts for mammalian internal organs, and their vasculature. *Nat Cell Biol* 14, 1251-1260.
- Schuffler, M.D., and Chaffee, R.G. (1979). Small intestinal biopsy in a patient with Crohn's disease of the duodenum. The spectrum of abnormal findings in the absence of granulomas. *Gastroenterology* 76, 1009-1014.
- Shepherd, A.P., and Kiel, J.W. (1992). A model of countercurrent shunting of oxygen in the intestinal villus. *Am J Physiol* 262, H1136-1142.
- Shiner, M., and Birbeck, M.S. (1961). The microvilli of the small intestinal surface epithelium in coeliac disease and in idiopathic steatorrhea. *Gut* 2, 277-284.

Smillie, C.S., Biton, M., Ordovas-Montanes, J., Sullivan, K.M., Burgin, G., Graham, D.B., Herbst, R.H., Rogel, N., Slyper, M., Waldman, J., *et al.* (2019). Intra- and Inter-cellular Rewiring of the Human Colon during Ulcerative Colitis. *Cell* *178*, 714-730 e722.

Specian, R.D., and Oliver, M.G. (1991). Functional biology of intestinal goblet cells. *Am J Physiol* *260*, C183-193.

Sprangers, J., Zaalberg, I.C., and Maurice, M.M. (2021). Organoid-based modeling of intestinal development, regeneration, and repair. *Cell Death Differ* *28*, 95-107.

Subramanian, A., Tamayo, P., Mootha, V.K., Mukherjee, S., Ebert, B.L., Gillette, M.A., Paulovich, A., Pomeroy, S.L., Golub, T.R., Lander, E.S., *et al.* (2005). Gene set enrichment analysis: a knowledge-based approach for interpreting genome-wide expression profiles. *Proc Natl Acad Sci U S A* *102*, 15545-15550.

Sun, S., Zhu, J., Ma, Y., and Zhou, X. (2019). Accuracy, robustness and scalability of dimensionality reduction methods for single-cell RNA-seq analysis. *Genome Biol* *20*, 269.

Tamagawa, H., Takahashi, I., Furuse, M., Yoshitake-Kitano, Y., Tsukita, S., Ito, T., Matsuda, H., and Kiyono, H. (2003). Characteristics of claudin expression in follicle-associated epithelium of Peyer's patches: preferential localization of claudin-4 at the apex of the dome region. *Lab Invest* *83*, 1045-1053.

Tran, Q.T., Kennedy, L.H., Leon Carrion, S., Bodreddigari, S., Goodwin, S.B., Sutter, C.H., and Sutter, T.R. (2012). EGFR regulation of epidermal barrier function. *Physiol Genomics* *44*, 455-469.

Tu, Y.H., Cooper, A.J., Teng, B., Chang, R.B., Artiga, D.J., Turner, H.N., Mulhall, E.M., Ye, W., Smith, A.D., and Liman, E.R. (2018). An evolutionarily conserved gene family encodes proton-selective ion channels. *Science* *359*, 1047-1050.

Van der Sluis, M., De Koning, B.A., De Bruijn, A.C., Velcich, A., Meijerink, J.P., Van Goudoever, J.B., Buller, H.A., Dekker, J., Van Seuningen, I., Renes, I.B., *et al.* (2006). Muc2-deficient mice spontaneously develop colitis, indicating that MUC2 is critical for colonic protection. *Gastroenterology* *131*, 117-129.

VanDussen, K.L., Stojmirovic, A., Li, K., Liu, T.C., Kimes, P.K., Muegge, B.D., Simpson, K.F., Ciorba, M.A., Perrigoue, J.G., Friedman, J.R., *et al.* (2018). Abnormal Small Intestinal Epithelial Microvilli in Patients With Crohn's Disease. *Gastroenterology* *155*, 815-828.

Vogel, G.F., Hess, M.W., Pfaller, K., Huber, L.A., Janecke, A.R., and Muller, T. (2016). Towards understanding microvillus inclusion disease. *Mol Cell Pediatr* *3*, 3.

Wang, Y., Chiang, I.L., Ohara, T.E., Fujii, S., Cheng, J., Muegge, B.D., Ver Heul, A., Han, N.D., Lu, Q., Xiong, S., *et al.* (2019). Long-Term Culture Captures Injury-Repair Cycles of Colonic Stem Cells. *Cell* *179*, 1144-1159 e1115.

Wang, Y., Song, W., Wang, J., Wang, T., Xiong, X., Qi, Z., Fu, W., Yang, X., and Chen, Y.G. (2020). Single-cell transcriptome analysis reveals differential nutrient absorption functions in human intestine. *J Exp Med* 217.

Xia, L., Yang, Y., Wang, J., Jing, Y., and Yang, Q. (2018). Impact of TGEV infection on the pig small intestine. *Virology* 15, 102.

Yui, S., Azzolin, L., Maimets, M., Pedersen, M.T., Fordham, R.P., Hansen, S.L., Larsen, H.L., Guiu, J., Alves, M.R.P., Rundsten, C.F., *et al.* (2018). YAP/TAZ-Dependent Reprogramming of Colonic Epithelium Links ECM Remodeling to Tissue Regeneration. *Cell Stem Cell* 22, 35-49 e37.

Zang, R., Gomez Castro, M.F., McCune, B.T., Zeng, Q., Rothlauf, P.W., Sonnek, N.M., Liu, Z., Brulois, K.F., Wang, X., Greenberg, H.B., *et al.* (2020). TMPRSS2 and TMPRSS4 promote SARS-CoV-2 infection of human small intestinal enterocytes. *Sci Immunol* 5.

Zheng, L., Kelly, C.J., and Colgan, S.P. (2015). Physiologic hypoxia and oxygen homeostasis in the healthy intestine. A Review in the Theme: Cellular Responses to Hypoxia. *Am J Physiol Cell Physiol* 309, C350-360.

Ziegler, T.R., Fernandez-Estivariz, C., Gu, L.H., Fried, M.W., and Leader, L.M. (2003). Severe villus atrophy and chronic malabsorption induced by azathioprine. *Gastroenterology* 124, 1950-1957.

Chapter 4

YAP Signaling Mediates Intestinal Barrier Re-establishment

4.1 Introduction

The intestinal tract exhibits an impressive capacity for repair after severe tissue damage. In the small intestine, where zones of proliferation and differentiation are anatomically separated, majority of studies have been focused on the regenerative response to stem cell or crypt loss. This has been extensively studied using the irradiation, LGR5-diphtheria toxin receptor (DTR), and graft-versus-host disease models (Kim et al., 2017; Metcalfe et al., 2014; Takashima et al., 2011; Tian et al., 2011). Understanding the mechanism behind crypt regeneration is important, as widespread crypt loss can result in intestinal failure and mortality (Kuhnert et al., 2004).

Importantly, LGR5⁺ ISC^s have been shown to be essential for radiation-induced epithelial regeneration (Metcalfe et al., 2014). This was surprising because LGR5⁺ ISC^s are largely thought to be dispensable for intestinal homeostasis, with other cells capable of taking over their stem cell function (Tian et al., 2011). It is therefore critical to recover the LGR5⁺ ISC pool during regeneration, and the mechanism behind this has been a subject of great interest. Initially, the predominant theory was that radioresistant +4 reserved ISC^s, marked by the expression of BMI1, LRIG1, HOPX, mTERT, and SOX9^{high}, were the major source of LGR5⁺ ISC after injury (Bankaitis et al., 2018; Yan et al., 2012). However, many subsequent studies thereafter have identified additional cell types with the ability to revert to a stem-like state. These cells include secretory and enterocyte progenitors and even fully mature enteroendocrine and Paneth cells (Beumer and Clevers, 2021). These studies have also called into question the identity of the +4 cells. Originally, +4 stem cells were defined by their slow cycling nature—the so-called label-retaining cells (LRCs) (Potten, 1977). However, with the availability of elegant genetic tools, intestinal LRCs have been defined to be secretory precursor cells (Buczacki et al., 2013). Additional +4 markers continue to expand today, including MEX3A and CLU, further

complicating the identity of these cells (Ayyaz et al., 2019; Barriga et al., 2017). It is likely that a heterogeneous population of cells exist at the +4 position, including various precursor cells and secretory cell types. Furthermore, a recent study has concluded that ISC regeneration is explained almost entirely by dedifferentiation of LGR5-progenitor cells (Murata et al., 2020). Therefore, ISC restoration relies predominantly on the plasticity of intestinal progenitors.

The colon, on the other hand, lacks villi and is instead made up of taller crypt units. While stem or progenitor cell-specific ablation can occur, for example after irradiation or chemotherapy treatment, often colonic injuries result in entire loss of crypt structures. Such wounds or ulcers can form in the small intestine as well, but these types of injuries have been more extensively studied in the colon. In contrast to the small intestine, the focus here is less on ISC regeneration and more on crypt reconstitution. Interestingly, during colonic inflammation induced by dextran sodium sulfate (DSS), LGR5⁺ ISCs are dispensable for repair (Metcalf et al., 2014). To better understand colonic wound repair, we and others have utilized an endoscopy-guided, biopsy forceps-mediated focal removal of the colonic mucosa (Seno et al., 2009). In comparison to chemical or infectious colitis, this biopsy injury system allows for far greater control over the location, timing, and degree of damage. Studies of these biopsy-generated wounds have revealed that colonic repair occurs through three distinct phases. In the first phase, CLDN4⁺ wound-associated epithelial (WAE) cells emerge from the adjacent crypts and cover the wound bed (Manieri et al., 2012; Seno et al., 2009). This step is independent of cell proliferation, primarily involving the migration of WAE cells, and has been traditionally referred to as restitution (Sturm and Dignass, 2008). In the second phase, there is extensive cell proliferation in the adjacent crypts that result in the formation of wound channels (Miyoshi et al., 2012). Finally, in the third phase, wound channels get partitioned into individual crypt structures.

This is achieved through focal inhibition of cell proliferation within the wound channel by WNT5A⁺ mesenchymal cells (Miyoshi et al., 2012). Due to the fact that entire epithelial structures (i.e. crypts) often need to be reconstructed following colonic injury, the repair process is generally much more involved and complex than simply restoring the ISC pool.

In determining what factors are essential for repair in adult animals, a growing body of work has recognized the Hippo signaling pathway as one of the most prominent regulators of tissue and organ regeneration. During development, the Hippo pathway negatively regulates organ size (Yu et al., 2015). Loss of the Hippo kinases, such as MST1/2, SAV1, and LATS1/2, results in a dramatic overgrowth phenotype in multiple organs (Yu et al., 2015). Importantly, the Hippo kinases work by actively inhibiting the activity of YAP and TAZ (YAP/TAZ) (Moya and Halder, 2019). YAP/TAZ are thus key effectors of the Hippo pathway and are largely thought to function by regulating gene transcription. However, YAP/TAZ do not bind DNA directly; instead they serve as transcriptional co-activators and bind to transcription factors, most notably the TEAD family of transcription factors (Dey et al., 2020). TEADs are the major partners of YAP and bind to a conserved sequence motif (Lin et al., 2017). Besides TEADs, YAP/TAZ have been shown to interact with a number of other transcription factors, including AP-1, SMADs, RUNX, and β -catenin (Yu et al., 2015). Unlike many of the other developmental pathways, there are no family of ligands or receptors that is specific to the Hippo pathway. Various cell-extrinsic cues have been shown to modulate YAP/TAZ activity, including mechanotransduction and inflammatory cytokines (Mohri et al., 2017; Zhou et al., 2018). Thus, YAP/TAZ act as sensors for changes in the microenvironment with the potential to influence many biological processes.

In general, YAP/TAZ act to promote proliferation and stem cell properties during tissue development, homeostasis, and regeneration. In the skin, YAP is required to maintain the basal

epidermal progenitor cell population at steady state (Zhang et al., 2011). In other organs, such as the liver and heart, YAP/TAZ have a more pronounced role in development and regeneration (Lu et al., 2018; Xin et al., 2013). In the intestine, YAP/TAZ appears to be largely dispensable for the development or homeostasis of this tissue. In contrast, YAP/TAZ is essential for intestinal regeneration and tumorigenesis (Gregorieff et al., 2015; Hong et al., 2016). When and how YAP/TAZ activity is induced or inhibited currently remain an area of intense investigation.

In the gut, majority of studies have focused on the role of YAP during intestinal regeneration. Following DSS or irradiation-induced injury, YAP localizes to the nucleus in regenerating crypts and promote epithelial survival and/or proliferation (Cai et al., 2010; Gregorieff et al., 2015). Overexpression of YAP, generally by relieving its inhibition from the Hippo kinases, results in crypt expansion, impaired epithelial differentiation, and adenoma formation (Cai et al., 2010; Zhou et al., 2011), thus making YAP an oncogene. Consistent with this, YAP is absolutely essential for the development of APC-deficient tumors through interaction with the AXIN- β -catenin complex (Azzolin et al., 2014; Cai et al., 2015). On the other hand, studies have also identified growth and tumor suppressive functions of YAP. This body of work largely comes from the finding that YAP can inhibit Wnt signaling. During intestinal injury-repair, YAP has been shown to be a key player in the resolution phase of the regenerative response. Loss of YAP leads to hyperactive Wnt signaling, crypt expansion, and persistent regeneration (Barry et al., 2013). Furthermore, activation of YAP leads to loss of ISCs, cancer stem cells, and tumor regression (Cheung et al., 2020). These seemingly conflicting reports likely reflect the complex interplay between the Hippo and Wnt signaling pathways, as well as the differential response of ISCs and progenitor cells to YAP signaling (Li et al., 2020).

While dedifferentiation represents a predominant means for ISC recovery, injury-induced ISC states have been recognized as well (Murata et al., 2020; Rees et al., 2020). In the parasitic helminth infection model, induction of the granuloma-associated LGR5⁻ fetal-like ISC state is mediated by an interferon-gamma transcriptional program (Nusse et al., 2018). In the irradiation injury model, YAP appears to reprogram LGR5⁺ ISCs to a LGR5⁻ state and promote cell survival while simultaneously inhibiting Paneth cell differentiation (Gregorieff et al., 2015). In the absence of YAP, LGR5⁺ ISC persisted after injury followed by increased cell death and an expansion of Paneth cell numbers (Gregorieff et al., 2015). Interestingly, YAP has also been shown to expand a rare population of quiescent “revival” stem cells (revSCs) in response to irradiation (Ayyaz et al., 2019). In this scenario, a +4-like stem cell population marked by clusterin (CLU) expression greatly expands in numbers in a YAP-dependent fashion and reconstitutes the ISC pool. In the DSS colitis model, where there is drastic tissue remodeling following injury, YAP is implicated in reprogramming the epithelium to a fetal-like state as a result of changes in the extracellular matrix (Yui et al., 2018). Therefore, YAP’s function in the gut appears to be manifold. We summarize these findings in **Figure 4.1**. However, the precise mechanism by which YAP orchestrates repair has been complicated by its crosstalk with the Wnt, Notch, and EGF pathways in the crypt (Hong et al., 2016). This has made data interpretation difficult, leading to conclusions that are at times incongruent. It remains largely unknown whether induction of the fetal-like program is unique to regenerative stem cells, and whether YAP is functional in other contexts of injury independent of ISC or crypt damage.

4.2 Materials and Methods

Animals

C57BL/6J, *Lgr5-EGFP-IRES-CreERT2*, *Rosa-LSL-tdTomato*, *Vill-Cre*, *Vill-CreERT2*, *Krt20-T2A-CreERT2*, and *Yap^{fllox}* mice were obtained from the Jackson Laboratory. *Yap^{fllox}* mice were further backcrossed to the C57BL/6J strain for more than 3 generations. Experiments that called for only wild-type mice used 8-week-old C57BL/6J male mice. All other experiments involving specific genetic strains used 7- to 10-week-old male and female mice with appropriate littermate controls. Mice were housed under specific pathogen-free conditions and were maintained on a strict 12 h light/dark cycle. All animal studies were conducted in compliance with protocols approved by the Washington University Institutional Animal Care and Use Committee.

Animal procedures

For intraperitoneal injections, the following reagents were prepared and administered at the indicated dose. 1 mg/mL poly(I:C) HMW (InvivoGen) was prepared in saline and 20 mg/kg was injected. 20 mg/mL tamoxifen (Sigma) was prepared in corn oil and 75 mg/kg was delivered. For intestinal permeability studies, mice were subjected to a 4 h fast, during which food, water, and bedding were withdrawn from the cage. 4-kDa FITC-dextran (Sigma) was dissolved in PBS to make 100mg/mL, and 44mg/100g was delivered by oral gavage. 3 h after gavage, blood was collected by cardiac puncture, and serum was obtained in Microtainer tubes (BD). FITC-dextran levels were measured based on a standard curve on the Cytation 5 instrument. For colonic biopsy injury, mucosal wounds were generated in the distal colon using biopsy forceps guided by a high-resolution miniaturized colonoscope as previously described (Seno et al., 2009).

Histology and immunostaining

The proximal small intestine was examined for histological studies. Intestinal tissues were pinned out and fixed in 10% neutral buffered formalin overnight at 4°C. Fixed samples were washed in 70% ethanol three times and embedded in 2% agar (Sigma). This was followed by paraffin embedding, sectioning, and hematoxylin & eosin staining. Unstained paraffin sections were de-paraffinized in xylene and rehydrated in isopropanol three times each. Antigen retrieval was performed in Trilogy solution (Sigma) for 20 min under boiling water. For immunohistochemistry (IHC), sections were additionally treated with 3% H₂O₂ in methanol to quench endogenous peroxidase activity. Slides were incubated in blocking solution (1% BSA/PBS containing 0.1% Triton X-100) for 1 h at room temperature before overnight treatment with primary antibodies diluted in blocking solution at 4°C. The following day, slides were treated with secondary antibodies diluted in blocking solution for 1 h at room temperature. For immunofluorescence (IF), sections were counterstained with Hoechst 33258 (Invitrogen) for 15 min and mounted in Fluoromount medium (Sigma). For IHC, sections were treated with VECTASTAIN Elite ABC-HRP Kit (Vector Laboratories), developed with DAB Peroxidase Substrate Kit (Vector Laboratories), counterstained with CAT hematoxylin (Biocare), and mounted in Cytoseal XYL (Thermo Scientific). Washes were performed in PBS. The following primary antibodies were used in this chapter: rabbit anti-Yap (Cell Signaling 14074), mouse anti-β-catenin (BD Transduction Laboratories 610154), rabbit anti-Cldn4 (Thermo Fisher 36-4800), rabbit anti-Car4 (gift from Dr. William Sly, St. Louis University), rabbit anti-Muc2 (Santa Cruz sc-15334), rabbit anti-RFP (Rockland 600-401-379), rabbit anti-cCasp3 (Cell Signaling 9664), rabbit anti-EpCAM (Abcam ab71916), guinea pig anti-Krt20 (Progen GP-K20), rabbit anti-Olfm4 (Cell Signaling 39141), rabbit anti-Lysozyme (Abcam ab108508), goat anti-Mmp7 (R&D

Systems AF2967), rabbit anti-Ki67 (Abcam ab15580), and goat anti-Ace2 (R&D Systems AF933). The following Thermo Fisher highly cross-absorbed IgG secondary antibodies were used in this chapter: goat anti-rabbit Biotin, donkey anti-mouse Alexa Fluor 488, donkey anti-rabbit Alexa Fluor 488/594, donkey anti-goat Alexa Fluor 488/594, and donkey anti-guinea pig Alexa Fluor 594. UEA1 (Vector Laboratories RL-1062-2) was used for goblet cell staining.

RNAscope in situ hybridization

Intestinal tissues were fixed in 4% PFA overnight at 4°C and then incubated in 20% sucrose/PBS overnight at 4°C. Fixed samples were cryo-embedded in O.C.T. and sectioned at 7 µm on a cryotome. *In situ* hybridization was carried out on frozen sections using a RNAscope 2.5 HD Assay-RED Kit (ACDBio) according to the manufacturer's instructions. The following probes were used in this chapter: *Clu* (427891), *Msln* (443241), *Areg* (430501), and *Ereg* (437981).

Imaging and quantification

Bright-field images were acquired with an Olympus BX51 microscope. Fluorescent images were acquired with a Zeiss Axiovert 200M inverted microscope and a Zeiss Axio Imager M2 Plus wide field fluorescent microscope. Whole mount images were acquired with an Olympus SZX12 stereo dissection microscope. The lengths of well-oriented villi/crypts were measured using the cellSens software (Olympus). For histology-based quantifications, each data point represents an average value across 30-50 well-oriented villi/crypts in the proximal small intestine per animal (see figure legends). Nearest neighbor distances (NNDs) were quantified on Fiji/ImageJ based on whole mount images using the NND plugin. Images were processed with Adobe Photoshop CC.

Comparative analysis of the aVEC and WAE LCM-microarray dataset

Microarray data from colonic WAE cells was previously reported and deposited (ArrayExpress E-MTAB-1175; Miyoshi et al., 2012). WAE cells (from day 2-4 post-injury) was compared with control cells (surface epithelium and control crypts from day 2-4 post-injury combined). Data normalization and differential gene expression analysis were performed on the Partek software. WAE and aVEC datasets were combined using Microsoft Excel and visualized with Graphpad Prism 8 or 9. Gene ontology analysis and transcription factor motif enrichment of signature genes were pulled from ToppGene Suite and Enrichr (Chen et al., 2013; Kuleshov et al., 2016).

Single-cell RNA-sequencing (scRNA-seq) and analysis

FACS purified IECs (see previous chapter for FACS process) were resuspended in 10% FBS in DMEM/F12 for single-cell capture and sequencing. Single-cell libraries were constructed using Chromium Single Cell 3' v3 reagents (10x Genomics) and sequenced on a NovaSeq6000 S4 system (Illumina) with around 50,000 reads per cell. Demultiplexing, alignment, and UMI (unique molecular identifier) counting were performed with Cell Ranger v4.0. For downstream analysis, filtered gene-barcode matrices generated by Cell Ranger were read into the Seurat package (v3.2.2) or Monocle 3 package (v0.2.3.0) on RStudio (v1.3.1056) (Butler et al., 2018; Cao et al., 2019; Trapnell et al., 2014). Plots generated were adjusted with ggplot2 and Adobe Illustrator CC. In Seurat, low-quality cells with high (>9,000) and low (<500) unique gene counts and high mitochondrial counts (>20%) were first filtered out. The resulting data was log-normalized, and paired samples were integrated. PCA scores were computed on scaled data based on 2,000 of the most highly variable features. The first 15 PCs were used for graph-based clustering (resolution = 0.2-0.3), which was visualized with UMAP-based dimensional reduction

(Becht et al., 2018). FindMarkers was used to identify cell types as well as to determine differentially expressed genes between *Yap^{fl/fl}* and *Yap^{AIEC}* cells. Immune cells (<1% of total cells) were removed from analysis. Gene expression levels were plotted with FeaturePlot, VlnPlot, and Dotplot functions. Enrichment of the fetal spheroid and YAP signatures were determined with the AddModuleScore function. GO analysis was performed with Enrichr. In Monocle 3, the standard PCA method with 100 PCs was adopted to normalize the data and remove batch effects. Dimensionality reduction was conducted with UMAP, and cells were clustered based on community detection (resolution = 0.5). Cell types were identified with top_markers and plot_cells functions. After learning the trajectory graph (learn_graph), cells were ordered in pseudotime (order_cells) and the root node was selected according to where ISC markers (i.e., *Olfm4*) were most highly expressed. The plot_genes_in_pseudotime function (minimum expression = 0.5) was used to visualize gene expression as a function of pseudotime.

Statistics and reproducibility

Statistical analyses were performed in GraphPad Prism 8 or 9. *P*-values are indicated in the plots or figure legends with *p* < 0.05 denoted as significant. Data are expressed as mean ± standard deviation (SD). An unpaired two-tailed Student's *t*-test was used when comparing two groups; a one-way ANOVA was used when comparing three or more groups; and a two-way ANOVA was used when comparing groups with two experimental variables. Data from independent experiments were pooled when possible. Otherwise, data are representative of at least two independent experiments. Animals that had near 0% weight loss one day after poly(I:C) injection (<10% of all mice) were excluded from the study as these mice did not exhibit intestinal damage. Further statistical details and quantification methods can be found in the figure legends.

Data and Code Availability

All sequencing data have been deposited in Gene Expression Omnibus (GEO) under the accession codes GSE168439 (for LCM-microarray) and GSE169718 (for scRNA-seq).

4.3 Results

YAP is activated in aVECs during villus repair

Immediately following poly(I:C)-induced villus injury, aVECs emerge and line the surface of damaged villi. Because aVECs express high levels of CLDN4, a tight junction protein involved in maintaining barrier integrity (Gunzel and Yu, 2013; Watari et al., 2017), and are enriched in wound healing-related programs (**Figure 3.2E**), we hypothesized that aVECs actively play a role in villus repair and barrier re-establishment. We tested intestinal permeability *in vivo* by measuring the serum levels of orally-gavaged FITC-dextran at different time points throughout the injury-repair process in the poly(I:C) model. Serum FITC-dextran levels peaked during the injury phase, reflecting barrier leakage, and returned to baseline levels during the atrophy phase, revealing that aVECs possess barrier restorative properties (**Figure 4.2A**).

The bulk and single-cell transcriptional data of aVECs show multiple candidate pathways that could control the form and function of these cells. To further refine candidate pathways, we cross-compared the aVEC dataset with the transcriptome of WAE cells that mediate the initial step of repair in severe colonic injury (Miyoshi et al., 2012; Seno et al., 2009). This analysis showed that 87 genes were commonly induced in both cell types, many of which were fetal markers (**Figure 4.2B; Table 4.1**). Pathways enriched in this shared signature included those previously implicated in repair, such as coagulation, EGFR, Hippo, and focal adhesion (**Figure 4.2C**; Cai et al., 2010; El-Assal and Besner, 2005; Kaiko et al., 2019; Yui et al., 2018). Importantly, TEAD4 and AP-1, which act downstream of Hippo signaling and synergize to regulate gene expression (Zanconato et al., 2015), were among the top transcription factors whose motifs were enriched in this signature (**Figure 4.2D**). Thus, we hypothesized that barrier restoration after villus injury required the involvement of the Hippo signaling pathway.

In the context of crypt injury induced by DSS or irradiation, Hippo signaling is required for epithelial regeneration through activation of the transcriptional regulator YAP (Cai et al., 2010; Gregorieff et al., 2015). To assess whether YAP is involved in aVECs during villus repair, we compared the localization of YAP between the homeostatic and atrophic intestine. At baseline, YAP was largely cytoplasmic throughout the epithelium with higher expression in the crypt compared to the villus compartment. This is consistent with the fact that YAP is largely inhibited by Hippo signaling in the adult intestinal epithelium (Xie et al., 2021). In contrast, YAP was predominantly nuclear in aVECs, suggestive of an activated state, and largely retained cytoplasmic localization in the crypt after poly(I:C)-induced injury (**Figure 4.3A,B**). In line with these observations, YAP signature genes were almost exclusively expressed by atrophy-associated cluster 7 cells (i.e., aVECs) (**Figure 4.3C,D**). These results suggest that YAP may act as a sensor of tissue integrity in multiple epithelial compartments in the gut, including villi.

We next mapped single cells in the villus atrophy sample along a pseudotime trajectory using the Monocle 3 algorithm (Cao et al., 2019), with cells expressing high levels of ISC markers as the starting point (**Figure 4.4A**). By ordering single cells according to their differentiation status, we can examine changes in gene expression as stem cells become progenitor cells and differentiate into aVECs (**Figure 4.4B**). This unsupervised approach revealed induction of YAP target genes over the course of epithelial differentiation, especially upon exit of the progenitor cell zone (**Figure 4.4C**). YAP activation in a post-mitotic cell type has also been previously reported in “resealing epithelial cells” in the ischemia-reperfusion small intestine damage model (Takeda and Kiyokawa, 2017). Thus, following intestinal villus injury, YAP induction promotes the adaptive differentiation of progenitor cells to facilitate repair.

YAP is activated in WAE cells during colonic repair

Given that aVECs and WAE cells both mediate barrier function in the gut post-injury, we next tested whether WAE cells also feature a YAP-activated profile. WAE cells immediately cover biopsy-induced wounds in the colon and is distinguished by the expression of CLDN4 (Seno et al., 2009). These cells are post-mitotic with short apical microvilli and a flattened cell morphology (Miyoshi et al., 2017). Immunostaining analysis of serial sections revealed that WAE cells were comprised of primitive-appearing CAR4⁺ colonocytes and MUC2⁺ goblet cells (**Figure 4.5A-C**). Furthermore, WAE cells had pronounced YAP nuclear staining, high *Clu* expression, and significant enrichment of the YAP transcriptional program (**Figure 4.6A-C**). Thus, WAE cells likely do not represent a unique cell lineage as we previously speculated. Consistent with TA progenitors as the major source of these cells (Seno et al., 2009; Takeda and Kiyokawa, 2017), WAE cells traced from LGR5⁺ lineage cells (**Figure 4.6D**). Together, these findings indicate that YAP activation may be a general feature of adaptively differentiated IECs.

YAP is critical for barrier function during villus atrophy

We next tested the role of YAP in barrier restoration and villus repair by performing poly(I:C) injury on mice lacking *Yap* in the intestinal epithelium using the *Vill^{Cre}* driver (*Yap^{ΔIEC}*) (**Figure 4.7A**). As previously reported, deletion of *Yap* did not perturb intestinal homeostasis (Cai et al., 2010). Importantly, the level of IEC death and villus atrophy induced by poly(I:C) was comparable between *Yap^{fl/fl}* and *Yap^{ΔIEC}* mice (**Figure 4.7B,C**). This offered the opportunity to examine the function of YAP specifically in the villus repair process.

Importantly, intestinal permeability to FITC-dextran was significantly elevated in *Yap^{ΔIEC}* mice during the atrophy phase (**Figure 4.8A**), demonstrating a compromised epithelial barrier.

Histological analysis revealed a greater number of fused atrophic villi with abnormal aVEC morphology in *Yap^{ΔIEC}* mice compared to littermate *Yap^{fl/fl}* controls (**Figure 4.8B,C**). Thus, YAP is required for the proper function of aVECs in restoring barrier integrity post-villus injury.

YAP controls epithelial wound healing programs in aVECs

To determine what genes are regulated by YAP specifically in the aVEC population, we performed scRNA-seq of IECs from the proximal intestine with roughly equivalent amount of the atrophic and distal non-atrophic regions of the gut to capture the full spectrum of cell states in *Yap^{fl/fl}* and *Yap^{ΔIEC}* mice (**Figure 4.9A-C**). UMAP identified all major intestinal cell lineages and revealed a similar clustering pattern between the two genotypes (**Figure 4.10A,B**).

Consistent with our prior scRNA-seq analysis, the fetal program emerged most prominently in the villus-top enterocyte (cluster 7) as well as the goblet cell (cluster 3) clusters (**Figure 4.10C**). Likewise, the villus-top enterocyte cluster could be further re-clustered into two distinct *Cldn4*-expressing clusters, one corresponding to *Enpp3⁺Ada⁺* homeostatic villus-top enterocytes (cluster 7a) and the other to *Il33⁺Suox⁺* atrophy-induced enterocytes (cluster 7b) (**Figure 4.10D**).

Homing in on the fetal program-enriched IECs (clusters 3 and 7b) and stem/progenitor cells (cluster 1), we performed comparative analysis between *Yap^{fl/fl}* and *Yap^{ΔIEC}* cells for each cluster, which revealed the most substantial gene expression difference in atrophy-induced enterocytes (**Figure 4.11A**). Many previously defined YAP target genes, including *Msln*, *Clu*, *Suox*, and *Il33*, were no longer induced in the absence of *Yap* (**Figure 4.11B**). *In situ* hybridization validated the loss of *Msln* and *Clu* expression in aVECs in *Yap^{ΔIEC}* mice (**Figure 4.12A**). However, the expression of some putative YAP target genes previously defined in intestinal crypts, such as *Areg* (Gregorieff et al., 2015), was not affected (**Figure 4.12B**). Top

pathways blunted by *Yap* deletion included cell-cell adhesion, cell migration, actin cytoskeleton, and focal adhesion (**Figure 4.12C**). Interestingly, similar YAP-dependent pathways were enriched in the organoid culture system (**Figure 4.12D**; Gregorieff et al., 2015). Finally, reconstruction of single cells along a pseudotime trajectory highlighted a requirement for YAP in invoking the adaptive differentiation program (**Figure 4.13A,B**). Without YAP, epithelial differentiation occurred but YAP target genes were no longer induced (**Figure 4.13A,B**). Together, these data establish a critical role for YAP in maintaining epithelial barrier integrity.

YAP deletion largely does not affect Wnt signaling or cell proliferation following villus injury

Upon damage to ISCs, YAP inhibits Wnt signaling, leading to loss of canonical ISC markers, in order to prevent excessive Paneth cell differentiation (Gregorieff et al., 2015). While we observed a minor increase in the expression of Wnt, stem cell, and Paneth cell genes upon *Yap* deletion, this was not unique to our stem/progenitor cell cluster (**Figure 4.14A**).

Quantification of ISCs and Paneth cells by immunostaining revealed no difference in numbers between *Yap^{fl/fl}* and *Yap^{ΔIEC}* crypts during villus atrophy (**Figure 4.14B**). The number of proliferating crypt cells also did not differ between the two genotypes (**Figure 4.14C**). These results are consistent with the lack of ISC damage in our model and the primary role of YAP in mediating adaptive differentiation in the villus compartment outside of the stem cell niche.

aVEC function but not formation depends on YAP

Given the mechanistic link between YAP activation and the fetal-like epithelial conversion seen in DSS-induced colitis (Yui et al., 2018), we next examined the extent to which YAP controls the aVEC state. In determining which of the fetal (Mustata et al., 2013) and YAP

signature (Gregorieff et al., 2015) genes were aVEC-specific and/or YAP-dependent in the poly(I:C) injury model, we discovered that many of the overlapping genes between the two datasets were uniquely expressed by aVECs. Importantly, only ~40% of these aVEC markers were impacted by *Yap* deletion (**Figure 4.15A,B; Table 4.2**). Outside of the overlapping genes, YAP had a very minor role in inducing the fetal program (**Figure 4.15A,B; Table 4.2**). These findings suggest that aVEC formation occurs to a certain extent after damage without *Yap*. Indeed, epithelial shortening and *Areg* expression still occurred in *Yap^{AIEC}* mice after poly(I:C)-induced villus injury (**Figure 4.8B** and **4.12B**). Thus, the YAP program serves to positively modulate aVEC function, and without it, aVECs enter a dysfunctional or maladapted state.

YAP deficiency impairs villus regeneration

To assess the consequence of maladaptive aVEC differentiation due to *Yap* deficiency, we examined the regenerative capacity of villi following injury. Notably, compared to *Yap^{fl/fl}* controls, villus regeneration was hampered in *Yap^{AIEC}* mice at 48 and 72 HPI. This was accompanied by compensatory expansion of the crypt at 72 HPI (**Figure 4.16A**). Histological analysis at 48 HPI during the regenerative phase revealed aggregates of fused and stunted villi in *Yap^{AIEC}* mice (**Figure 4.16B**). Whole mount imaging and spatial distribution analysis revealed that villus regeneration occurred in a more clustered pattern in the absence of *Yap* at 48 HPI (**Figure 4.16C,D**). While our collective data position YAP's activity primarily in the villus compartment in our model, we were unable to specifically delete *Yap* in differentiated cells using *Krt20^{CreER}/Yap^{fl/fl}* mice to confirm this (**Figure 4.17**). This is likely due to the fact that YAP is produced in the crypt and the protein persists in the villus epithelium (Camargo et al., 2007).

Further characterization of the stunted *Yap^{AIEC}* villi revealed that the epithelium was in a persistent maladapted aVEC state, exemplified by the continued expression of *Areg* (**Figure 4.18A**). Differentiation was impaired as evidenced by the reduction of ACE2⁺ enterocytes and presence of abnormal goblet cells in regenerating *Yap^{AIEC}* villi (**Figure 4.18B-D**). Proliferation was not affected, suggesting a comparable crypt response. By 72 HPI, *Yap^{AIEC}* villi were still not recovered and continued to show diminished ACE2 expression. The crypts at this time point were hyperproliferative (**Figure 4.18E,F**). Overall, villus regeneration was significantly delayed in *Yap^{AIEC}* mice, likely due to the presence of a weakened barrier during villus atrophy.

YAP is essential during the early stages of villus repair and regeneration

By one-week post-injury, *Yap^{AIEC}* mice had largely restored their villus architecture. Crypts were slightly still taller and villi were just a few μm shorter in *Yap^{AIEC}* compared to *Yap^{fl/fl}* mice, but otherwise, YAP did not appear to be crucial during the later stages of villus regeneration (**Figure 4.19A**). *Yap^{AIEC}* mice also displayed signs of normal epithelial differentiation one-week post-injury (**Figure 4.19B**). The eventual recovery of villi in *Yap^{AIEC}* mice was associated with heightened stromal *Ereg* expression (**Figure 4.19C,D**). Similar compensatory responses are also seen in the irradiation model (Gregorieff et al., 2015). Thus, YAP's early role in villus repair can profoundly impact the regenerative outcome of villi.

4.4 Discussion

Severe tissue injury triggers unique cellular states and responses that are not observed under normal physiological conditions. Stem and progenitor cells must not only replenish lost cells to restore tissue function but also properly attend to the damage itself. Upon injury to the villus epithelium, TA cells rapidly migrate upward and adaptively differentiate into aVECs to cover damaged villi. In addition to possessing a fetal-like profile, here we found that aVECs feature a YAP-activated state. This transcriptional response is likely important for re-establishing the barrier following villus collapse. Indeed, in the absence of YAP, barrier integrity failed to restore completely after injury. This is consistent with YAP's role in promoting wound healing behaviors in other cell types through modification of cell mechanics, cell adhesion, and actin cytoskeleton (Calvo et al., 2013; Lee et al., 2014; Nardone et al., 2017; Neto et al., 2018; Park et al., 2019). Once the damaged villi were fully covered with aVECs and the injury stimulus was no longer present, proliferation dramatically increased in the crypt and the production of differentiated IECs shifted back to a more normal program as villi began regenerating.

Historically, restoration of epithelial continuity after disruption of the gastrointestinal mucosa has been referred to as “restitution” (Lacy, 1988; Sturm and Dignass, 2008). The term was first utilized by Svanes et al. to describe the rapid repair of the amphibian gastric lining following severe hypertonic chemical injury (Svanes et al., 1982). Yet, the literal meaning of restitution is “restoration or return of something to its normal position” (Oxford English Dictionary, 2021). However, Svanes et al. and others that followed recognized that the repairing epithelium went through a phase where the cell shape changed dramatically, implying that tissue repair did not simply involve the production of new fully differentiated cells. In addition, restitution was initially thought to involve a partial dedifferentiation step (Sturm and Dignass,

2008). However, the molecular features of these transient cells remained largely enigmatic. Using a biopsy injury system, we previously described a WAE cell population in the colon that repairs wounds after extensive crypt loss (Miyoshi et al., 2017; Seno et al., 2009). However, the paucity of these cells in this model, the severe disruption of mucosal architecture caused by the injury, and the lack of high-resolution transcriptomic analysis limited our ability to define the lineage properties of WAE cells and the mechanisms responsible for their barrier function.

In many ways, aVECs can be considered as the small intestine counterpart of WAE cells. While the poly(I:C) injury system and colonic biopsy model differ in several key regards—the main one being that the latter involves wound formation while the former does not—the morphology and function of these two damage-induced cell types are strikingly similar. Superimposing the transcriptional profiles of aVECs and WAE cells uncovered a core gene signature that distinguishes these cells from homeostatic IECs. This shared signature includes many genes related to cell migration, cell adhesion, and ECM re-organization, which is consistent with the primary function of these cells: to re-establish the intestinal barrier after injury. Importantly, we discovered that WAE cells also possess a YAP-activated profile and are composed of wound-adapted versions of colonocytes and goblet cells. Whether YAP is important in mediating WAE cell function and colonic repair remains to be addressed.

Several mutually non-exclusive mechanisms have been proposed for YAP's regenerative function in the gut (Ayyaz et al., 2019; Cheung et al., 2020; Gregorieff et al., 2015; Yui et al., 2018). As crypt-based cells are pliable to cell fate changes, depletion or overexpression of YAP induces profound cellular remodeling, including alteration of ISC identity, unintended lineage skewing, and loss or gain of proliferative activity. The action of YAP on other signaling pathways in the crypt likely explains a large portion of these effects. In the poly(I:C) injury

model, we examined the function of YAP outside of the crypt niche, potentially exposing the true nature of its reparative program. In doing so, we established a proliferation, survival, and reprogramming-independent function of YAP during adaptive differentiation. In support of this, deletion of YAP did not block aVEC formation as one might expect if these cells were converted from another cell type. Instead, in the absence of YAP, aVECs were dysfunctional and maladapted for repair. YAP-deficient aVECs were unable to properly restore the barrier after injury. Thus, our data uncover a requirement for YAP in carefully tuning aVEC function.

An unresolved question stemming from our work is how and when YAP is induced following injury. Recent work using the LGR5-DTR mouse model found minimal activation of YAP and fetal markers following ISC-specific ablation (Murata et al., 2020), suggesting that stem cell loss alone and injury-induced dedifferentiation do not trigger YAP activation. To induce YAP activity, there is likely a threshold of damage that needs to be surpassed, coupled with an appropriate microenvironment (Romera-Hernandez et al., 2020; Taniguchi et al., 2015; Xu et al., 2020; Yui et al., 2018). Our study suggests that recovery from severe injury involves a transient intermediate step that is tailored to meet the demands of the repairing tissue prior to entering a pro-regenerative state. Thus, YAP is not only essential for crypt regeneration but also for the rapid re-sealing of the intestinal barrier following drastic loss of surface epithelial cells.

Villus fusion is a phenomenon often associated with villus atrophy in several different enteropathies, particularly during recurrent or chronic disease (Dickson et al., 2006; Rutgeerts et al., 1984; Townley et al., 1964). We observed some level of villus fusion in wild-type mice after poly(I:C)-induced injury; however, this event was prominent in *Yap^{AIEC}* mice, likely due to the presence of defective aVECs. While questions remain on the exact reason for this increase, prior studies indicate a need for maintaining proper epithelial integrity. Disruption of epithelial

proteins involved in stabilizing the membrane-cytoskeleton interface, such as ezrin and crumbs3, result in defective epithelial morphogenesis and villus fusion (Casaletto et al., 2011; Whiteman et al., 2014). Therefore, in promoting epithelial integrity in aVECs, YAP may be preventing atrophic villi from fusing, which could otherwise impede their regenerative capacity. Eventually, *Yap^{ΔIEC}* mice fully recover their villi and return to normalcy, likely owing to the elevated crypt response and heightened stromal *Ereg* expression observed in these mice. Similar compensatory responses are also seen in the irradiation injury model (Gregorieff et al., 2015).

This work has important implications for human enteropathies such as Crohn's disease, in which YAP is upregulated in the epithelium in ~60% of patients (Taniguchi et al., 2015; Yu et al., 2018). Furthermore, villus atrophy caused by small bowel injury is observed in a variety of enteropathies in both children and adults (Jansson-Knodell et al., 2018). Therapies designed around enhancing endogenous mechanisms of villus recovery (i.e. adaptive differentiation) may provide clinical benefit for patients with impaired healing capacity. Additionally, the delayed villus regeneration phenotype we observed in the absence of YAP may help explain why certain patients with villus damage fail to restore their villi despite treatment efforts. This is known as persistent villus atrophy (Lebwohl et al., 2014; Rubio-Tapia and Murray, 2010), but the underlying reason for why this occurs is not known. Our work suggests the inability to properly form aVECs (i.e., maladaptive differentiation) results in barrier leakage and a persistently damaged state. Therefore, not only is it important to form aVECs, but the proper functioning of these cells during repair is just as critical. Given that YAP activation in the stem cell compartment could lead to tumorigenesis (Choi et al., 2018), targeting this signaling pathway specifically in the differentiated compartment could be a potential avenue for future therapeutics.

4.5 Figures

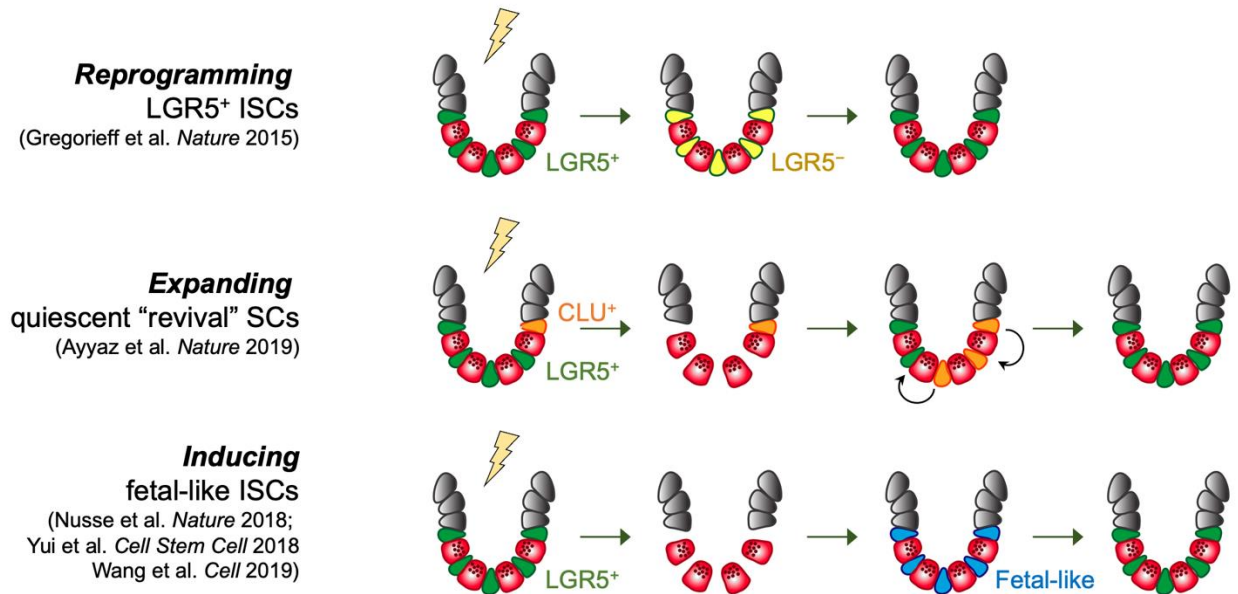


Figure 4.1. YAP-dependent mechanisms of ISC recovery after injury

The Hippo-YAP pathway has been described as a key mediator of stem cell recovery. Three major mechanisms have been proposed for how YAP achieves this in the gut. In the first scenario, LGR5⁺ ISCs are in fact not lost during irradiation injury but rather are transiently reprogrammed to a LGR5⁻ state. This reprogramming process involves an inhibition of Wnt signaling to prevent Paneth cell differentiation as well as EGF pathway activation to promote cell survival. In the second scenario, a rare CLU⁺ cell population near the +4 position responds to injury and expands in a YAP-dependent manner. These “revival” stem cells (revSCs) contribute to epithelial regeneration by reconstituting the LGR5⁺ ISC pool. In the third scenario, a fetal-like stem cell population arises after injury and participates in epithelial regeneration. Induction of the fetal program appears to require IFN-gamma or YAP signaling depending on the injury context. The source of these fetal-like stem cells and their relationship to revSCs remain unclear.

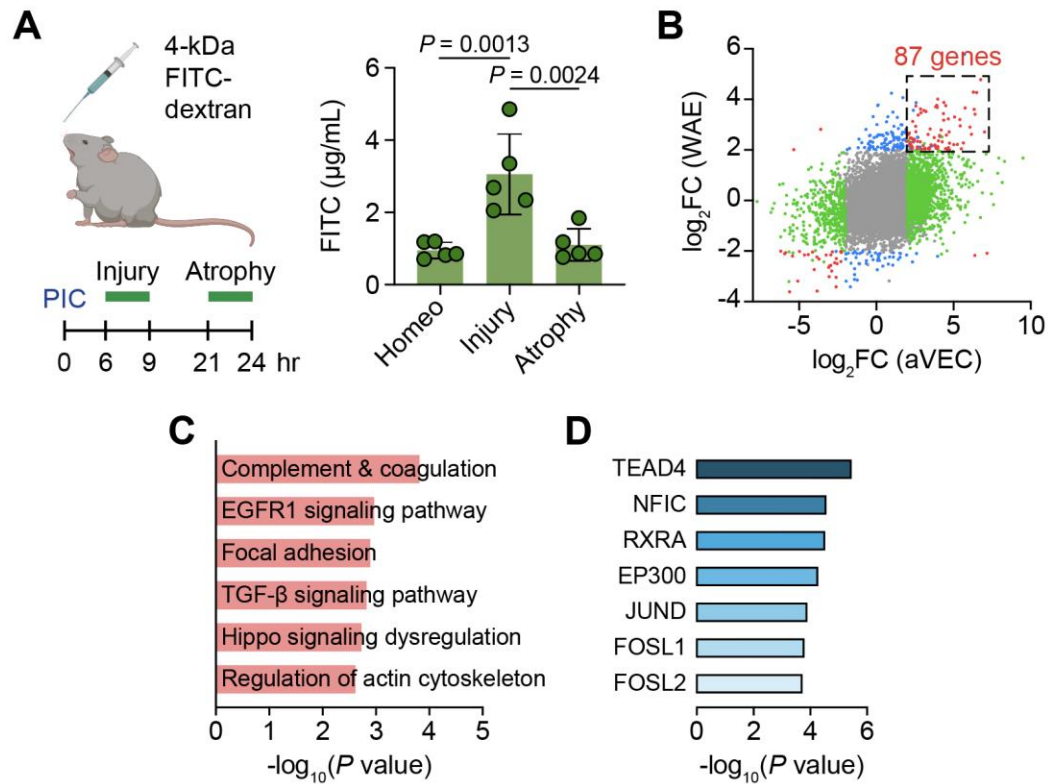


Figure 4.2. Defining a core transcriptional signature for intestinal barrier restoration

(A) Schematic of FITC-dextran permeability assay (left). 4-kDa FITC-dextran was orally gavaged and serum was obtained 3 h later at the indicated time points. Serum FITC-dextran levels were measured and plotted as mean \pm SD (right). $n = 5$ mice/group. Significance was determined by one-way ANOVA and Tukey's multiple comparison test. (B) Fold change values for each gene from the aVEC and wound-associated epithelial (WAE) cell LCM-microarray datasets were plotted. Differentially expressed genes in only the aVEC dataset were colored green, in only the WAE dataset were colored blue, and in both datasets were colored red. 87 genes were commonly upregulated in both aVECs and WAE cells. (C and D) Pathway analysis (C) and transcription factor motif analysis (D) of the aVEC-WAE shared signature gene set.

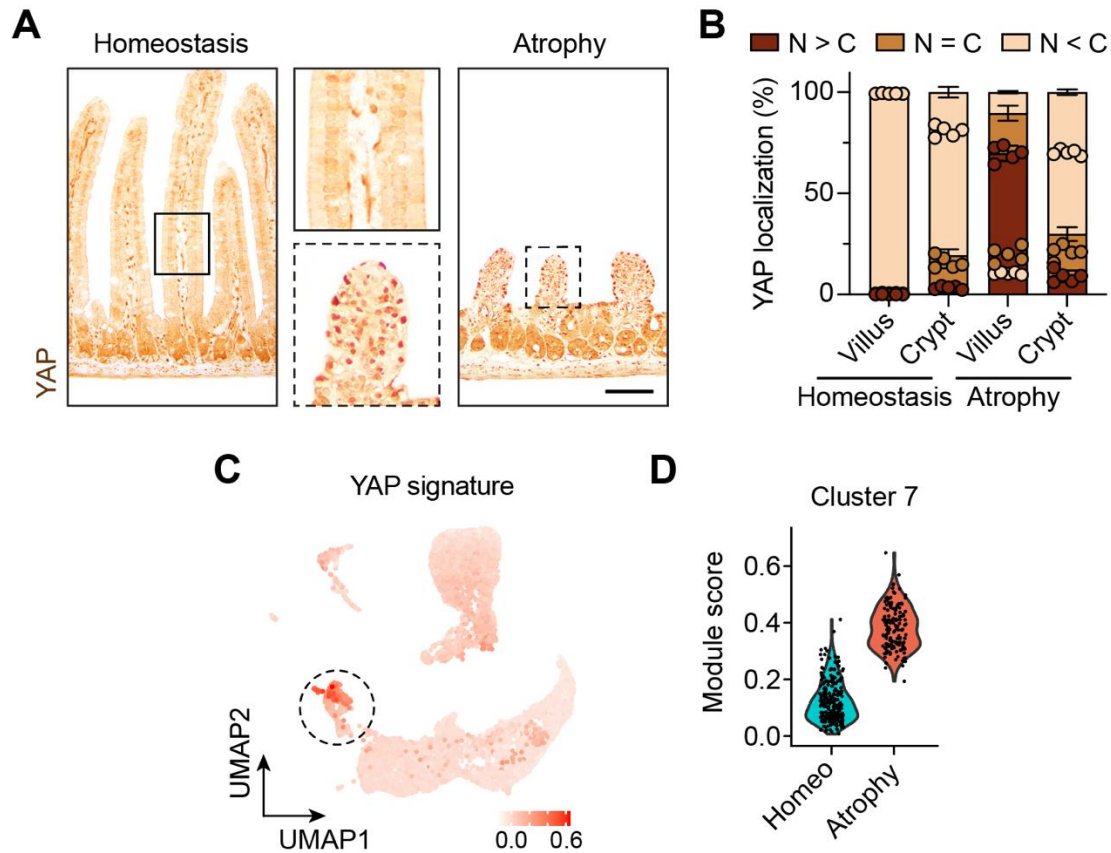


Figure 4.3. YAP is activated in aVECs

(A) IHC for YAP (brown) in the homeostatic and atrophic intestine. Bar: 100 μ m. (B) Percent of epithelial cells with predominantly nuclear ($N > C$), equally nuclear and cytoplasmic ($N = C$), or predominantly cytoplasmic ($N < C$) localization of YAP was quantified across 30 villi/crypts based on IF images and plotted as mean \pm SD. $n = 5$ mice/group. (C and D) Expression of a YAP signature was overlaid on the UMAP plot from **Figure 3.6** (C) and enrichment scores were plotted for each cell in cluster 7 (dashed circle, villus-top enterocyte) separated by sample (D).

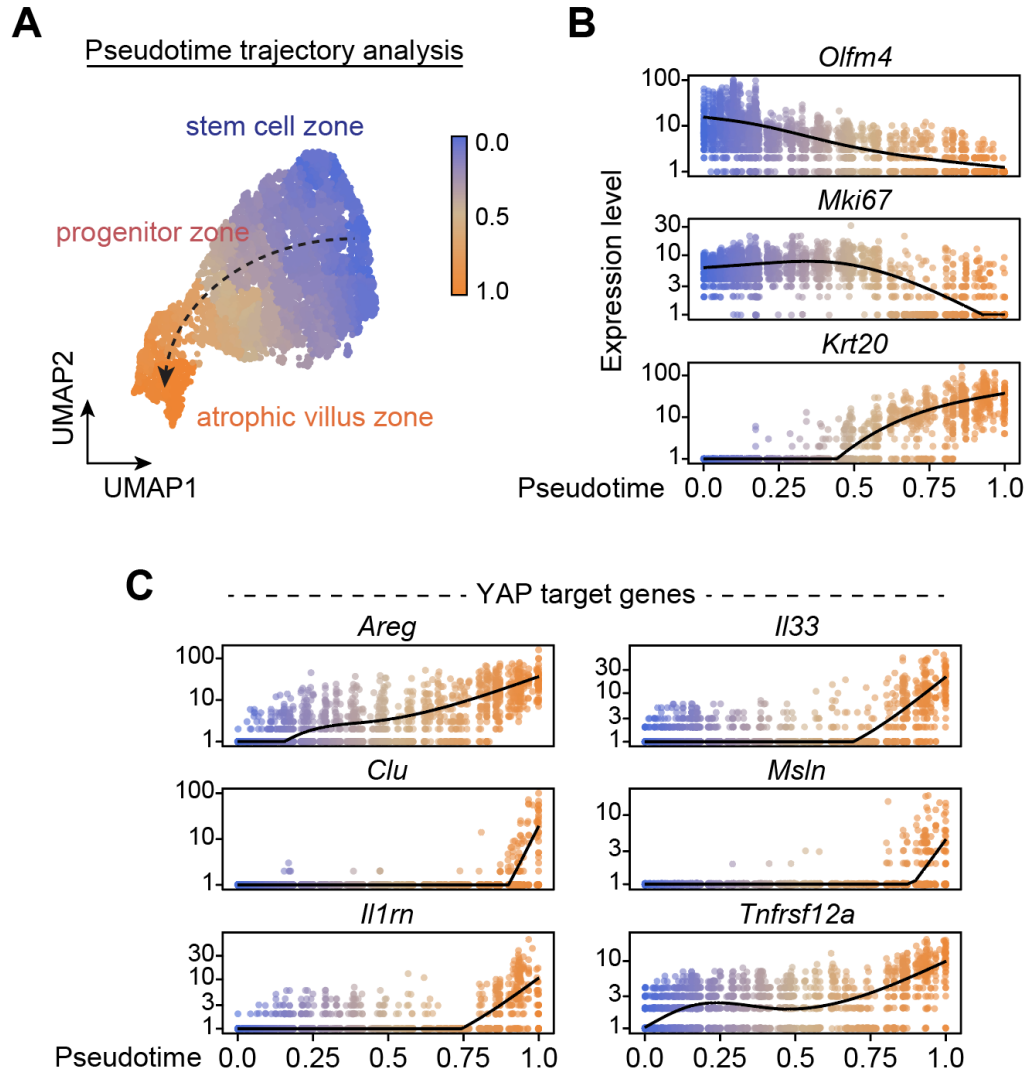


Figure 4.4. YAP promotes adaptive epithelial differentiation

(A) Pseudotime analysis of IECs during villus atrophy based on single cell transcriptomes. Cells were colored by progression through a pseudotime differentiation trajectory. Black dashed arrow indicates direction of fate progression. (B and C) Single cells were plotted according to their pseudotime position and their expression level of stem cell (*Olfm4*), proliferation (*Mki67*), differentiation (*Krt20*) (B), and YAP target genes (*Areg*, *Clu*, *Il1rn*, *Il33*, *Msln*, *Tnfrsf12a*) (C).

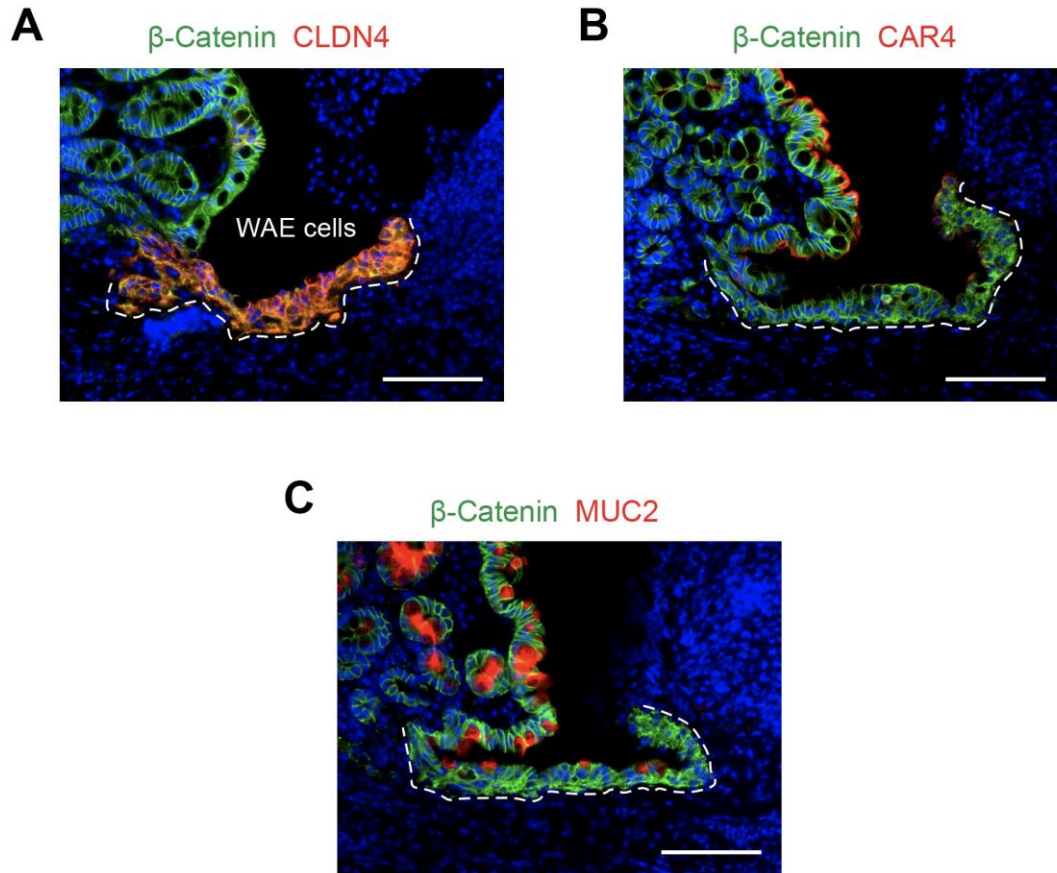


Figure 4.5. WAE cells retain remnants of colonocyte and goblet cell identity

(A-C) IF for CLDN4 (A), CAR4 (B), and MUC2 (C) in day 2 colonic biopsy wounds. β-Catenin (green) marks epithelial cells. Serial sections were stained to examine the expression of CAR4 (colonocyte marker) and MUC2 (goblet cell marker) in CLDN4⁺ WAE cells (white dashed line). Bars: 100 μm. Immunofluorescence (IF) images are representative of at least 3 animals.

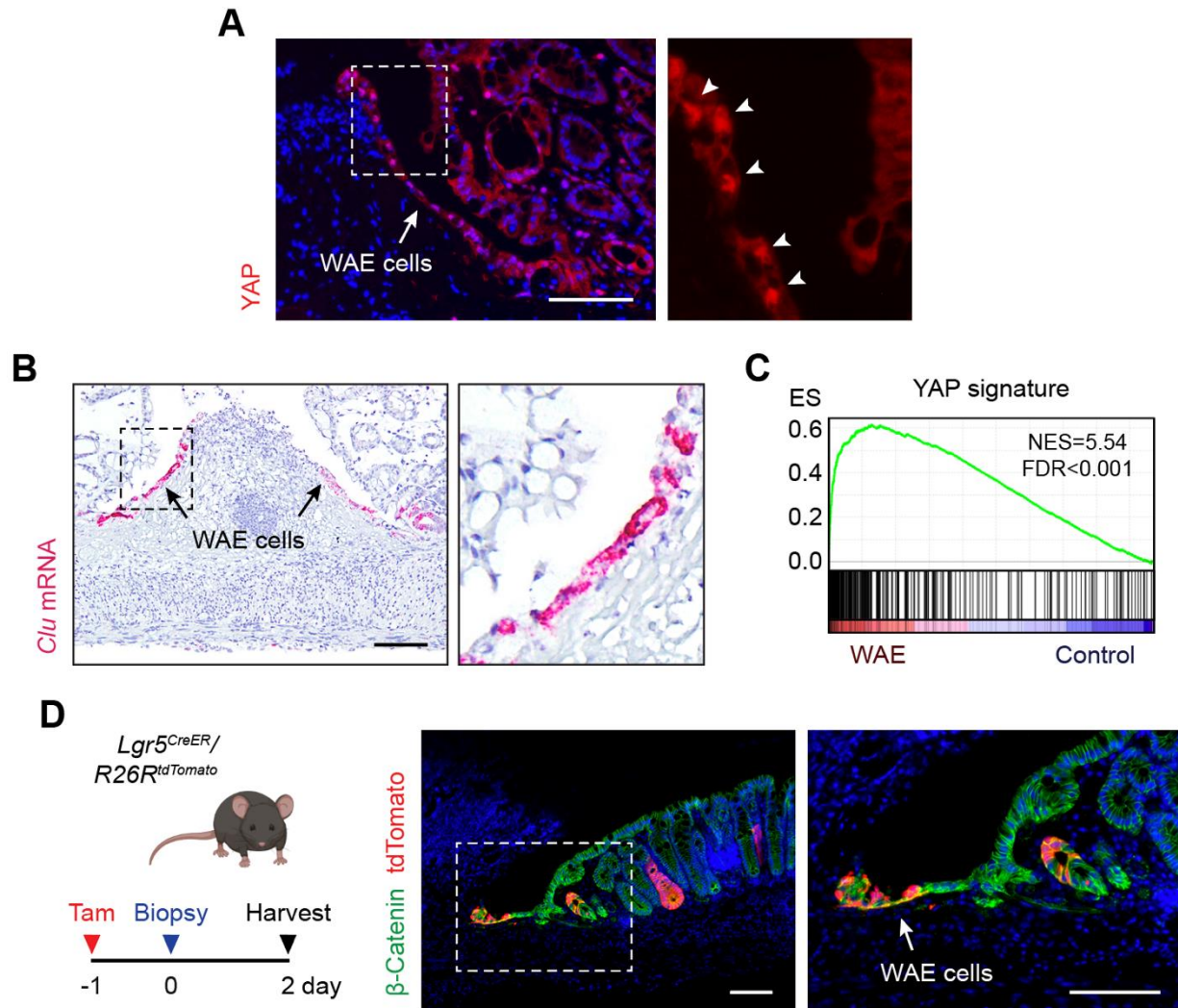


Figure 4.6. YAP is activated in WAE cells

(A and B) IF for YAP protein (A) and RNAscope for *Clu* mRNA (B) in day 2 colonic biopsy wounds reveal nuclear YAP expression and high *Clu* expression in WAE cells (arrows). (C) Gene set enrichment analysis (GSEA) of YAP target genes in WAE cells (day 2 and 4 post-injury) compared with control cells (adjacent uninjured surface epithelium and crypts on day 2 and 4 post-injury). (D) Fate mapping of LGR5⁺ lineage cells following colonic biopsy injury. LGR5⁺ ISC were labeled with tamoxifen 1 day prior to injury in *Lgr5^{CreER}/R26^{tdTomato}* mice. LGR5⁺ lineage cells contribute to the generation of WAE cells (white arrow) on day 2 post-injury. All bars: 100 μ m. IF and RNAscope images are representative of at least 3 animals.

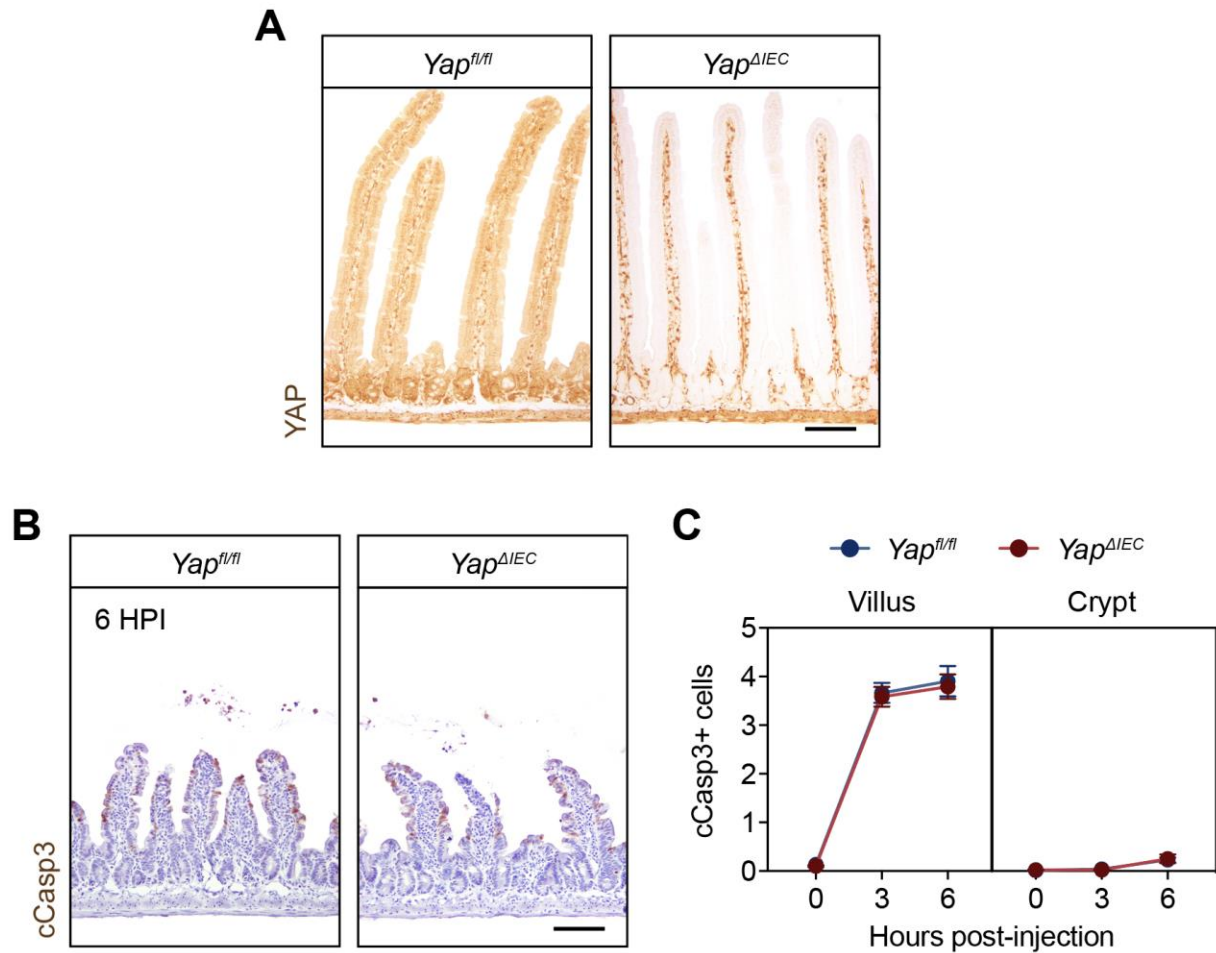


Figure 4.7. *Yap^{AIEC}* and *Yap^{fl/fl}* mice exhibit a similar level of poly(I:C)-induced damage

(A) IHC for YAP (brown) in the homeostatic intestine from *Yap^{fl/fl}* and *Yap^{AIEC}* mice validating the loss of YAP expression in the intestinal epithelium in *Yap^{AIEC}* mice. Bar: 100 μ m. (B and C) IHC for cleaved-caspase 3 (cCASP3) (brown) at 6 HPI (B). Bar: 100 μ m. Average number of cCASP3⁺ cells across 50 villi/crypts at the indicated time points in *Yap^{fl/fl}* and *Yap^{AIEC}* mice was plotted as mean \pm SD (C). n = 3 mice/group. No significant difference was observed by two-way ANOVA with Tukey's multiple comparisons test. Images are representative of at least 3 animals.

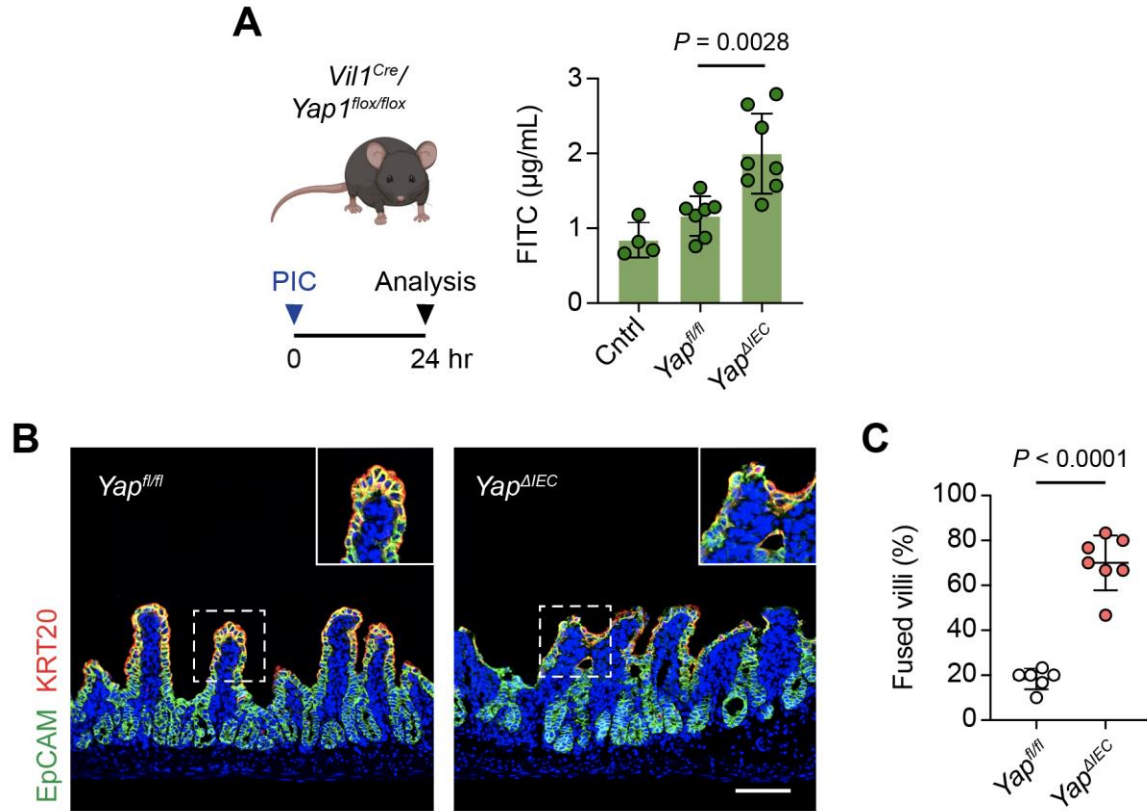


Figure 4.8. Proper barrier re-establishment and aVEC morphology depend on YAP

(A) 4-kDa FITC-dextran was orally gavaged at 24 HPI and serum was obtained 3 h later from *Yap^{fl/fl}* and *Yap^{ΔIEC}* mice. Serum FITC-dextran levels were measured and plotted as mean \pm SD to assess intestinal permeability *in vivo* (right). Control (cntrl) were *Yap^{fl/fl}* mice without poly(I:C) injection. $n = 4-8$ mice/group. Significance was determined by one-way ANOVA and Tukey's multiple comparison test. (B) IF for EpCAM (green) and KRT20 (red) in the atrophic intestine from *Yap^{fl/fl}* and *Yap^{ΔIEC}* mice. Bar: 100 μm . Images are representative of at least 3 animals. (C) Percent of atrophic villi that were fused to other villi was quantified across 50 villi and plotted as mean \pm SD. $n = 6-7$ mice/group. Significance was determined by unpaired *t*-test.

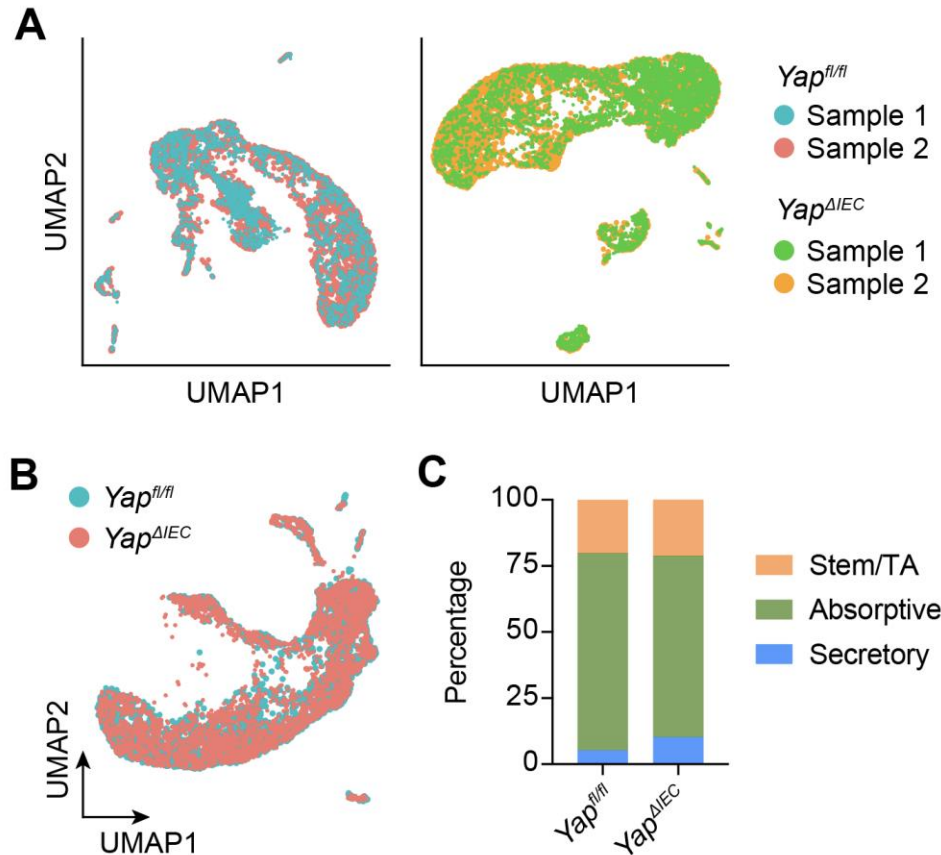


Figure 4.9. scRNA-seq overview of the damaged intestine from *Yap^{AIEC}* and *Yap^{fl/fl}* mice

(A) UMAP visualization of scRNA-seq libraries from two independent *Yap^{fl/fl}* samples and two independent *Yap^{AIEC}* samples reveals minimal batch-to-batch variation. (B and C) UMAP visualization of IECs from *Yap^{fl/fl}* and *Yap^{AIEC}* mice with similar level of damage (containing roughly equivalent amount of the atrophic and distal non-atrophic regions of the gut) colored by genotype (B). Proportion of stem/progenitor cells, absorptive enterocytes, and secretory cells (i.e., Paneth, goblet, enteroendocrine, and tuft cells) based on scRNA-seq clusters (C).

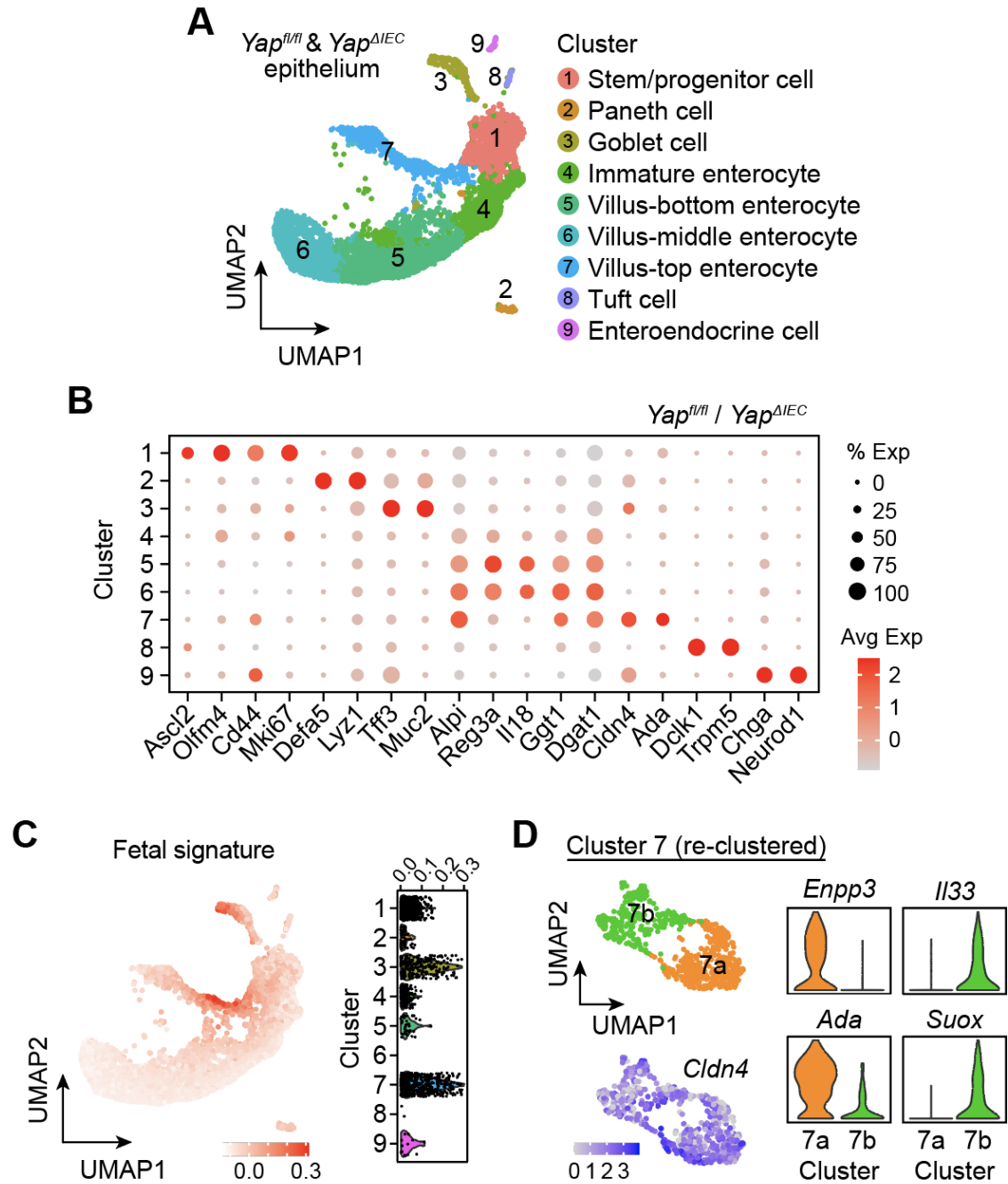


Figure 4.10. scRNA-seq analysis of the damaged intestine from *Yap^{ΔIEC}* and *Yap^{fl/fl}* mice

(A) UMAP visualization of IECs from *Yap^{fl/fl}* (3,571 cells) and *Yap^{AIEC}* (4,013 cells) mice colored by cell type. Clusters were annotated based on expression of known and top marker genes. (B) Dot plot of cell type-specific and enterocyte zonation markers in the *Yap^{fl/fl}* vs *Yap^{AIEC}* IEC scRNA-seq dataset. (C) Expression of a fetal spheroid signature was overlaid on the UMAP plot (left) and enrichment scores were plotted for each cell separated by cluster (right). Cells with the highest enrichment were found in cluster 3 (goblet cells) and cluster 7 (villus-top enterocyte). A greater spread is appreciated here than before (which showed two distinct populations) likely because half of the cells lack YAP. (D) UMAP visualization of cluster 7 sub-clusters colored by cell type (left top) and relative *Cldn4* expression (left bottom). Expression of villus-top (*Enpp3*, *Ada*) and fetal (*Il33*, *Suox*) markers in each sub-cluster (right). Note that aVECs (cluster 7b) can be distinguished from homeostatic villus-top enterocytes (cluster 7a) using this analysis.

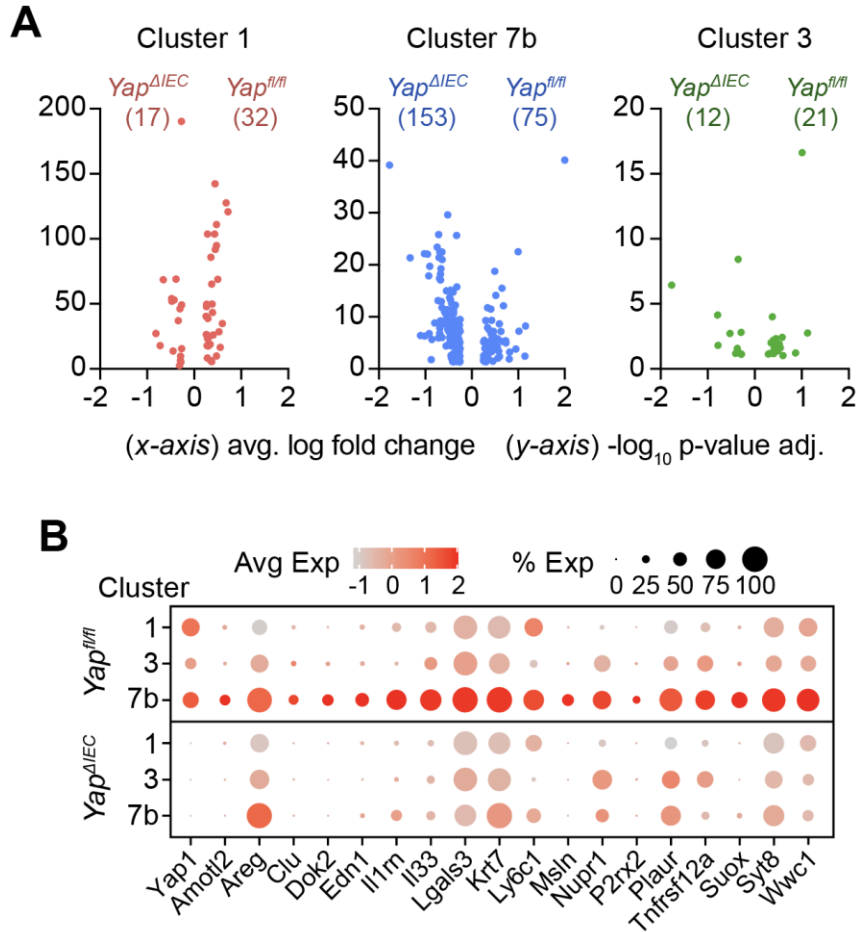


Figure 4.11. Cell-type specific responses to YAP deficiency during villus atrophy

(A) Differentially expressed genes between *Yap*^{fl/fl} and *Yap*^{ΔIEC} cells were plotted for stem/progenitor cells (cluster 1), atrophy-induced enterocytes (cluster 7b), and goblet cells (cluster 3). Note that *Yap* deficiency had the most impact on gene expression in atrophy-induced enterocytes. (B) Dot plot of previously defined YAP target genes in stem/progenitor cells (cluster 1), goblet cells (cluster 3), and atrophy-induced enterocytes (cluster 7b) separated by genotype.

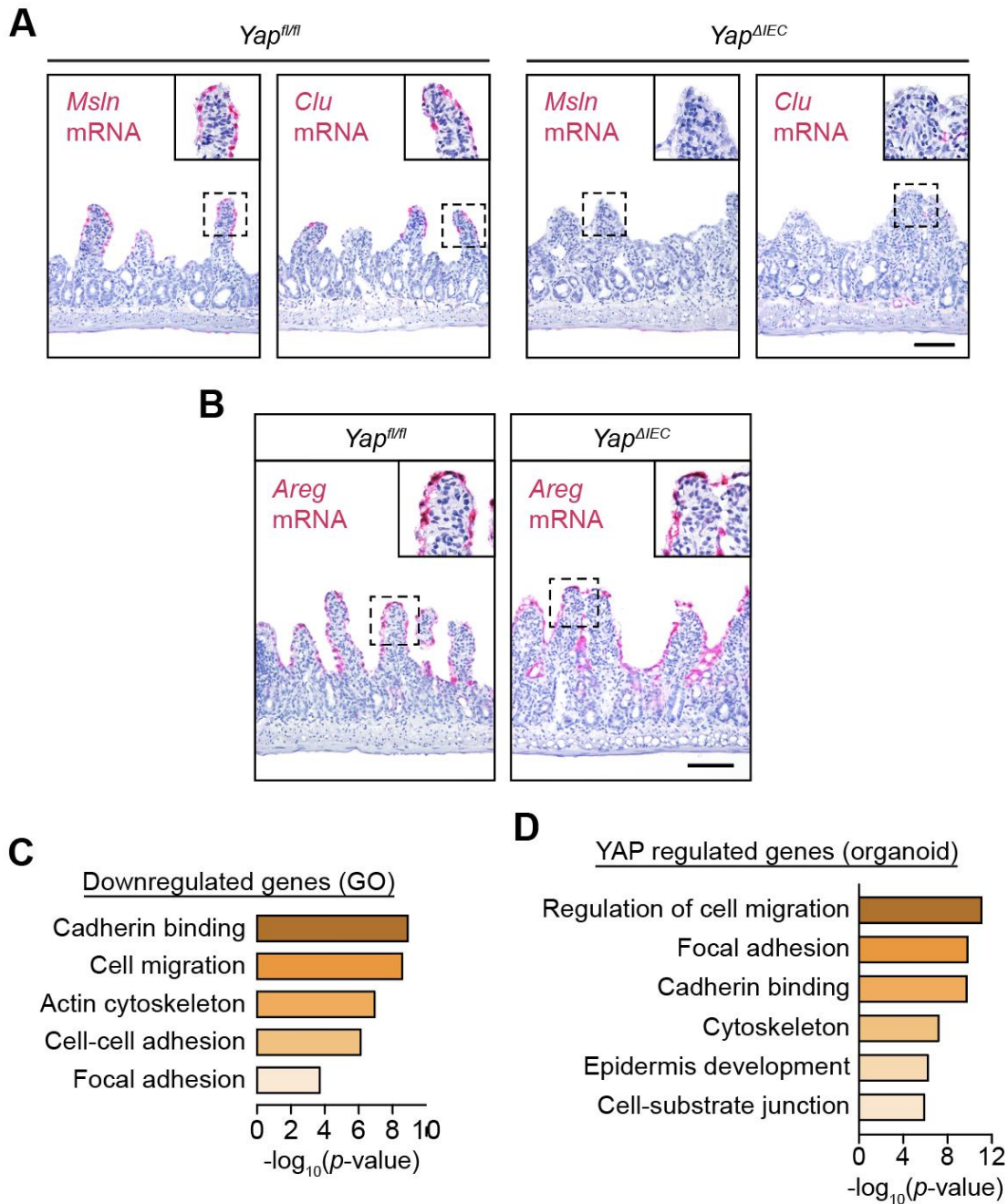


Figure 4.12. *In situ* hybridization validation and pathway analysis of scRNA-seq data

(A and B) RNAscope for *Msln* and *Clu* mRNA (A) and *Areg* mRNA (B) in the atrophic intestine from *Yap^{fl/fl}* and *Yap^{AIEC}* mice. Bars: 100 μ m. In the absence of YAP, aVECs no longer express *Msln* and *Clu* expression but maintain *Areg* expression. This suggests that aVECs still form without YAP, but they lose a YAP-specific transcriptional program. All RNAscope images are representative of at least 3 animals. (C) Gene ontology (GO) analysis of downregulated genes in *Yap^{AIEC}* cells compared with *Yap^{fl/fl}* cells. (D) Pathway analysis of the top 300 YAP regulated genes in the intestinal organoid culture system reveals induction of similar programs as aVECs.

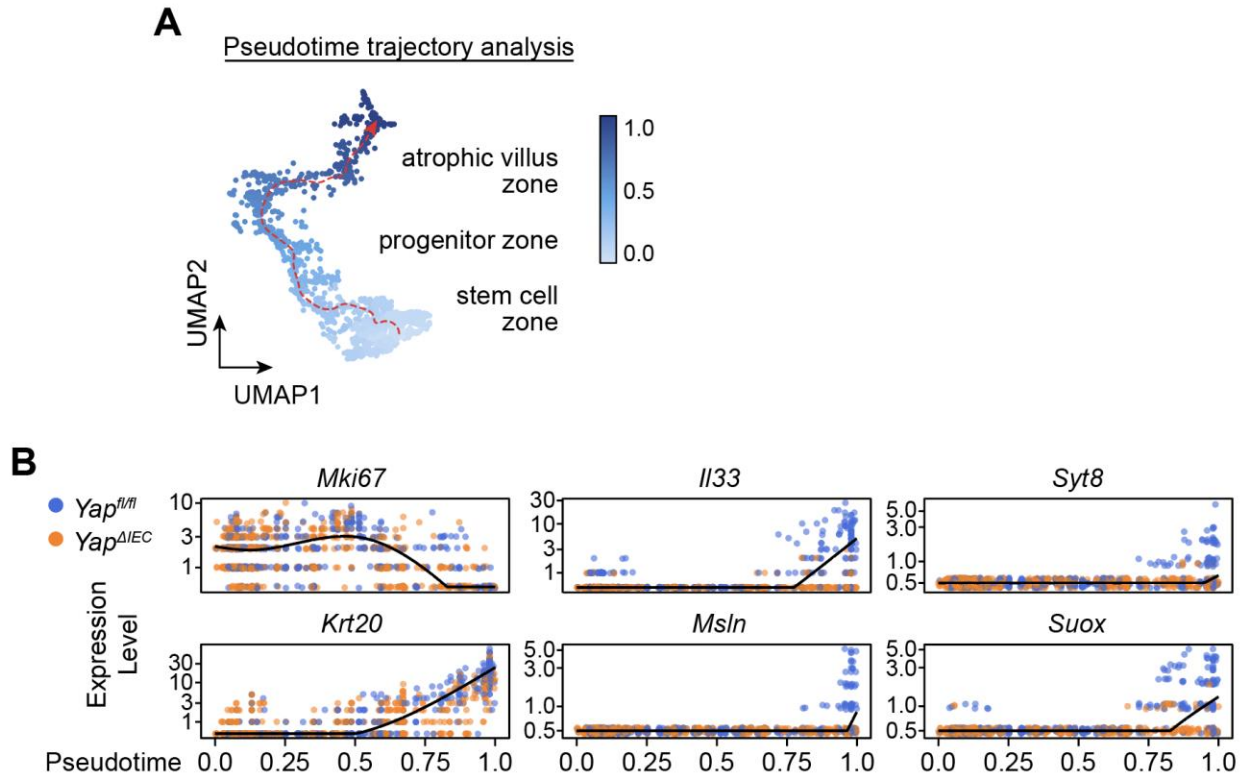


Figure 4.13. YAP is functionally required for proper adaptive differentiation

(A) Pseudotime analysis of *Yap^{fl/fl}* and *Yap^{ΔIEC}* IECs associated with villus atrophy based on single cell transcriptomes. Cells were colored by progression through a pseudotime differentiation trajectory (i.e., from the stem cell zone to the atrophic villus zone). Red dashed arrow indicates direction of fate progression. (B) Single *Yap^{fl/fl}* cells (blue) and *Yap^{ΔIEC}* cells (orange) were plotted according to their pseudotime position and their expression level of proliferation (*Mki67*), differentiation (*Krt20*), and YAP target genes (*Il33*, *Syt8*, *Msln*, *Suox*).

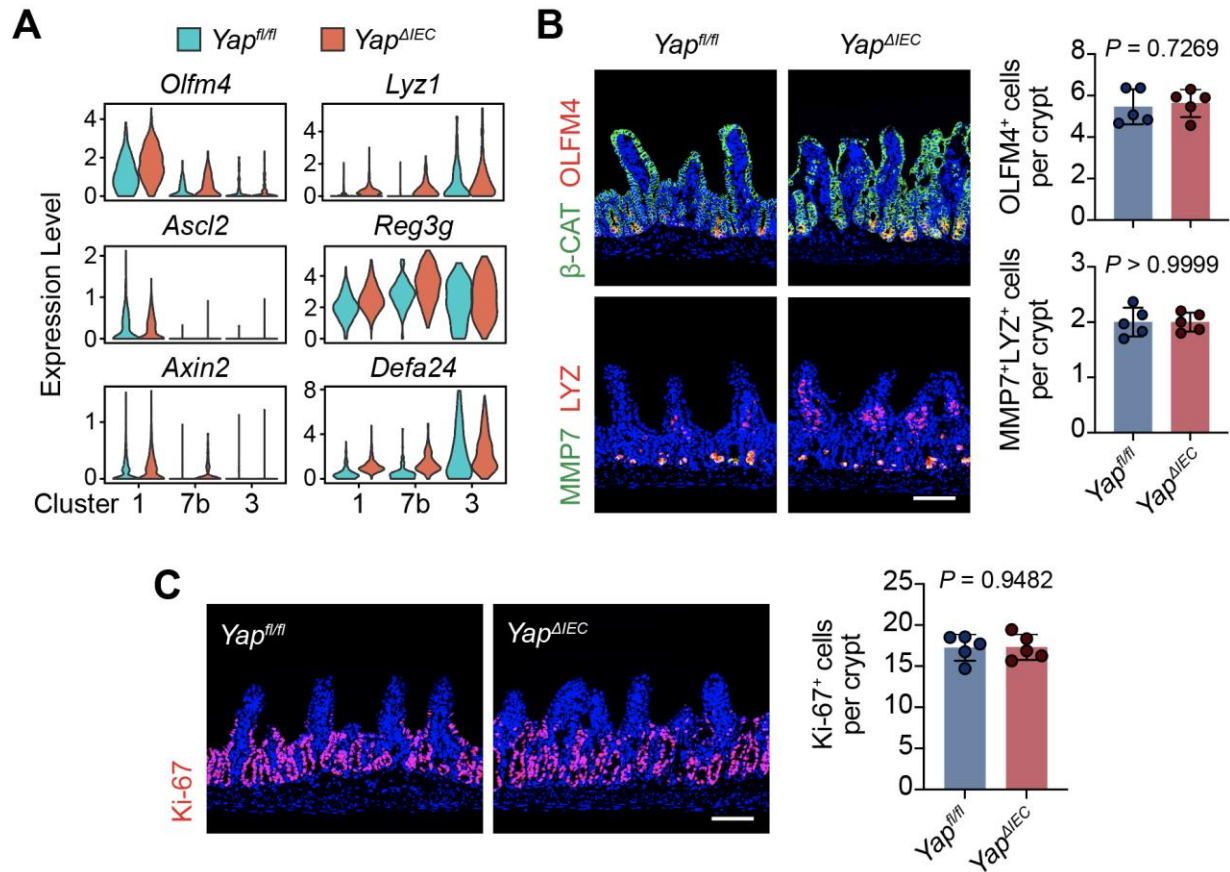


Figure 4.14. Analysis of Wnt signaling and cell proliferation in the absence of YAP

(A) Expression of stem cell (*Olfm4*, *Ascl2*), Wnt (*Axin2*), and Paneth cell (*Lyz1*, *Reg3g*, *Defa24*) markers in stem/progenitor cells (cluster 1), atrophy-induced enterocytes (cluster 7b), and goblet cells (cluster 3) separated by genotype. (B and C) IF and quantification of OLFM4⁺ ISCs (B, top), MMP7⁺LYZ⁺ Paneth cells (B, bottom), and Ki-67⁺ cells (C) in the crypt. Average number of cells across 30 crypts was plotted as mean \pm SD. n = 5 mice/group. Significance was determined by unpaired *t*-test. Bars: 100 μ m. Images are representative of at least 3 animals.

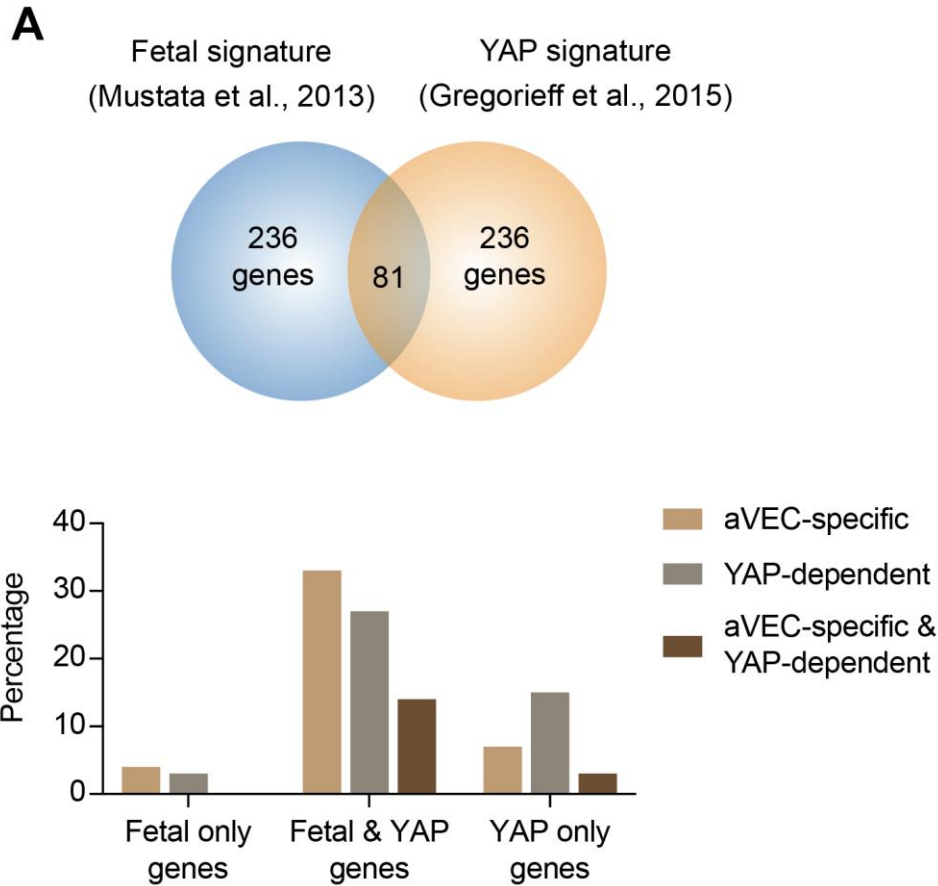


Figure 4.15. Defining the extent to which YAP controls the fetal and aVEC program

(A) Venn diagram of all the fetal signature genes (317 total) and the top 317 YAP signature genes reveals 81 overlapping targets. (B) Every gene from this merged dataset (indicated as fetal only, fetal and YAP, or YAP only genes) was assessed for its specificity as an aVEC marker (as determined by our scRNA-seq data in **Figure 3.6**) and its dependency on YAP in aVECs (as determined by our scRNA-seq data in **Figure 4.10**). Percentage of genes that meet these criteria was plotted. Note that many of the fetal-YAP overlapping genes were expressed in aVECs. Of these overlapping genes, only ~40% of aVEC markers were impacted by *Yap* deletion.

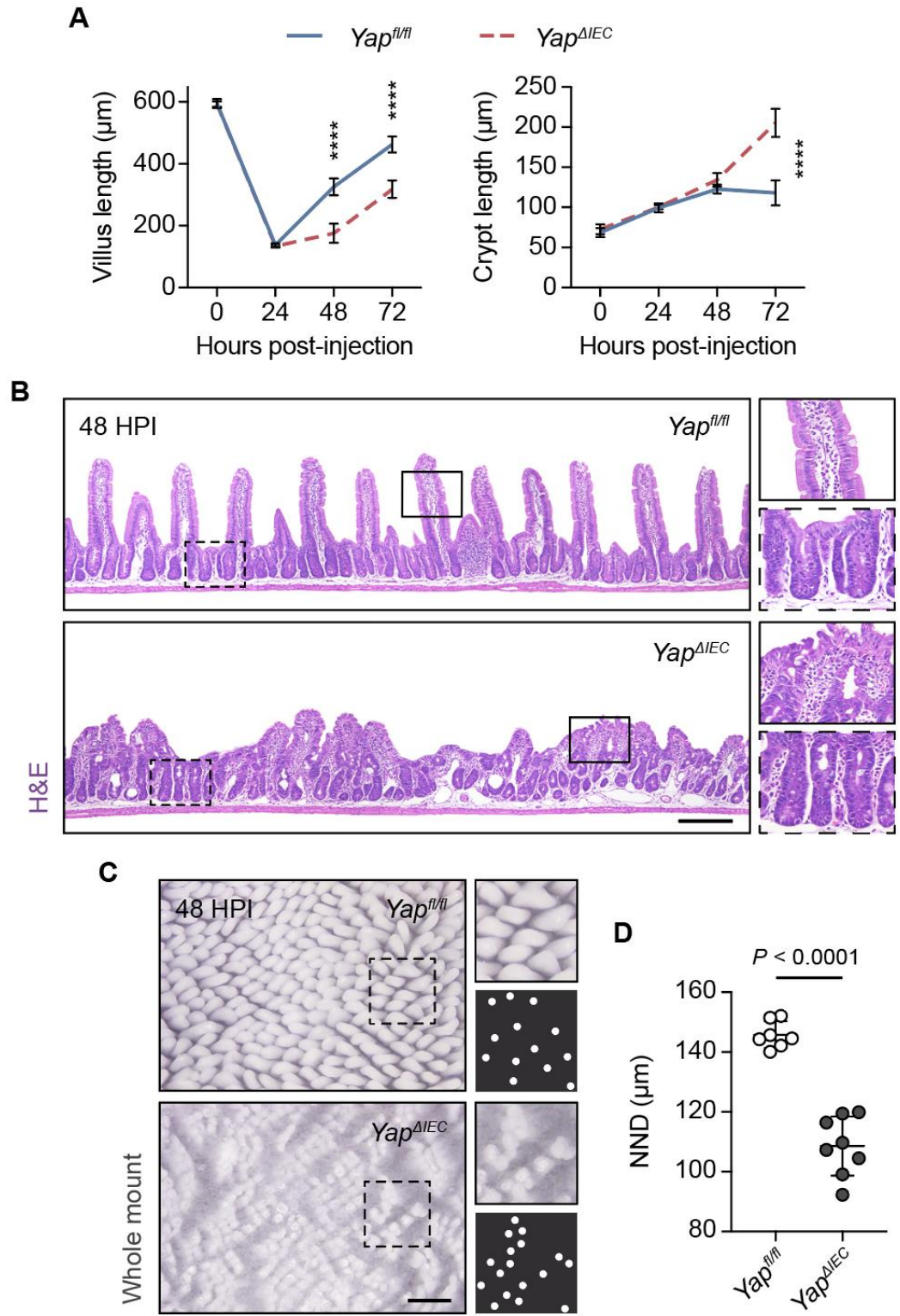


Figure 4.16. Loss of YAP results in impaired villus regeneration

(A) Average villus/crypt length across 50 villi/crypts for each time point based on H&E images was plotted as mean \pm SD. n = 6-8 mice/group. Significance was determined by unpaired *t*-test with Welch's correction. ****p < 0.0001. (B) H&E images of the regenerating intestine at 48 HPI from *Yap^{fl/fl}* and *Yap^{ΔIEC}* mice. Bar: 200 μ m. (C and D) Whole mount luminal view of regenerating villi at 48 HPI from *Yap^{fl/fl}* and *Yap^{ΔIEC}* mice (C). Bar: 500 μ m. White dots represent individual villus tips. The distance between a villus and its closest neighboring villus, known as the nearest neighbor distance (NND), was calculated based on the whole-mount images, and the average value was plotted as mean \pm SD (D). n = 7-8 mice/group. Significance was determined by unpaired *t*-test. H&E and whole mount images are representative of at least 3 animals.

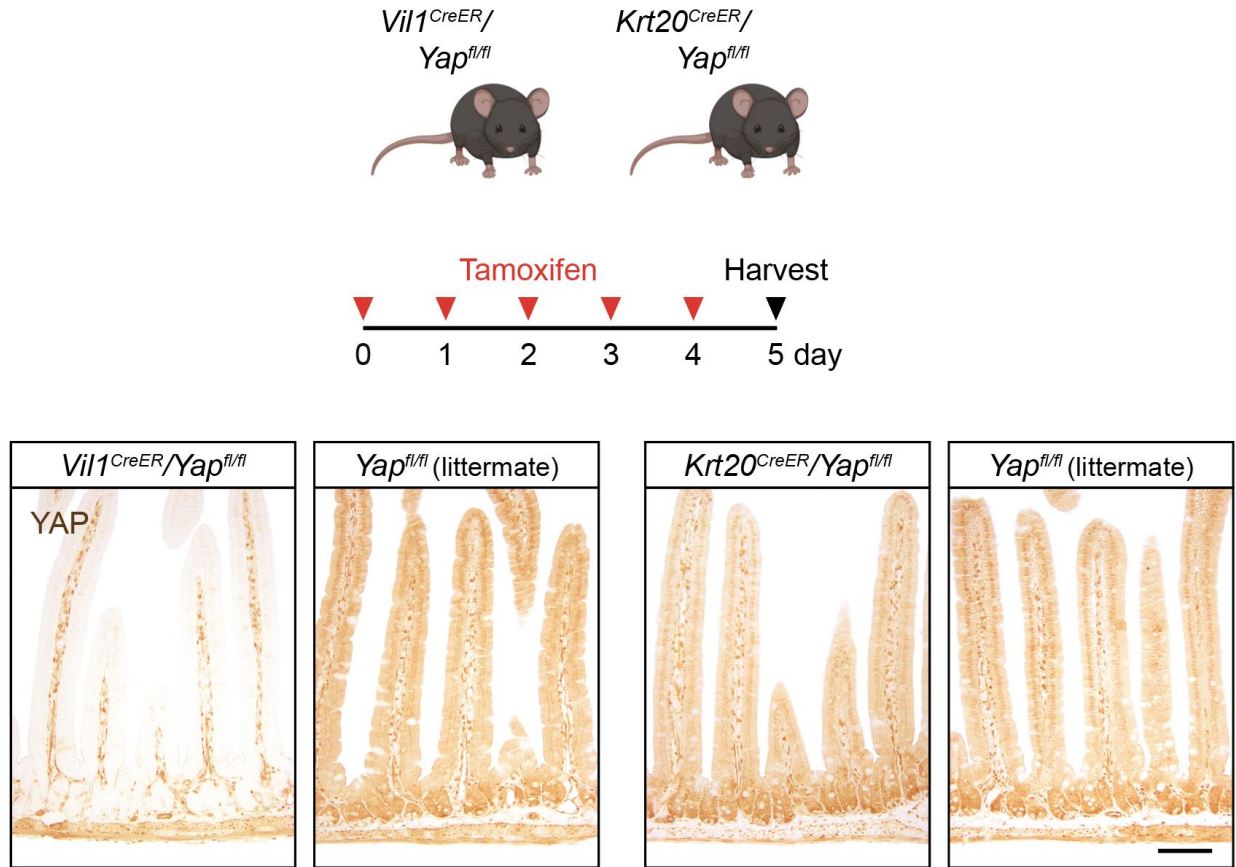


Figure 4.17. Inability to delete YAP in differentiated cells using $Krt20^{CreER}/Yap^{fl/fl}$ mice

$Vil1^{CreER}/Yap^{fl/fl}$, $Krt20^{CreER}/Yap^{fl/fl}$, and $Yap^{fl/fl}$ littermate control mice were given 5 consecutive injections of tamoxifen and examined on the 6th day (top). IHC for YAP (brown) in the homeostatic intestine from these mice (bottom). Loss of YAP expression was seen in $Vil1^{CreER}/Yap^{fl/fl}$ mice (positive control) but not in $Krt20^{CreER}/Yap^{fl/fl}$ mice. This is likely because *Yap* mRNA is generated in the crypt and the protein persists in the villus. Thus, we were unable to specifically assess the function of Yap in the differentiated villus compartment after injury.

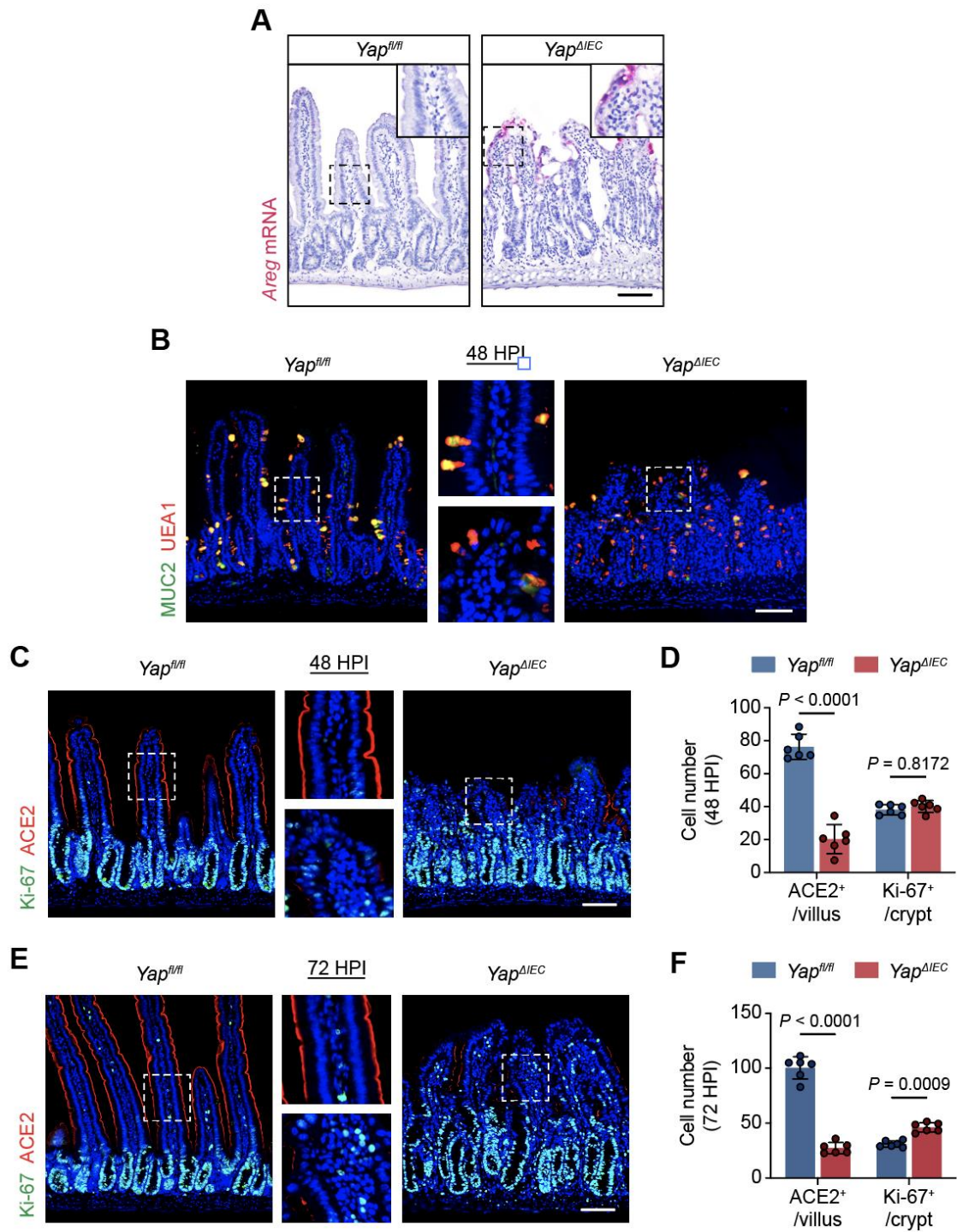


Figure 4.18. Impaired villus regeneration in *Yap*^{ΔIEC} mice is accompanied by a persistent maladapted aVEC state and abnormal epithelial differentiation

(A) RNAscope for *Areg* in the regenerating intestine at 48 HPI from *Yap^{fl/fl}* and *Yap^{ΔIEC}* mice.

(B) IF for MUC2 (green) and UEA1 (red) in the regenerating intestine at 48 HPI from *Yap^{fl/fl}* and *Yap^{ΔIEC}* mice. (C-F) IF for Ki-67 (green) and ACE2 (red) in the regenerating intestine at 48 HPI (C) and 72 HPI (E) from *Yap^{fl/fl}* and *Yap^{ΔIEC}* mice. Average number of Ki-67⁺ and ACE2⁺ cells across 30 villi/crypts at 48 HPI (D) and 72 HPI (F) was plotted and displayed as mean ± SD. n = 6 mice/group. Significance was determined by two-way ANOVA and Sidak's multiple comparisons test. All bars: 100 μm. RNAscope/IF images are representative of at least 3 animals.

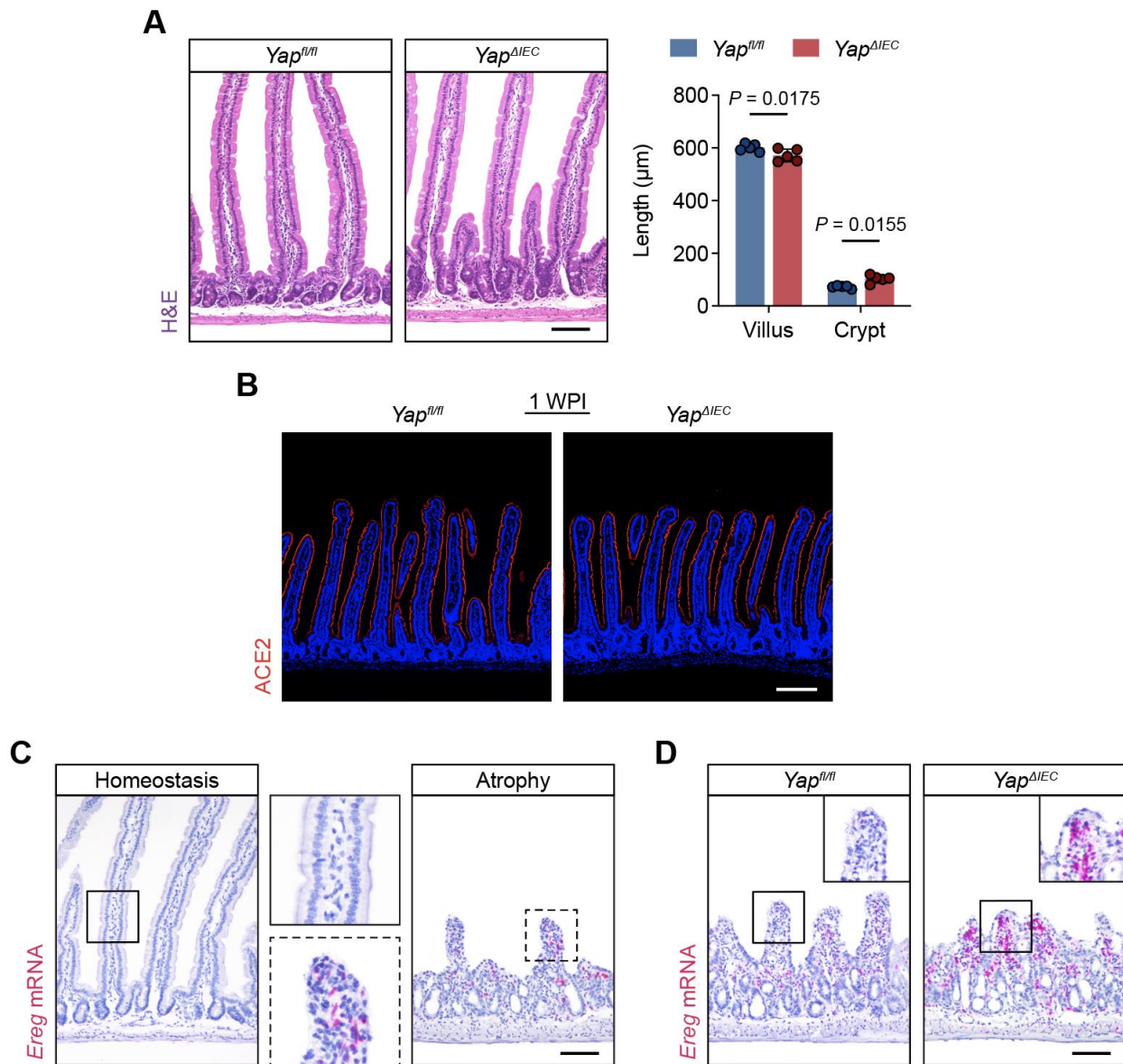


Figure 4.19. Eventual recovery of villus structures in *Yap^{ΔIEC}* mice one-week post-injury and possible compensation by stromal EREG

(A) H&E images of the regenerating intestine at one-week post-injury from *Yap^{fl/fl}* and *Yap^{AIEC}* mice (left). Average villus/crypt length across 50 villi/crypts was plotted as mean \pm SD (right). n = 5 mice/group. Significance was determined by two-way ANOVA and Sidak's multiple comparisons test. Bar: 100 μ m. (B) IF for ACE2 (red) in the regenerating intestine at one-week post-injury from *Yap^{fl/fl}* and *Yap^{AIEC}* mice. Bar: 200 μ m (C and D) RNAscope for *Ereg* in the homeostatic and atrophic intestine from wild-type mice (C) and the atrophic intestine from *Yap^{fl/fl}* and *Yap^{AIEC}* mice (D). Bars: 100 μ m. Note that *Ereg* expression is induced during villus atrophy and even more upregulated in the stroma of atrophic villi in *Yap^{AIEC}* mice, suggesting a possible compensatory response. H&E, IF, and RNAscope images are representative of at least 3 animals.

4.6 Tables

Table 4.1. Genes commonly induced in aVECs and WAE cells, related to Figure 4.2

Gene	(aVEC)- log10 P- value	(aVEC) log2 FC	(WAE)- log10 P- value	(WAE) log2 FC
Clu	6.67	7.00	1.49	2.71
Msln	3.88	6.76	2.42	4.78
Sprr1a	4.70	6.50	1.97	4.27
Adam8	5.31	6.39	8.48	3.41
Plaur	2.90	6.34	2.81	3.60
Ly6d	5.70	6.28	4.43	4.29
Plat	4.59	6.16	2.66	2.62
Acsbg1	6.50	6.07	3.56	2.90
Mal	3.91	5.75	2.46	3.66
Anxa1	4.57	5.64	2.39	2.28
Trim10	3.85	5.51	1.94	2.04
Isg20	6.33	5.44	3.82	2.96
Il1r1	4.61	5.41	2.19	3.21
Anxa5	4.79	5.25	2.91	2.22
Inhba	4.24	5.07	2.83	3.31
Vill	5.16	5.02	2.63	2.21
Cd44	5.52	4.74	3.05	2.27
Emp2	4.82	4.74	1.43	2.00
F3	7.18	4.71	2.26	2.71
Hmox1	5.27	4.67	6.04	2.09
Il11	4.62	4.66	5.23	3.23
Krt7	5.76	4.62	2.99	2.02
Ap1s2	4.87	4.54	3.34	2.58
Bmp8b	5.47	4.50	3.09	3.76
Pdlim7	6.28	4.48	2.74	2.06
Aldh1a3	2.06	4.38	2.74	3.88
Dok2	4.92	4.36	2.53	3.18
Egfr	6.27	4.34	2.81	3.44
Phldb2	5.90	4.27	2.38	2.32
Ubd	2.69	4.20	2.81	2.79
Phlda3	4.42	4.10	2.76	2.54
Fgd3	6.11	4.10	2.53	2.58
Tnfrsf22	5.04	4.01	2.40	2.36
Rap2b	3.72	3.99	3.62	2.13
Lox	3.09	3.98	2.56	2.03
Akr1b8	4.09	3.98	5.58	2.05
Sprr2h	4.20	3.97	4.14	4.02
Prss12	3.19	3.95	2.97	3.68
Mmp10	3.91	3.91	2.42	3.76
Dyrk3	3.32	3.87	1.34	2.07
Rbp1	5.01	3.84	2.54	3.70
Tnfrsf12a	5.54	3.81	2.18	2.15
Atg9b	4.32	3.79	2.31	2.19
Stx11	3.77	3.75	4.56	2.49
Las1l	4.73	3.54	3.38	2.21
Stx1a	2.85	3.49	3.50	2.83
Phlda1	5.38	3.46	2.28	2.10
Arid5a	3.94	3.45	1.86	2.04
Sh3kbp1	4.42	3.37	2.75	2.06
Marcksl1	6.19	3.35	2.56	2.61
Osmr	4.50	3.22	5.13	3.52
Actn1	5.53	3.17	3.16	2.04
Plekhg3	4.69	3.16	3.60	2.06
Dusp1	4.15	3.10	1.90	2.05
Rgs12	2.79	3.07	2.72	3.56
Pls3	4.42	3.04	3.04	2.17
Slc39a6	3.69	2.92	1.68	2.03
Tgm2	3.46	2.89	3.02	3.47
Serpine1	2.70	2.86	3.54	3.62
Ppfbp1	4.06	2.85	2.78	2.32
Dusp4	4.89	2.71	3.77	3.38
Slc15a3	2.16	2.69	5.61	2.50
Glis2	3.82	2.67	2.13	2.06
Cxcr4	2.86	2.67	3.65	2.34
Ephb2	4.95	2.66	2.65	2.12
Ctgf	2.93	2.57	2.76	2.72
Clec4d	2.32	2.57	6.23	3.74
Cldn4	3.98	2.54	1.87	2.94
Ier3	3.67	2.46	2.66	2.40
Gcnt2	2.46	2.45	1.56	2.43
Thbs1	2.84	2.42	7.28	2.38
Trim15	4.09	2.39	1.63	2.32
Bdh2	3.68	2.36	3.04	3.13
Enc1	4.57	2.33	2.40	2.11
Abl2	4.20	2.32	3.59	2.04
Arf2	4.27	2.28	2.37	2.46
Spire1	3.46	2.27	4.20	2.17
Uchl1	2.74	2.25	2.71	2.47
Mthfd1l	3.22	2.20	2.20	2.23
Ecm1	4.54	2.19	3.42	2.47
Parvb	1.62	2.16	2.57	2.27
Trim29	3.20	2.14	2.41	2.67
Myadm	4.46	2.14	3.47	2.16
Itga2	3.48	2.08	2.76	2.61
Crip2	2.78	2.00	2.55	2.34
Slc16a3	2.46	-3.60	1.61	2.82
Ccl24	3.65	-5.34	1.71	2.01

Comparison of the aVEC and WAE LCM-microarray datasets reveals 87 commonly induced genes. These genes are likely responsible for the barrier function of these damaged-induced cells.

Table 4.2. Genes expressed by aVECs and/or YAP-dependent, related to Figure 4.15

Fetal Genes	YAP Genes	Mtap6	Mtap6	Ak1	Ankrd35	Escr	Fam83h	Il4ra	Lgals3	Rdh10	Ptpn21
Abcc5	Abcc5	Paqr8	Paqr8	Akap13	Ano1	Eda2r	Fgd3	Inf2	Lhfp2	Rgs17	Ptfr
Ahnak	Ahnak	Pdzk1ip1	Pdzk1ip1	Akr1b10	Anxa2	Efem1	Fina	Itgb4	Ltaf	Rgs19	Pthr1
Akr1b8	Akr1b8	Phlda2	Phlda2	Akr1b3	Apo19a	Efn5	Flnb	Ivl	Lmo7	Rps19	Pvr
Anxa1	Anxa1	Plat	Plat	Alcam	Apo19b	Enah	Fos	Kcnn4	Lrfip1	S100a4	Pwwp2b
Anxa3	Anxa3	Plaur	Plaur	Anxa8	Areg	Endod1	Gjb4	Klhl13	Ly6c1	S100a7A	Raph1
Anxa5	Anxa5	Plk2	Plk2	Ap1s3	Arhgap29	Epha4	Gli2	Krt4	Ly6c2	Samd5	Rassf1
Bmp8b	Bmp8b	Ppl	Ppl	Aqp5	Arhgap40	Eps811	Gm10129	Lama3	Macf1	Sca10	Rbpm5
Capn2	Capn2	Psc	Psc	Arhgap44	Atf3	Erc5	Gm10393	Laptm5	Maff	Scel	Rhof
Capn5	Capn5	Rbms1	Rbms1	Arhgef3	Atp11a	Exoc4	Gm10972	Ldh2	Mmp23	Scmh1	Rin1
Car2	Car2	Rhod	Rhod	Arhgef4	Bcam	Exp1	Gm14446	Ly6c	Mndal	Serpinb11	Rin3
Cd55	Cd55	S100a11	S100a11	Ar1	Bex1	Fabp5	Gm16721	Ly6d	Mrc1	Serpinb6b	Rnf208
Cgnl1	Cgnl1	S100a14	S100a14	Ar14c	Bmp2	Fam129b	Gm17237	Ly6f	Myadm	Serpinh1	Rnf39
Chmb1	Chmb1	S100a16	S100a16	Avp1	Btn1a1	Fam149a	Gm17622	Mai	Myo1c	Serpinh1	Rras2
Clic3	Clic3	S100a6	S100a6	B9d1	Calcb	Fam198b	Gm7008	Mcam	Myo1e	Sfpc	Rsd2
Clu	Clu	Serpinb5	Serpinb5	Baiap2	Camk1	Fam212b	Gm7665	Mcpt2	Myo1h	Sfpc	Rtp4
Cnn2	Cnn2	Serpinb9b	Serpinb9b	Basp1	Ccdc120	Fam64a	Gngt2	Mdm2	Myof	Sh3kbp1	S1pr2
Crip2	Crip2	Slc25a48	Slc25a48	Bax	Cdce68	Far1	Gprc5a	Mfsd4	Nbl1	Slc19a2	Samd9l
Cryab	Cryab	Slc44a2	Slc44a2	Bok	Ci20	Fbw9	Grasp	Mgat4c	Neu1	Slc39a10	Sema3c
Ctgf	Ctgf	Spr1a	Spr1a	Btdb11	Cdkn1c	Fer113	Hbegf	Mgmt	Ngfrap1	Slc45a3	Serpinb9
Cxcl16	Cxcl16	Suox	Suox	Chac1	Cidec	Fkbp9	Hdac7	Mkl1	Nid1	Slc4a11	Skg2
E130012A19Rik	E130012A19Rik	Syt8	Syt8	Camkk1	Cidec	Fln	Hsd17b2	Msantd3	Npnt	Slco4a1	Sh3bp5
Emp1	Emp1	Tead4	Tead4	Camsap2	Clca6	Flot2	Hsp110	Msn	Oas3	Sln2	Sh3t1
Emp2	Emp2	Tinag1	Tinag1	Cdc92	Cldn4	Fmn12	Hsp110	Ncmip	Oas11	Soga2	Sh3t2
Epn3	Epn3	Trex2	Trex2	Cnd1	Cld4	Fmx2	Id1	Nfe2l3	Oas12	Sox21	Slamf9
Ereg	Ereg	Vangl1	Vangl1	Cnd2	Cnks1r	Frdm6	Id3	Nox1	Omp	Sox21	Slc35a4
Fosl1	Fosl1	Vnn1	Vnn1	Cng1	Crf3	Fut2	Ifi271l	Oas1f	Otd7b	Spat6	Slc5a5
Gadd45b	Gadd45b	Wfdc2	Wfdc2	Ccp110	Csrp1	Fxyd3	Ifit1	Osbp15	P2x2	Spp1	Slc5a6
Gcnt1	Gcnt1	Whip	Whip	Cd14	G6pdx	Gatm	Ifit3	P2ry2	Pak6	Sptssb	Slc7a11
Ggta1	Ggta1	Wwc2	Wwc2	Cd44	Cyr61	Gcm3	Ifrd1	P2ry6	Pallid	Stb11	Sorbs2
Gjb3	Gjb3	Wwtr1	Wwtr1	Cd68	Ddx60	Gja1	Il28ra	Pdlim4	Pard6b	Susd4	Spr2a1
Glpr1	Glpr1	1110028F11Rik	1110032A04Rik	Cd99i2	Dnahc2	Gkn1	Isq15	Pdlim7	Pcolce	Syt14l	Spr2a2
Hspa1b	Hspa1b	1700007K13Rik	1700019G06Rik	Cdh13	Dok2	Glis3	Isx	Pir	Pcsk6	Tacstd2	Spr2a3
Id2	Id2	1700066819Rik	1700019L03Rik	Cdkn2a	Dusp1	Gnai1	Itgb6	Phlda3	Pey11a	Tbc1d2	Spr2b
Ier3	Ier3	2210011C24Rik	2010002M12Rik	Ckap2	Dusp10	Golg2	Jag2	Picd3	Pear1	Timp2	Spr2c
Il1m	Il1m	2310002J15Rik	2010109I03Rik	Cicf1	Dusp14	Gpc1	Jdp2	Plekhs1	Pgap1	Tir4	Steap1
Il33	Il33	4632434I11Rik	2310002L13Rik	Col18a1	Dusp3	Gpr120	Kctd10	Pif	Phid1a	Tmem34	Steap2
Ildr1	Ildr1	4833427G06Rik	2310007B03Rik	Col4a1	Dusp8	Gpr137b	Klf4	Pmepa1	Phidb2	Tmem40	Stk32c
Jub	Jub	4930461G14Rik	A430105I19Rik	Col4a2	Dusp9	Gpx2	Klf6	Pmm1	Pim1	Tmem43	Syde1
Klf3	Klf3	5730416F02Rik	AA986860	Cpt1c	Edn1	Gsn	Krt14	Ppp1r2	Plau	Tnfrsf10b	Syt12
Klrg2	Klrg2	5830408B19Rik	Abhd2	Ctsb	Ehd2	Gtse1	Krt16	Ppcc	Plec	Tnni2	Tagln2
Krt18	Krt18	Aaas	Acot10	Cugbp2	Epha2	Gusb	Krt17	Prkar1a	Plec	Tnni2	Tgfb2
Krt23	Krt23	Abcb1b	Acot9	Dap1	Ezr	Hsf6t2	Krt19	Prkcdp	Plekhh3	Tns4	Thbs1
Krt7	Krt7	Abcc4	Acot2	Dcxr	F2r1	Hspa2	Krt42	Pri2c3	Pmaip1	Tpm2	Tjp1
Lamc2	Lamc2	Abhd4	Adam8	Ddah1	F3	Hspb1	Krt8	Prss22	Pmp22	Trp5inp1	Tln2
Lmna	Lmna	Abi3	Adamts15	Ddit4l	Fam101b	Hyal1	Krt80	Psap1l	Pparg	Tspan2	Tm4sf1
Lor	Lor	Acsm3	Adm2	Dhh	Fam129a	Ica1	Krt9	Psc1	Ppp1r15a	Tspan4	Tm4sf4
Ly6a	Ly6a	Adam9	AF064781	Discr6	Fam160a1	Icam1	Lama5	Ptp4a3	Ppp1r2	Tspan6	Tmem188
Mboat1	Mboat1	Aen	Akap2	Dusp22	Fam189a2	Igf7	Lamb3	Rab11fip5	Prrg4	Tuba1	Tnks1bp1
Mras	Mras	Al647606	Als2c4	Dyrk3	Fam46b	Igf7	Lats2	Rab15	Prss23	Tubb6	Tnb3
Msln	Msln	Aim1	Amot2	Ecm1	Fam59a	Il17re	Ldh	Rab27b	Psat1	Usp46	Trim15

Fetal signature genes: Mustata et al., 2013	
YAP signature genes: Gregorieff et al., 2015	
	= Common to both datasets (Fetal & YAP genes)
Vamp5	Tsc22d2
Vax1	Tuft1
Vsig1	Unc13d
Wnt4	Usp18
Zbtb32	Wnt7a
Zfp365	Wwc1
Zfp52	Zfp185
Zic4	Zfp37
Zmat3	Zmynd15
	Blue text = aVEC-specific genes
	Red text = YAP-dependent genes in aVECs
	Green text = aVEC-specific & YAP-dependent genes

Fetal signature genes (317 total) and the top 317 YAP signature genes were compared. 81 genes were shared between the two datasets (shaded in yellow). Every gene here was examined for its specificity as an aVEC marker (blue and green texts) and as a YAP target gene in aVECs (red and green texts). This analysis helps determine the extent to which YAP controls the aVEC state.

4.7 References

- Ayyaz, A., Kumar, S., Sangiorgi, B., Ghoshal, B., Gosio, J., Ouladan, S., Fink, M., Barutcu, S., Trcka, D., Shen, J., *et al.* (2019). Single-cell transcriptomes of the regenerating intestine reveal a revival stem cell. *Nature* *569*, 121-125.
- Azzolin, L., Panciera, T., Soligo, S., Enzo, E., Bicciato, S., Dupont, S., Bresolin, S., Frasson, C., Basso, G., Guzzardo, V., *et al.* (2014). YAP/TAZ incorporation in the beta-catenin destruction complex orchestrates the Wnt response. *Cell* *158*, 157-170.
- Bankaitis, E.D., Ha, A., Kuo, C.J., and Magness, S.T. (2018). Reserve Stem Cells in Intestinal Homeostasis and Injury. *Gastroenterology* *155*, 1348-1361.
- Barriga, F.M., Montagni, E., Mana, M., Mendez-Lago, M., Hernando-Momblona, X., Sevillano, M., Guillaumet-Adkins, A., Rodriguez-Esteban, G., Buczacki, S.J.A., Gut, M., *et al.* (2017). Mex3a Marks a Slowly Dividing Subpopulation of Lgr5+ Intestinal Stem Cells. *Cell Stem Cell* *20*, 801-816 e807.
- Barry, E.R., Morikawa, T., Butler, B.L., Shrestha, K., de la Rosa, R., Yan, K.S., Fuchs, C.S., Magness, S.T., Smits, R., Ogino, S., *et al.* (2013). Restriction of intestinal stem cell expansion and the regenerative response by YAP. *Nature* *493*, 106-110.
- Becht, E., McInnes, L., Healy, J., Dutertre, C.A., Kwok, I.W.H., Ng, L.G., Ginhoux, F., and Newell, E.W. (2018). Dimensionality reduction for visualizing single-cell data using UMAP. *Nat Biotechnol.*
- Beumer, J., and Clevers, H. (2021). Cell fate specification and differentiation in the adult mammalian intestine. *Nat Rev Mol Cell Biol* *22*, 39-53.
- Buczacki, S.J., Zecchini, H.I., Nicholson, A.M., Russell, R., Vermeulen, L., Kemp, R., and Winton, D.J. (2013). Intestinal label-retaining cells are secretory precursors expressing Lgr5. *Nature* *495*, 65-69.
- Butler, A., Hoffman, P., Smibert, P., Papalexi, E., and Satija, R. (2018). Integrating single-cell transcriptomic data across different conditions, technologies, and species. *Nat Biotechnol* *36*, 411-420.
- Cai, J., Maitra, A., Anders, R.A., Taketo, M.M., and Pan, D. (2015). beta-Catenin destruction complex-independent regulation of Hippo-YAP signaling by APC in intestinal tumorigenesis. *Genes Dev* *29*, 1493-1506.
- Cai, J., Zhang, N., Zheng, Y., de Wilde, R.F., Maitra, A., and Pan, D. (2010). The Hippo signaling pathway restricts the oncogenic potential of an intestinal regeneration program. *Genes Dev* *24*, 2383-2388.

- Calvo, F., Ege, N., Grande-Garcia, A., Hooper, S., Jenkins, R.P., Chaudhry, S.I., Harrington, K., Williamson, P., Moeendarbary, E., Charras, G., *et al.* (2013). Mechanotransduction and YAP-dependent matrix remodelling is required for the generation and maintenance of cancer-associated fibroblasts. *Nat Cell Biol* *15*, 637-646.
- Camargo, F.D., Gokhale, S., Johnnidis, J.B., Fu, D., Bell, G.W., Jaenisch, R., and Brummelkamp, T.R. (2007). YAP1 increases organ size and expands undifferentiated progenitor cells. *Curr Biol* *17*, 2054-2060.
- Cao, J., Spielmann, M., Qiu, X., Huang, X., Ibrahim, D.M., Hill, A.J., Zhang, F., Mundlos, S., Christiansen, L., Steemers, F.J., *et al.* (2019). The single-cell transcriptional landscape of mammalian organogenesis. *Nature* *566*, 496-502.
- Casaleto, J.B., Saotome, I., Curto, M., and McClatchey, A.I. (2011). Ezrin-mediated apical integrity is required for intestinal homeostasis. *Proc Natl Acad Sci U S A* *108*, 11924-11929.
- Chen, E.Y., Tan, C.M., Kou, Y., Duan, Q., Wang, Z., Meirelles, G.V., Clark, N.R., and Ma'ayan, A. (2013). Enrichr: interactive and collaborative HTML5 gene list enrichment analysis tool. *BMC Bioinformatics* *14*, 128.
- Cheung, P., Xiol, J., Dill, M.T., Yuan, W.C., Panero, R., Roper, J., Osorio, F.G., Maglic, D., Li, Q., Gurung, B., *et al.* (2020). Regenerative Reprogramming of the Intestinal Stem Cell State via Hippo Signaling Suppresses Metastatic Colorectal Cancer. *Cell Stem Cell* *27*, 590-604 e599.
- Choi, W., Kim, J., Park, J., Lee, D.H., Hwang, D., Kim, J.H., Ashktorab, H., Smoot, D., Kim, S.Y., Choi, C., *et al.* (2018). YAP/TAZ Initiates Gastric Tumorigenesis via Upregulation of MYC. *Cancer Res* *78*, 3306-3320.
- Dey, A., Varelas, X., and Guan, K.L. (2020). Targeting the Hippo pathway in cancer, fibrosis, wound healing and regenerative medicine. *Nat Rev Drug Discov* *19*, 480-494.
- Dickson, B.C., Streutker, C.J., and Chetty, R. (2006). Coeliac disease: an update for pathologists. *J Clin Pathol* *59*, 1008-1016.
- Dictionary, O.E. (2021). "restitution, n." (Oxford University Press).
- El-Assal, O.N., and Besner, G.E. (2005). HB-EGF enhances restitution after intestinal ischemia/reperfusion via PI3K/Akt and MEK/ERK1/2 activation. *Gastroenterology* *129*, 609-625.
- Gregorieff, A., Liu, Y., Inanlou, M.R., Khomchuk, Y., and Wrana, J.L. (2015). Yap-dependent reprogramming of Lgr5(+) stem cells drives intestinal regeneration and cancer. *Nature* *526*, 715-718.
- Gunzel, D., and Yu, A.S. (2013). Claudins and the modulation of tight junction permeability. *Physiol Rev* *93*, 525-569.

Hong, A.W., Meng, Z., and Guan, K.L. (2016). The Hippo pathway in intestinal regeneration and disease. *Nat Rev Gastroenterol Hepatol* 13, 324-337.

Jansson-Knodell, C.L., Hujoel, I.A., Rubio-Tapia, A., and Murray, J.A. (2018). Not All That Flattens Villi Is Celiac Disease: A Review of Enteropathies. *Mayo Clin Proc* 93, 509-517.

Kaiko, G.E., Chen, F., Lai, C.W., Chiang, I.L., Perrigoue, J., Stojmirovic, A., Li, K., Muegge, B.D., Jain, U., VanDussen, K.L., *et al.* (2019). PAI-1 augments mucosal damage in colitis. *Sci Transl Med* 11.

Kim, C.K., Yang, V.W., and Bialkowska, A.B. (2017). The Role of Intestinal Stem Cells in Epithelial Regeneration Following Radiation-Induced Gut Injury. *Curr Stem Cell Rep* 3, 320-332.

Kuhnert, F., Davis, C.R., Wang, H.T., Chu, P., Lee, M., Yuan, J., Nusse, R., and Kuo, C.J. (2004). Essential requirement for Wnt signaling in proliferation of adult small intestine and colon revealed by adenoviral expression of Dickkopf-1. *Proc Natl Acad Sci U S A* 101, 266-271.

Kuleshov, M.V., Jones, M.R., Rouillard, A.D., Fernandez, N.F., Duan, Q., Wang, Z., Koplev, S., Jenkins, S.L., Jagodnik, K.M., Lachmann, A., *et al.* (2016). Enrichr: a comprehensive gene set enrichment analysis web server 2016 update. *Nucleic Acids Res* 44, W90-97.

Lacy, E.R. (1988). Epithelial restitution in the gastrointestinal tract. *J Clin Gastroenterol* 10 Suppl 1, S72-77.

Lebwohl, B., Murray, J.A., Rubio-Tapia, A., Green, P.H., and Ludvigsson, J.F. (2014). Predictors of persistent villous atrophy in coeliac disease: a population-based study. *Aliment Pharmacol Ther* 39, 488-495.

Lee, M.J., Byun, M.R., Furutani-Seiki, M., Hong, J.H., and Jung, H.S. (2014). YAP and TAZ regulate skin wound healing. *J Invest Dermatol* 134, 518-525.

Li, Q., Sun, Y., Jarugumilli, G.K., Liu, S., Dang, K., Cotton, J.L., Xiol, J., Chan, P.Y., DeRan, M., Ma, L., *et al.* (2020). Lats1/2 Sustain Intestinal Stem Cells and Wnt Activation through TEAD-Dependent and Independent Transcription. *Cell Stem Cell* 26, 675-692 e678.

Lin, K.C., Park, H.W., and Guan, K.L. (2017). Regulation of the Hippo Pathway Transcription Factor TEAD. *Trends Biochem Sci* 42, 862-872.

Lu, L., Finegold, M.J., and Johnson, R.L. (2018). Hippo pathway coactivators Yap and Taz are required to coordinate mammalian liver regeneration. *Exp Mol Med* 50, e423.

Manieri, N.A., Drylewicz, M.R., Miyoshi, H., and Stappenbeck, T.S. (2012). Igf2bp1 is required for full induction of Ptg2 mRNA in colonic mesenchymal stem cells in mice. *Gastroenterology* 143, 110-121 e110.

- Metcalf, C., Kljavin, N.M., Ybarra, R., and de Sauvage, F.J. (2014). Lgr5⁺ stem cells are indispensable for radiation-induced intestinal regeneration. *Cell Stem Cell* 14, 149-159.
- Miyoshi, H., Ajima, R., Luo, C.T., Yamaguchi, T.P., and Stappenbeck, T.S. (2012). Wnt5a potentiates TGF-beta signaling to promote colonic crypt regeneration after tissue injury. *Science* 338, 108-113.
- Miyoshi, H., VanDussen, K.L., Malvin, N.P., Ryu, S.H., Wang, Y., Sonnek, N.M., Lai, C.W., and Stappenbeck, T.S. (2017). Prostaglandin E2 promotes intestinal repair through an adaptive cellular response of the epithelium. *EMBO J* 36, 5-24.
- Mohri, Z., Del Rio Hernandez, A., and Krams, R. (2017). The emerging role of YAP/TAZ in mechanotransduction. *J Thorac Dis* 9, E507-E509.
- Moya, I.M., and Halder, G. (2019). Hippo-YAP/TAZ signalling in organ regeneration and regenerative medicine. *Nat Rev Mol Cell Biol* 20, 211-226.
- Murata, K., Jadhav, U., Madha, S., van Es, J., Dean, J., Cavazza, A., Wucherpfennig, K., Michor, F., Clevers, H., and Shivdasani, R.A. (2020). Ascl2-Dependent Cell Dedifferentiation Drives Regeneration of Ablated Intestinal Stem Cells. *Cell Stem Cell* 26, 377-390 e376.
- Mustata, R.C., Vasile, G., Fernandez-Vallone, V., Strollo, S., Lefort, A., Libert, F., Monteyne, D., Perez-Morga, D., Vassart, G., and Garcia, M.I. (2013). Identification of Lgr5-independent spheroid-generating progenitors of the mouse fetal intestinal epithelium. *Cell Rep* 5, 421-432.
- Nardone, G., Oliver-De La Cruz, J., Vrbsky, J., Martini, C., Pribyl, J., Skladal, P., Pesl, M., Caluori, G., Pagliari, S., Martino, F., *et al.* (2017). YAP regulates cell mechanics by controlling focal adhesion assembly. *Nat Commun* 8, 15321.
- Neto, F., Klaus-Bergmann, A., Ong, Y.T., Alt, S., Vion, A.C., Szymborska, A., Carvalho, J.R., Hollfinger, I., Bartels-Klein, E., Franco, C.A., *et al.* (2018). YAP and TAZ regulate adherens junction dynamics and endothelial cell distribution during vascular development. *Elife* 7.
- Nusse, Y.M., Savage, A.K., Marangoni, P., Rosendahl-Huber, A.K.M., Landman, T.A., de Sauvage, F.J., Locksley, R.M., and Klein, O.D. (2018). Parasitic helminths induce fetal-like reversion in the intestinal stem cell niche. *Nature* 559, 109-113.
- Park, J., Kim, D.H., Shah, S.R., Kim, H.N., Kshitiz, Kim, P., Quinones-Hinojosa, A., and Levchenko, A. (2019). Switch-like enhancement of epithelial-mesenchymal transition by YAP through feedback regulation of WT1 and Rho-family GTPases. *Nat Commun* 10, 2797.
- Potten, C.S. (1977). Extreme sensitivity of some intestinal crypt cells to X and gamma irradiation. *Nature* 269, 518-521.
- Rees, W.D., Tandun, R., Yau, E., Zachos, N.C., and Steiner, T.S. (2020). Regenerative Intestinal Stem Cells Induced by Acute and Chronic Injury: The Saving Grace of the Epithelium? *Front Cell Dev Biol* 8, 583919.

- Romera-Hernandez, M., Aparicio-Domingo, P., Papazian, N., Karrich, J.J., Cornelissen, F., Hoogenboezem, R.M., Samsom, J.N., and Cupedo, T. (2020). Yap1-Driven Intestinal Repair Is Controlled by Group 3 Innate Lymphoid Cells. *Cell Rep* 30, 37-45 e33.
- Rubio-Tapia, A., and Murray, J.A. (2010). Classification and management of refractory coeliac disease. *Gut* 59, 547-557.
- Rutgeerts, P., Geboes, K., Vantrappen, G., Kerremans, R., Coenegrachts, J.L., and Coremans, G. (1984). Natural history of recurrent Crohn's disease at the ileocolonic anastomosis after curative surgery. *Gut* 25, 665-672.
- Seno, H., Miyoshi, H., Brown, S.L., Geske, M.J., Colonna, M., and Stappenbeck, T.S. (2009). Efficient colonic mucosal wound repair requires Trem2 signaling. *Proc Natl Acad Sci U S A* 106, 256-261.
- Sturm, A., and Dignass, A.U. (2008). Epithelial restitution and wound healing in inflammatory bowel disease. *World J Gastroenterol* 14, 348-353.
- Svanes, K., Ito, S., Takeuchi, K., and Silen, W. (1982). Restitution of the surface epithelium of the in vitro frog gastric mucosa after damage with hyperosmolar sodium chloride. Morphologic and physiologic characteristics. *Gastroenterology* 82, 1409-1426.
- Takashima, S., Kadowaki, M., Aoyama, K., Koyama, M., Oshima, T., Tomizuka, K., Akashi, K., and Teshima, T. (2011). The Wnt agonist R-spondin1 regulates systemic graft-versus-host disease by protecting intestinal stem cells. *J Exp Med* 208, 285-294.
- Takeda, H., and Kiyokawa, E. (2017). Activation of Erk in ileal epithelial cells engaged in ischemic-injury repair. *Sci Rep* 7, 16469.
- Taniguchi, K., Wu, L.W., Grivennikov, S.I., de Jong, P.R., Lian, I., Yu, F.X., Wang, K., Ho, S.B., Boland, B.S., Chang, J.T., *et al.* (2015). A gp130-Src-YAP module links inflammation to epithelial regeneration. *Nature* 519, 57-62.
- Tian, H., Biehs, B., Warming, S., Leong, K.G., Rangell, L., Klein, O.D., and de Sauvage, F.J. (2011). A reserve stem cell population in small intestine renders Lgr5-positive cells dispensable. *Nature* 478, 255-259.
- Townley, R.R., Cass, M.H., and Anderson, C.M. (1964). Small Intestinal Mucosal Patterns of Coeliac Disease and Idiopathic Steatorrhoea Seen in Other Situations. *Gut* 5, 51-55.
- Trapnell, C., Cacchiarelli, D., Grimsby, J., Pokharel, P., Li, S., Morse, M., Lennon, N.J., Livak, K.J., Mikkelsen, T.S., and Rinn, J.L. (2014). The dynamics and regulators of cell fate decisions are revealed by pseudotemporal ordering of single cells. *Nat Biotechnol* 32, 381-386.
- Watari, A., Kodaka, M., Matsuhisa, K., Sakamoto, Y., Hisaie, K., Kawashita, N., Takagi, T., Yamagishi, Y., Suzuki, H., Tsujino, H., *et al.* (2017). Identification of claudin-4 binder that attenuates tight junction barrier function by TR-FRET-based screening assay. *Sci Rep* 7, 14514.

- Whiteman, E.L., Fan, S., Harder, J.L., Walton, K.D., Liu, C.J., Soofi, A., Fogg, V.C., Hershenson, M.B., Dressler, G.R., Deutsch, G.H., *et al.* (2014). Crumbs3 is essential for proper epithelial development and viability. *Mol Cell Biol* *34*, 43-56.
- Xie, Z., Wang, Y., Yang, G., Han, J., Zhu, L., Li, L., and Zhang, S. (2021). The role of the Hippo pathway in the pathogenesis of inflammatory bowel disease. *Cell Death Dis* *12*, 79.
- Xin, M., Kim, Y., Sutherland, L.B., Murakami, M., Qi, X., McAnally, J., Porrello, E.R., Mahmoud, A.I., Tan, W., Shelton, J.M., *et al.* (2013). Hippo pathway effector Yap promotes cardiac regeneration. *Proc Natl Acad Sci U S A* *110*, 13839-13844.
- Xu, J., Tang, Y., Sheng, X., Tian, Y., Deng, M., Du, S., Lv, C., Li, G., Pan, Y., Song, Y., *et al.* (2020). Secreted stromal protein ISLR promotes intestinal regeneration by suppressing epithelial Hippo signaling. *EMBO J* *39*, e103255.
- Yan, K.S., Chia, L.A., Li, X., Ootani, A., Su, J., Lee, J.Y., Su, N., Luo, Y., Heilshorn, S.C., Amieva, M.R., *et al.* (2012). The intestinal stem cell markers *Bmi1* and *Lgr5* identify two functionally distinct populations. *Proc Natl Acad Sci U S A* *109*, 466-471.
- Yu, F.X., Zhao, B., and Guan, K.L. (2015). Hippo Pathway in Organ Size Control, Tissue Homeostasis, and Cancer. *Cell* *163*, 811-828.
- Yu, M., Luo, Y., Cong, Z., Mu, Y., Qiu, Y., and Zhong, M. (2018). MicroRNA-590-5p Inhibits Intestinal Inflammation by Targeting YAP. *J Crohns Colitis* *12*, 993-1004.
- Yui, S., Azzolin, L., Maimets, M., Pedersen, M.T., Fordham, R.P., Hansen, S.L., Larsen, H.L., Guiu, J., Alves, M.R.P., Rundsten, C.F., *et al.* (2018). YAP/TAZ-Dependent Reprogramming of Colonic Epithelium Links ECM Remodeling to Tissue Regeneration. *Cell Stem Cell* *22*, 35-49 e37.
- Zanconato, F., Forcato, M., Battilana, G., Azzolin, L., Quaranta, E., Bodega, B., Rosato, A., Bicciato, S., Cordenonsi, M., and Piccolo, S. (2015). Genome-wide association between YAP/TAZ/TEAD and AP-1 at enhancers drives oncogenic growth. *Nat Cell Biol* *17*, 1218-1227.
- Zhang, H., Pasolli, H.A., and Fuchs, E. (2011). Yes-associated protein (YAP) transcriptional coactivator functions in balancing growth and differentiation in skin. *Proc Natl Acad Sci U S A* *108*, 2270-2275.
- Zhou, D., Zhang, Y., Wu, H., Barry, E., Yin, Y., Lawrence, E., Dawson, D., Willis, J.E., Markowitz, S.D., Camargo, F.D., *et al.* (2011). Mst1 and Mst2 protein kinases restrain intestinal stem cell proliferation and colonic tumorigenesis by inhibition of Yes-associated protein (Yap) overabundance. *Proc Natl Acad Sci U S A* *108*, E1312-1320.
- Zhou, Y., Huang, T., Zhang, J., Cheng, A.S.L., Yu, J., Kang, W., and To, K.F. (2018). Emerging roles of Hippo signaling in inflammation and YAP-driven tumor immunity. *Cancer Lett* *426*, 73-79.

Chapter 5

Characterizing Atrophy-Induced Stromal Changes

5.1 Introduction

The process of tissue repair and regeneration is complex and involves inputs from multiple cell types and cell-extrinsic factors. By virtue of being exposed to the external environment, epithelial cells receive cues from a diverse array of local and systemic factors. In the gut, stromal cells, and particularly fibroblasts, are essential for maintaining the normal turnover of the epithelium. PDGFRA⁺FOXL1⁺ subepithelial telocytes and PDGFRA⁺GLI1⁺ subepithelial mesenchymal cells locally provide essential Wnt factors to support stem cell function (Degirmenci et al., 2018; Shoshkes-Carmel et al., 2018), thus serving as one of the most important components of the stem cell niche. Beyond the stem cell compartment, these PDGFRA⁺ fibroblast populations also establish the Bmp signaling gradient that promotes epithelial differentiation (Brugger et al., 2020; McCarthy et al., 2020). Additional stromal cell types, such as myofibroblasts, have also been shown to secrete Wnt, R-spondin, and Bmp ligands/inhibitors (Powell et al., 2011). Various immune populations that reside in the intestinal lamina propria, including innate lymphoid cells (ILCs), macrophages, and dendritic cells also play unique roles in intestinal biology (Hou et al., 2020). Recently, T-helper subsets have been reported to interact directly with LGR5⁺ ISC and regulate their self-renewal capacity and cell fate choices through secretion of specific cytokines (Biton et al., 2018). In addition to providing physical support, the extracellular matrix also regulates epithelial biology (Meran et al., 2017). Distinct laminins help establish the small intestine and colonic tissue identity. For example, loss of laminin- α 5 results in a transformation of the small intestine to a colonic-type mucosal architecture (Mahoney et al., 2008). Furthermore, in the organoid culture system, alteration of basement membrane components, including matrix stiffness, can drastically impact the growth, differentiation, and transcriptional profile of intestinal organoids (Gjorevski et al., 2016; Yui et

al., 2018). Given that epithelial cells are the workhorse of many tissues, it is no surprise that various cell types, cytokines, and matrix factors act together to support this layer of cells.

The intestine also harbors an incredibly rich and large community of microorganisms. IECs are uniquely situated between the microbiota and host immune system and actively sense microbial signals (Okumura and Takeda, 2017). Currently, it is widely appreciated that dysbiosis, or abnormal alteration of the microbiota, is a key feature of inflammatory bowel disease (Tamboli et al., 2004). How certain microbial species and metabolites affect host physiology is an area of great interest. A key challenge is sifting out relationships that are mere correlations to those that are in fact causative (Stappenbeck and Virgin, 2016). An accumulating body of work have established an essential role for the microbiota in shaping host immunity. Germ-free animals that lack commensal microbes are deficient in secondary gut lymphoid tissues, CD4⁺ T cell numbers, and IgA producing plasma cells (Belkaid and Hand, 2014). As a result, these animals are more susceptible to certain bacterial, viral, and parasitic infections (Round and Mazmanian, 2009). Microbial sensing by IECs through pattern recognition receptors, such as Toll-like receptors (TLRs) and NOD-like receptors (NLRs), is a key mediator of this host-microbial crosstalk. Moreover, proper epithelial barrier function against pathogen invasion, including the ability to produce antimicrobial peptides and mucus, relies on signals from commensal microbes and the immune system (Okumura and Takeda, 2017).

Epithelial cells and the underlying stroma must not only defend themselves against pathogens but also swiftly respond to breaches in the intestinal barrier. We and others have shown that signals from both the overlying microbiota and underlying host cells can influence epithelial repair (Alam and Neish, 2018; Owens and Simmons, 2013; Stappenbeck and Miyoshi, 2009; Yu et al., 2012b). Using the colonic biopsy injury system, we have previously shown that

PTGS2 (also known as COX2)-expressing mesenchymal stem cells (MSCs) localize to the wound bed in response to TLR signaling and are major players in orchestrating the healing process (Jackstadt and Sansom, 2017). Prostaglandin E2 (PGE2) secreted from these cells act through its receptor PTGER4 (also known as EP4 receptor) on IECs to induce WAE cell differentiation (Miyoshi et al., 2017). Genetic deletion of *Ptgs2* or *Ptger4* significantly impairs WAE cell formation and delays colonic wound healing (Manieri et al., 2012; Miyoshi et al., 2017). *In vitro*, PGE2 treatment is sufficient to generate spheroids that morphologically and transcriptionally resemble WAE cells (Miyoshi et al., 2017). Similarly in the small bowel irradiation injury model, PTGS2⁺ MSCs are also thought to play a protective role especially in combination with *Lactobacillus* probiotic or lipopolysaccharide treatment (Ciorba et al., 2012; Riehl et al., 2000). Following barrier re-establishment, PGE2 levels must reduce to baseline levels to permit wound channel formation and crypt regeneration. This downmodulation is mediated by the bacterial metabolite deoxycholate (DCA), which inhibits PGE2 production in MSCs. Sustained PGE2 production or depletion of DCA by antibiotic treatment blocks the latter phases of wound repair (Jain et al., 2018). Once wound channels form, WNT5A generated by mesenchymal cells focally inhibit proliferation to initiate crypt fission events. In the absence of WNT5A, wound channels form normally but crypt regeneration is impeded (Miyoshi et al., 2012). Therefore, epithelial wound repair and crypt regeneration involves a complex cross-talk between microbes, epithelial cells, and stromal cells with other players likely involved as well.

A large majority of studies have examined the role of the microbiota during colonic injury-repair. It is well established that germ-free, antibiotic-treated, MYD88 knockout, and TLR knockout mice are all more prone to DSS-induced rectal bleeding, epithelial damage, and mortality compared to conventional mice (Hernandez-Chirlaque et al., 2016; Rakoff-Nahoum et

al., 2004). Interestingly, these mice display less signs of colonic inflammation, suggesting that the heightened susceptibility is due to weakening of the intestinal barrier and impaired epithelial regeneration. On the other hand, there are few studies that examine the contribution of the microbiota within the small intestine. This is likely because there is significantly less microbes in this region (Kastl et al., 2020). However, a recent study has unveiled a role for the small intestine microbiota in dietary lipid absorption (Martinez-Guryn et al., 2018). Furthermore, in children with environmental enteric dysfunction, alteration of the duodenal microbiota as shown to be causal in triggering enteropathy and villus blunting (Chen et al., 2021). Whether the microbiota is functional during injury-repair in the proximal small intestine is an open question.

In the poly(I:C) injury model that we have developed and characterized so far, we show that a WAE-like cell type, which we call aVECs, cover the surface of damaged villi to re-establish the barrier. We also established that this function depends on the Hippo-YAP signaling pathway. However, key questions remaining from our work is how YAP activation is triggered following villus injury and whether or not this involves certain microbial or stromal signals. Unlike other developmental pathways, the Hippo-YAP pathway is not under the control of a specific ligand-receptor interaction. A number of cell-extrinsic and cell-intrinsic factors can modulate the activity of YAP in a Hippo-dependent and -independent manner (Meng et al., 2016). In many ways, YAP acts as a sensor for the tissue environment, incorporating biomechanical, inflammatory, and growth factor cues to carry out cell- and context-specific responses (Totaro et al., 2018). In the gut, several different upstream factors have been proposed to induce YAP activation during epithelial regeneration, including g130 ligands (IL-6, IL-11), PGE2, collagen/focal adhesion kinase signaling, and stromal ILSR (Kim et al., 2017; Taniguchi et al., 2015; Xu et al., 2020; Yui et al., 2018). In addition to producing IL-22 to facilitate

epithelial regeneration, ILC3s have also been shown to drive tissue regeneration through activation of YAP in an IL-22-independent manner (Lindemans et al., 2015; Romera-Hernandez et al., 2020). So far, there are no reports of a microbial contribution to the regulation of Hippo-YAP signaling. Importantly, the same stromal-epithelial interactions that drive intestinal repair also play major roles in tumorigenesis. This is consistent with the adage, “cancer is a wound that never heals,” by Rudolf Virchow in the 1800’s. Initiation of colorectal cancer is mediated by induction of YAP activity via the PGE2-PTGER4 axis (Kim et al., 2017; Roulis et al., 2020). Additionally, epithelial gp130 and STAT3 signaling, which is often triggered in response to cytokine production by stromal cells, facilitates the growth of gastrointestinal tumors (Ernst et al., 2014; Nishina et al., 2021). With this body of literature in mind, we sought to define the cell-extrinsic factors that contribute to aVEC-mediated villus repair in the poly(I:C) injury model.

5.2 Materials and Methods

Animals

C57BL/6J, *APC^{Min/+}*, *Vill-Cre*, *Yap^{fllox}*, *Yap-Taz^{fllox}*, *Ptger4^{fllox}*, and *Ptgs2^{-/-}* mice were obtained from the Jackson Laboratory or available in-house. *Yap^{fllox}* mice were further backcrossed to the C57BL/6J strain for more than 3 generations. Experiments that called for only wild-type mice used 8-week-old C57BL/6J male mice. All other experiments involving specific genetic strains used 7 to 10-week-old littermate male and female mice. Mice were housed under specific-pathogen-free conditions with free access to autoclaved food and water and were maintained on a 12 h light/dark cycle. C57BL/6J germ-free mice were bred and housed at the Washington University Gnotobiotic Core Facility. All animal studies were conducted in compliance with protocols approved by the Washington University Institutional Animal Care and Use Committee.

Animal procedures

1 mg/mL poly(I:C) HMW (InvivoGen) was made according to the manufacturer's instructions and 20 mg/kg was injected intraperitoneally. For permeability assays, mice were subjected to a 4 h fast, during which food, water, and bedding were withdrawn. 4-kDa FITC-dextran (Sigma) was dissolved in PBS to make 100 mg/mL, and 44 mg/100g was delivered by oral gavage. 3 h after gavage, blood was collected by cardiac puncture, and serum was obtained in Microtainer tubes.

Primary epithelial culture

The establishment, maintenance, and differentiation of mouse IECs as spheroids or air-liquid interface (ALI) monolayers were previously described (Miyoshi and Stappenbeck, 2013; Miyoshi et al., 2017; Wang et al., 2019). In brief, intestinal crypts were harvested by collagenase

type I (Gibco) digestion, and stem cell spheroids were grown in 50% L-WRN conditioned medium in Matrigel (Corning 354234) and passaged every 3 days via trypsinization. To induce epithelial differentiation, dissociated stem cells were grown in differentiation medium containing 10 μ M EP₄ receptor antagonist (R&D Systems) or 1 μ M dmPGE₂ (R&D Systems) and supplemented with 50 ng/mL EGF (PeproTech) for 24 h. Dissociated stem cells seeded onto transwells (Corning 3470) for ALI culture were initially submerged in 50% L-WRN medium for 6 days before media was removed in the upper chamber. ALI transwells were maintained with 50% L-WRN medium in the bottom chamber for another 14-21 days to reach maturity. For intestinal organoid culture, crypts were grown in IntestiCult Organoid Growth Medium (STEMCELL Technologies) and passaged according to the manufacturer's instructions. All media, with the exception of the IntestiCult medium, were supplemented with 10 μ M Y-27632 (R&D Systems). Cell culture treatments used in this chapter were 2 μ M verteporfin (Sigma) in DMSO, 1 μ g/mL mouse epiregulin (R&D Systems) in PBS, and appropriate vehicle controls. All reagents were added on the day of passage unless otherwise stated. Cell viability was determined with CellTiter-Glo 3D Cell Viability Assay (Promega) on the Cytation 5 instrument (BioTek). Mouse spheroid transcriptomes were previously reported and deposited (ArrayExpress E-MTAB-3952; Miyoshi et al., 2017). Enrichment analysis of the top YAP target genes (Gregorieff et al., 2015) was performed using the GSEA v4 software (Subramanian et al., 2005).

Histology and immunostaining

The proximal small intestine (duodenum or proximal jejunum) was pinned out and fixed in 10% neutral buffered formalin overnight at 4°C. Spheroids were incubated in Cell Recovery Solution (Corning) for 1 h prior to overnight formalin fixation. ALI transwells were directly fixed in

formalin overnight at 4°C. Fixed samples were washed in 70% ethanol three times and reoriented with warm 2% agar solution. This was followed by paraffin embedding, sectioning, and hematoxylin and eosin staining. Unstained paraffin sections were de-paraffinized in xylene and rehydrated in isopropanol each for 5 min three times. Antigen retrieval was performed in Trilogy solution (Sigma) for 20 min under boiling water. For immunohistochemistry (IHC), sections were additionally treated with 3% H₂O₂ in methanol to quench endogenous peroxidase activity. Slides were blocked for 1 h at room temperature in 1% BSA/PBS containing 0.1% Triton X-100 and incubated with primary antibodies diluted in blocking solution overnight at 4°C. The following day, slides were incubated with secondary antibodies diluted in blocking solution for 1 h at room temperature. For immunofluorescence (IF), sections were stained with Hoechst 33258 (Invitrogen) for 15 min and mounted with Fluoromount medium (Sigma). For IHC, sections were treated with VECTASTAIN Elite ABC-HRP Kit (Vector Laboratories), developed with DAB Peroxidase Substrate Kit (Vector Laboratories), counterstained with CAT hematoxylin (Biocare), and mounted with Cytoseal XYL (Thermo Scientific). Washes were performed between each step in PBS without any detergent. The following primary antibodies were used in this chapter: rabbit anti-Fabp1 (Novus Biologicals NBP1-87695), goat anti-IL-33 (R&D Systems AF3626), rabbit anti-Cldn4 (Thermo Fisher 36-4800), rabbit anti-Yap (Cell Signaling 14074), guinea pig anti-Krt20 (Progen GP-K20), rabbit anti-Ki67 (Abcam ab15580), mouse anti- β -catenin (BD Transduction Laboratories 610154), goat anti-Ace2 (R&D Systems AF933), goat anti-Trop2 (R&D Systems AF1122), and rabbit anti-EpCAM (Abcam ab71916). The following Thermo Fisher highly cross-absorbed IgG secondary antibodies were used in this chapter: goat anti-rabbit Biotin, donkey anti-mouse Alexa Fluor 488, donkey anti-rabbit Alexa Fluor 488/594, donkey anti-goat Alexa Fluor 488/594, and donkey anti-guinea pig Alexa Fluor 488.

RNAscope in situ hybridization

Intestinal tissues and spheroids (after incubation in Cell Recovery Solution) were fixed in 4% PFA overnight at 4°C and then incubated in 20% sucrose/PBS overnight at 4°C. Fixed samples were cryo-embedded in O.C.T. compound (Fisher Scientific) and sectioned at 7 µm on a cryotome. *In situ* hybridization was carried out on frozen sections using a RNAscope 2.5 HD Assay-RED Kit (ACDBio) according to the manufacturer's instructions. The following probes were used: *Msln* (443241), *Clu* (427891), *Ptgs2* (316621), *Il11* (552461), and *Mmp3* (480961).

Imaging and quantification

Bright-field images were acquired with an Olympus BX51 microscope. Fluorescent images were acquired with a Zeiss Axiovert 200M inverted microscope and a Zeiss Axio Imager M2 Plus wide field fluorescent microscope. Whole mount images were acquired with an Olympus SZX12 stereo dissection microscope. Live spheroid images were acquired with a Zeiss Cell Observer inverted microscope with color camera. The lengths of well-oriented villi were measured using the cellSens software (Olympus). For histology-based quantifications, each data point represents an average value across 30-100 villi/crypts in the proximal small intestine per animal (see figure legends). Nearest neighbor distances (NNDs) were quantified based on whole mount images on Fiji/ImageJ using the NND plugin. Images were further processed with Adobe Photoshop CC.

Cytokine array and ELISA

Intestinal tissues (<1 cm) were placed in Lysing Matrix D tubes (MP Biomedicals) containing RIPA buffer (Sigma) and protease/phosphatase inhibitors (Thermo Scientific) and

homogenized/lysed using the FastPrep-24 5G homogenizer (MP Biomedicals). Lysates were centrifuged for 10 min, and supernatants were collected for downstream applications. Protein concentration was measured with the Pierce BCA Protein Assay Kit (Thermo Fisher). After normalizing for total protein amount, cytokine levels were assessed using the Proteome Profile Mouse XL Cytokine Array (R&D Systems) according to the manufacturer's instructions. Fiji/ImageJ was used to calculate pixel densities. PGE2 levels were measured using the Monoclonal PGE2 ELISA Kit (Cayman Chemical) according to the manufacturer's instructions.

Quantitative real-time PCR (qRT-PCR)

Intestinal tissues (<5 mg) were homogenized and lysed in Buffer RLT Plus containing β -mercaptoethanol (β ME) using the FastPrep system (MP Biomedicals). Total RNA was isolated using the RNeasy Plus Micro Kit (Qiagen). cDNA was synthesized using iScript Reverse Transcription Supermix reagents (Bio-Rad). qPCR was performed using iTaq Universal SYBR Green Supermix reagents (Bio-Rad) on a StepOne RT-PCR System (Applied Biosystems). Expression levels were normalized to β 2m. Primers used in this chapter are listed in **Table 5.1**.

Statistics and reproducibility

Statistical analyses were performed in GraphPad Prism 8 or 9. *P*-values are indicated in the plots or figure legends with $p < 0.05$ denoted as significant. Data are expressed as mean \pm standard deviation (SD). An unpaired two-tailed Student's *t*-test was used when comparing two groups; a one-way ANOVA was used when comparing three or more groups; and a two-way ANOVA was used when comparing groups with two experimental variables. Data from independent experiments were pooled when possible. Otherwise, data are representative of at least two

independent experiments. Animals that had near 0% weight loss one day after poly(I:C) injection (<10% of all mice) were excluded from the study as these mice did not exhibit intestinal damage. Further statistical details and quantification methods can be found in the figure legends.

5.3 Results

Partial villus atrophy triggers the aVEC state

To determine whether YAP activation requires total villus damage and atrophy in the poly(I:C) injury model, we took advantage of the fact that poly(I:C) induces partial damage in the proximal jejunum. The damage appears to be confined to the villus tip (**Figure 5.1A**). Interestingly, at 24 HPI, during which robust villus atrophy occurs in the duodenum, the blunted villi in the jejunum featured epithelial cells expressing low levels of FABP1 in the tip region (**Figure 5.1B**). Reduced expression of FABP1 is also seen in aVECs (**Figure 3.1E**). Therefore, we wondered whether these FABP1⁻ cells in the jejunum were enriched for fetal-like markers. *In situ* hybridization demonstrated that *Msln* and *Clu* mRNAs were induced in these cells. Furthermore, immunostaining revealed prominent expression of IL-33 in the tip of blunted villi. Together, these findings reveal that aVECs are also induced even during partial villus atrophy.

Germ-free mice have normal aVECs following villus injury

We next tested whether microbes were necessary for aVEC formation. Poly(I:C) injection of germ-free mice induced robust villus atrophy in the proximal small intestine similar to conventionally-raised mice (**Figure 5.2A**). This indicated that poly(I:C)-induced epithelial cell death and villus injury are not influenced by the presence of commensal microbes. Close inspection of atrophic villi in germ-free mice revealed robust expression of CLDN4 and IL-33 in aVECs (**Figure 5.2B,C**), revealing that aVEC formation does not depend on microbial signals.

PGE2 and gp130 ligands are induced in the stroma of atrophic villi

Stromal factors play a crucial role in facilitating wound repair in epithelium-lined organs (Stappenbeck and Miyoshi, 2009). In the setting of irradiation injury or chemically-induced colitis, YAP can be activated by multiple cell-extrinsic cues, including prostaglandin E2 (PGE2), gp130 cytokines (i.e. IL-6 and IL11), and ECM components (Kim et al., 2017; Taniguchi et al., 2015; Yui et al., 2018). Additionally, mesenchymal cells that express PTGS2 have been shown to induce revSCs and WAE cells via PGE2-PTGER4 signaling (Manieri et al., 2012; Miyoshi et al., 2017; Roulis et al., 2020). We therefore addressed whether these stromal factors were also induced during villus atrophy. qPCR analysis showed a robust increase in *Ptgs2* and *Il11* transcript levels in the atrophic intestine (**Figure 5.3A**). PGE2 was also elevated specifically during atrophy and diminished during villus regeneration (**Figure 5.3B**). Notably, while *Ptgs2* and *Il11* expression were low in the homeostatic intestine, these transcripts were strongly induced within the atrophic stroma (**Figure 5.3C**). These results demonstrate a remodeling of the stromal microenvironment during villus atrophy that corresponds with the generation of aVECs.

The PGE2-PTGER4 axis is dispensable for villus repair and regeneration

As *Ptgs2* and PGE2 levels were upregulated during villus atrophy, we next examined the requirement of the PGE2-PTGER4 pathway in YAP nuclear localization and expression of fetal markers in aVECs. Whole body knockout of *Ptgs2* (*Ptgs2*^{-/-}) or conditional deletion of *Ptger4* in the intestinal epithelium (*Ptger4*^{ΔIEC}) did not affect the localization of YAP to the nucleus in aVECs compared to littermates (**Figure 5.4A,B**). Furthermore, the expression of *Msln* and *Clu* was not affected by the lack of *Ptgs2* or epithelial *Ptger4*, suggesting that this signaling pathway is largely dispensable for adaptive differentiation and villus repair in the poly(I:C) injury model.

As such, villus regeneration was not impaired in *Ptgs2*^{-/-} or *Ptger4*^{ΔIEC} mice, while *Yap*-*Taz*^{ΔIEC} mice, which lack both YAP and TAZ Hippo pathway effectors, displayed a similar phenotype as *Yap*^{ΔIEC} mice (**Figure 5.5A-C**). Thus, these results do not support a role for the PGE2-PTGER4 signaling axis in atrophy-induced YAP activation and villus regeneration.

Identification of other secreted factors induced during villus atrophy

Taking a more unbiased approach, we performed a cytokine array on whole tissue lysates from the atrophic intestine. To identify factors that are induced in response to villus damage and not to poly(I:C) itself, we used tissues distal to the injury site from the same mice as a control. Among the 35 factors that were detected, 10 were differentially expressed in the atrophic region compared to the distal non-atrophic region of the gut, including IL1-RA, F3 (tissue factor), several chemokines, and MMP3 (**Figure 5.6A**). IL1-RA and F3 are both highly expressed in aVECs (**Figure 3.7A and 3.8B**), thus serving as positive controls. MMP3 is a factor elevated in both Crohn's and celiac disease mucosa (Bragde et al., 2018; Haberman et al., 2014). Interestingly, *in situ* hybridization revealed that *Mmp3* mRNA was strongly upregulated around the crypts during villus atrophy (**Figure 5.6B**). This suggests a modification of the stem cell niche as well as a potential mechanism for the enhanced epithelial migratory phenotype observed during this stage. Collectively, we show that adaptive differentiation is accompanied by an altered stromal microenvironment with YAP-activating and ECM-modifying characteristics.

YAP activation is necessary for adaptive differentiation in vitro

To this end, we aimed to understand the extent to which YAP activation in adaptive differentiation is epithelial-cell intrinsic. We utilized our short-term culture system, which

involves enzymatic dissociation of stem cell spheroids and culturing the dissociated cells in L-WRN or differentiation media for at least 24 h (Miyoshi and Stappenbeck, 2013; Miyoshi et al., 2017). We also examined our recently developed long-term culture system, which involves plating dissociated stem cell spheroids on a transwell and establishing air-liquid interface (ALI) to induce differentiation (Wang et al., 2019). Surprisingly, we found that many of the top YAP target genes were highly expressed in both our stem cell and differentiated intestinal spheroids (**Figure 5.7A**). *In situ* hybridization confirmed high levels of *Msln* and *Clu* mRNA in both short-term culture conditions (**Figure 5.7B**). WAE-like spheroids, through addition of PGE2 to the differentiation media, also expressed high levels of YAP target genes (**Figure 5.7C**). Moreover, nuclear localization of YAP was observed in all culture conditions except for mature ALI cultures (**Figure 5.8**), which possess a transcriptional profile that resembles a steady-state intestinal epithelium (Wang et al., 2019). Intriguingly, differentiated spheroids had more varied levels of YAP expression and localization (**Figure 5.8**), possibly reflecting a symmetry-breaking event (Serra et al., 2019). These results demonstrate that epithelial cells are wired to undergo adaptive differentiation when subjected to short-term culture in differentiation conditions.

Importantly, treatment of epithelial cultures with the YAP-TEAD inhibitor verteporfin caused loss of cell viability in short-term cultures, especially in differentiated spheroids, but not in mature ALI culture (**Figure 5.9A**). *Yap^{ΔIEC}* crypts also saw decreased viability when subjected to short-term culture conditions compared to *Yap^{fl/fl}* crypts (**Figure 5.9B**). Additionally, in budding intestinal organoids, which go through an early transient YAP-activated state (Serra et al., 2019), VP treatment greatly affected organoid growth early in culture but to a much lesser extent late in culture (**Figure 5.9C**). The impact of YAP inhibition was not on spheroid formation but rather on maintaining the adaptive differentiation state (**Figure 5.10A**). Notably,

epiregulin supplementation partially rescued the viability of *Yap^{AIEC}* cells (**Figure 5.10B**). Taken together, we demonstrate that stem cells have an intrinsic capacity to adaptively differentiate. Further, we establish an essential role for YAP in mediating adaptive differentiation *in vitro*.

Maladaptive differentiation occurs in intestinal tumors

Wound repair mechanisms are often hijacked by cancer cells, making them appear to be in a persistent wound healing state (Ge et al., 2017). We thus examined whether intestinal tumors were lined with a VEC-like cells with an altered differentiation state. *APC^{Min/+}* mice develop spontaneous intestinal adenomas throughout the length of the small intestine and serve as a model of familial adenomatous polyposis (Moser et al., 1990; Su et al., 1992). Examination of *APC^{Min/+}* tumors revealed high expression of CLDN4 and loss of FABP1 and ACE2 expression in the differentiated epithelial compartment (**Figure 5.11A,B**). In addition, *Msln* and *Clu* expression were strongly induced in the differentiated tumor cells (**Figure 5.11C**). Within the proliferative compartment of the tumor, we detected expression of TROP2, a prominent fetal marker (Fernandez Vallone et al., 2016; Wang et al., 2019). Thus, we see evidence of both fetal-like stem cell reprogramming and adaptive epithelial differentiation in *APC^{Min/+}* tumors.

YAP is essential for maintaining epithelial integrity in response to severe poly(I:C) injury

Finally, we determined what happens when mice receive continuous bouts of poly(I:C) injury in the proximal small intestine without YAP. At most, mice can tolerate two consecutive injections of poly(I:C) (**Figure 5.12**). Remarkably, *Yap^{AIEC}* mice showed near complete loss of the epithelial layer, including the crypt compartment, while *Yap^{fl/fl}* mice appeared comparable to mice that received just one dose of poly(I:C) (**Figure 5.12B,C**). Not surprisingly, serum FITC-

dextran levels were dramatically elevated in *Yap^{ΔIEC}* compared to *Yap^{fl/fl}* mice following double poly(I:C) injury, revealing a significantly weakened barrier. Together, these results highlight a requirement for YAP in sustaining epithelial integrity in the face of severe intestinal damage.

5.4 Discussion

Here, we took a deeper dive into the specific contexts in which YAP signaling is activated in the intestinal epithelium. In the duodenum, poly(I:C) injection results in near total loss of differentiated IECs, leading to severe villus atrophy. In the proximal jejunum, poly(I:C)-induced damage is more confined to the upper villus compartment, resulting in partial villus atrophy. Despite this, we still observed induction of aVECs in the jejunum in the tip portion of the villi. This is consistent with the notion that aVEC formation is triggered once the level of IEC loss exceeds that of the normal homeostatic turnover of the epithelium. Interestingly, this finding calls into question the source of aVECs in this scenario. In the duodenum, aVECs are derived from TA cells in the crypt, which expresses high levels of YAP. However, in the jejunum, the likely source of aVECs would be the differentiated VECs. Thus, our data suggests that aVECs do not necessarily have to come from TA cells; rather, even fully mature IECs can acquire the aVEC state. Using germ-free animals, we further show that commensal microbes are not required for the induction of aVECs following villus injury. This could be a location-specific phenomenon, as the proximal intestine contains a relatively less diverse and abundant microbial community compared to the distal intestine (Donaldson et al., 2016). It could also be that there are other signals that contribute to YAP activation and mediate adaptive differentiation.

The Hippo-YAP pathway is regulated by a number of factors, including various cell-extrinsic cues (Yu et al., 2012a). In order to determine the mechanism behind YAP activation during poly(I:C)-induced villus atrophy, we examined previously known upstream inducers of YAP in the gut. We identified several secreted factors such as PGE2 (Kim et al., 2017) and IL-11 (Taniguchi et al., 2015) that were upregulated in the atrophic intestine. Localization of *Ptgs2*⁺ cells, which are the major PGE2-producing cells (Manieri et al., 2012; Roulis et al., 2020), and

Il11⁺ cells by *in situ* hybridization revealed that these cells were induced in the stroma of atrophic villi beneath the aVEC layer. Despite this finding and the fact that PGE2 is crucial for WAE cell differentiation (Miyoshi et al., 2017), we found the PTGS2-PGE2-PTGER4 axis to be largely dispensable for aVEC formation, YAP activation, and villus regeneration. Interestingly, IL-11 has been recently proposed as a mediator of crypt regeneration in response of ISC depletion, but this study did not find significant YAP activation in dedifferentiating crypt cells (Murata et al., 2020). It is possible that there are redundant sources of YAP-activating factors induced during villus injury-repair, and loss of any one of these factors can be compensated.

Our results thus reveal a key difference between aVECs and WAE cells. WAE cells require PGE2 signaling while aVECs do not. This discrepancy could be a reflection of the biological difference between the small intestine and colon. Additionally, it could be due to the distinct nature of the poly(I:C) and colonic biopsy injury models. WAE cells, as the name implies, cover the surface of wounds, which contains a mixture of tissue-resident and infiltrating immune cells, ECM constituents, and vascular components. The presence of *Ptgs2*⁺ mesenchymal stem cells (MSCs) in the wound bed appears to be critical for WAE cell formation (Jain et al., 2018; Manieri et al., 2012). On the other hand, aVECs cover atrophic villi, with little or no granulation tissue formation. Despite this, we also saw induction of *Ptgs2*⁺ stromal cells and PGE2 levels in the atrophic intestine, but whether these are equivalent to the *Ptgs2*⁺ MSCs in the colon remains to be addressed. Given the speed at which aVECs and WAE cells are generated following injury, it is likely that there is an immediate signal that gets triggered when the intestinal barrier is breached, resulting in YAP activation during barrier restoration.

The activity of YAP can also be modulated through cell mechanics, cell shape, and cytoskeletal changes (Halder et al., 2012). Dramatic alterations in the tissue architecture

following injury can alter local mechanical forces, influencing the behavior of individual cells. During DSS-induced regeneration, there is increased deposition of type I collagen in the extracellular space adjacent to the epithelium (Yui et al., 2018). Changes in the ECM are sensed through integrins, leading to activation of focal adhesion kinase (FAK) and Src signaling (Kim and Gumbiner, 2015). These signals can ultimately converge on YAP/TAZ, which, in the case of DSS-induced regeneration, promotes epithelial reprogramming to a fetal-like state (Yui et al., 2018). An important distinction between the DSS and poly(I:C)-induced injury model is that the DSS-induced repairing epithelium is much thicker than the homeostatic epithelium. Additionally, the repairing epithelium appears much later in the regenerative phase (~2 weeks). In contrast, aVECs are much shorter than the homeostatic epithelium and appear very early during repair (1 day). Therefore, the regulation of YAP may be very different between the two injury models. While *in vitro* studies suggest that collagen signaling is sufficient to activate YAP-dependent cellular reprogramming (Yui et al., 2018), changes in cytoskeletal dynamics and cell-cell junctions could also direct YAP activity (Halder et al., 2012). Regardless, mechanical and cytoskeletal cues may be an important driver of aVEC formation in the poly(I:C) injury model.

Intestinal organoids recapitulate the process of crypt regeneration *in vitro*, and mature organoids contain all the cell types found in the adult epithelium (Sato et al., 2009). YAP deficient organoids fail to grow, and it was postulated that this is due to precocious Paneth cell differentiation as a result of overactive Wnt signaling (Gregorieff et al., 2015). It was also recently discovered that stem cells go through a transient YAP-activated spheroid stage prior to crypt budding and organoid maturation (Serra et al., 2019). These studies highlight an epithelial-intrinsic regulation of YAP activity. Surprisingly, using our primary spheroid culture system, we observed signs of YAP activation in our stem cell and differentiated spheroids cultures.

Inhibition of YAP with verteporfin impaired spheroid viability, revealing that YAP is functional. Why YAP is triggered in our spheroid cultures is unclear, but it may be that the initial formation of the spheroid structure mimics a wound healing event. In line with this, long-term ALI cultures did not express YAP target genes. The fact that even differentiated spheroids possess a YAP-activated state means that we can model the process of adaptive differentiation *in vitro*.

Lastly, we examined whether adaptive differentiation could become maladaptive in the setting of tumorigenesis. It has been recently appreciated that SCA1⁺, revSC-like cells expand in tumors in a YAP-dependent manner (Roulis et al., 2020). We also identified fetal-like proliferating cells (marked by TROP2 expression) in *APC^{Min/+}* tumors that is independent of the LGR5⁺ ISC population. Intriguingly, we found that epithelial differentiation in these tumors was drastically altered, which has not been previously appreciated. While tumor-associated IECs did not appear shorter, they lacked expression of mature enterocyte markers such as ACE2 and FABP1 and instead expressed high levels of CLDN4, *Msln*, and *Clu* similar to aVECs in the poly(I:C) injury model. The biological reason for this remains to be investigated, but given the barrier protective role of aVECs during repair, it is possible that tumors hijack this wound healing mechanism to strengthen their barrier function and protect themselves against damage.

5.5 Figures

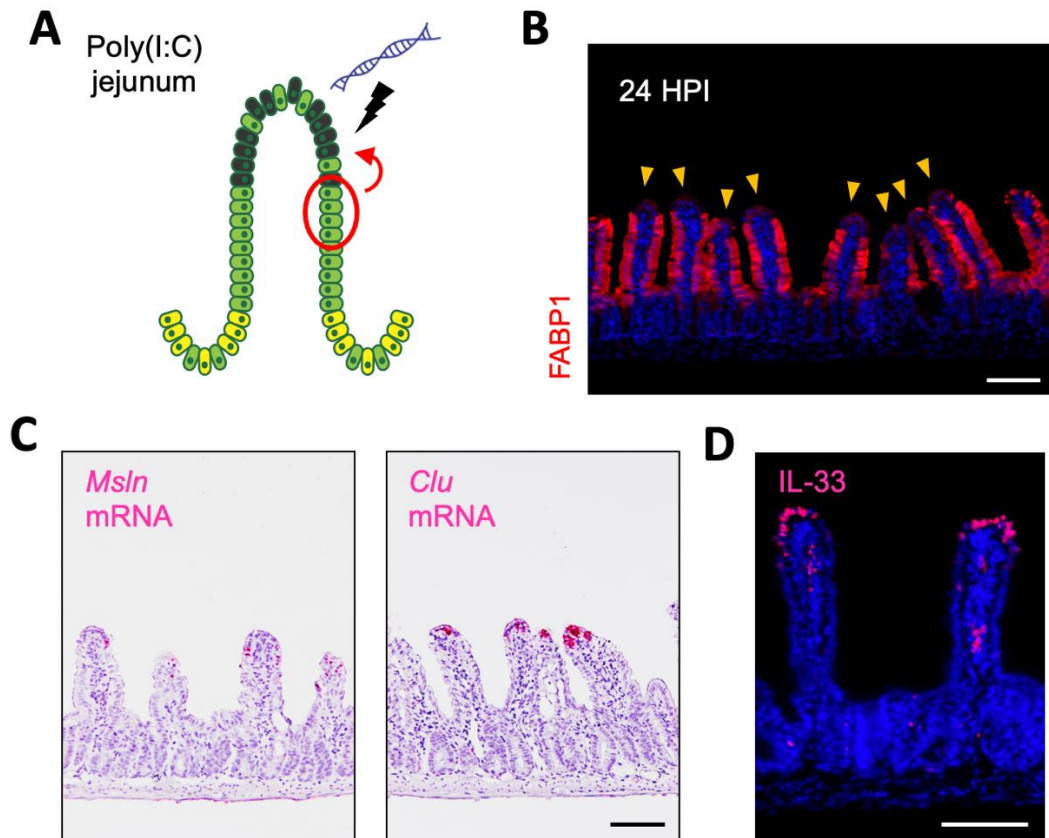


Figure 5.1. aVECs are induced at the tip region of partially blunted villi

(A) Schematic of poly(I:C)-induced injury in the proximal jejunum. In this segment, apoptotic cells (black) are largely confined to the villus tip region, resulting in partial villus blunting. (B) Immunofluorescence (IF) for FABP1 (red) in the proximal jejunum at 24 HPI. (C) RNAscope *in situ* hybridization for *Msln* and *Clu* in partially blunted villi in the proximal jejunum. Each red dot represents a single mRNA molecule. (D) IF for IL-33 (red) in partially blunted villi in the jejunum. All bars: 100 μm. IF and RNAscope images are representative of at least 3 animals.

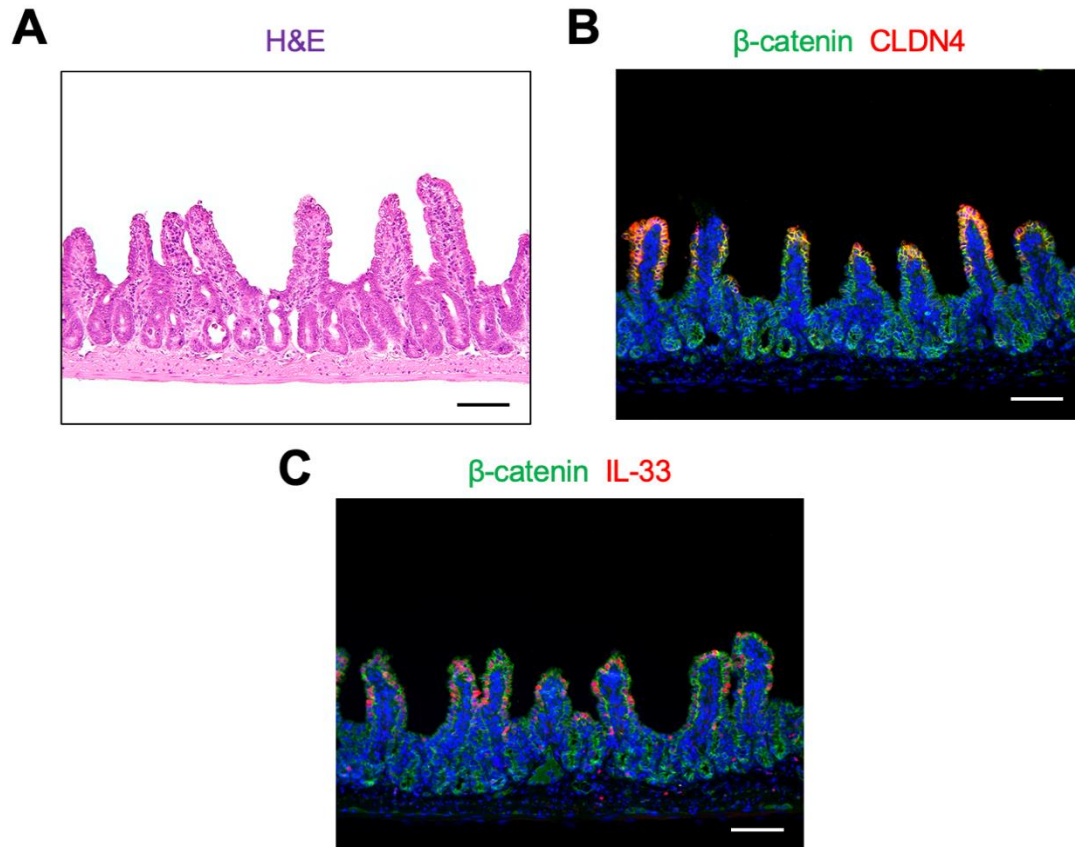


Figure 5.2. aVECs are present on atrophic villi in germ-free mice

(A) H&E images of the atrophic intestine at 24 HPI in germ-free mice. (B and C) IF for β -catenin (green, epithelium), CLDN4 (red, B), and IL-33 (red, C) in the atrophic intestine from germ-free mice. Bars: 100 μ m. H&E and IF images are representative of at least 3 animals.

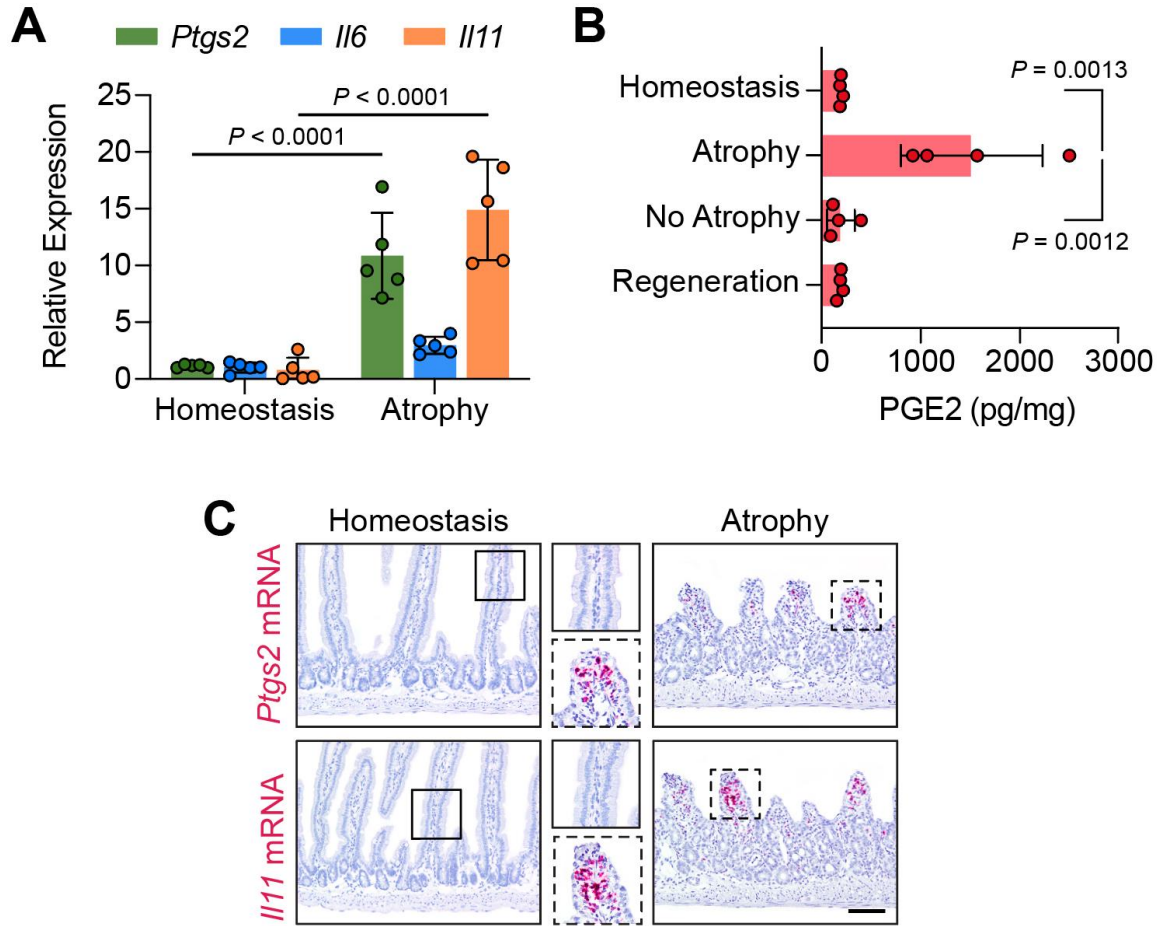


Figure 5.3. Remodeling of the stromal microenvironment following villus injury

(A) qPCR analysis of *Ptgs2* and gp130 cytokines (*Il6*, *Il11*) in whole tissue lysates from the homeostatic and atrophic intestine. Expression values are relative to one of the homeostatic samples for each gene. n = 5 mice/group. (B) PGE₂ levels were measured by ELISA in whole tissue lysates from the homeostatic, atrophic (24 HPI), non-atrophic (distal uninjured region at 24 HPI), and regenerating (48 HPI) intestine. n = 4 mice/group. (C) RNAscope for *Ptgs2* (top) and *Il11* (bottom) in the homeostatic and atrophic intestine. Bar: 100 μm. Note that *Ptgs2* and *Il11* transcripts are induced in the stroma of atrophic villi beneath the aVECs. All values in (A) and (B) are displayed as mean ± SD. Unpaired *t*-test in (A). One-way ANOVA and Tukey's multiple comparisons test in (B). RNAscope images are representative of at least 3 animals.

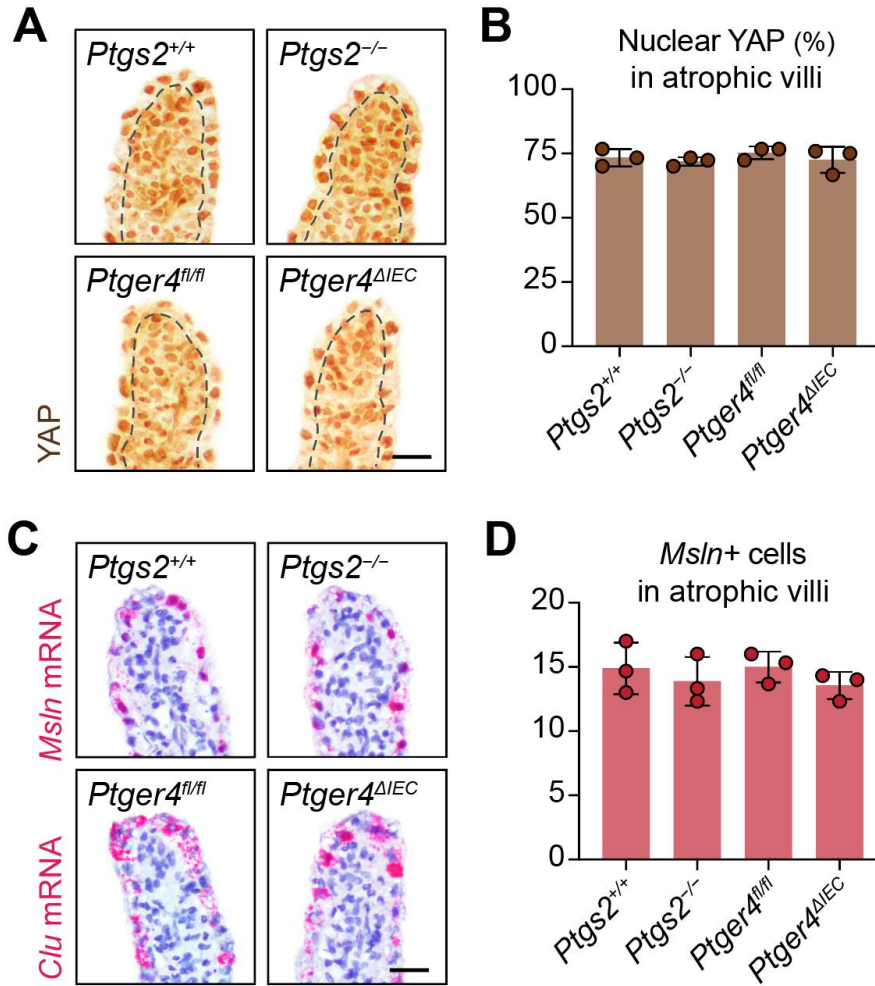


Figure 5.4. The PGE2-PTGER4 axis is not required for YAP nuclear localization and aVEC formation

(A and B) IHC for YAP (brown) in a representative atrophic villus from *Ptgs2*^{+/+}, *Ptgs2*^{-/-}, *Ptger4*^{fl/fl}, and *Ptger4*^{ΔIEC} mice (A). Dashed line represents the epithelial-stromal border. Percent of epithelial cells with predominantly nuclear localization of YAP was quantified across 30 atrophic villi (B). n = 3 mice/group. Values were not significantly different across samples. (C and D) RNAscope for *Msln* and *Clu* in a representative atrophic villus from *Ptgs2*^{+/+}, *Ptgs2*^{-/-}, *Ptger4*^{fl/fl}, and *Ptger4*^{ΔIEC} mice (C). Average number of *Msln*⁺ cells across 30 atrophic villi was plotted (D). n = 3 mice/group. Values were not significantly different across samples. All values in (B) and (D) are plotted as mean ± SD. One-way ANOVA and Tukey's multiple comparisons test in (B) and (D). Bars: 20 μm. IHC/RNAscope images are representative of at least 3 animals.

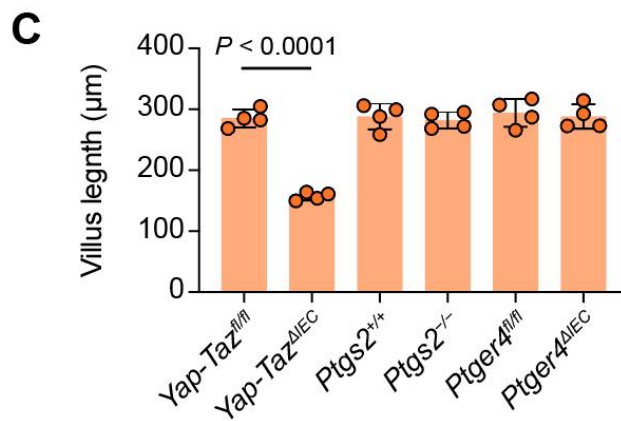
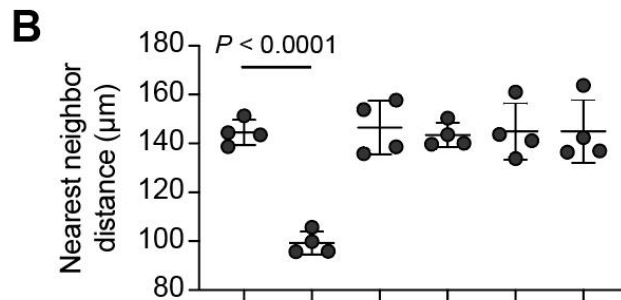
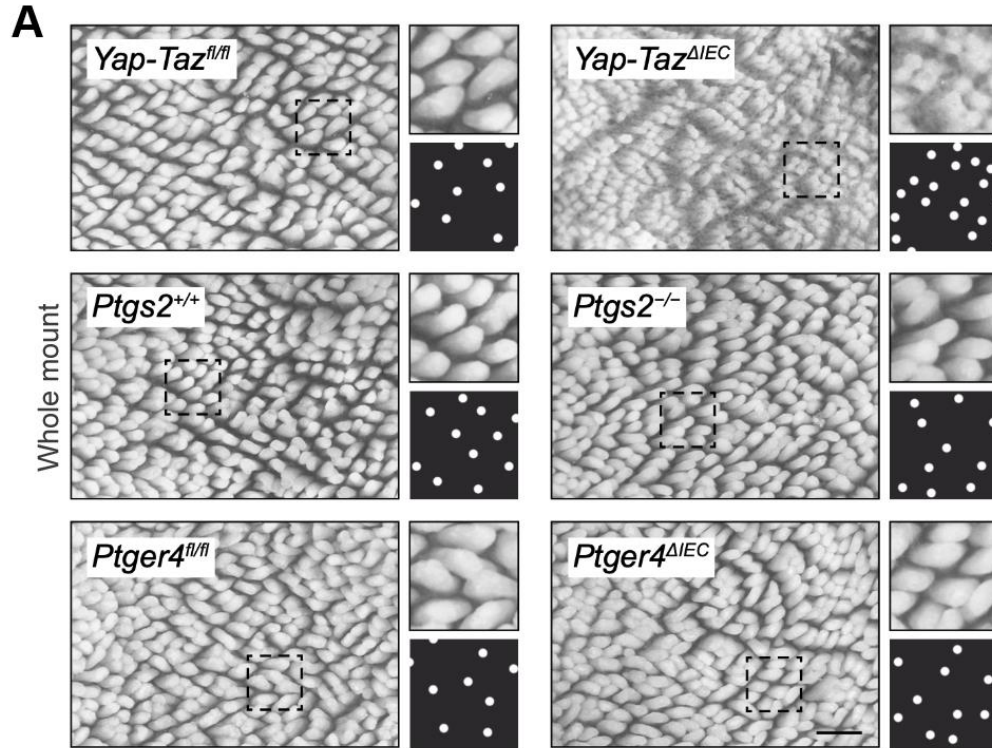


Figure 5.5. The PGE2-PTGER4 axis is dispensable for villus regeneration

(A) Whole mount luminal view of regenerating villi at 48 HPI from *Yap-Taz^{fl/fl}*, *Yap-Taz^{AIEC}*, *Ptgs2^{+/+}*, *Ptgs2^{-/-}*, *Ptger4^{fl/fl}*, and *Ptger4^{AIEC}* mice. Bar: 500 μ m. (B) Average nearest neighbor distance (NND) value was calculated based on the whole-mount images and plotted as mean \pm SD. n = 4 mice/group. (C) Average villus length across 50 villi for each genotype was plotted as mean \pm SD. n = 4 mice/group. Significance was determined by one-way ANOVA and Tukey's multiple comparisons test in (B) and (C). Images are representative of at least 3 animals.

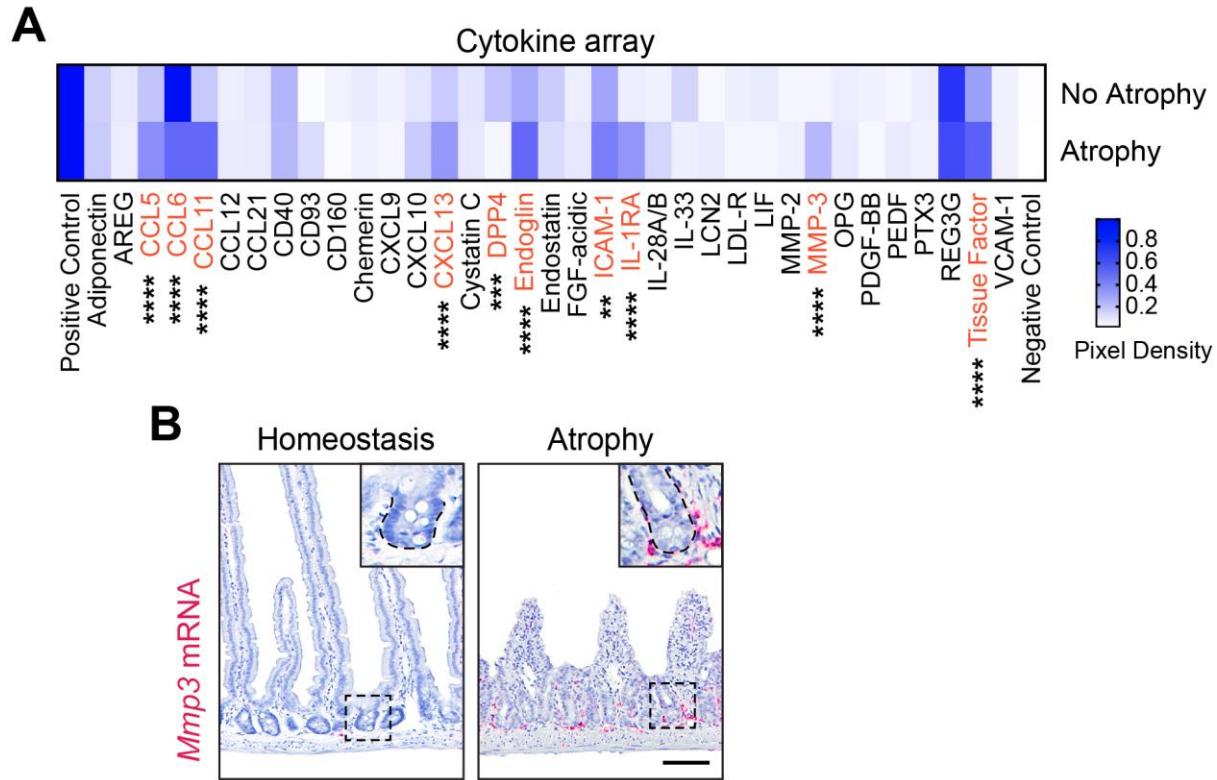


Figure 5.6. Defining the villus atrophy-induced intestinal secretome

(A) Cytokine array analysis of whole tissue lysates comparing the atrophic (Atrophy) and distal non-atrophic (No Atrophy) regions of the intestine following poly(I:C)-induced villus injury.

Proteins that were above the level of detection are shown. Scale represents mean pixel densities from $n = 4$ mice/group. Significance was determined by two-way ANOVA and Sidak's multiple comparisons test. ** $p < 0.01$, *** $p < 0.001$, **** $p < 0.0001$ (B) RNAscope for *Mmp3* mRNA in the homeostatic and atrophic intestine. Bar: 100 μm . Note that *Mmp3* transcripts are upregulated in the stroma around the crypts. RNAscope images are representative of at least 3 animals.

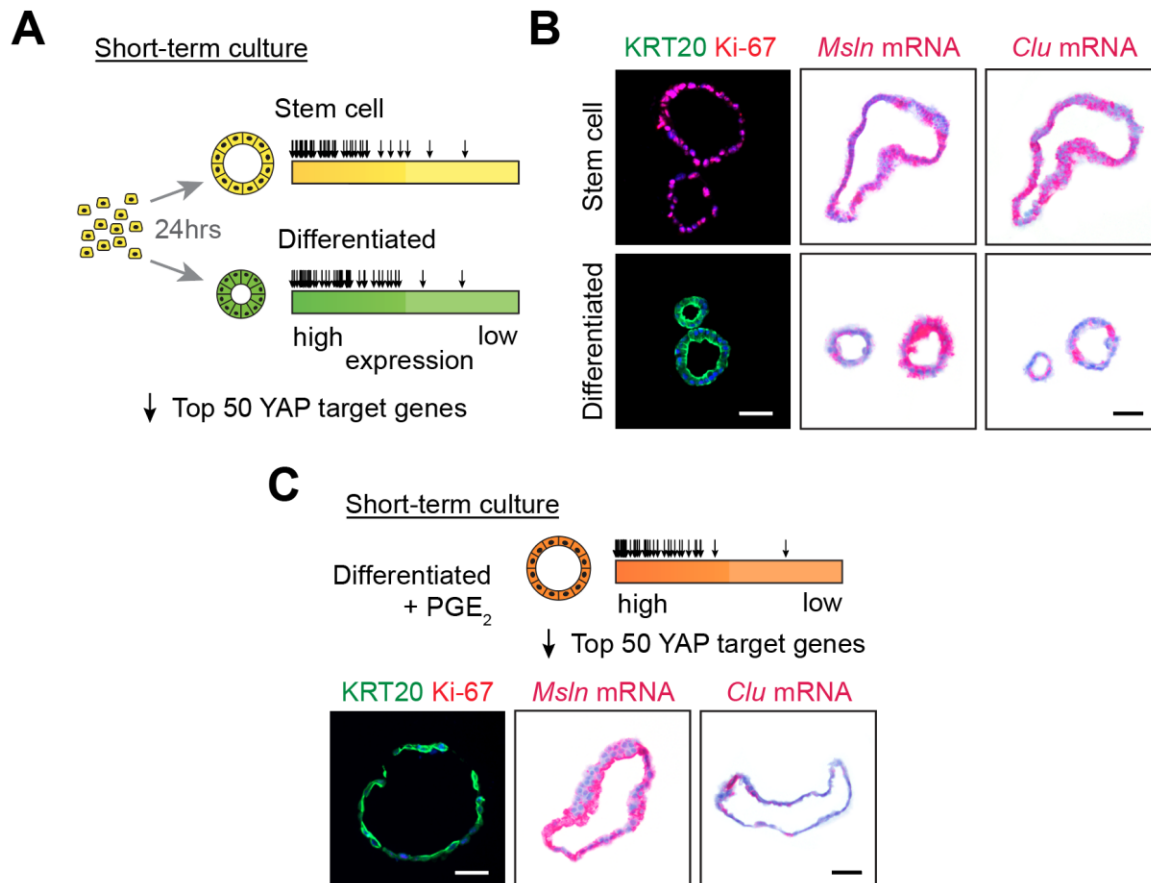


Figure 5.7. Induction of a fetal-like, YAP-activated program in intestinal spheroids regardless of differentiation status or PGE2 treatment

Enzymatically dissociated stem cell spheroids were cultured in either 50% L-WRN media or differentiation media for 24 h to establish short-term cultures. The top 50 YAP target genes were mapped to the transcriptome of stem cell spheroids (A, top), differentiated spheroids (A, bottom), and WAE-like differentiated spheroids treated with dmPGE2 (C, top). Each arrow represents a YAP target gene. IF/RNAscope for KRT20 (green), Ki-67 (red), *Msln* (red), and *Clu* (red) in stem cell spheroids (B, top), differentiated spheroids (B, bottom), and WAE-like spheroids (C, bottom). Note the expression of *Msln* and *Clu* in all three culture conditions.

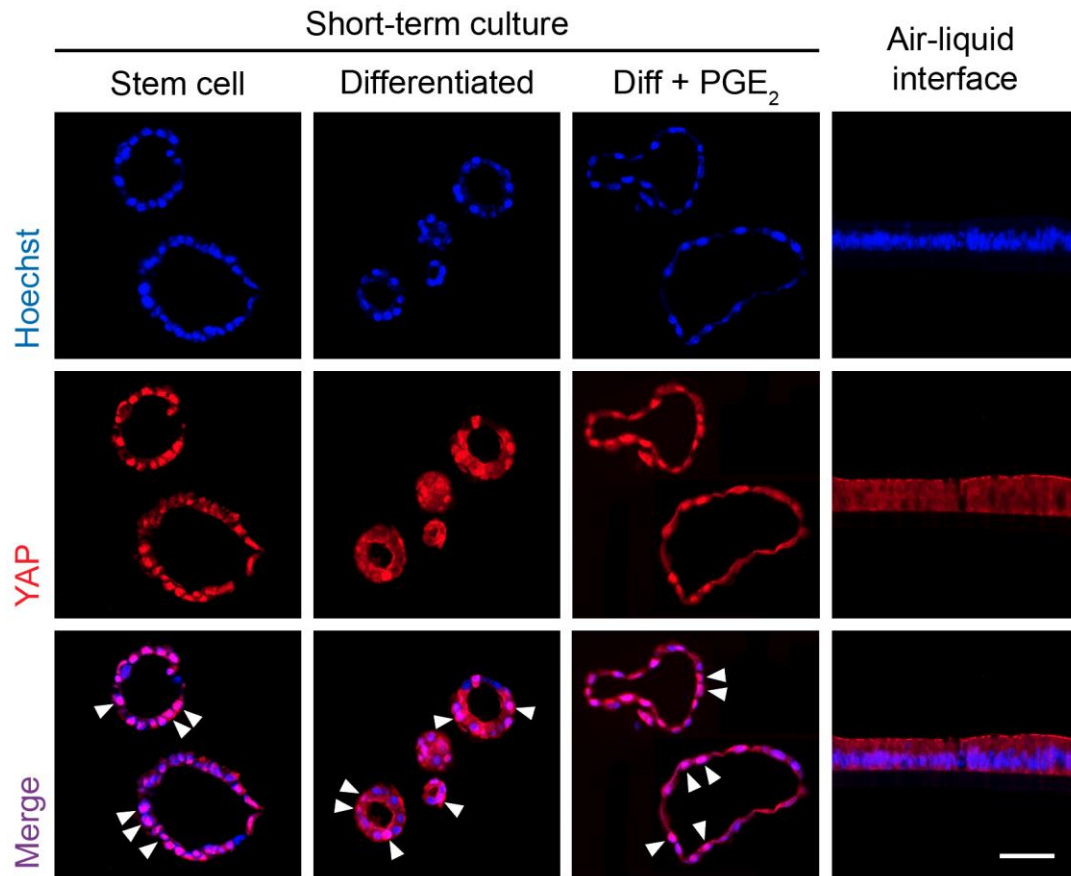


Figure 5.8. Differentiated spheroids, but not ALI cells, feature nuclear YAP expression

IF for YAP (red) in short-term spheroid cultures and in mature air-liquid interface cultures (ALI day 21). Bar: 50 μ m. White arrowheads indicate examples of cells with nuclear YAP expression. In stem cell spheroids, nuclear YAP staining was prominent in nearly all cells. In differentiated spheroids (with or without PGE₂), some cells had nuclear YAP staining whereas other cells lacked YAP expression entirely or expressed cytoplasmic YAP. In ALI day 21 cells, nearly all cells had diffuse cytoplasmic YAP staining. IF images are representative of at least 3 samples.

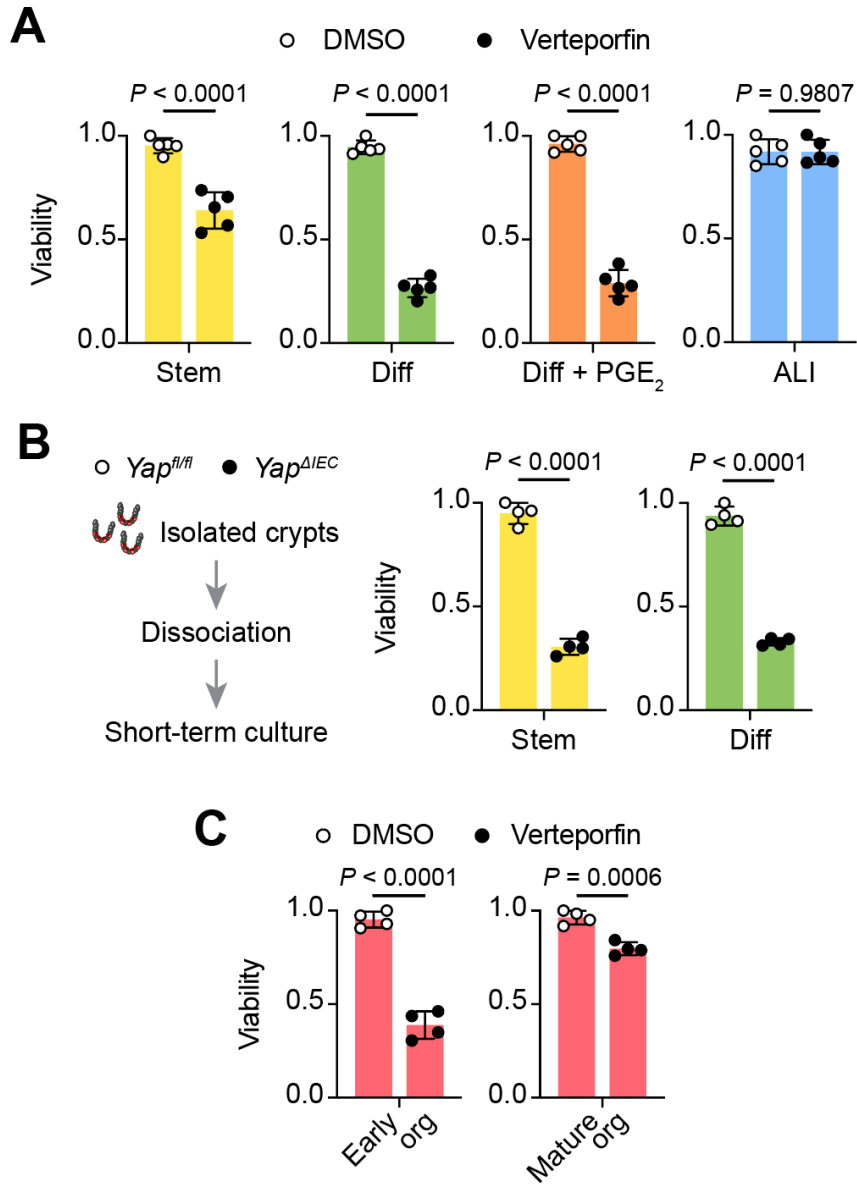


Figure 5.9. YAP is essential for adaptive differentiation *in vitro*

(A) CellTiter-Glo assay of spheroids (stem cell, differentiated without PGE2, differentiated with PGE2) and ALI day 21 cells treated with DMSO (vehicle control) or verteporfin (VP), a small molecule inhibitor of YAP. Values are relative to the most viable sample. n = 5 samples/group.

(B) *Yap^{fl/fl}* and *Yap^{ΔIEC}* intestinal crypts were subjected to short-term culture and assessed for cell viability. n = 4 samples/group. (G) Intestinal organoids were treated with DMSO or VP on day 1 (early) or day 5 (mature) of culture for 24 h and assessed for cell viability. n = 4 samples/group.

All values in (A), (B), and (C) are displayed as mean ± SD. Unpaired *t*-test in (A), (B), and (C).

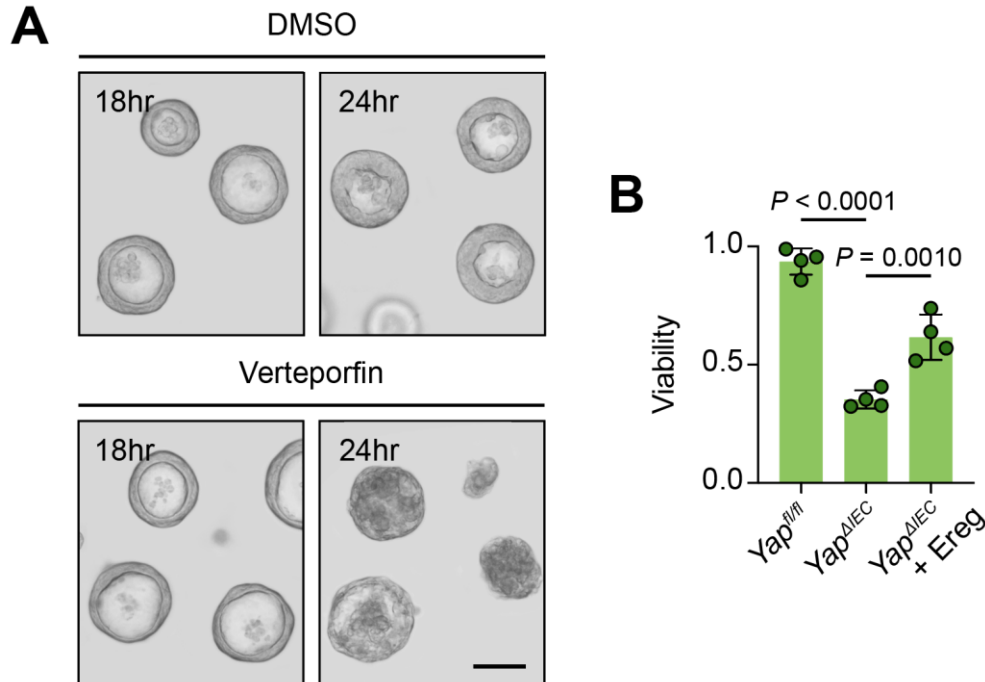


Figure 5.10. EREG supplementation partially rescues YAP deficiency

(A) Bright-field images of differentiated spheroids (without PGE2 supplementation) treated with DMSO or VP at 18 and 24 h. Bar: 50 μ m. (B) *Yap^{AIEC}* crypts subjected to short-term differentiation culture was partially rescued by addition of 1 μ g/mL epiregulin (Ereg). Data are displayed as mean \pm SD. Significance was determined by one-way ANOVA and Tukey's multiple comparison test. Bright-field images are representative of at least 3 samples.

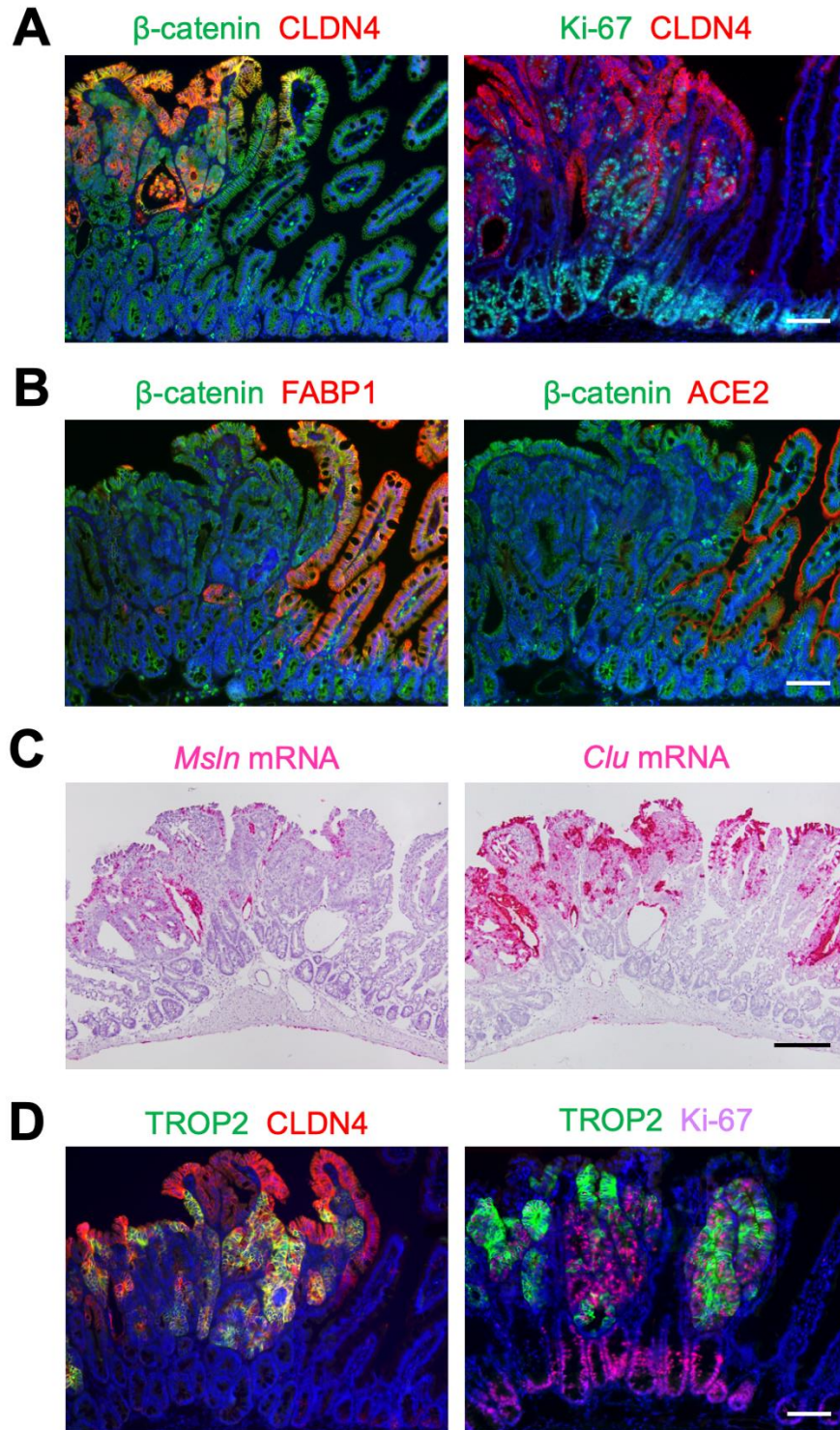


Figure 5.11. Maladaptive differentiation in $APC^{Min/+}$ tumors

(A, B, and D) IF for β -catenin (green), CLDN4 (red), Ki-67 (green or purple), FABP1 (red), ACE2 (red), and TROP2 (green) in $APC^{Min/+}$ intestinal adenomas. Adjacent non-tumorigenic regions are included on the right side for each image. (C) RNAscope for *Msln* and *Clu* (red) in $APC^{Min/+}$ intestinal adenomas. Bars: 100 μ m. Intestinal tumors express the fetal marker TROP2 within the proliferative compartment. Importantly, tumors exhibit an altered differentiation state that reflects many of the same changes observed in aVECs following intestinal villus injury.

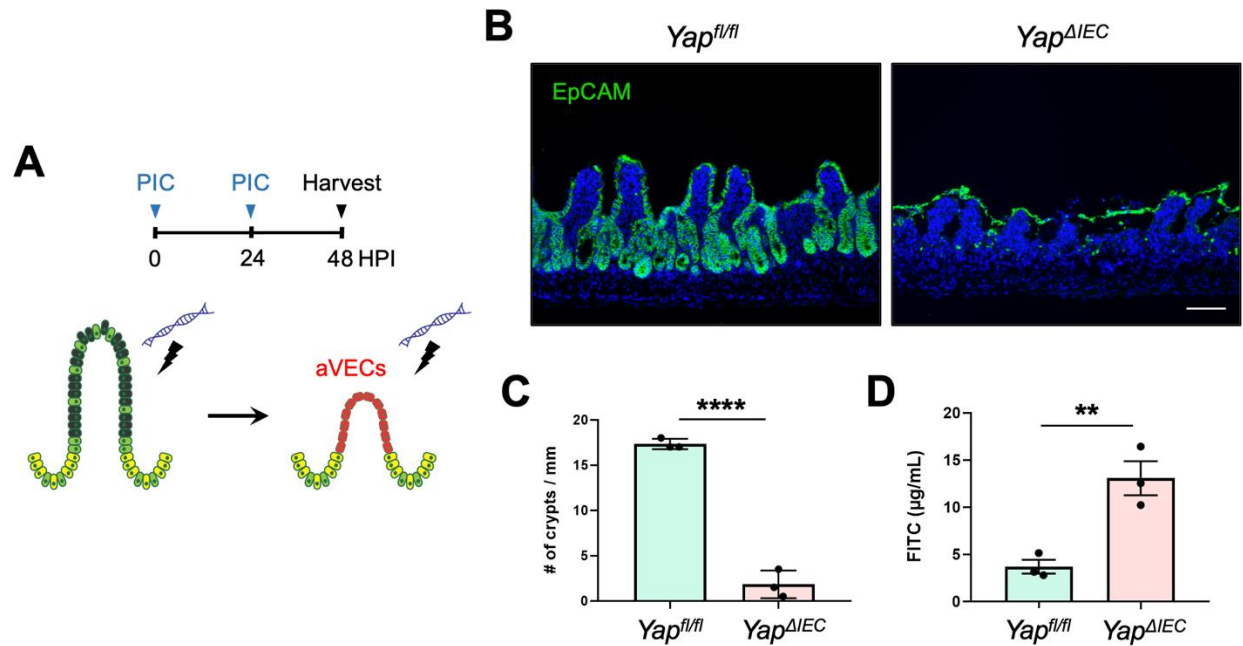


Figure 5.12. YAP deficient mice are highly susceptible to double-poly(I:C) challenge

(A) Schematic of double poly(I:C) challenge in mice. 20 mg/kg poly(I:C) was injected consecutively for two days and the proximal intestine was examined on the third day (24 h after the second dose). (B) IF for EpCAM (green) in the proximal intestine from *Yap^{fl/fl}* and *Yap^{ΔIEC}* mice. Bar: 100 μm. (C) Average number of crypts per mm was plotted and displayed as mean ± SD. n = 3 mice/group. (D) Serum FITC-dextran levels were measured and plotted as mean ± SD. n = 3 mice/group. For both (C) and (D), significance was determined by unpaired *t*-test.

5.6 Tables

Table 5.1. Primers used for qRT-PCR, related to Figure 5.3

<u>Primer Name</u>	<u>Species</u>	<u>Primer Sequence (5' to 3')</u>	<u>Primer Length</u>	<u>Tm (°C)</u>	<u>GC (%)</u>	<u>Product Size</u>	<u>Target</u>	<u>RefSeq</u>
mPts2-F	Mouse	TCCAACCTCTCCTACTACACCAG	23	60.56	52.17	146	Exon 4	NM_011198
mPts2-R	Mouse	GGGTCAGGGATGAACTCTCTC	21	59.24	57.14	146	Exon 5	NM_011198
mll6-F	Mouse	CTGGGACTGATGCTGGTGACA	22	62.52	54.55	118	Exon 2	NM_031168
mll6-R	Mouse	GCCTCCGACTTGTGAAGTGGA	22	62.24	54.55	118	Exon 2	NM_031168
mll11-F	Mouse	AATCCCAGCTGACGGAGATCACA	24	63.96	50.00	112	Exon 3	NM_008350
mll11-R	Mouse	TCTACTCGAAGCCTTGTCAGCACA	24	63.85	50.00	112	Exon 4	NM_008350
B2m-F	Mouse	TTCTGGTGCTTGTCTCACTGA	21	59.24	47.62	104	Exon 1	NM_009735
B2m-R	Mouse	CAGTATGTTCGGCTTCCCATTC	22	59.39	50.00	104	Exon 2	NM_009735

5.7 References

- Alam, A., and Neish, A. (2018). Role of gut microbiota in intestinal wound healing and barrier function. *Tissue Barriers* 6, 1539595.
- Belkaid, Y., and Hand, T.W. (2014). Role of the microbiota in immunity and inflammation. *Cell* 157, 121-141.
- Biton, M., Haber, A.L., Rogel, N., Burgin, G., Beyaz, S., Schnell, A., Ashenberg, O., Su, C.W., Smillie, C., Shekhar, K., *et al.* (2018). T Helper Cell Cytokines Modulate Intestinal Stem Cell Renewal and Differentiation. *Cell* 175, 1307-1320 e1322.
- Bragde, H., Jansson, U., Fredrikson, M., Grodzinsky, E., and Soderman, J. (2018). Celiac disease biomarkers identified by transcriptome analysis of small intestinal biopsies. *Cell Mol Life Sci* 75, 4385-4401.
- Brugger, M.D., Valenta, T., Fazilaty, H., Hausmann, G., and Basler, K. (2020). Distinct populations of crypt-associated fibroblasts act as signaling hubs to control colon homeostasis. *PLoS Biol* 18, e3001032.
- Chen, R.Y., Ahmed, T., and Gordon, J.I. (2021). Duodenal Microbiota in Stunted Undernourished Children with Enteropathy. Reply. *N Engl J Med* 384, 1778.
- Ciorba, M.A., Riehl, T.E., Rao, M.S., Moon, C., Ee, X., Nava, G.M., Walker, M.R., Marinshaw, J.M., Stappenbeck, T.S., and Stenson, W.F. (2012). Lactobacillus probiotic protects intestinal epithelium from radiation injury in a TLR-2/cyclo-oxygenase-2-dependent manner. *Gut* 61, 829-838.
- Degirmenci, B., Valenta, T., Dimitrieva, S., Hausmann, G., and Basler, K. (2018). GLI1-expressing mesenchymal cells form the essential Wnt-secreting niche for colon stem cells. *Nature* 558, 449-453.
- Donaldson, G.P., Lee, S.M., and Mazmanian, S.K. (2016). Gut biogeography of the bacterial microbiota. *Nat Rev Microbiol* 14, 20-32.
- Ernst, M., Thiem, S., Nguyen, P.M., Eissmann, M., and Putoczki, T.L. (2014). Epithelial gp130/Stat3 functions: an intestinal signaling node in health and disease. *Semin Immunol* 26, 29-37.
- Fernandez Vallone, V., Leprovots, M., Stollo, S., Vasile, G., Lefort, A., Libert, F., Vassart, G., and Garcia, M.I. (2016). Trop2 marks transient gastric fetal epithelium and adult regenerating cells after epithelial damage. *Development* 143, 1452-1463.
- Ge, Y., Gomez, N.C., Adam, R.C., Nikolova, M., Yang, H., Verma, A., Lu, C.P., Polak, L., Yuan, S., Elemento, O., *et al.* (2017). Stem Cell Lineage Infidelity Drives Wound Repair and Cancer. *Cell* 169, 636-650 e614.

Gjorevski, N., Sachs, N., Manfrin, A., Giger, S., Bragina, M.E., Ordonez-Moran, P., Clevers, H., and Lutolf, M.P. (2016). Designer matrices for intestinal stem cell and organoid culture. *Nature* 539, 560-564.

Gregorieff, A., Liu, Y., Inanlou, M.R., Khomchuk, Y., and Wrana, J.L. (2015). Yap-dependent reprogramming of Lgr5(+) stem cells drives intestinal regeneration and cancer. *Nature* 526, 715-718.

Haberman, Y., Tickle, T.L., Dexheimer, P.J., Kim, M.O., Tang, D., Karns, R., Baldassano, R.N., Noe, J.D., Rosh, J., Markowitz, J., *et al.* (2014). Pediatric Crohn disease patients exhibit specific ileal transcriptome and microbiome signature. *J Clin Invest* 124, 3617-3633.

Halder, G., Dupont, S., and Piccolo, S. (2012). Transduction of mechanical and cytoskeletal cues by YAP and TAZ. *Nat Rev Mol Cell Biol* 13, 591-600.

Hernandez-Chirlaque, C., Aranda, C.J., Ocon, B., Capitan-Canadas, F., Ortega-Gonzalez, M., Carrero, J.J., Suarez, M.D., Zarzuelo, A., Sanchez de Medina, F., and Martinez-Augustin, O. (2016). Germ-free and Antibiotic-treated Mice are Highly Susceptible to Epithelial Injury in DSS Colitis. *J Crohns Colitis* 10, 1324-1335.

Hou, Q., Huang, J., Ayansola, H., Masatoshi, H., and Zhang, B. (2020). Intestinal Stem Cells and Immune Cell Relationships: Potential Therapeutic Targets for Inflammatory Bowel Diseases. *Front Immunol* 11, 623691.

Jackstadt, R., and Sansom, O.J. (2017). The Wae to repair: prostaglandin E2 (PGE2) triggers intestinal wound repair. *EMBO J* 36, 3-4.

Jain, U., Lai, C.W., Xiong, S., Goodwin, V.M., Lu, Q., Muegge, B.D., Christophi, G.P., VanDussen, K.L., Cummings, B.P., Young, E., *et al.* (2018). Temporal Regulation of the Bacterial Metabolite Deoxycholate during Colonic Repair Is Critical for Crypt Regeneration. *Cell Host Microbe* 24, 353-363 e355.

Kastl, A.J., Jr., Terry, N.A., Wu, G.D., and Albenberg, L.G. (2020). The Structure and Function of the Human Small Intestinal Microbiota: Current Understanding and Future Directions. *Cell Mol Gastroenterol Hepatol* 9, 33-45.

Kim, H.B., Kim, M., Park, Y.S., Park, I., Kim, T., Yang, S.Y., Cho, C.J., Hwang, D., Jung, J.H., Markowitz, S.D., *et al.* (2017). Prostaglandin E2 Activates YAP and a Positive-Signaling Loop to Promote Colon Regeneration After Colitis but Also Carcinogenesis in Mice. *Gastroenterology* 152, 616-630.

Kim, N.G., and Gumbiner, B.M. (2015). Adhesion to fibronectin regulates Hippo signaling via the FAK-Src-PI3K pathway. *J Cell Biol* 210, 503-515.

Lindemans, C.A., Calafiore, M., Mertelsmann, A.M., O'Connor, M.H., Dudakov, J.A., Jenq, R.R., Velardi, E., Young, L.F., Smith, O.M., Lawrence, G., *et al.* (2015). Interleukin-22 promotes intestinal-stem-cell-mediated epithelial regeneration. *Nature* 528, 560-564.

- Mahoney, Z.X., Stappenbeck, T.S., and Miner, J.H. (2008). Laminin alpha 5 influences the architecture of the mouse small intestine mucosa. *J Cell Sci* *121*, 2493-2502.
- Manieri, N.A., Drylewicz, M.R., Miyoshi, H., and Stappenbeck, T.S. (2012). Igf2bp1 is required for full induction of Ptg2 mRNA in colonic mesenchymal stem cells in mice. *Gastroenterology* *143*, 110-121 e110.
- Martinez-Guryn, K., Hubert, N., Frazier, K., Urlass, S., Musch, M.W., Ojeda, P., Pierre, J.F., Miyoshi, J., Sontag, T.J., Cham, C.M., *et al.* (2018). Small Intestine Microbiota Regulate Host Digestive and Absorptive Adaptive Responses to Dietary Lipids. *Cell Host Microbe* *23*, 458-469 e455.
- McCarthy, N., Manieri, E., Storm, E.E., Saadatpour, A., Luoma, A.M., Kapoor, V.N., Madha, S., Gaynor, L.T., Cox, C., Keerthivasan, S., *et al.* (2020). Distinct Mesenchymal Cell Populations Generate the Essential Intestinal BMP Signaling Gradient. *Cell Stem Cell* *26*, 391-402 e395.
- Meng, Z., Moroishi, T., and Guan, K.L. (2016). Mechanisms of Hippo pathway regulation. *Genes Dev* *30*, 1-17.
- Meran, L., Baulies, A., and Li, V.S.W. (2017). Intestinal Stem Cell Niche: The Extracellular Matrix and Cellular Components. *Stem Cells Int* *2017*, 7970385.
- Miyoshi, H., Ajima, R., Luo, C.T., Yamaguchi, T.P., and Stappenbeck, T.S. (2012). Wnt5a potentiates TGF-beta signaling to promote colonic crypt regeneration after tissue injury. *Science* *338*, 108-113.
- Miyoshi, H., and Stappenbeck, T.S. (2013). In vitro expansion and genetic modification of gastrointestinal stem cells in spheroid culture. *Nat Protoc* *8*, 2471-2482.
- Miyoshi, H., VanDussen, K.L., Malvin, N.P., Ryu, S.H., Wang, Y., Sonnek, N.M., Lai, C.W., and Stappenbeck, T.S. (2017). Prostaglandin E2 promotes intestinal repair through an adaptive cellular response of the epithelium. *EMBO J* *36*, 5-24.
- Moser, A.R., Pitot, H.C., and Dove, W.F. (1990). A dominant mutation that predisposes to multiple intestinal neoplasia in the mouse. *Science* *247*, 322-324.
- Murata, K., Jadhav, U., Madha, S., van Es, J., Dean, J., Cavazza, A., Wucherpfennig, K., Michor, F., Clevers, H., and Shivdasani, R.A. (2020). Ascl2-Dependent Cell Dedifferentiation Drives Regeneration of Ablated Intestinal Stem Cells. *Cell Stem Cell* *26*, 377-390 e376.
- Nishina, T., Deguchi, Y., Ohshima, D., Takeda, W., Ohtsuka, M., Shichino, S., Ueha, S., Yamazaki, S., Kawauchi, M., Nakamura, E., *et al.* (2021). Interleukin-11-expressing fibroblasts have a unique gene signature correlated with poor prognosis of colorectal cancer. *Nat Commun* *12*, 2281.
- Okumura, R., and Takeda, K. (2017). Roles of intestinal epithelial cells in the maintenance of gut homeostasis. *Exp Mol Med* *49*, e338.

- Owens, B.M., and Simmons, A. (2013). Intestinal stromal cells in mucosal immunity and homeostasis. *Mucosal Immunol* 6, 224-234.
- Powell, D.W., Pinchuk, I.V., Saada, J.I., Chen, X., and Mifflin, R.C. (2011). Mesenchymal cells of the intestinal lamina propria. *Annu Rev Physiol* 73, 213-237.
- Rakoff-Nahoum, S., Paglino, J., Eslami-Varzaneh, F., Edberg, S., and Medzhitov, R. (2004). Recognition of commensal microflora by toll-like receptors is required for intestinal homeostasis. *Cell* 118, 229-241.
- Riehl, T., Cohn, S., Tessner, T., Schloemann, S., and Stenson, W.F. (2000). Lipopolysaccharide is radioprotective in the mouse intestine through a prostaglandin-mediated mechanism. *Gastroenterology* 118, 1106-1116.
- Romera-Hernandez, M., Aparicio-Domingo, P., Papazian, N., Karrich, J.J., Cornelissen, F., Hoogenboezem, R.M., Samsom, J.N., and Cupedo, T. (2020). Yap1-Driven Intestinal Repair Is Controlled by Group 3 Innate Lymphoid Cells. *Cell Rep* 30, 37-45 e33.
- Roulis, M., Kaklamanos, A., Scherthanner, M., Bielecki, P., Zhao, J., Kaffe, E., Frommelt, L.S., Qu, R., Knapp, M.S., Henriques, A., *et al.* (2020). Paracrine orchestration of intestinal tumorigenesis by a mesenchymal niche. *Nature* 580, 524-529.
- Round, J.L., and Mazmanian, S.K. (2009). The gut microbiota shapes intestinal immune responses during health and disease. *Nat Rev Immunol* 9, 313-323.
- Sato, T., Vries, R.G., Snippert, H.J., van de Wetering, M., Barker, N., Stange, D.E., van Es, J.H., Abo, A., Kujala, P., Peters, P.J., *et al.* (2009). Single Lgr5 stem cells build crypt-villus structures in vitro without a mesenchymal niche. *Nature* 459, 262-265.
- Serra, D., Mayr, U., Boni, A., Lukonin, I., Rempfler, M., Challet Meylan, L., Stadler, M.B., Strnad, P., Papasaikas, P., Vischi, D., *et al.* (2019). Self-organization and symmetry breaking in intestinal organoid development. *Nature* 569, 66-72.
- Shoshkes-Carmel, M., Wang, Y.J., Wangenstein, K.J., Toth, B., Kondo, A., Massasa, E.E., Itzkovitz, S., and Kaestner, K.H. (2018). Subepithelial telocytes are an important source of Wnts that supports intestinal crypts. *Nature* 557, 242-246.
- Stappenbeck, T.S., and Miyoshi, H. (2009). The role of stromal stem cells in tissue regeneration and wound repair. *Science* 324, 1666-1669.
- Stappenbeck, T.S., and Virgin, H.W. (2016). Accounting for reciprocal host-microbiome interactions in experimental science. *Nature* 534, 191-199.
- Su, L.K., Kinzler, K.W., Vogelstein, B., Preisinger, A.C., Moser, A.R., Luongo, C., Gould, K.A., and Dove, W.F. (1992). Multiple intestinal neoplasia caused by a mutation in the murine homolog of the APC gene. *Science* 256, 668-670.

- Subramanian, A., Tamayo, P., Mootha, V.K., Mukherjee, S., Ebert, B.L., Gillette, M.A., Paulovich, A., Pomeroy, S.L., Golub, T.R., Lander, E.S., *et al.* (2005). Gene set enrichment analysis: a knowledge-based approach for interpreting genome-wide expression profiles. *Proc Natl Acad Sci U S A* *102*, 15545-15550.
- Tamboli, C.P., Neut, C., Desreumaux, P., and Colombel, J.F. (2004). Dysbiosis in inflammatory bowel disease. *Gut* *53*, 1-4.
- Taniguchi, K., Wu, L.W., Grivnenkov, S.I., de Jong, P.R., Lian, I., Yu, F.X., Wang, K., Ho, S.B., Boland, B.S., Chang, J.T., *et al.* (2015). A gp130-Src-YAP module links inflammation to epithelial regeneration. *Nature* *519*, 57-62.
- Totaro, A., Panciera, T., and Piccolo, S. (2018). YAP/TAZ upstream signals and downstream responses. *Nat Cell Biol* *20*, 888-899.
- Wang, Y., Chiang, I.L., Ohara, T.E., Fujii, S., Cheng, J., Muegge, B.D., Ver Heul, A., Han, N.D., Lu, Q., Xiong, S., *et al.* (2019). Long-Term Culture Captures Injury-Repair Cycles of Colonic Stem Cells. *Cell* *179*, 1144-1159 e1115.
- Xu, J., Tang, Y., Sheng, X., Tian, Y., Deng, M., Du, S., Lv, C., Li, G., Pan, Y., Song, Y., *et al.* (2020). Secreted stromal protein ISLR promotes intestinal regeneration by suppressing epithelial Hippo signaling. *EMBO J* *39*, e103255.
- Yu, F.X., Mo, J.S., and Guan, K.L. (2012a). Upstream regulators of the Hippo pathway. *Cell Cycle* *11*, 4097-4098.
- Yu, L.C., Wang, J.T., Wei, S.C., and Ni, Y.H. (2012b). Host-microbial interactions and regulation of intestinal epithelial barrier function: From physiology to pathology. *World J Gastrointest Pathophysiol* *3*, 27-43.
- Yui, S., Azzolin, L., Maimets, M., Pedersen, M.T., Fordham, R.P., Hansen, S.L., Larsen, H.L., Guiu, J., Alves, M.R.P., Rundsten, C.F., *et al.* (2018). YAP/TAZ-Dependent Reprogramming of Colonic Epithelium Links ECM Remodeling to Tissue Regeneration. *Cell Stem Cell* *22*, 35-49 e37.

Chapter 6

Summary and Future Directions

6.1 Summary

In this thesis, I provided a detailed understanding of how intestinal villi repair after injury. These findings are illustrated in **Figure 6.1**. Thus far, majority of studies have focused on elucidating the mechanisms behind crypt and stem cell regeneration in the small intestine and colon. However, one of the most crucial and prominent features of the small bowel are the villi that project into the luminal space. From the duodenum to the terminal ileum, millions of these finger-like structures cover the surface of the small bowel and provide an enormous surface area for nutrient digestion and absorption. Breakdown of the villus architecture can occur due to certain infections, medications, ischemic events, and inflammatory responses, leading to villus atrophy and symptoms of diarrhea and malabsorption. Villus atrophy is a hallmark of several enteropathies in children and adults, and if left untreated, can have far-reaching impacts on their lives. Yet, how intestinal villi cope with damage and restore their architecture are not well understood. A large reason for this is the lack of a robust villus injury-repair model that enables detailed mechanistic studies. To this end, I employed a mouse model of acute viral gastroenteritis using poly(I:C) to delineate the steps involved in repairing the intestinal villus structure.

Poly(I:C) is a double-stranded RNA analog that is often used to mimic a viral infection. Consistent with previous studies, I found that a single intraperitoneal injection of poly(I:C) in mice caused immediate and near complete loss of VECs in the proximal small intestine. This resulted in severe villus atrophy, yet due to the localized damage, these mice tolerated the injury well. Poly(I:C) appeared to directly and preferentially kill differentiated IECs in a TLR3-dependent manner without any bias toward a specific intestinal lineage. Despite the severity of the injury, atrophic villi were capable of restoring back to their original height in less than a week. This was likely because ISCs were spared from poly(I:C) injury and capable of

regenerating the villus epithelium. Thus, the poly(I:C) injury model offered a unique system to investigate the process and mechanism of villus repair without affecting the crypt compartment.

Using this model, I discovered that mature enterocyte markers became transiently suppressed during villus atrophy. The epithelial cells that line atrophic villi, named atrophy-induced villus epithelial cells (aVECs), lacked expression of ACE2, FABP1, and ALDOB despite their villus localization. Microarray analysis of laser-capture microdissected aVECs revealed a transcriptional profile that resembled disease-associated IECs observed in Crohn's and celiac disease mucosal samples. Morphologically, aVECs were short with underdeveloped microvilli and contained extensive lipid droplets, likely a result of their impaired metabolic capacity. Importantly, aVECs possessed a fetal-like transcriptional profile similar to previously identified regenerative stem cell populations in the irradiation, DSS, and helminth infection models. They expressed high levels of *Ly6a*, *Msln*, and *Clu* transcripts. By scRNA-seq, aVECs clustered separately as their own distinct cell population, and they were most closely related to homeostatic villus-top enterocytes. Similar aVEC-like cells were present in scRNA-seq datasets of Crohn's disease samples, highlighting the potential relevance of these cells in disease.

Unlike regenerative stem cells, aVECs were terminally differentiated and lineage-committed. Lineage analysis revealed that aVECs still retained either an enterocyte or goblet cell identity by the expression of *Alpi* or MUC2. Taking advantage of the fact that aVECs expressed the pan-differentiation marker KRT20, I used *Krt20^{CreER}/R26^{RtdTomato}* mice to definitively show that aVECs did not possess stem cell capacity *in vitro* or *in vivo*. Furthermore, aVECs were derived from TA cells and transiently covered damaged villi. This aVEC coverage was important for restoring the epithelial barrier after villus injury. Once villus regeneration resumed and

epithelial differentiation switched back to a more normal program, aVECs that once covered atrophic villi were pushed up by newly generated IECs and sloughed off into the lumen. Given that aVEC formation cannot be explained by current models of repair, as it did not involve a cell type conversion, I coined this process “adaptive differentiation.” I propose that adaptive differentiation is a key repair mechanism that involves the activation of a wound-adapted program, such as a fetal-like transcriptional profile, during injury-induced differentiation. How adaptive differentiation fits with other mechanisms of tissue repair is illustrated in **Figure 6.2**.

As aVECs were morphologically and functionally similar to WAE cells in the colon, I compared the transcriptomes of these two cell populations and identified a shared gene signature. Analysis of this gene signature revealed the Hippo-YAP-TEAD pathway as one of the top candidates for controlling aVEC/WAE cell identity and function. This was also an interesting pathway because Hippo-YAP signaling was shown to be essential for crypt regeneration and fetal reprogramming in the irradiation and DSS injury models. Indeed, YAP was localized to the nucleus and YAP target genes were induced in aVECs/WAE cells. Functionally, YAP was crucial for the barrier restorative properties of aVECs. In comparison to *Yap^{fl/fl}* controls, *Yap^{ΔIEC}* mice had a weakened intestinal barrier post-injury with increased numbers of fused atrophic villi. Transcriptional analysis determined that many YAP target genes were no longer induced in YAP-deficient aVECs. Importantly, stem cell, TA cell, and Paneth cell numbers were not altered between *Yap^{fl/fl}* and *Yap^{ΔIEC}* mice. An impaired ability for the epithelium to undergo adaptive differentiation post-injury appeared to be the root cause for the compromised epithelial barrier. Additionally, *Yap^{ΔIEC}* mice displayed a significant delay in their ability to regenerate their villi. Together, these results establish a crucial role for YAP in aVEC-mediated barrier restoration.

To determine what cell-extrinsic factors may be responsible for triggering YAP activation during villus repair, I examined germ-free mice as well as mice deficient in the PTGS2-PGE2-PTGER4 axis. Induction of aVECs and YAP activity following poly(I:C) injury was intact in all of these mice, suggesting that other factors are likely involved. Importantly, the dispensable nature of PGE2 signaling for aVEC formation distinguishes these cells from colonic WAE cells. Using our primary spheroid culture system, I further demonstrated that the process of adaptive differentiation can be modeled *in vitro* and that YAP activation could partly be a cell-intrinsic phenomenon. Lastly, I showed that intestinal tumors display signs of maladaptive differentiation, in which the aVEC state was hijacked by tumor-associated surface IECs.

6.2 Future Directions

Examine whether adaptive differentiation occurs in other tissues

Here, we propose a novel mechanism of repair involving the direct differentiation of intestinal progenitor cells into a post-mitotic cell type specialized for repair while still retaining lineage identity. We call this process “adaptive differentiation.” We distinguish this repair mechanism from cellular reprogramming, which involves conversion of one cell type to another. Generally, cellular reprogramming involves loss of features of the original cell type and gain of features of the new cell type (Aydin and Mazzone, 2019; Jessen et al., 2015). This is best exemplified by pioneering studies by Takahashi and Yamanaka, who showed that differentiated cells can be reprogrammed to a pluripotent state (Takahashi and Yamanaka, 2016). In the case of aVECs, there isn’t necessarily a loss of features involved. Epithelial differentiation occurs as usual, with progenitors making cell fate choices during their exit from the crypt compartment. However, during adaptive differentiation, progenitors prioritize the reparative program, and this comes with a price. The progenitors do not fully mature into the original intended cell type and gain all the features needed for the homeostatic function of the tissue. This is why we think *Alpi*⁺ aVECs express *Alpi* transcripts but lack protein expression of ACE2, FABP1, and ALDOB. Similarly, this is why we think *Muc2*⁺ aVECs express some levels of MUC2 protein, but the mucus theca is much smaller than a typical goblet cell. The primary goal of aVECs is to seal the epithelial barrier and not to take up and metabolize dietary nutrients or secrete mucus.

It will be important to determine whether adaptive differentiation occurs in other mammalian tissues. Such a process will likely occur in tissues with dedicated pools of stem and progenitor cells, including the skin and airway epithelium. In fact, skin re-epithelialization likely involves adaptive differentiation as various stem cell populations migrate into the wound field to

help re-establish the barrier (Pastar et al., 2014). Interestingly, upon epidermal wounding, hair follicle stem cells, which normally produce hair cells, upregulate epidermal markers, thus creating a dual hair follicle-epidermal state known as “lineage infidelity” (Ge et al., 2017). Other transitional stem cell states have been identified in the lung and olfactory epithelium (Gadye et al., 2017; Kobayashi et al., 2020). Ultimately, these studies may be capturing an early stage of adaptive differentiation as stem cells acquire unique repair features that are separate from enhanced proliferation or differentiation capacity while committing to a certain cell fate.

Clarify the relationship between fetal reprogramming and YAP activation

One of the major conundrum in the field is understanding the relationship between injury-induced fetal reprogramming and YAP activation in the gut. Reprogramming of the adult epithelium to a fetal-like state was first recognized in the stomach (LGR5⁺ stem cell ablation and indomethacin-induced injury) and then in the colon (DSS-induced chemical injury) (Fernandez Vallone et al., 2016; Yui et al., 2018). A fetal-like program was also identified in the small intestinal ISC compartment in response to parasitic helminth infection (Nusse et al., 2018). This study concluded that this crypt response was a generalized response to tissue injury when there is loss of LGR5⁺ ISCs. The latter two studies utilized SCA1 as the main marker of the fetal program. While Yui et al. attributed YAP/TAZ signaling as being upstream of this program, Nusse et al. pointed toward IFN-gamma signaling. It has also been appreciated that YAP/TAZ signaling is essential for stem cell and crypt regeneration in the small intestine and colon.

Interestingly, there is a lot of overlap between the so-called fetal program and YAP target genes, leading some investigators to believe that YAP is responsible for fetal reprogramming in the gut (Rees et al., 2020; Seo et al., 2020). However, one issue is that there is no consensus for

which marker(s) best represent the fetal program. TROP2 (TACSTD2) and GJA1 (CNX43) were originally identified as the major injury-induced fetal markers (Fernandez Vallone et al., 2016). However, more recent studies have begun to utilize SCA1, likely due to the availability of reagents as it is a stem cell marker in various other tissues (Holmes and Stanford, 2007). It is unclear whether any of these three markers are direct targets of YAP signaling. Another issue is the way the fetal program was initially described and characterized. Unlike adult stem cells, which grow as budding organoids in ENR media, fetal cells grow as spheroids (Fordham et al., 2013; Mustata et al., 2013). While this suggested that fetal cells behave differently than their adult counterpart even when isolated in culture, and fetal spheroids clearly retain their fetal identity, it has also become apparent that culture conditions mimic an injury-like environment. YAP signaling is dispensable for intestinal homeostasis, yet becomes indispensable for organoid development (Gregorieff et al., 2015). Adult ISCs, when cultured, go through a YAP-activated state in media containing Wnt ligands, as we have also shown in our study (**Figure 5.7**; Serra et al., 2019). Many investigators use the fetal spheroid signature to define the fetal transcriptome, but it could very well be influenced by culture-related artifacts. There is a need to better define the fetal IEC program *in vivo* and its reliance on YAP/TAZ signaling during development.

Given that aVECs also expressed a fetal-like, YAP-activated profile, I was able to examine the extent to which YAP controlled the fetal program using YAP-deficient mice. This analysis revealed that YAP only partially controls fetal genes. Thus, we concluded that aVECs do not necessarily become fetal cells. Rather, these cells are better described as possessing a YAP-activated state, which happens to partly overlap with fetal markers. aVECs also do not express *Trop2* or *Gjal*. They express high levels of *Ly6a* but we found this marker to be expressed throughout the atrophic intestinal epithelium and not just in aVECs. We speculate that

Ly6a is upregulated in response to inflammatory cues and is not a specific repair cell marker. It will be interesting to compare and contrast the transcriptomic and proteomic profiles among aVECs, WAE cells, irradiation-induced revSCs, DSS-induced regenerative cells, and fetal IECs.

Identify downstream YAP target genes that are crucial for aVEC function

We demonstrated that YAP is essential for aVEC function, specifically in re-establishing the intestinal barrier post-villus injury. However, because YAP functions as a transcriptional co-activator, we found that over 150 genes were significantly downregulated in the absence of YAP (**Figure 4.11**). It remains unclear which of these genes are responsible for the function of aVECs. Following damage to the crypt compartment, YAP appears to be essential for stem cell regeneration, but the specific target genes that mediate ISC survival and/or proliferation are not known. It has been postulated that clusterin, which is the defining marker of revSCs, may also be functional in the context of ISC regeneration as it is involved in cell survival pathways (Li, 2019; Trougakos et al., 2005). Complicating the matter is the cross-talk that occurs between YAP and Wnt signaling in the crypt niche. In addition to promoting a regenerative program, YAP also has a dual role in suppressing Wnt signaling and preventing excessive Paneth cell differentiation (Gregorieff et al., 2015). While an unbiased screen to determine which YAP target genes are functionally important will be useful, doing so *in vivo* will be technically challenging.

Using our primary spheroid culture system, I was able to successfully model adaptive differentiation *in vitro* by growing dissociated stem cell spheroids in serum-free media devoid of Wnt signaling (**Figure 5.7**). We also previously established an ALI culture method to model cycles of colonic injury-repair *in vitro* (Wang et al., 2019). These spheroid/organoid/ALI culture systems provide a powerful means to perform unbiased screens. Tools to edit the genome of

intestinal organoids using CRISPR-Cas9 technology have become widely accessible (Artegiani et al., 2020; Fujii et al., 2019; Schwank and Clevers, 2016). In addition, the ability to expand organoids indefinitely make them ideal to perform drug screens (Kim et al., 2020; Yoshida et al., 2020). Recently, an image-based screening platform enabled the identification of novel pathways that regulate intestinal organoid formation and regeneration (Lukonin et al., 2020). Therefore, these tools provide a powerful opportunity to perform detailed mechanistic studies of repair.

Determine upstream regulators of YAP during villus injury-repair

A key question remaining from our work is how YAP activation is triggered following villus injury in aVECs. Examination of previously known upstream regulators of YAP revealed that multiple factors, including PGE2, IL-6, and IL-11, were induced in the underlying stroma of atrophic villi. Unlike previous studies (Kim et al., 2017; Miyoshi et al., 2017; Roulis et al., 2020), we found the PGE2-PTGER4 signaling axis to be dispensable for YAP activation and aVEC formation in our model. Recent evidence suggests that group 3 innate lymphoid cells (ILC3s) and stromal ISLR also control YAP activity during intestinal regeneration (Romera-Hernandez et al., 2020; Xu et al., 2020). Deciphering which of these components are relevant under different injury contexts will be vital going forward. Since YAP is also induced in our epithelial spheroid culture system, we also cannot discount the contribution of mechanical, ECM, and epithelial-intrinsic forces (Gjorevski et al., 2016; Panciera et al., 2017; Yui et al., 2018).

The advantage of the poly(I:C) injury model is that it can be done in nearly any genetic mouse strains as it entails a simple intraperitoneal injection. Therefore, it will be feasible to conduct *in vivo* studies and examine the role of IL-11, FAK, Src, and other signaling pathways in aVEC formation, YAP activation, and villus regeneration. An *in vitro* screen using epithelial

spheroids and organoids can also be performed as described above. Before conducting these studies, it may be valuable to further characterize the stromal changes of the atrophic intestine. We performed targeted *in situ* hybridization studies as well as a cytokine array, but scRNA-seq of the whole tissue or just the mesenchymal compartment or a proteomics study would be informative. In addition to laser-capture microdissection, more complex spatial transcriptomics methodologies are beginning to emerge (Burgess, 2019; Marx, 2021), enabling high-resolution, single-cell transcriptome-wide sequencing while preserving spatial tissue information.

Analyze the importance of adaptive differentiation in the context of an infection

Why atrophic villi assume a primitive-type epithelium, rather than a polarized and absorptive one, remains to be determined. Given that the injury model uses poly(I:C), a dsRNA analog and a viral mimic, there may be a biological reason for the generation of aVECs from a host-pathogen interaction perspective. During enteric infection, brush border proteins often serve as receptors for entry of viruses and bacteria (Delacour et al., 2016; Lamers et al., 2020). Remodeling of the epithelium may therefore be a key defense mechanism granted in a high-turnover tissue—rapidly eliminate infected cells, replacing them with “immature” cells with less capacity for infection, to prevent further spread of the pathogen at the cost of temporarily losing absorptive function. Consistent with this idea, in transmissible gastroenteritis in pigs, IECs lining atrophic villi were comparatively more resistant to viral infection than those lining normal villi (Pensaert et al., 1970). While the mechanism for this is not clear, a coronavirus related to transmissible gastroenteritis virus, known as SARS-CoV-2, which is currently circulating in the world during the COVID-19 pandemic, infects epithelial cells via ACE2 (Hoffmann et al., 2020). SARS-CoV-2 can also infect enterocytes in the gut, as these cells express high levels of ACE2

(Lamers et al., 2020). As aVECs lack expression of ACE2 protein, it will be interesting to assess whether SARS-CoV-2 has less capacity for gut infection following intestinal villus injury.

Another intriguing possibility is that aVECs and YAP signaling may have roles outside of tissue repair. In addition to ECM-modifying genes, aVECs express genes related to immune function and pathogen defense, including *Il33* (a type 2 cytokine), *Il1rn* (an inhibitor of IL-1 signaling), *Duox2* (a hydrogen-peroxide generator), and *Lcn2* (an anti-microbial peptide). Therefore, aVECs may also be an active participant of host defense. Furthermore, epithelial YAP has recently been shown to confer protection against pathogens upon barrier loss. In this study, YAP activation following disruption of the intestinal barrier was required for resistance to infections with pathogenic bacteria in both worms and mice (Ma et al., 2020). Here, YAP appeared to directly regulate immune response-related genes. Thus, adaptive differentiation may not only be important for injury-repair but also in modulating host immunity to pathogens.

Determine if maladaptive differentiation occurs in chronic inflammation and tumorigenesis

While the adaptive cellular response described in this study appears to be beneficial in the setting of injury-repair and possibly in infection, it will be important to determine whether this process can go awry (i.e. maladaptive differentiation) during chronic inflammation and tumorigenesis. We illustrate this concept in **Figure 6.3**. In celiac disease, villus atrophy is a hallmark feature, and patients placed on a gluten-free diet generally enables villus recovery and symptomatic relief. However, over one-third of patients placed on a strict gluten-free diet have persistent villus atrophy and chronic symptoms (Lebwohl et al., 2014; Rubio-Tapia and Murray, 2010). This is known as refractory sprue/ceeliac disease/enteropathy (Cellier et al., 2000). Crohn's disease patients can also present with villus atrophy (Culliford et al., 2004; Jansson-Knodell et

al., 2018). In Crohn's disease, a major goal of treatment is to achieve mucosal healing and restoration of the epithelial architecture (Baert et al., 2010; Rutgeerts et al., 2007). Impaired barrier function and healing is thought to be one of the major problems in these patients (Rieder et al., 2007). Understanding how healing can be hindered in human enteropathies may provide novel therapeutics for patients with refractory or chronic disease. Additionally, inflammatory diseases are often thought to be precursors to metaplasia and cancer (Coussens and Werb, 2002). While small bowel tumors are quite rare, inflammatory bowel disease is an important risk factor for the development of colorectal cancer (Axelrad et al., 2016; Ullman and Itzkowitz, 2011). While a lot is known about the mechanisms that underly tumor initiation and progression in colorectal cancer (Bajaj et al., 2020; La Vecchia and Sebastian, 2020), less is known about how established tumors and cancers maintain their architecture and resist against damage signals.

We discovered that when adaptive differentiation does not occur properly, which occurs in mice lacking YAP, villus regeneration is impaired. In addition, atrophic villi fused with each other, and the epithelium persisted in a maladapted state. As villus fusion is a phenomenon that often occurs in human enteropathies (Dickson et al., 2006; Rutgeerts et al., 1984), this provides a possible explanation for why certain patients with damage to their villi fail to recover these structures. It will be interesting to examine Crohn's and celiac disease patients and assess whether their lack of ability to activate YAP signaling in the intestinal epithelium and generate normal aVECs are what could be behind their pathology. Furthermore, it would be important to determine whether aVEC-like cells are present in human cancers and assess the functional role of these cells using mouse models. Developing ways to target therapies to the differentiated villus compartment without affecting the crypt compartment may be of immense value in the future.

6.3 Closing Remarks

In conclusion, I have identified a damaged-induced cell type, named atrophy-induced villus epithelial cells (aVECs), that covers the surface of injured intestinal villi. These cells possess an altered differentiation state that is specialized for repair. They promote repair by quickly re-establishing the intestinal barrier following villus collapse. This function is dependent on the Hippo effector YAP. In the absence of YAP, aVEC function is impaired and barrier function is compromised. As a result, villus repair is delayed, leading to a diminished capacity for atrophic villi to regenerate back to their original height. These findings have important implications for diseases states with villus damage, including Crohn's and celiac disease.

Importantly, I have discovered a repair mechanism that has not been previously described in the literature. In this process, which I call "adaptive differentiation," stem and progenitor cells directly differentiate into a specialized cell type not present during homeostasis that is essential for meeting the current demands of the tissue (i.e., repair, pathogen defense, etc.). Generally this process is transient and does not involve a cell type conversion. Rather, lineage identity is retained, but instead of fully committing to the intended cell type, the programs that drives the adaptive function of these cells become prioritized. In the context of villus injury, progenitor cells differentiate into aVECs to seal the intestinal barrier. These cells still technically commit to the usual enterocyte or goblet cell lineages, but their repair signature and function predominates.

We predict that aVECs play a unique role in villus repair and perhaps in the pathogenesis of intestinal diseases. To our knowledge, the connection between cell differentiation and reactivation of a developmental program has not been made before. We believe our findings will set a precedent for how differentiated cells can have altered states in injury-repair and disease.

6.4 Figures

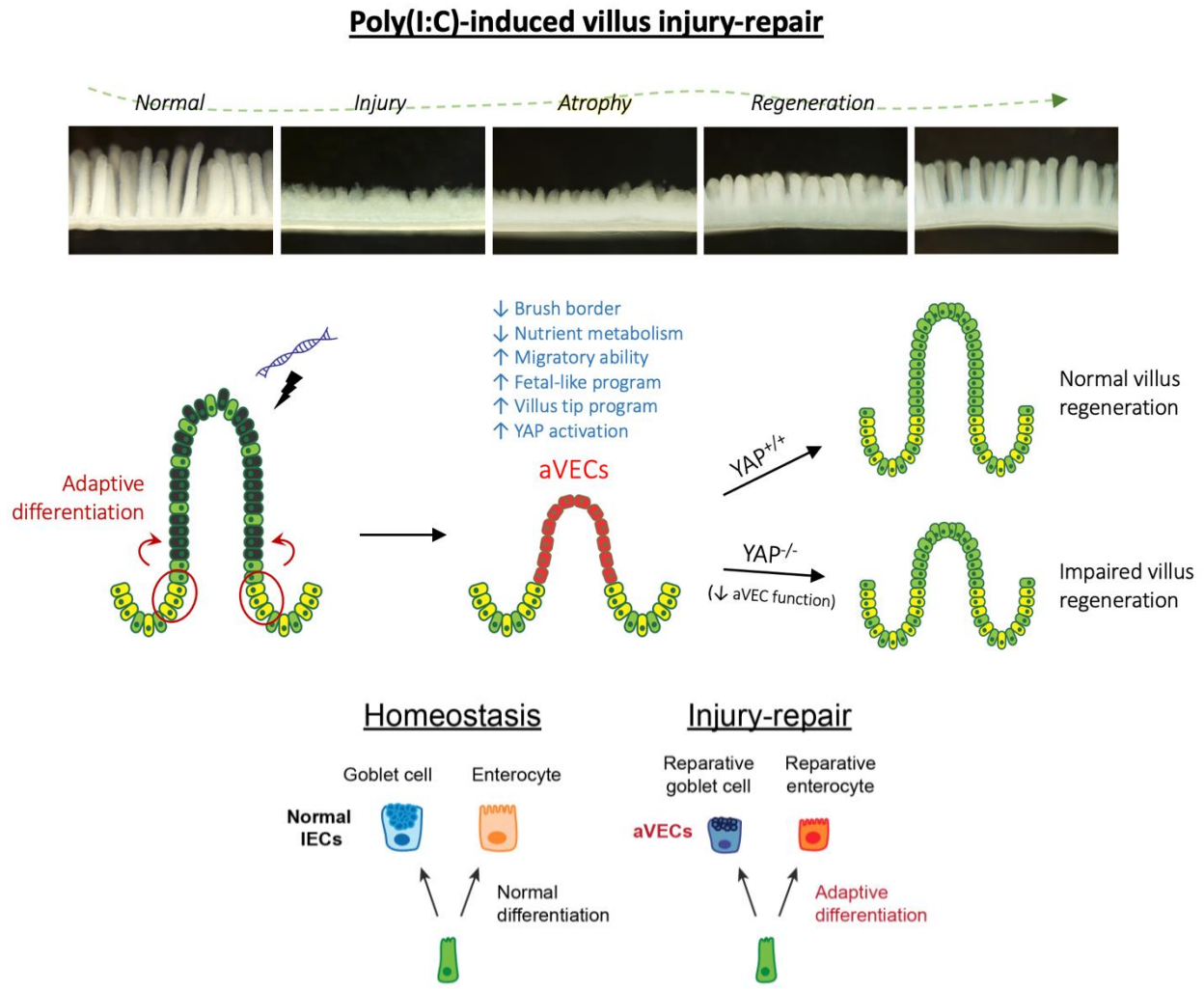


Figure 6.1. Overall summary of findings

Using a poly(I:C)-mediated intestinal injury model, we provide a detailed cellular and molecular understanding of how villi repair and regenerate after damage. We describe two key steps of repair: (1) formation of aVECs and barrier recovery during villus atrophy and (2) increase in cell proliferation and differentiation during villus regeneration. The first step involves the adaptive differentiation of progenitor cells to reparative enterocytes and goblet cells (i.e., aVECs). This step depends on YAP and must occur properly in order to proceed to the second repair phase.

Mechanisms of Tissue Repair

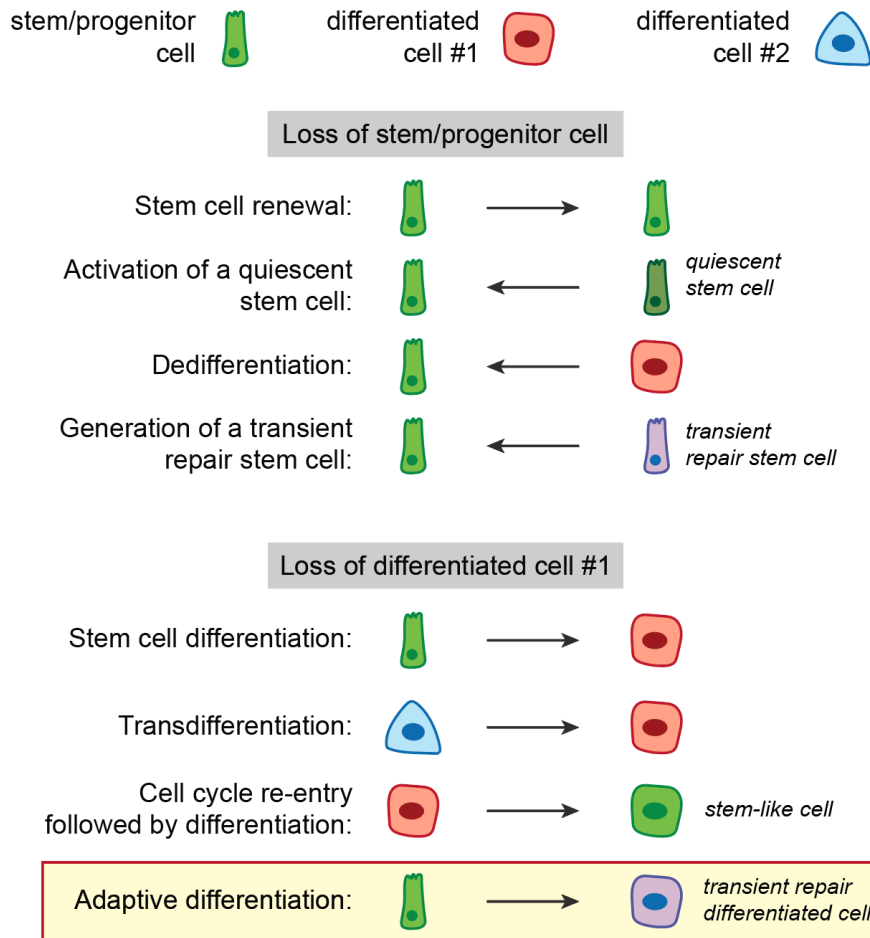


Figure 6.2. Mechanisms of tissue repair

Various mechanisms of repair have been proposed to occur in response to injury in mammals. Generally, these include stem cell activation (expansion and differentiation of tissue-resident stem cells), dedifferentiation (mature cells reverting back to an immature state), and transdifferentiation (conversion of one cell type to another). In these cases, the goal is to replenish the lost cells. However, in certain contexts, tissues may need to first attend to the damage itself before resuming regeneration. These transient repair processes, including the one we describe here (i.e., adaptive differentiation), are just beginning to be appreciated.

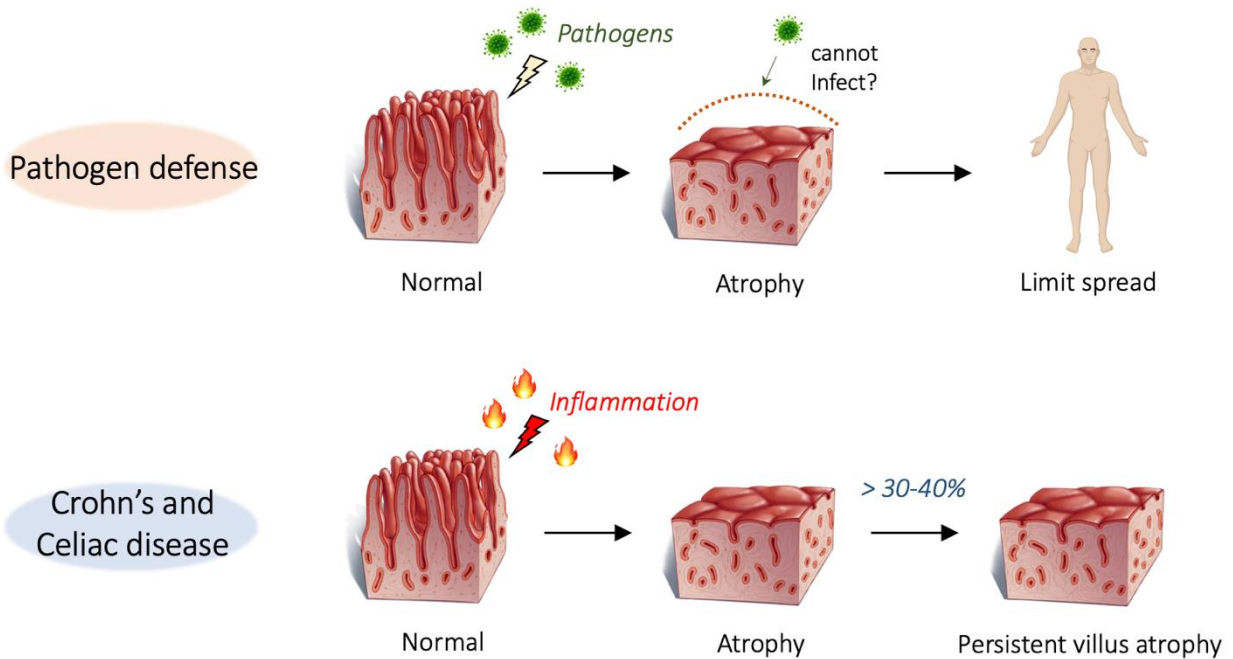


Figure 6.3. Role of adaptive differentiation in pathogen defense and disease

In addition to being an important repair mechanism, adaptive differentiation may be applicable in other contexts such as pathogen defense and diseases such as Crohn's and celiac disease. One idea is that after injury, adaptive differentiation is triggered to prevent further spread of the infectious agent. Another idea is that when adaptive differentiation is impaired (i.e. maladaptive differentiation occurs), mucosal healing is impaired, resulting in a persistent state of damage.

6.5 References

- Artegiani, B., Hendriks, D., Beumer, J., Kok, R., Zheng, X., Joore, I., Chuva de Sousa Lopes, S., van Zon, J., Tans, S., and Clevers, H. (2020). Fast and efficient generation of knock-in human organoids using homology-independent CRISPR-Cas9 precision genome editing. *Nat Cell Biol* 22, 321-331.
- Axelrad, J.E., Lichtiger, S., and Yajnik, V. (2016). Inflammatory bowel disease and cancer: The role of inflammation, immunosuppression, and cancer treatment. *World J Gastroenterol* 22, 4794-4801.
- Aydin, B., and Mazzoni, E.O. (2019). Cell Reprogramming: The Many Roads to Success. *Annu Rev Cell Dev Biol* 35, 433-452.
- Baert, F., Moortgat, L., Van Assche, G., Caenepeel, P., Vergauwe, P., De Vos, M., Stokkers, P., Hommes, D., Rutgeerts, P., Vermeire, S., *et al.* (2010). Mucosal healing predicts sustained clinical remission in patients with early-stage Crohn's disease. *Gastroenterology* 138, 463-468; quiz e410-461.
- Bajaj, J., Diaz, E., and Reya, T. (2020). Stem cells in cancer initiation and progression. *J Cell Biol* 219.
- Burgess, D.J. (2019). Spatial transcriptomics coming of age. *Nat Rev Genet* 20, 317.
- Cellier, C., Delabesse, E., Helmer, C., Patey, N., Matuchansky, C., Jabri, B., Macintyre, E., Cerf-Bensusan, N., and Brousse, N. (2000). Refractory sprue, coeliac disease, and enteropathy-associated T-cell lymphoma. French Coeliac Disease Study Group. *Lancet* 356, 203-208.
- Coussens, L.M., and Werb, Z. (2002). Inflammation and cancer. *Nature* 420, 860-867.
- Culliford, A., Markowitz, D., Rotterdam, H., and Green, P.H. (2004). Scalloping of duodenal mucosa in Crohn's disease. *Inflamm Bowel Dis* 10, 270-273.
- Delacour, D., Salomon, J., Robine, S., and Louvard, D. (2016). Plasticity of the brush border - the yin and yang of intestinal homeostasis. *Nat Rev Gastroenterol Hepatol* 13, 161-174.
- Dickson, B.C., Streutker, C.J., and Chetty, R. (2006). Coeliac disease: an update for pathologists. *J Clin Pathol* 59, 1008-1016.
- Fernandez Vallone, V., Leprovots, M., Strollo, S., Vasile, G., Lefort, A., Libert, F., Vassart, G., and Garcia, M.I. (2016). Trop2 marks transient gastric fetal epithelium and adult regenerating cells after epithelial damage. *Development* 143, 1452-1463.
- Fordham, R.P., Yui, S., Hannan, N.R., Soendergaard, C., Madgwick, A., Schweiger, P.J., Nielsen, O.H., Vallier, L., Pedersen, R.A., Nakamura, T., *et al.* (2013). Transplantation of

expanded fetal intestinal progenitors contributes to colon regeneration after injury. *Cell Stem Cell* *13*, 734-744.

Fujii, M., Clevers, H., and Sato, T. (2019). Modeling Human Digestive Diseases With CRISPR-Cas9-Modified Organoids. *Gastroenterology* *156*, 562-576.

Gadye, L., Das, D., Sanchez, M.A., Street, K., Baudhuin, A., Wagner, A., Cole, M.B., Choi, Y.G., Yosef, N., Purdom, E., *et al.* (2017). Injury Activates Transient Olfactory Stem Cell States with Diverse Lineage Capacities. *Cell Stem Cell* *21*, 775-790 e779.

Ge, Y., Gomez, N.C., Adam, R.C., Nikolova, M., Yang, H., Verma, A., Lu, C.P., Polak, L., Yuan, S., Elemento, O., *et al.* (2017). Stem Cell Lineage Infidelity Drives Wound Repair and Cancer. *Cell* *169*, 636-650 e614.

Gjorevski, N., Sachs, N., Manfrin, A., Giger, S., Bragina, M.E., Ordonez-Moran, P., Clevers, H., and Lutolf, M.P. (2016). Designer matrices for intestinal stem cell and organoid culture. *Nature* *539*, 560-564.

Gregorieff, A., Liu, Y., Inanlou, M.R., Khomchuk, Y., and Wrana, J.L. (2015). Yap-dependent reprogramming of Lgr5(+) stem cells drives intestinal regeneration and cancer. *Nature* *526*, 715-718.

Hoffmann, M., Kleine-Weber, H., Schroeder, S., Kruger, N., Herrler, T., Erichsen, S., Schiergens, T.S., Herrler, G., Wu, N.H., Nitsche, A., *et al.* (2020). SARS-CoV-2 Cell Entry Depends on ACE2 and TMPRSS2 and Is Blocked by a Clinically Proven Protease Inhibitor. *Cell* *181*, 271-280 e278.

Holmes, C., and Stanford, W.L. (2007). Concise review: stem cell antigen-1: expression, function, and enigma. *Stem Cells* *25*, 1339-1347.

Jansson-Knodell, C.L., Hujoel, I.A., Rubio-Tapia, A., and Murray, J.A. (2018). Not All That Flattens Villi Is Celiac Disease: A Review of Enteropathies. *Mayo Clin Proc* *93*, 509-517.

Jessen, K.R., Mirsky, R., and Arthur-Farraj, P. (2015). The Role of Cell Plasticity in Tissue Repair: Adaptive Cellular Reprogramming. *Dev Cell* *34*, 613-620.

Kim, H.B., Kim, M., Park, Y.S., Park, I., Kim, T., Yang, S.Y., Cho, C.J., Hwang, D., Jung, J.H., Markowitz, S.D., *et al.* (2017). Prostaglandin E2 Activates YAP and a Positive-Signaling Loop to Promote Colon Regeneration After Colitis but Also Carcinogenesis in Mice. *Gastroenterology* *152*, 616-630.

Kim, J., Koo, B.K., and Knoblich, J.A. (2020). Human organoids: model systems for human biology and medicine. *Nat Rev Mol Cell Biol* *21*, 571-584.

Kobayashi, Y., Tata, A., Konkimalla, A., Katsura, H., Lee, R.F., Ou, J., Banovich, N.E., Kropski, J.A., and Tata, P.R. (2020). Persistence of a regeneration-associated, transitional alveolar epithelial cell state in pulmonary fibrosis. *Nat Cell Biol* *22*, 934-946.

- La Vecchia, S., and Sebastian, C. (2020). Metabolic pathways regulating colorectal cancer initiation and progression. *Semin Cell Dev Biol* 98, 63-70.
- Lamers, M.M., Beumer, J., van der Vaart, J., Knoops, K., Puschhof, J., Breugem, T.I., Ravelli, R.B.G., Paul van Schayck, J., Mykytyn, A.Z., Duimel, H.Q., *et al.* (2020). SARS-CoV-2 productively infects human gut enterocytes. *Science* 369, 50-54.
- Lebwohl, B., Murray, J.A., Rubio-Tapia, A., Green, P.H., and Ludvigsson, J.F. (2014). Predictors of persistent villous atrophy in coeliac disease: a population-based study. *Aliment Pharmacol Ther* 39, 488-495.
- Li, V.S.W. (2019). Yap in regeneration and symmetry breaking. *Nat Cell Biol* 21, 665-667.
- Lukonin, I., Serra, D., Challet Meylan, L., Volkmann, K., Baaten, J., Zhao, R., Meeusen, S., Colman, K., Maurer, F., Stadler, M.B., *et al.* (2020). Phenotypic landscape of intestinal organoid regeneration. *Nature* 586, 275-280.
- Ma, Y.C., Yang, Z.S., Ma, L.Q., Shu, R., Zou, C.G., and Zhang, K.Q. (2020). YAP in epithelium senses gut barrier loss to deploy defenses against pathogens. *PLoS Pathog* 16, e1008766.
- Marx, V. (2021). Method of the Year: spatially resolved transcriptomics. *Nat Methods* 18, 9-14.
- Miyoshi, H., VanDussen, K.L., Malvin, N.P., Ryu, S.H., Wang, Y., Sonnek, N.M., Lai, C.W., and Stappenbeck, T.S. (2017). Prostaglandin E2 promotes intestinal repair through an adaptive cellular response of the epithelium. *EMBO J* 36, 5-24.
- Mustata, R.C., Vasile, G., Fernandez-Vallone, V., Strollo, S., Lefort, A., Libert, F., Monteyne, D., Perez-Morga, D., Vassart, G., and Garcia, M.I. (2013). Identification of Lgr5-independent spheroid-generating progenitors of the mouse fetal intestinal epithelium. *Cell Rep* 5, 421-432.
- Nusse, Y.M., Savage, A.K., Marangoni, P., Rosendahl-Huber, A.K.M., Landman, T.A., de Sauvage, F.J., Locksley, R.M., and Klein, O.D. (2018). Parasitic helminths induce fetal-like reversion in the intestinal stem cell niche. *Nature* 559, 109-113.
- Panciera, T., Azzolin, L., Cordenonsi, M., and Piccolo, S. (2017). Mechanobiology of YAP and TAZ in physiology and disease. *Nat Rev Mol Cell Biol* 18, 758-770.
- Pastar, I., Stojadinovic, O., Yin, N.C., Ramirez, H., Nusbaum, A.G., Sawaya, A., Patel, S.B., Khalid, L., Isseroff, R.R., and Tomic-Canic, M. (2014). Epithelialization in Wound Healing: A Comprehensive Review. *Adv Wound Care (New Rochelle)* 3, 445-464.
- Pensaert, M., Haelterman, E.O., and Burnstein, T. (1970). Transmissible gastroenteritis of swine: virus-intestinal cell interactions. I. Immunofluorescence, histopathology and virus production in the small intestine through the course of infection. *Arch Gesamte Virusforsch* 31, 321-334.

- Rees, W.D., Tandun, R., Yau, E., Zachos, N.C., and Steiner, T.S. (2020). Regenerative Intestinal Stem Cells Induced by Acute and Chronic Injury: The Saving Grace of the Epithelium? *Front Cell Dev Biol* 8, 583919.
- Rieder, F., Brenmoehl, J., Leeb, S., Scholmerich, J., and Rogler, G. (2007). Wound healing and fibrosis in intestinal disease. *Gut* 56, 130-139.
- Romera-Hernandez, M., Aparicio-Domingo, P., Papazian, N., Karrich, J.J., Cornelissen, F., Hoogenboezem, R.M., Samsom, J.N., and Cupedo, T. (2020). Yap1-Driven Intestinal Repair Is Controlled by Group 3 Innate Lymphoid Cells. *Cell Rep* 30, 37-45 e33.
- Roulis, M., Kaklamanos, A., Scherthanner, M., Bielecki, P., Zhao, J., Kaffe, E., Frommelt, L.S., Qu, R., Knapp, M.S., Henriques, A., *et al.* (2020). Paracrine orchestration of intestinal tumorigenesis by a mesenchymal niche. *Nature* 580, 524-529.
- Rubio-Tapia, A., and Murray, J.A. (2010). Classification and management of refractory coeliac disease. *Gut* 59, 547-557.
- Rutgeerts, P., Geboes, K., Vantrappen, G., Kerremans, R., Coenegrachts, J.L., and Coremans, G. (1984). Natural history of recurrent Crohn's disease at the ileocolonic anastomosis after curative surgery. *Gut* 25, 665-672.
- Rutgeerts, P., Vermeire, S., and Van Assche, G. (2007). Mucosal healing in inflammatory bowel disease: impossible ideal or therapeutic target? *Gut* 56, 453-455.
- Schwank, G., and Clevers, H. (2016). CRISPR/Cas9-Mediated Genome Editing of Mouse Small Intestinal Organoids. *Methods Mol Biol* 1422, 3-11.
- Seo, Y., Park, S.Y., Kim, H.S., and Nam, J.S. (2020). The Hippo-YAP Signaling as Guardian in the Pool of Intestinal Stem Cells. *Biomedicines* 8.
- Serra, D., Mayr, U., Boni, A., Lukonin, I., Rempfler, M., Challet Meylan, L., Stadler, M.B., Strnad, P., Papasaikas, P., Vischi, D., *et al.* (2019). Self-organization and symmetry breaking in intestinal organoid development. *Nature* 569, 66-72.
- Takahashi, K., and Yamanaka, S. (2016). A decade of transcription factor-mediated reprogramming to pluripotency. *Nat Rev Mol Cell Biol* 17, 183-193.
- Trougakos, I.P., Lourda, M., Agiostratidou, G., Kletsas, D., and Gonos, E.S. (2005). Differential effects of clusterin/apolipoprotein J on cellular growth and survival. *Free Radic Biol Med* 38, 436-449.
- Ullman, T.A., and Itzkowitz, S.H. (2011). Intestinal inflammation and cancer. *Gastroenterology* 140, 1807-1816.

Wang, Y., Chiang, I.L., Ohara, T.E., Fujii, S., Cheng, J., Muegge, B.D., Ver Heul, A., Han, N.D., Lu, Q., Xiong, S., *et al.* (2019). Long-Term Culture Captures Injury-Repair Cycles of Colonic Stem Cells. *Cell* *179*, 1144-1159 e1115.

Xu, J., Tang, Y., Sheng, X., Tian, Y., Deng, M., Du, S., Lv, C., Li, G., Pan, Y., Song, Y., *et al.* (2020). Secreted stromal protein ISLR promotes intestinal regeneration by suppressing epithelial Hippo signaling. *EMBO J* *39*, e103255.

Yoshida, S., Miwa, H., Kawachi, T., Kume, S., and Takahashi, K. (2020). Generation of intestinal organoids derived from human pluripotent stem cells for drug testing. *Sci Rep* *10*, 5989.

Yui, S., Azzolin, L., Maimets, M., Pedersen, M.T., Fordham, R.P., Hansen, S.L., Larsen, H.L., Guiu, J., Alves, M.R.P., Rundsten, C.F., *et al.* (2018). YAP/TAZ-Dependent Reprogramming of Colonic Epithelium Links ECM Remodeling to Tissue Regeneration. *Cell Stem Cell* *22*, 35-49 e37.